DIAGNOZA - GENEZA - PROGNOZA => PODSTAWA KAŻDEJ DECYZJI

POLSKIE TOWARZYSTWO DIAGNOSTYKI TECHNICZNEJ

PTDT

afiliowane przy

Wydziale Nauk
Technicznych
Polskiej Akademii Nauk

Diagnostyka

ISSN 1641-6414

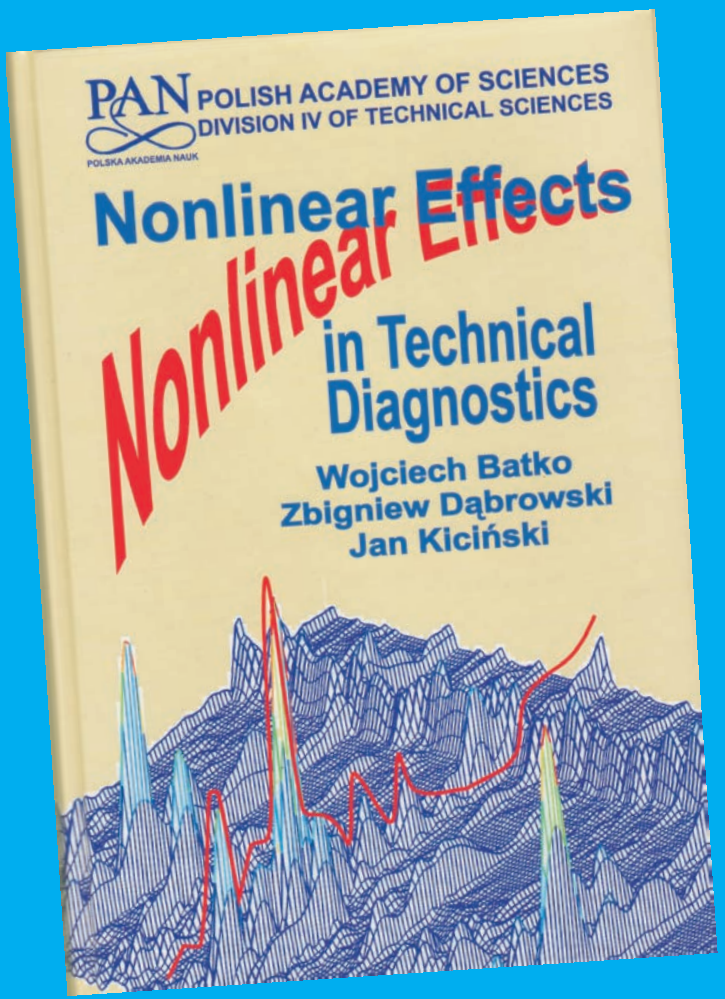

Nr 2(50) / 2009

WYDAWCA:
Polskie Towarzystwo Diagnostyki Technicznej
02-981 Warszawa
ul. Augustówka 5

REDAKTOR NACZELNY:
prof. dr hab. inż. **Ryszard MICHALSKI**

SEKRETARZ REDAKCJI:
dr inż. **Sławomir WIERZBICKI**

CZŁONKOWIE KOMITETU REDAKCYJNEGO:
dr inż. **Krzysztof LIGIER**
dr inż. **Paweł MIKOŁAJCZAK**

ADRES REDAKCJI:
UWM w Olsztynie
Redakcja Diagnostyki
ul. Oczapowskiego 11
10-736 Olsztyn
Poland
tel.: 089-523-48-11, fax: 089-523-34-63
www.diagnostyka.net.pl
e-mail: diagnostyka@uwm.edu.pl

KONTO PTDT:
Bank PEKAO SA O/Warszawa
nr konta: 33 1240 5963 1111 0000 4796 8376

NAKŁAD: **350 egzemplarzy**

Wydanie dofinansowane przez Ministra Nauki i Szkolnictwa Wyższego

Spis treści / Contents

HARMONISATION OF MAINTENANCE PERFORMANCE INDICATORS

Juraj GRENCIK

University of Zilina, Faculty of Mechanical Engineering,
Univerzitna 1, 010 26 Zilina, Slovakia, e-mail: juraj.grencik@fstroj.utc.sk

Summary

Globalization process brought the need for a common understanding of the indicators that are used to measure maintenance and availability performance. There have been numerous systems of indicators developed virtually by each larger company or organisation around the world. However, a common set of indicators and definitions would facilitate the ability of an international company to accurately perform benchmarking between facilities in different counties or continents. To resolve this problem, a team comprised of EFNMS and SMRP representatives is working toward a common set of indicators that can be applied globally. This cooperative effort is termed harmonisation.

Keywords: maintenance, key performance indicators, EFNMS, SMRP, harmonisation.

1. INTRODUCTION

Maintenance performance has always been of great interest of both company managers as well as active maintenance staff. The managers always want to know if the money spent on maintenance is spent effectively and is not just wasted. Maintenance staff on the other hand wants to show that they are doing perfect job with top results. The easiest way to show the results is to measure them. But the main obstacle in measuring maintenance performance is in difficulty to find objective criteria or indicators to measure its performance. Unlike production, where outputs can easily be measured in manufactured numbers, tons, etc. per manufacturing costs, it is impossible to give single indicator of maintenance output.

Maintenance process is very complex one and its performance depends on number of factors. Perfect work of maintenance staff quite often brings unsatisfactory results in reliability performance, just because of outdated unreliable machinery. On the other hand reliable advanced equipment may require virtually no maintenance thus resulting in high equipment availability.

Some principal efforts on international level can be recognized in the area of maintenance performance measurement, very often called maintenance benchmarking. Benchmarking uses a set of indicators that can be used for comparison of own results with results being achieved by the others, if possible by the so called world class. In Europe a principal role was played by EFNMS (European Federation of National Maintenance Societies), its working group 7 – Maintenance Benchmarking, which had set up 13 principal indicators in 2002. Later on, this effort was transformed into European standard bringing 71 indicators divided into 3 main categories – economical, technical and organizational. In parallel, in the North America, a SMRP (Society of Maintenance and Reliability Professionals) has been developing system of maintenance performance metrics, as they called them, but divided into 5 groups – Business and Management, Manufacturing Process Reliability, Equipment Reliability, People Skills and Work Management. As the world is only one and globalization is an ongoing process, in 2006 during the Euromaintenance 2006 /3rd world congress on maintenance, held in Basel, representatives of these groups met and decided to start process of harmonization of both system which should bring a commonly defined and commonly used indicators of maintenance performance.

By the April 2008, seventeen indicators have been harmonized, that is compared and recognized as identical, similar or measure same performance, but using different definitions. Objective the harmonization effort is to bring a common set of indicators and definitions, and thus the ability of an international company to accurately perform benchmarking between facilities in different counties or continents by using a set of indicators that can be applied globally.

2. EUROPEAN SET OF INDICATORS

The European Federation of National Maintenance Societies vzw (EFNMS) is non-profit organization with the objective of improvement of maintenance for the benefit of the peoples of Europe. In 1998, Working Group 7 (WG7) was formed and continually selected a number of benchmark indicators that were regarded as important when measuring maintenance performance [1]. In 2002 they published a set of thirteen indicators.

Members of Working Group 7 actively participated in the standardisation activities of the European Committee for Standardization Technical Committee 319 - Maintenance (CEN/TC 319). The technical committee's efforts resulted in publication of 71 in European Standard EN:15341 Maintenance Key Performance Indicators in early 2007 [2].

The EFNMS Benchmarking Committee (previously called WG 7) utilizes the indicators (selected ones, corresponding to the former 13 EFNMS indicators) in EN: 15341:2007 to conduct workshops through Europe and the Middle East, at which more than 150 participants in twelve countries (among them Slovakia) have been given the opportunity to calculate indicators on their company's maintenance and availability performance, and to gain a deeper understanding in the use of indicator.

The new standard let the users decide which indicators will be utilised, but this on the other hand brings a problem of mutual comparison when companies will not use the same indicators.

The objective of indicators is to help management to support management in achieving maintenance excellence and utilize technical assets in a competitive manner. Most of the indicators apply to all industrial and supporting facilities.

These indicators should be used to:

a) measure the status;
b) compare (internal and external benchmarks);
c) diagnose (analysis of strengths and weaknesses);
d) identify objectives and define targets to be reached;
e) plan improvement actions;
f) continuously measure changes over time.

To select relevant indicators, the first step is to define the objectives to be reached at each level of the enterprise. At the company level, the requirement is to identify how maintenance can be managed in order to improve global performance (profits, market shares, competitiveness etc). At the systems level and production lines, the maintenance objectives can address some particular performance factors, which have been identified through previous analysis, such as improvement of availability, improvement on cost-effective maintenance, retaining health, safety and environment preservation, improvement in cost-effective management of the value of the maintenance inventory, control of contracted services, etc. At the equipment level, machines or types of machines, better control of reliability costs; maintainability and maintenance supportability, etc may be desirable.

When the objectives have been defined and the performance parameters to be measured have been identified, the next step is to find the indicators that allow measuring these parameters. The system can include capacity of maintaining the equipment, reliability of the equipment, efficiency of the maintenance activities, health, safety and the environment, etc. An indicator is relevant when its value or its evaluation is correlated with the evaluation of the performance parameter to be measured. A relevant indicator shall be one element of decision making.

It is necessary to precisely define:

– data to be collected to determine the values required for the indicator;
– measurement method (operating mode);
– tools required for the measurement (documents, counters, sensors, analyzers, computerized maintenance management system, etc.).

To make the possible evaluation and comparisons easier, it is necessary that the collected data are in conformity with the standardized definitions (e.g. EN 13306).

It is necessary to predetermine the frequency of the calculation and consider availability and time delay of the relevant data, changes over time and reactivity of the system to the actions undertaken.

Out of the scope of this standard remain definition of score, analysis and adopting required measures. The standard itself comprises a set of indicators, but their analysis will require additional projects.

3. SMRP (USA) METRICS

Society for Maintenance and Reliability Professionals (SMRP) has defined and continually has been developing indicators (metrics as they call them) of the best practices to measure maintenance performance. This process is ongoing and metrics can be found at www.smrp.org. The SMRP is active mostly in the USA and Canada, has over 1500 members of which 150 are executive company members.

Objective of the SMRP committee is to define best practices in maintenance and reliability and gradually create a set of the most frequently used metrics and definitions.

The SMRP best practices committee has selected over 70 metrics that will be gradually defined in the following categories:

- business and management.
- manufacturing process reliability.
- equipment reliability.
- people skills.
- work management.

4. HARMONISATION PROCESS WITH KPI'S

At Euromaintenance 2006 in Basel, Switzerland, key members of the EFNMS WG 7 and the SMRP Best Practices Committee met for the first time. The purpose of the meeting was to exchange information and to explore possible cooperation efforts [3].

It was decided to form a joint EFNMS-SMRP working group to resolve differences between the EN:15341 indicators and those being developed by

the SMRP Best Practices Committee. Side-by-side comparisons were made of both the indicator formulas and definitions of terms. The basis for the European terms was EN:13306:2001 Maintenance Terminology and IEC 60050-191:1990 Dependability and Quality of Service. The SMRP definitions are contained within each indicator (metric) description, and have been compiled in a Glossary of Terms. This resulted in two extensive lists, as there were either terms or formulas that were not common to both sets.

An indicator is determined to be common if it has the same basic formula or could be universally applied. For these common indicators, it is first determined whether any differences can be eliminated. If there are differences that cannot be eliminated, the differences are qualified or explained. This is the essence of the harmonisation process.

It should be noted that the grouping of indicators is different. In EN:15341, the indicators are grouped into economic, technical and organizational sets. The SMRP indicators are categorized in accordance with the five pillars of the SMRP Body of Knowledge: Business and Management, Manufacturing Process Reliability, Equipment Reliability, People Skills and Work Management.

The joint working group made very good progress, announcing the first harmonisation results in January 2007.

To date, the seventeen indicators listed in Table 1 have been harmonized. An additional eleven indicators have been identified for harmonisation. Each is classified as:

- IDENTICAL – the bases of the indicators are the same, although there may be some differences in how they are presented. The differences are detailed in the comments.
- SIMILAR – there are some differences in the differences that are detailed in the comments.
- SAME PERFORMANCE – the indicators measure the same performance area, but there are significant differences in the definitions or calculations that are detailed in the comments.

When an indicator is harmonized, a statement declaring this fact is added to the SMRP metric description.

Furthermore, the SMRP metric is recommended for use by EFNMS as a guideline or supporting document for the European Indicator.

The harmonised indicators were used in the first world's SMRP-EFNMS Benchmarking Workshop held at Euromaintenance 2008 in Brussels.

The harmonisation work will continue until the list of SMRP indicators currently under development has been exhausted. It is desired to initiate similar harmonisation efforts with other international maintenance organizations, such as COPIMAN (Technical Committee on Maintenance of the Pan American Federation of Engineering Societies) or MESA (Maintenance Engineering Society of Australia).

It is also desired to promulgate the use of these indicators as accepted standards. Discussions are ongoing with CEN/TC 319 to consider proposing the harmonized metrics as global standards or guidelines.

Table 1 – EFNMS-SMRP Harmonized Indicators

SMRP Metrics		EN 15341 Indicators	
Metric No.	Metric name	Indicator No	Indicator Ratio
5.5.33	Stock outs	O26	Number of the spare parts supplied by the warehouse as requested x 100/ Total number of spare parts required by maintenance
1.4	Stores value/RAV	E7	Average inventory value of maintenance materials x 100/ Asset Replacement Value
1.5	Annual maintenance cost per RAV	E1	Total Maintenance Cost x 100/ Assets Replacement Value
3.5.1	MTBF	T17	Total operating time x 100/ Number of failures
3.5.2	MTTR	T21	Total time to restore x 100/ Number of failures
4.2.1	Maintenance training costs	E21	Cost of training for maintenance/ Number of maintenance personnel
4.2.2.	Maintenance Training hours	O23	Number of maintenance internal personnel man-hours for training x 100/ Total internal maintenance man-hours
5.4.1	Reactive work	O17	Immediate Corrective maintenance man-hours x 100/ Total maintenance man-hours
5.4.2	Proactive Work	O18	Preventive maintenance man hours x 100/ Total maintenance man hours

5.7.1	Continious improvement hours	O8	Man-hours used for continuous improvement x 100/ Total maintenance personnel man-hours
5.5. 71	Contractor maintenance cost	E10	Total contractor cost x 100/ Total maintenance cost
5.5.8	Overtime maintenance hours	O21	Overtime internal maintenance man hours x 100/ Total internal maintenance man hours
5.1.1	Corrective maintenance cost	E15	Corrective maintenance cost x 100/ Total Maintenance Cost
5.1.2	Corrective maintenance hours	O16	Corrective maintenance man hours x 100/ Total maintenance man hours
5.4.4	Work orders performed as scheduled	O22	Number of work orders performed as scheduled x 100/ Total number of scheduled work orders
5.5.6	Craft workers on shift ratio	O10	Direct maintenance personnel on shift x 100 Total direct maintenance personnel
5.5.31	Stores Inventory Turns	E12	Total cost of maintenance materials x 100 Average inventory value of Maintenance materials Warehouse turnover

5. SUMMARY

Although much has been done in the field of KPIs, there are some weaknesses in the area of structuring and hierarchical composition of these KPIs. Another problem is definition of "top" or leading indicators, which was discussed in [4]. Frequently used OEE is only partly affected by maintenance and maintenance costs do not characterize quality of work performed (not considering age and inherent reliability of equipment). And none of these systems, although declaring technical indicators, have nothing to say about technical basis or diagnostics used in maintenance process, which is a fundamental for the maintenance.

REFERENCES

[1] Svantesson T.: *Nordic Benchmarking Analysis and EFNMS Key Figures*. Euromaintenance 2002, Helsinki, Finland, 2002.
[2] EN 15341, Maintenance Key Performance Indicators, 2007.
[3] Svantesson T., Olver R., Kahn J. D.: *EFNMS-SMRP maintenance and reliability indicator harmonisation project*. Euromaintenance 2008, Brussels, Belgium, April, 2008.
[4] Grencik J., Legat V.: *Maintenance audit and benchmarking - search for evaluation criteria on global scale*. Eksploatacja i niezawodność. Nr. 3 (35) 2007, PNTTE, Warszawa, Oct 2007, ISSN 1507-2711, pp. 34 – 39.

Author: Doc. Ing. **Juraj GRENCIK**, PhD. University of Zilina, Faculty of Mechanical Engineering. At present a chairman of the Slovak Maintenance Society, member of the EFNSM Benchmarking Committee.

APPLICATION OF DIAGNOSTIC ALGORITHMS FOR WIND TURBINES

Tomasz BARSZCZ

Department of Robotics and Mechatronics, AGH University of Science and Technology,
Al. Mickiewicza 30, 30-059 Cracow, fax: (012) 634-35-05, email: tbarszcz@agh.edu.pl

Summary

The paper presents the choice of diagnostic algorithms for condition monitoring of wind turbines. The device under monitoring is the power train, i.e. a main bearing, gears and a generator. The object also contains several roller bearings. The typical mechanical structure and characteristic frequencies are shown. The next chapter presents the sensor location and choice of sampling parameters. Additionally the monitoring should include a few key process parameters (output power, wind speed and rotational speed). Quick changes of the operational point are an important feature of wind turbines and should be addressed.

There are several diagnostic methods which could be used for the monitoring of a wind turbine. A few of them should be selected for the proper detection and identification of the most important faults. The main part of the paper presents malfunctions and diagnostic algorithms which should be used to detect those malfunctions. To avoid the influence of varying operational point, some additional preprocessing should take place. Apart from relatively simple methods mentioned above, there is a number of more advanced methods. The example of such an algorithm based on the spectral kurtosis is also presented.

Keywords: vibration, monitoring, diagnostics, wind turbines.

DOBÓR ALGORYTMÓW DIAGNOSTYCZNYCH DLA TURBIN WIATROWYCH

Streszczenie

Artykuł przedstawia dobór algorytmów diagnostycznych do nadzorowania stanu turbiny wiatrowej. Nadzorowanymi elementami są: główne łożysko wirnika, przekładnie i generator wraz z ich łożyskami. Przedstawiono typową strukturę i zaprezentowano częstotliwości charakterystyczne obiektu. Kolejny rozdział omawia lokalizację czujników drgań oraz parametry próbkowania sygnałów. Dodatkowo monitorowanie powinno obejmować najważniejsze parametry procesowe (tj. moc generatora, prędkość wiatru i prędkość obrotową). Charakterystyczną cechą turbin wiatrowych są szybkie zmiany punktu pracy, które należy brać pod uwagę.

Istnieją liczne algorytmy diagnostyczne, które mogą być wykorzystane do monitorowania turbin wiatrowych. Wybrane algorytmy zostały zastosowane do właściwego wykrywania i identyfikacji najważniejszych uszkodzeń. Kolejny rozdział przedstawia typowe uszkodzenia i algorytmy, które powinny być zastosowane do ich detekcji. Aby uniknąć wpływu zmian punktu pracy, konieczny jest dodatkowy preprocessing sygnałów. Oprócz stosunkowo prostych metod, stosowane są również metody bardziej zaawansowane. Przedstawiono przykład takiego algorytmu opartego na kurtozie widmowej.

Słowa kluczowe: drgania, monitorowanie, diagnostyka, turbina wiatrowa.

1. INTRODUCTION

The paper presents the selection of diagnostic algorithms for condition monitoring of wind turbines. In recent years wind energy has been the fastest growing branch of the power generation industry. Development of renewable energy sources is one of EU priorities. The goal for Poland is that in year 2020 15% of installed power generation capacity should come from green sources. It is estimated that every year new wind power turbines having total power output of 450 MW should be commissioned from now till 2020 [1]. The distribution of costs during the lifecycle of the unit for wind energy is significantly different from that of traditional fossil fired plants [2]. Initial investment costs are relatively higher but during operation the maintenance is the biggest cost. With proper maintenance policies wind turbines can achieve very high availability – even up to 98%. The basis of proper maintenance is continuous monitoring of transmission of a wind turbine.

Fig. 1 [3] presents typical layout of the wind turbine. The main rotor with three blades is supported by the main bearing and transmits the torque to the planetary gear [4]. The planetary gear

input is the plate, to which the main rotor is connected. The planetary gear has three planets, with their shafts attached to the plate. The planets roll over the stationary ring and transmit the torque to the sun. The sun shaft is the output of the planetary gear. Further, the sun drives the two-stage parallel gear. The parallel gear has three shafts: the slow shaft connected to the sun shaft, the intermediate shaft and the fast shaft, which drives the generator. The generator produces AC current of slightly varying frequency. This current is converted first into DC power and then into AC power of frequency equal to the grid frequency. Electric transformations are performed by the controller at the base of the tower. There exist other configurations of wind turbines, where e.g. only parallel gear is used. It has typically three stages, to be able to change the rotational speed from ca. 25 rpm on the main rotor to ca. 1500 rpm at the generator.

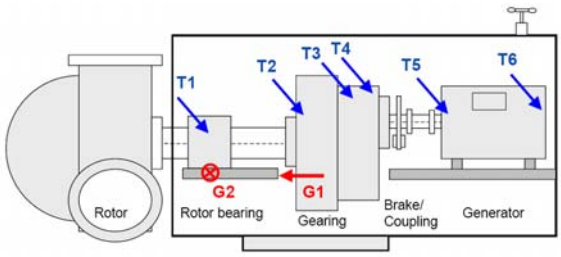

Fig. 1. Typical layout of the wind turbine. Gx and Tx present recommended locations of vibration sensors [3]

The device under monitoring is the power train, i.e. a main bearing, gears and a generator. Every of mentioned elements also contains several roller bearings. Gears and bearings are the most vulnerable parts of the structure and the monitoring should be first of all focused on them.

In order to enforce high standards of maintenance, since the year 2003 insurance companies in European markets introduced certification of condition monitoring systems for the wind power segment [3, 5]. The further part of the paper is based on such requirements, literature and experience of the author.

2. MEASUREMENTS

Since few years more and more wind turbines are equipped with condition monitoring systems. All such systems are based on measurement of vibration and key process variables. In general, number of sensors depends on the design of the wind turbine. There are several setups, but the most popular one includes
8 vibration sensors (see Fig. 1). Sensors G1 and G2 are used to monitor structural vibrations of the nacelle and the tower. Sensors T1 … T6 measure vibration of the drive train. On some installations it is possible to combine G1 with T1 and G2 with T2 and only 6 sensors are sufficient for the monitoring. One of those sensors (typically G2/T2) must monitor the transversal direction. T1/G1 measures axial vibration and all the others – vertical.

All used sensors are accelerometers, in most cases with ICP® output. Proper selection of frequency range and acquisition length are also very important. The combined gear ratio is in the range of approx. two decades, typically from 25 rpm on the main rotor to 1500 rpm on the generator. Thus, sensors close to the main bearing should have relatively low band (in the range of 100 Hz). Those ones close to the generator should monitor frequencies up to 10 kHz or even more. On the other hand even sensors on the main bearing should have high frequency band, because it is necessary for the detection of bearing faults. Another problem is the frequency resolution of the spectrum. The number of characteristic frequencies in a wind turbine is in the range of one hundred, and many of them and placed close to each other. If we want to be able to distinguish such frequencies, spectral resolution must be in the range of 0.1 Hz. For lower frequencies it is even 0.01 Hz or less. All those considerations lead to the measurement system having sampling frequency of 25 kHz and sampling signals for 10 or even 100 s. These are rather high requirements, especially when we consider storage of data in the database.

Additionally the monitoring should include a few key process parameters, like the output power, wind speed and the rotational speed of a generator. Rotational speed has special importance, as it is used for advanced processing of signals. In order to that, it must have a once-per-revolution form which is next transformed into the analogue value. The exact location of once-per-rev signal must be correlated with vibration signals. Additionally such signals like: ambient, bearing temperatures, oil and generator windings temperatures can be monitored. Also wind direction and activity of yaw drive should be taken into account. During operation of the yaw drive vibration should not be monitored due to excessive disturbances it has to the structure.

Quick changes of the operational point are an important feature of wind turbines. The example of such changes is presented on the Fig. 2. During 120 seconds the generator output power varies between 400 and 1400 kW. Such a changes have significant influence on vibration and can blur the changes caused by a malfunction.

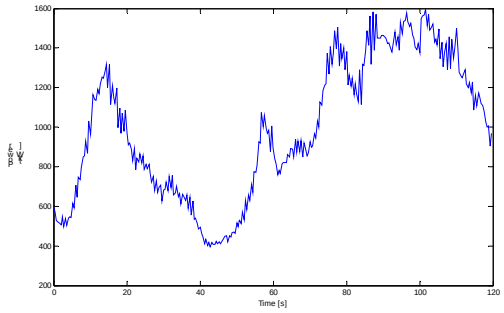

Fig. 2. Changes of generator output power during 120 seconds

Those problems can be overcome with proper signal preprocessing. In most cases, one can define states of the machine (e.g. depending on the power). Next, vibration signals are assigned the state they were acquired in and limits for this state are applied to the signal [6]. There are also other methods, like e.g. model based scaling, but due to complexity of this method it is not used in practice.

3. SELECTION OF DIAGNOSTIC ALGORITHMS

Condition monitoring based on analysis of vibration is a discipline developed for several decades. There are well established methods and a variety of new methods, alike. Broad survey of many methods can be found e.g. in [7] or in shorter form and very practice oriented form in [8]. The work [9] presented many basic and advanced methods with several application, but didn't cover wind turbines. Some guidelines towards condition monitoring of wind turbines can be found in [5], where the insurance company attempted to standardize methods for monitoring of wind turbines.

Out of many developed algorithms, some should be selected for the monitoring of a wind turbine. The process of selection should be based on two key elements:

- key components;
- most common malfunctions.

As listed in the fist section, the supervised components are:

- generator (shaft, bearings);
- gearbox (shafts, teeth, bearings);
- main rotor (shaft, blade pass, main bearing);
- structure (tower, nacelle).

There are three types of vibrations which should be investigated. Most common ones are excitation frequencies, generated by rotors and gears. Another type of excitation frequencies are impulses generated by bearing faults. The last group are resonance frequencies generated by tower, main rotor blades and machinery casings. Methods depend on those types of vibrations, so in total a 3D matrix of components (generator, gear, …), parts (shaft, teeth, bearing, blade,…) and algorithms should be created. In other words, an algorithm should be selected for every part of a component.

Special group of algorithms are **general signal estimates** which show overall technical state of the machinery. Such estimates are so called broadband parameters: rms, pp, crest and kurtosis. They serve as a general warning and are important when develops a malfunction, which is not covered by any other algorithm or when such other algorithms are not configured properly. This algorithms should be used as a fault detection tool. Since a very important part in the wind turbine are roller bearings, it is necessary to analyze the vibration signal envelopes, which show malfunctions earlier than the original signal [10]. The group of general signal estimates should also include broadband parameters from the **envelope signal**. It is very important that envelopes are obtained after high-pass filtering. Choice of the filter cut off frequency is very important parameter of the algorithm and must be adjusted to the monitored machine. It should be higher than frequencies excited by shafts and meshings. For most types of wind turbines this is in the range of a few kHz.

Second group of algorithms are **frequency selective estimates** from the vibration signal spectra. All relevant characteristic frequencies should be monitored. Most important ones are:

- main rotor (1X, blade pass);
- shafts (1X, 2X);
- gears (1X, 2X, meshing with sidebands);
- roller bearings (inner and outer rings, rolling elements, overroll, cage);
- structural (resonances).

Presented characteristic frequencies should be extracted from appropriate spectra. In general rotor, shafts and gear frequencies should be extracted from amplitude spectra, whereas roller bearings – from envelope spectra. There are also situations, where envelope spectra should be also investigated for the first group of components. There are cases when monitoring of the envelope spectrum can lead to detection of a tooth fault. One has to remember that similarly to general signal estimates, algorithm to obtain envelope spectra should be configured to cut off unwanted frequencies and carry impulses induced by bearing faults.

Another important problem is variability of the rotational speed. Frequency selective components depend linearly on the rotational speed, since they are defined as multiplies of the reference shaft rotational speed (this reference shaft is typically the generator shaft). Large part of wind turbines have variable speed. In such cases spectra should be monitored in the order domain, not the frequency domain. To obtain the **order spectrum**, the acquired vibration signal should be resampled so that the output signal has a constant number of samples per revolution, not a constant number of samples per a unit of time. Choice of resampling parameters

should be also done with care. Detailed discussion of resampling parameters can be found in [11].

General and frequency selective parameters form basic set of monitored vibration signal estimates. All those estimates are scalar values and can be easily checked against defined warning and alarm levels. After generation of such a warning, complete signal spectra should be investigated by a vibration expert.

4. CASE STUDY

Presented algorithms were implemented in an on-line vibration monitoring system on a 1.5 MW wind turbine.

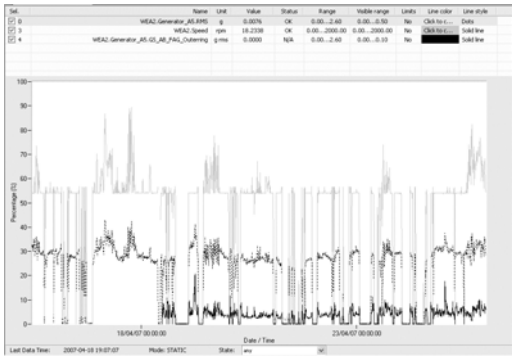

Fig. 3. Trend of BPFO on the wind turbine

Frequency selective parameter, monitoring the outer ring ball pass frequency (BPFO) on the generator bearing, showed increased value (see solid black line on the bottom of Fig. 3). The figure also presents rotational speed (grey, top) and rms (dotted black line, middle). The rms did not show any significant increase and seems to follow the rotational speed. The hypothesis of faulty outer ring was confirmed by investigation of the order spectrum of the signal envelope (see Fig. 4).

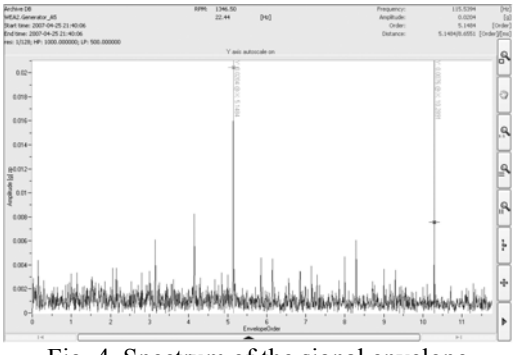

Fig. 4. Spectrum of the signal envelope

The characteristic frequency of the outerring is 5.14X. The cursors on the plot are set on 5.14X and its second harmonics (10.28X). Those components are dominating the spectrum of the envelope. Additionally, the original spectrum was also investigated (see Fig. 5).

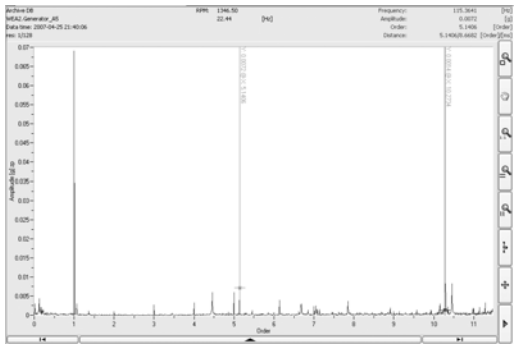

Fig. 5. Spectrum of the signal

The first vertical line is the fundamental frequency (1X). The first two harmonics of the ORBP (middle and right vertical lines) can be clearly seen, but are much smaller than on the envelope spectrum.

5. CONCLUSIONS

The paper presented set of diagnostic algorithms, which can be used for monitoring of the wind turbines. Presented case study shows that generator bearing fault could be detected. Care must be taken when data are analyzed, especially due to excessive changes of the operating point of the machine, which causes vibration changes much higher than those caused by a malfunction. Some more algorithms can be used (e.g. cepstrum), but were not discussed. They should be used when necessary at later stages of diagnostic investigations.

Apart from relatively simple methods discussed in the paper, there is a number of more advanced ones. They require more complex data acquisition and processing, but may deliver better results. One of such algorithms can be application of spectral kurtosis [12] to detect tooth fillet crack on the ring of the planetary gear. Such a crack can not be detected by standard methods and was successfully detected by application of SK for preprocessing of the vibration signal [13].

REFERENCES

[1] Polskie Stowarzyszenie Energetyki Wiatrowej. www.psew.pl
[2] European Wind Energy Association: *Wind Energy. The facts. An analysis of wind energy in the EU-25*, EWEA, 2005.
[3] Gellermann T.: *Requirements for Condition Monitoring Systems for Wind Turbines*, AZT Expertentage, 10-11.11.2003, Allianz 2003.
[4] Gasch R., Twele J., *Wind Power Plants – Fundamentals, Design, Construction and Operation*, James & James, 2002.
[5] Germanischer Lloyd: *Richtlinien für die Zertifizierung von Condition Monitoring Systemen für Windenergieanlagen*, Vorschriften und Richtlinien, Selbstverlag Germanischer Lloyd 2007.

[6] Barszcz T.: *Koncepcja monitorowania i diagnostyki maszyn wirujących małej i średniej mocy*, Diagnostyka vol. 35, Warszawa 2005.
[7] Cempel Cz.: *Diagnostyka wibroakustyczna maszyn*, PWN, Warszawa 1989.
[8] Klein U.: *Schwingungsdiagnostische Beurteilung von Maschinen und Anlagen*, Duesseldorf, Stahleisen Verlag 2003.
[9] Żółtowski B., Cempel Cz. (eds.): *Inżynieria diagnostyki maszyn*, ITE, Warszawa 2004.
[10] Ho D., Randall R. B.: *Optimisation of bearing diagnostics techniques using simulated and actual bearing fault signals*, Mechanical Systems and Signal Processing, vol. 14, 2000/5.
[11] Mc Fadden P. D.: *Interpolation techniques for time domain averaging of gear vibration*, MSSP vol. 3, 1989/1.
[12] Antoni J., Randall R. B.: *The spectral kurtosis: application to the vibratory surveillance and diagnostics of rotating machines*, MSSP vol. 20 (2006).
[13] Barszcz T., Randall R. B.: *Application of spectral kurtosis for detection of a tooth crack in the planetary gear of a wind turbine*, MSSP vol. 22 (2008, accepted).

Tomasz BARSZCZ, Ph D. Employed at Dept. of Robotics and Mechatronics, on AGH Univ. of Science and Technology, Cracow, Poland. His main field of research is design and applications of systems for machinery monitoring and diagnostics. He is author of two books, numerous papers and applications in this field.

VIBRATION BASED DIAGNOSIS OF INTERNAL COMBUSTION ENGINE VALVE FAULTS

Bogusław ŁAZARZ, Henryk MADEJ, Grzegorz PERUŃ, Zbigniew STANIK

Faculty of Transport, Silesian University of Technology
40-019 Katowice, ul. Krasińskiego 8, fax (+48) 32 603 41 08, email: boguslaw.lazarz@polsl.pl

Summary

Internal combustion (IC) engine is classical rotating machine that must be operated under various conditions. Sound and vibration signal of IC engine often give much dynamic information of mechanical system condition.

Vibration and angular velocity of crankshaft signal on Ford Fiesta engine 1,3 dm^3 were used for the tests. The tests were carried out in Bosch FLA 203 roller bench. The sampling frequency was 25 kHz and during data acquisition process, the rotating speed of the engine was kept at a constant rpm and at run up condition.

The energy state of the pistons and the connecting rods is determined by the mean angular speed and the angular positions of the crankshaft. Changes in the pressure in cylinder caused by compression faults or misfire will affect directly the instantaneous angular speed of the crankshaft and vibration energy. In this paper engine exhaust valve fault and its influence over the instantaneous angular speed waveform and vibration of engine head is presented.

Engine position sensor is one of part of the IC engine control system, thus an instantaneous angular speed based fault detection system does not require additional sensors.

It can be seen from example of the present paper, when the valve worked abnormally, the vibration energy is moved forward towards the high frequency region (larger than 8 kHz).

Keywords: IC engine, fault, diagnostics, valve.

DIAGNOZOWANIE USZKODZEŃ ZAWORÓW SILNIKA SPALINOWEGO NA PODSTAWIE ANALIZY DRGAŃ

Streszczenie

Silniki spalinowe są klasycznymi maszynami wirującymi pracującymi w zmiennych warunkach obciążenia i prędkości obrotowych. Drgania i hałas silnika spalinowego są nośnikiem informacji o stanie jego podzespołów mechanicznych.

Podczas prezentowanych badań, których obiektem był silnik samochodu osobowego Ford Fiesta o pojemności 1,3 dm^3, rejestrowano przyspieszenia drgań głowicy oraz prędkość obrotową wału korbowego. Badania przeprowadzono na hamowni podwoziowej FLA203 firmy Bosch. Częstotliwość próbkowania sygnałów drgań i prędkości obrotowej wynosiła 25 kHz. Badania przeprowadzono w warunkach ustalonej prędkości obrotowej oraz podczas rozbiegu.

Energia sygnału drganiowego generowanego w układzie tłokowo-korbowym zależy od średniej prędkości obrotowej oraz położenia kątowego wału korbowego. Uszkodzenia mechaniczne mające wpływ na ciśnienie sprężania oraz zjawisko wypadania zapłonów wywołują chwilowe zmiany prędkości obrotowej wału korbowego i chwilowej gęstości widmowej energii sygnału drgań. W artykule przedstawiono wyniki badań mających na celu określenie wpływu symulowanego lokalnego uszkodzenia zaworu wylotowego na zmianę chwilowej prędkości obrotowej i charakterystyk widmowych drgań głowicy.

Do pomiaru chwilowej prędkości obrotowej wału korbowego wykorzystano czujnik indukcyjny, stanowiący osprzęt silnika. Z przeprowadzonych badań wynika, że w przypadku pracy silnika z uszkodzonym zaworem wylotowym następuje widoczne przesunięcie energii drgań w kierunku wyższych częstotliwości (powyżej 8 kHz).

Słowa kluczowe: silniki spalinowe, uszkodzenia zaworów, diagnostyka drganiowa.

1. INTRODUCTION

The timing gear system is one of the principal, and precise in their operation, components of the combustion engine. Operational and breakdown wear of such components as the camshaft, pushers, valve springs and levers, as well as valves themselves, has a significant influence on the work of the engine, its performance and reliability. The timing gear system component subject to the highest load, both mechanical and thermal, is the exhaust valve. The valve head temperature reaches locally the value of 700÷800°C, and in engines subject to the highest thermal load, it reaches 900°C. This happens as a result of the action of combustion gases, the temperature of which amounts to 900÷1000°C, and their speed reaches a value of 600 m/s in the initial phase of opening the valve. The high temperature of the valve head results also from the lack of possibility of its cooling, which only takes place at the moment of contacting the valve-seat. The higher the rotational speed, the less heat will be taken by the head which has a direct contact with the coolant. The seat face of the valve and of the valve head wears out mostly as a result of exposure to streams of combustion gases. The wear of the exhaust valve is a consequence of joint action of repeated strokes during the valve closing, erosive influence of combustion gases with products of incomplete combustion and corrosive effect of flames [4].

A particularly important issue in case of valves is to maintain, for as long as possible, their satisfactory tightness during periods of closure, for insufficient tightness of inlet valves causes a reduction of engine power and an increase of specific fuel consumption. Leakage of exhaust valves affects the engine power to a lesser degree, while the main problem here is a rapid increase of their wear intensity as a result of combustion gas blow-by, which very often leads to a complete damage of valve heads, caused by their burn-out.

Damage of this type results in a reduction of effectiveness of action and durability of the catalyst, or its complete destruction. The symptoms of valve burn-out in its first stage can be effectively camouflaged by adaptive systems of control of the combustion engine operation [1, 3]. The modern control systems allow taking into account the differences which result from the scatter of parameters connected with tolerances in workmanship of a given engine, and with changes of characteristics caused by wear, which considerably hinders diagnosing of the engine. Detection of valve faults is also quite difficult in case of 6- and 8-cylinder engines. For this reason, it is justified to search for effective methods of processing vibroacoustic signals, which will allow detecting those faults in valves which cause leakage of a combustion chamber already in their initial stage.

2. RESEARCH OBJECT AND TESTING PROCEDURE

The object of tests was a 1.3 dm^3 engine of a Ford Fiesta personal car. During tests, carried out on a Bosch FLA203 chassis test bench, acceleration of the head vibration and rotational speed of crankshaft were recorded. The frequency of sampling of vibration signals and rotational speed was 25 kHz. The tests were performed in conditions of a steady rotational speed and during starting. An inductive sensor, being part of engine tooling, was used to measure the instantaneous rotational speed of the crankshaft.

The main purpose of the study was to determine the effect of the simulated local fatigue crack of an exhaust valve of the first cylinder on the changing instantaneous rotational speed and spectrum characteristics of head vibration.

In Figure 1, an engine head with a damaged exhaust valve is presented.

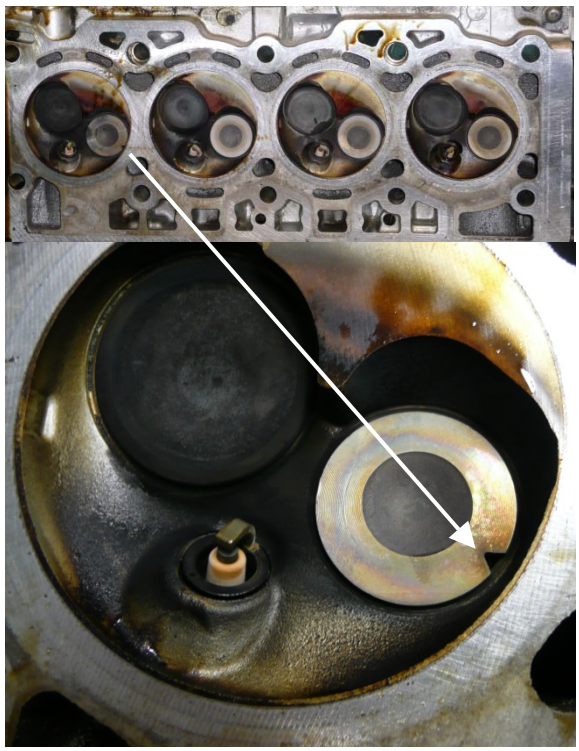

Fig. 1. Simulated damage of exhaust valve

Measurement of compression pressure has shown that the simulated damage caused its decrease by ca. 20%. The tests made on a chassis test bench have shown an insignificant power reduction caused by the introduced damage of the valve (Fig. 2).

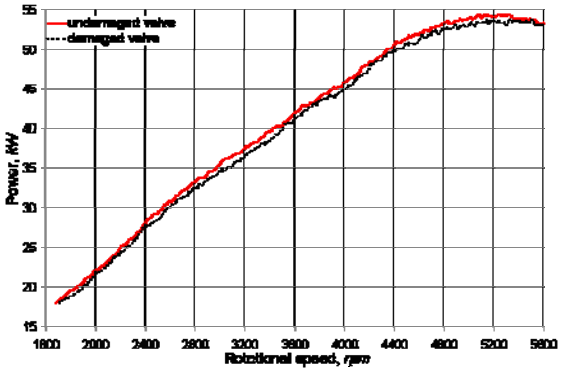

Fig. 2. Engine power as a function of rotational speed for two states of the exhaust valve

3. RESEARCH RESULTS

It appears from the previous research that mechanical damage which affects compression pressure induces instantaneous changes of rotational speed of the crankshaft and of instantaneous spectral concentration of the vibration signal energy [2, 5].

The signal obtained from an inductive sensor, the latter being usually placed over the toothed rim of a wheel rigidly connected with a crankshaft, is one of basic diagnostic signals used by the EOBD system during detection of misfiring. This signal enables determining the rotational speed and instantaneous changes in angular velocity and angular position of the crankshaft.

To identify instantaneous changes of rotational speed as a function of the crankshaft rotation angle, the signal from the inductive sensor, sampled at a frequency of 25 kHz, was appropriately processed by means of a procedure specially developed to this end. Damage of the valve caused increased non-uniformity of rotational speed, clearly visible during both, idle running (Fig. 3) and under load at different rotational speeds (Fig. 4).

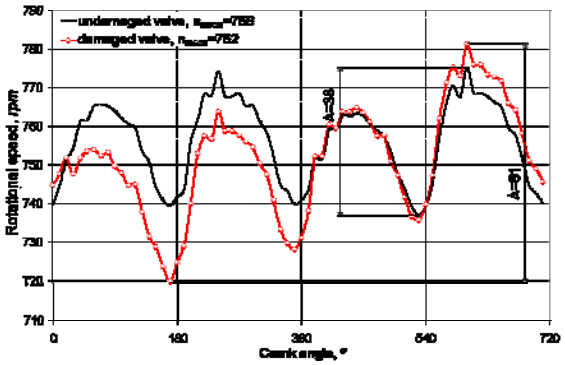

Fig. 3. Course of instantaneous rotational speed (idle run)

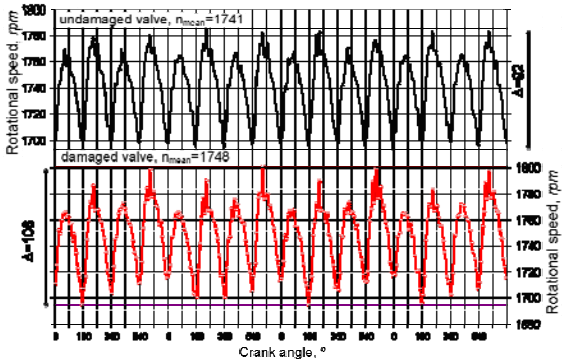

Fig. 4. Course of instantaneous rotational speed for four working cycles (13.2 kW – good valve, 11.6 kW – damaged valve, full load)

Vibration acceleration of the tested engine head in a vertical direction was recorded by means of a piezoelectric sensor. Simultaneous recording of the head acceleration and the crankshaft position signal enabled an analysis of further working cycles of the engine. For the purpose of separating the predominating low-frequency components, preliminary high-pass filtration of the signal was carried out, based on wavelet transform. In this way, a residual signal containing high-frequency components, induced, inter alia by pulse excitation, was obtained. Figure 5 presents an example of a signal of head vibration acceleration during a full working cycle before and after filtration.

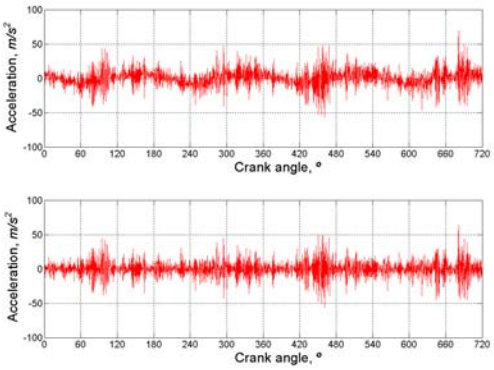

Fig. 5. Signal of head vibration accelerations before and after filtering with use of Daubechies 4 wavelet

An initial spectrum analysis of the head vibration acceleration has shown that in the case of an engine working with a damaged exhaust valve, a visible shift of vibration energy took place in the direction of higher frequencies (above 8 kHz). For the purpose of identifying resonance frequencies of the investigated engine, tests were conducted under conditions of unsteady work. Transitory or unsteady conditions are the conditions of start-up or coasting. Tests in such conditions enable observation of the system's response to various, often non-stationary, forcing. In the process of determining resonance frequencies of the engine during start-up or coasting,

there are forcing functions which affect its structure. In a modal analysis (classical or experimental), modal parameters of the identified object are determined on the basis of frequency characteristics obtained in the process of controlled forcing of vibration and measurement of response. In comparison to modal analysis, in this experiment, resonance frequencies can be determined in a much wider range.

Figure 6 shows the courses of changes of rotational speeds with an indicated interval used for determining the start-up characteristics.

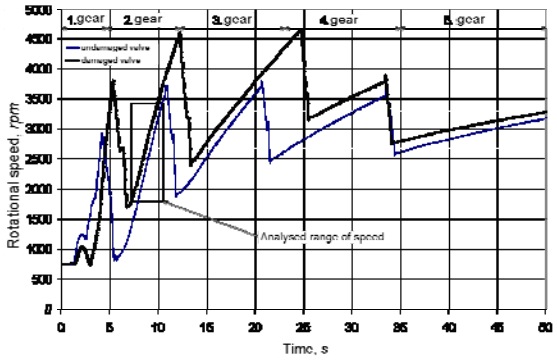

Fig. 6. Course of rotational speed of the engine during coasting performed on a chassis test bench

Spectral concentrations of power, determined based on residual signals of the head vibration accelerations for an engine working with a fully operational valve and with a damaged valve, as a function of rotational speed, reflect the changes of signal energy induced by valve damage (Fig. 7 and 8).

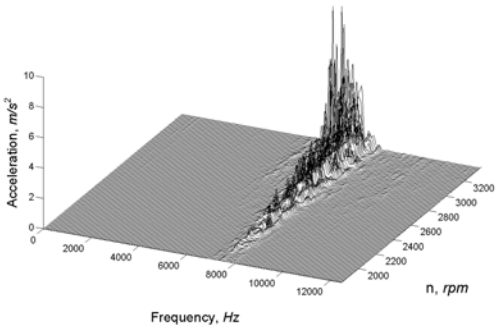

Fig. 7. Time and frequency distribution of the head vibration acceleration; undamaged valve

As can be seen in the above figures, the damage of the valve which caused leakage of the combustion chamber, stimulated the head to vibration in the range of higher frequencies. In order to accurately identify those frequencies, average values were determined of instantaneous amplitudes in the investigated range of changes in rotational speeds (Fig. 9).

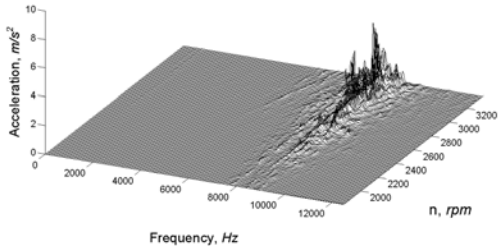

Fig. 8. Time and frequency distribution of the head vibration acceleration; damaged valve

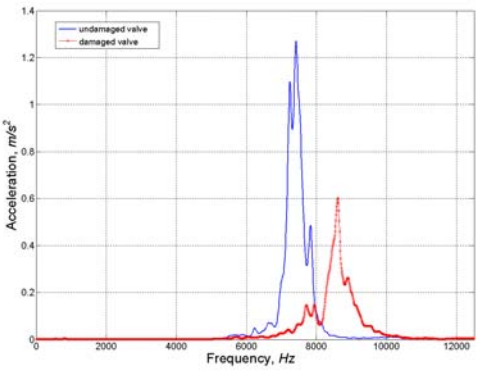

Fig. 9. Average values of instantaneous amplitudes of the head vibration acceleration

In the case of the undamaged valve, the highest energy of the vibration acceleration signal is contained in the range of 6.5 ÷ 8 kHz. Damage to the valve causes a shift of the energy maximum to a range of above 8 kHz.

Taking advantage of the phenomenon described here, dimensionless coefficients of valve damage were proposed: S_1, S_2 and S_3, described by the dependencies:

$$S_1 = \frac{\sum_{i=A}^{B} p_i}{\sum_{i=1}^{N} p_i} \tag{1}$$

$$S_2 = \frac{\sum_{i=B}^{N} p_i}{\sum_{i=1}^{N} p_i} \tag{2}$$

$$S_3 = \frac{S_2}{S_1} \tag{3}$$

where:

A and B mean the number of the first and last component, p_i, of spectrum in the range of 6.5 ÷ 8 kHz, and N corresponds to the upper limit of the spectral analysis made (12.5 kHz).

Fig. 10 presents the vibration acceleration spectra for the head of an engine working at different rotational speeds and under different loads.

a)

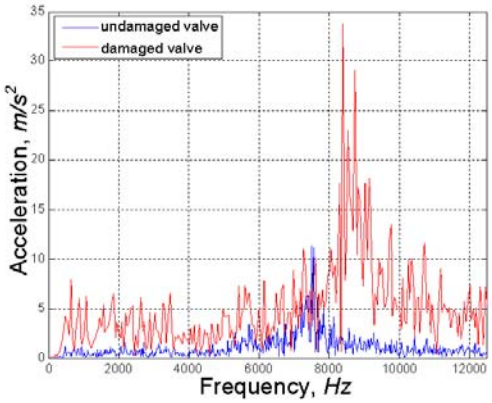

b)

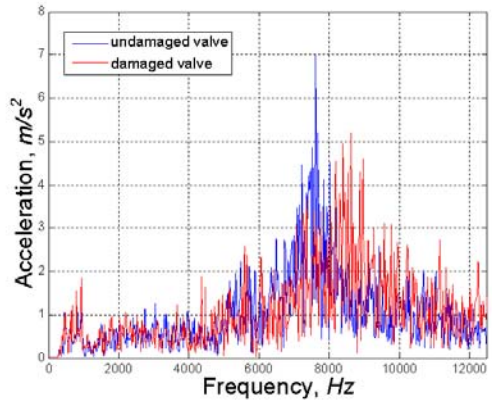

c)

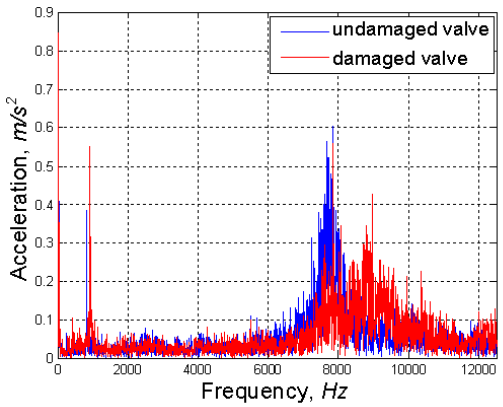

Fig. 10. Spectra of head vibration accelerations a) n=2945 r.p.m., N_{und}=25,7 kW, N_{dam}=25,9 kW, b) n=2905 r.p.m. N_{und}=23,7 kW, N_{dam}=21,8 kW, c) n=754 r.p.m., idle run

The effect of damage and working conditions on the proposed measures, S_1, S_2 and S_3, is presented in Figs 11 ÷ 13.

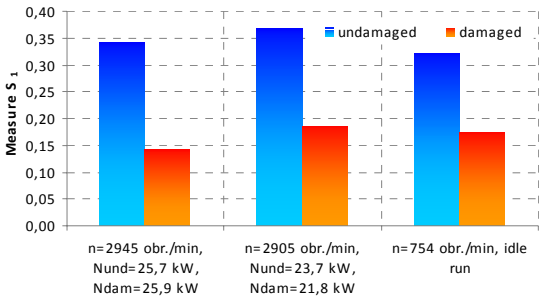

Fig. 11. Values of measure S_1 for an engine working at different rotational speeds and loads

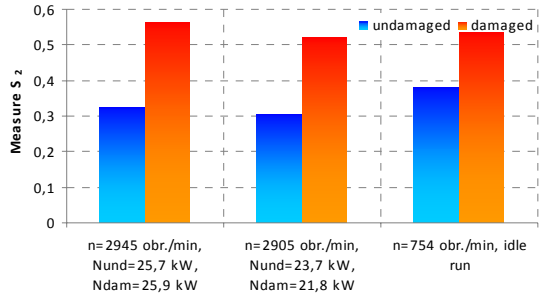

Fig. 12. Values of measure S_2 for an engine working at different rotational speeds and loads

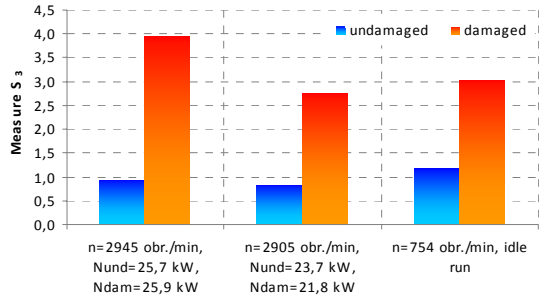

Fig. 13. Values of measure S_3 for an engine working at different rotational speeds and loads

4. CONCLUSIONS

Due to the phenomenon of vibration energy relocation towards higher frequencies during the work of an engine with a damaged exhaust valve, changes in values of the proposed measures detect well a local damage to the exhaust valve, irrespective of the engine operation conditions.

The measure S_3, which takes account of changes in vibration energy in the bands of 6.5 ÷ 8 kHz and 8 ÷ 12.5 kHz simultaneously, has turned out to be particularly sensitive to faults.

The values of measure S_3 for an engine with undamaged valves were contained in the range of 0.83 ÷ 1.35, while in the case with a damaged exhaust valve, they were contained in the range of 2.34 ÷ 3.95.

The proposed measure can be useful in diagnosing faults of valves.

REFERENCES

[1] Dąbrowski Z., Madej H.: *Masking mechanical damages in the modern control systems of combustion engines*. Journal of KONES, Vol. 13, No 3/2006.
[2] Geveci M.: *An investigation of crankshaft oscillations for cylinder health diagnostics*. Mechanical Systems and Signal Processing 19 (2005) 1107–1134.
[3] Iserman R.: *Diagnosis methods for electronic controlled vehicles*, Vehicle System Dynamics, Vol. 36, No. 2-3.
[4] Janecki J., Gołąbek S.: *Zużycie części i zespołów pojazdów samochodowych*. Warszawa, WKiŁ 1984.
[5] Yang W. X.: *Establishment of the mathematical model for diagnosing the engine valve faults by genetic programming*. Journal of Sound and Vibration 293 (2006) 213–226.

Bogusław ŁAZARZ Ph. D., D.Sc. Eng. professor of The Silesian University of Technology. Scientific interest: modelling of dynamic processes, diagnostics of tooth gear, machine design and vibroacoustic signal processing. Member of Machines Construction Committee and Polish Society of Technical Diagnostics.

Henryk MADEJ, Ph. D., D. Sc. Eng. work as a professor in the Department of Automotive Vehicle Construction Silesian University of Technology in Katowice. He deals with IC engines and powertrains diagnostics with the application of vibroacustical signal analysis, also with minimization of machine vibroactivity. Member of Polish Society of Technical Diagnostics.

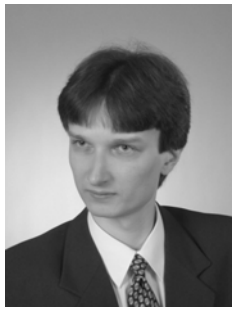

Grzegorz PERUŃ is Ph. D. student in the Department of Automotive Vehicle Construction Silesian University of Technology in Katowice.
Scientific interest: modelling of power transmission systems, machine design and vibroacoustic signal processing.

Zbigniew STANIK is Ph. D. in the Department of Automotive Vehicle Service Silesian University of Technology in Katowice.
His interests are connected with analysis of exploitation and emergency attrition of frictional coupe elements. His doctoral thesis about excessive wear of camshaft eams and followers was published in year 2002.

The results presented in the paper were obtained with the support of the Polish Scientific Committee.

DETERMINATION OF INFLUENCE OF THERMO-CYCLES ON HYDROGEN CRACKING OF STEEL

Valentyn SKALSKY, Denys RUDAVSKYY, Yurij MATVIJIV

H. V. Karpenko Physico-Mechanical Institute of National Academy of Sciences of Ukraine, Lviv, Naukova Str5., Lviv, 79601,Ukraine, skal@ipm.lviv.ua

Summary

Influence of thermo-cycles "heating-cooling" on the hydrogen induced cracking of structural steels, which are widely used in the heat-power equipment is investigated in this paper. An acoustic emission method of diagnostics of specimens made of exploited and non-exploited material of steam pipelines is described. Effective diagrams of dependence of number of events on heat cycle number for the all groups of specimens are plotted.

Keywords: heat cycling, hydrogen concentration, acoustic emission.

1. INTRODUCTION

For express-evaluation of material liability to hydrogen degradation, it is heat cycled in hydrogen of pressure higher then the working one, from working temperature that is characteristic for concrete technological process to the room temperature [1]. Then the nucleation and growth of crack type defects is conducted by radiation of elastic waves known as acoustic emission (AE). Its parameters allow estimating an intensity of initiation and equivalent areas of mentioned defects during heat cycling. The results obtained in this experimental research are described below.

It is generally known that the amount of hydrogen, which can dissolve in a metal, increases with temperature. This phenomenon and high diffusive mobility of hydrogen atoms in α-Fe at high temperature could be the ground of the laboratory express-method of accelerated high temperature hydrogen steel degradation [1]. The abrupt temperature decrease at the cooling stage considerably retards diffusive processes (diffusion coefficient of hydrogen in α-Fe decreases from $1.8 \cdot 10^{-4}$ to $4.4 \cdot 10^{-5}$ sm^2/s with decrease of temperature from 540 to 100°C [2-4]) and is accompanied by localization of dissolved hydrogen in metal at lower temperature, which concentration is over-equilibrium (from 0.1 to 1.0 $sm^3/100$ g of metal, according to [5]). In consequence of cooling, approximately the same concentration of hydrogen as an equilibrium one for temperature of 540 °C is observed inside a specimen. Obviously, that this hydrogenation assists in active migration of hydrogen to the nearest free surfaces, regardless of their location (internal or external). Thus residual hydrogen either goes out from a metal (from the subsurface layers of specimen) or gathers in traps at structural defects, grain or phase boundaries, which from the view point of energy expenditures are the advantageous places of its location (inside the specimen). As hydrogen fills any defects, its migration assists in moving of carbon atoms and alloying elements. It occurs because of degrees of energy barrier (affected by hydrogen) to moving of atoms of any element [6]. It is clear that such redistribution of elements accelerates the redistribution of carbides and formation of net of the fine-dispersed special or alloyed carbides in places with high concentration of alloying elements.

During the cooling, the redundant hydrogen goes to the traps at grain, phase boundaries or structural defects. Migration of hydrogen creates a track of high-gradient tensile field, assisting in the redistribution of carbon and alloying elements in a metal and, therefore, intensifies microstructure transformation of steel. As hydrogen localizes at these defects, it creates additional tension at interphases. At the frequent reiteration of this cycle pre-conditions for the formation of microscopic damages as micro-voids and micro-cracks are created. After each heat cycle the pressure of hydrogen grows, deformation of linkages between micro-voids and micro-cracks and their creep growth as result of the combined action of high temperature and loading becomes possible. These processes are conducted by the radiation of elastic AE waves [7].

In addition, such heat cycling of specimens in hydrogen creates pre-conditions for cyclic deformation of metal near the defects, which accumulate hydrogen. Amplitude of deformation is determined by many factors: distribution of defects by their sizes and amount, temperature range of heat cycling, pressure of hydrogen in a chamber, number of heat cycles etc.

Thus, the abrupt cooling of hydrogenated metal, at first, causes an increase of internal stresses in metal as a result of over-equilibrium concentration of hydrogen in metal, secondly, assists in the initiation of micro voids filled by hydrogen, thirdly, intensifies diffusion, in particular of carbon, assists in transformation of microstructure. All these processes assist in intensive crack formation in

steels and can be effectively detected by AE signals.

2. METHOD OF AE TESTING

Experiments were carried out for the four groups of smooth beam specimens of 12H1MF steel of sizes 12×18×180 mm^3. Chemical composition (%) of steel is: S - 0,1; Cr - 1,1; Mo - 0,26; V - 0,17; Mn - 0,54; Si - 0,26; S - 0,019; P - 0,015. The specimens of first and third groups were made of basic (not operated) material and second and fourth groups - of material, which operated in steam pipes of power station about 150 thousand hours (540 Ms). Specimens of first and second groups were heat cycled in air, third and fourth - in the environment of gaseous hydrogen. "Heating - holding – cooling" cycles are shown in Fig. 1 for the specimens of all four groups (pressure of hydrogen environment for the 3rd and 4th groups of specimens is shown in the Table 1). Heating of specimens up to the temperature of 813 °C and its maintenance was carried out by an alternating electric current. Its value is shown in the Table 1.

Table 1. Characteristics of specimen heating modes

Group of specimen	Heating current, кА	Supplied energy, MJ	Pressure in autoclave, MPa
1	3,6	1,017	atmospheric
2	2,88	0,587	atmospheric
3	3,84	1,615	0,14
4	2,58	0,334	0,4

AE signals were recorded using waveguide. The specimen and one end of the waveguide were placed in the autoclave. The other end of waveguide was placed outside of autoclave through the special airtight knot. On this end, the primary piezoelectric AE transducer (AET) was located. Calculation of geometry of waveguide and matching of its response characteristic with the similar characteristics of AET was made using the method described in [8].

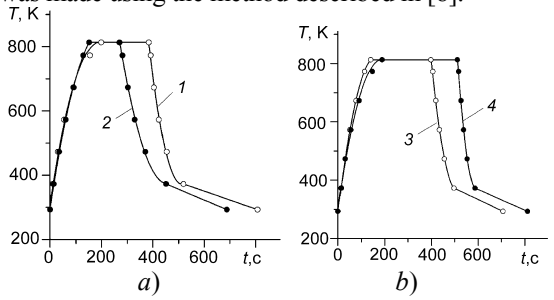

Fig. 1. Time variations of temperature in cycles of heating for four groups of specimens (the numeration of curves corresponds to the numbers of groups of specimens)

2. RESULTS OF AE RESEARCHES

In the temperature-cycle testing of the first group of specimens AE was emitted, mainly, during the specimen cooling. A tendency of its activity decaying with growth of temperature-cycles number was observed. The results of tests are shown in Fig. 2.

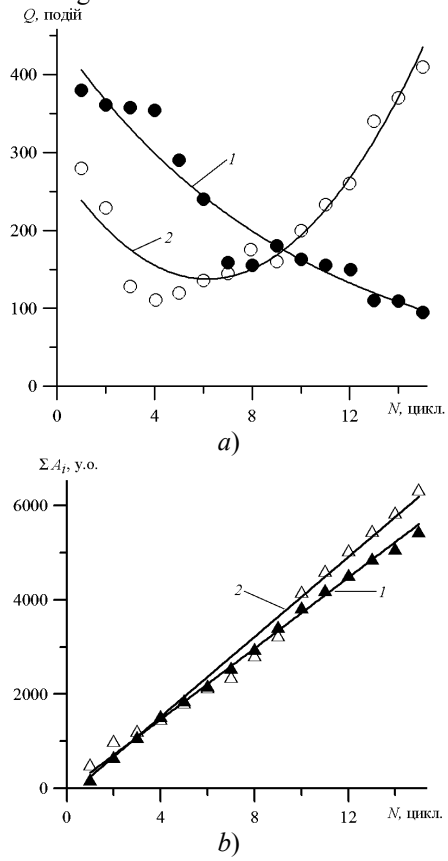

Fig. 2. Dependence of the number of events Q (*a*) and the sum of amplitudes ΣA_i of AE signals (*b*) on the number of heat cycles N for the specimens of first and second groups

Fig. 2a shows that for 1st and 2nd groups of the specimens the number of events Q, which was recorded during 15 cycles in air (specimens of steel 12H1MFA of base material), decreases with the number of cycles increase, starting from the first cycles. This experimentally obtained dependence is well approximated by exponential function of the form $Q = a \cdot \exp(bN+c)$ with the correlation factor $r = 0{,}912$. The coefficients of approximation are resulted in Table 2a. The second group of specimens made of the operated steel has shown complicated character of AE events number variation depending on the number of heat cycles in air. For the first cycles a tendency to their decreasing was observed, then the AE activity increased with growth of the number of heat cycles (curve 2 in the Fig. 2a). Experimental points for this group of specimens are approximated by expression $Q = aN^2+bN+c$ (the parameters of approximation are given in Table 2*a*).

In relation to the sum of amplitudes, which contains an information on bulk damaging of material [9], we notice that for the specimens of the specified 2 groups it varies linearly (see Table 2b and Fig. 2b) with the number of heat cycles. The

absolute values of this index for specimens made of the operated material are higher, starting from 10th heat cycle.

Table 2*a*. Parameters of approximation of experimental results

Group of specimens	Parameter of approximation			
	a	*b*	*c*	*r*
1	210,863	-0,102	0,758	0,912
2	3,808	-46,941	282,235	0,903
1	376,307	-43,39	--	0,997
2	423,907	-178,89	--	0,983
3	0,31	1,344	2,794	0,901
4	23,607	76,06	-60,25	0,99

Table 2*b*. Dependences of approximation of experimental results

Group of specimens	Type of dependence	Note
1	$Q = a\exp(bN+c)$	Fig. 4,a
2	$Q = aN^2+bN+c$	
1	$\Sigma A_i = aN+b$	Fig. 4,б
2	$\Sigma A_i = aN+b$	
3	$\Sigma A_i = aN^2+bN+c$	Fig.10,б
4	$\Sigma A_i = aN^2+bN+c$	

Similarly to the previous, specimens of third and fourth groups were tested in the environment of gaseous hydrogen. Time character of change in temperature of cycles heating - holding - cooling is shown in Fig. 1b. Having this data, firstly, we calculated the number of cycles to complete saturation of specimens of third and fourth groups by numerical methods for parameters of hydrogen environment indicated in Table 1. A mathematical model of temperature condition changing for each cycles was developed for this purpose. In this model the time interval of heating is described by the function $T = at^2+bt+c$, the interval of specimen holding for temperature 813 K was approximated by constant $T = B = const$ (where B = 256,6 s for the specimens of third group and B = 323,3 s for the specimens of fourth group). For the time interval of cooling two intervals of approximation were defined: for the temperature range 813...373 K the dependence $T = at^2+bt+c$ was used and for the temperature range 373...293 K $T = at+c$.

Using the data collected in Tables 1 and 3 and calculation method developed in paper [10], we determined the number of cycles for attaining equilibrium saturation of specimens of third and fourth groups with hydrogen. They were, respectively, 7 and 6 heat cycles [10]. Basing on results of these computations, we conducted heat cycling of specimens of these groups in gaseous hydrogen. The results of these tests are shown in Fig. 3, in Tables 1 and 2.

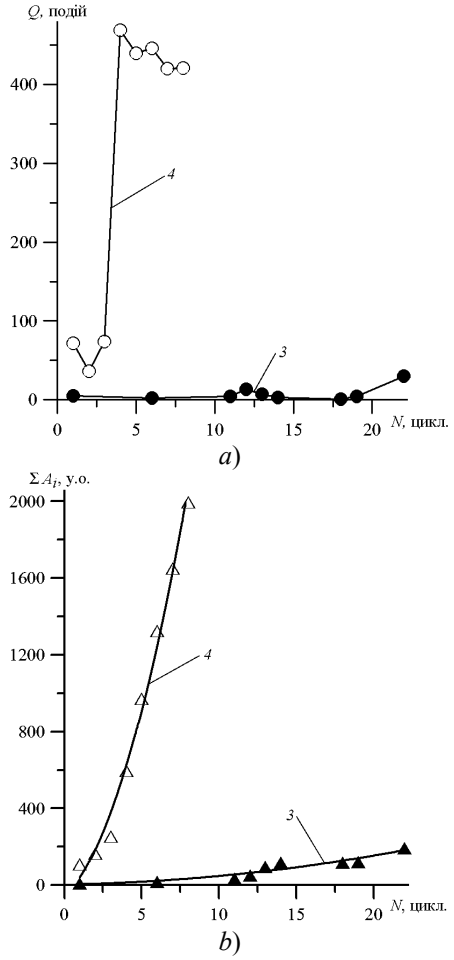

Fig. 3. Dependence of number of events Q (a) and sum of amplitudes $\sum A_i$ of the AE signals (b) on the number of cycles N of the heating and cooling of specimens of third and fourth groups

As it is shown in Fig. 3 AE for the specimens of third group sporadically observed only at the 2nd and 6th cycles with negligible indexes: 5 and 2 AE event, respectively, with approximately the same sum of amplitudes of 9 a. u. Starting from 11th cycle AE increased slightly: the activity increased to 7...13 events (for 13th and 12th cycles, respectively). The sum of amplitudes increased to 16...44 a. u. for these cycles. Later with growth of number of heat cycles, the radiating of AE was interrupted, which finished mainly, at the 20th cycle and monotonous growth of mentioned indexes of AE activity was observed. Thus, AE activity during heat cycling of initial material in the hydrogen environment is insignificant that confirms insignificant damaging of material.

The activity of AE in the tests of specimens of 4th group in the hydrogen environment is in orders higher. At the first 3 cycles it slightly decreases (by analogy with heat cycling of this material in air, see Fig. 2*a*; curve 2), and later abruptly increases showing a tendency to smooth decaying with the increase of cycles number. For 5th cycle the dependence between the variation of number of events and the number of cycles is approximated by

straight line: $Q = aN + c$, where a = -11,6; c = 508,8 and the coefficient of correlation is r = 0,823. The sum of amplitudes depends on the number of heat cycles. The approximation parameters of this dependence are shown in Table 2. Having these distinctions in AE generation, we decided to test the specimens of 4th group on the base of 8 cycles, because the tendency of their AE activity in these experiments is determined precisely from the test start.

As it follows from the obtained results, the used material taking substantially less energy (see Table 1) generates during the heat cycling in hydrogen and air considerably more of the AE signals. Therefore, it means it is more damaged.

Thus, AE method gives an effectively assessment of heat cycling effect in various environments on the bulk damaging in steels of heat-power equipment depending on the level of their degradation.

5. CONCLUSIONS

Heat cycling of steels both in air and hydrogen environment leads to growth of bulk damaging, which kinetics well correlates with activity of AE signals.

It is stated using the parameters of AE signals that the used material is more disposed to the micro- and macro crack initiation under influencing of temperature factor and service environment.

The dynamics AE signals development has showed that heat cycling of steels in the environment of gaseous hydrogen can be used for the accelerated obtaining of the prescribed index of their degradation during exploitation of steels operating conditions.

REFERENCES

[1] Student O. Z.: *Accelerated method of hydrogen degradation of structural steels*//Phys.-chem. mechanics of materials. 1998, №4, P. 45.

[2] Geller W., Sun T.: *Influence of alloy additions on hydrogen diffusion in iron and contributions to the system iron-hydrogen*// Arch. Eisenhuttenw. 1950, 21, P. 423.

[3] Johnson E. W., Hill M. L.: *The diffusivity of hydrogen in alpha iron*// Trans. AIME, 1960, 218, P. 1104.

[4] Hobson J. D.: *The diffusion of hydrogen in steel at temperatures of –78 °C to 200 °C*// LSI, 1958, 189, P. 315.

[5] *Metal Handbook*, ASM International, Metal Park, OH, 1948, P. 1208.

[6] Pohmurskiy V. I., Fedorov V. V.: *Effect of hydrogen on diffusive processes in metals*. Lviv: Publishing House Enej, 1998, 207 p.

[7] Skalskyi V. R., Koval P. M.: *Some methodological aspects of application of acoustic emission*. Lviv: Publishing House Spolom, 2007, 336 p.

[8] Skalskyi V. R., Sergienko O. M., Selivonchic T. V.: *Computation and optimization of geometry of waveguide of acoustic emission signals*// Engineering science, 2005, №9, P. 41.

[9] Skalskiy V. R., Andreykiv O. E.: *Estimation of bulk damaging in materials by the method of acoustic emission*. Lviv: Publishing House Franco Lviv National state University, 2006, 330 p.

[10] Skalskyi V. R., Rudavskiy D. V., Selivonchic T. V.: *Estimation of concentration and pressure of molecular hydrogen in a metal after heat cycling*// In Proc. 53-rd Internat. conf. "Hydrogen economy and hydrogen treatment of materials BOM-2007", May, 21-26 2007, Donetsk, 2007, P.815.

Valentine SKALSKY, Dr. Sci (Engineering Sciences), the head of department "Acoustic emission diagnostics of structural elements" of Karpenko Physico-mechanical Institute of National Academy of Sciences of Ukraine. He is the author over 230 papers in area of technical diagnostics and non-destructive testing of materials and structural elements.

MODELING OF VIBRATION SIGNAL FOR RECIPROCATING ENGINE DIAGNOSTICS

Iwona KOMORSKA

Politechnika Radomska, Instytut Eksploatacji Pojazdów i Maszyn, Zakład Elektroniki Samochodowej
Al. Bolesława Chrobrego 45, 26-600 Radom, email: iwona.komorska@pr.radom.pl

Summary

Vibration signal of the reciprocating engine may be described in several ways depend on the diagnostic purpose. For detecting non-uniform cylinder operation, for instance, lower harmonics of shaft vibration are interested. Then the signal can be assumed as stationary, ergodic and harmonic and may be expressed as a Fourier series. Assuming that transients are statistically independent some vibrations can be modeled as periodic transients, for instance piston slap. Transients may overlap each other and are buried in additive noise. Then the statistical methods are useful like periodically time-varying autoregressive model. In the paper different approaches to modeling of engine vibration signal are proposed. Particular methods of signal describing are dedicated to diagnostics of different components or processes of the reciprocating engine. Described diagnostic model propositions are illustrated by examples of four stroke spark ignition engine.

Keywords: internal combustion engine, diagnostic model, engine vibrations.

MODELOWANIE SYGNAŁU DRGAŃ SILNIKA SPALINOWEGO DLA POTRZEB DIAGNOSTYKI

Streszczenie

Sygnał drgań silnika spalinowego może być opisywany na wiele różnych sposobów w zależności od diagnozowanego podzespołu lub procesu. W celu obserwacji nierównomiernej pracy cylindrów, na przykład, monitorowanych jest kilka harmonicznych, czyli niskie częstotliwości sygnału. W takim przypadku sygnał może być opisany w postaci szeregu Fouriera. W innym przypadku, zakładając że odpowiedzi systemu na różne wymuszenia jednostkowe, jak zamykanie zaworów lub zwrot tłoka w cylindrze występują niezależnie i w ustalonej kolejności, drgania można opisać jako ciąg drgań przejściowych. Często jednak jest to sygnał zaszumiony, a drgania zachodzą na siebie. Wtedy użyteczne okazują się statystyczne modele, jak opisany w artykule model autoregresyjny ze zmiennymi w czasie współczynnikami. Wymienione wyżej metody modelowania zostały opisane w artykule w zastosowaniu do silnika czterocylindrowego o zapłonie iskrowym.

Słowa kluczowe: silnik spalinowy, model diagnostyczny, drgania silnika.

1. INTRODUCTION

The process of vibration and noise generation by an internal combustion engine is very complex. The measured vibrations are a mixture of periodic waves due to the rotating components and transient waves due to the reciprocating components of the engine and pressure forces. Strong transients come from exhaust and inlet valve operations, fuel injection, combustion, piston slap. For machine condition monitoring or design improvement purposes, it is necessary to separate the vibration signals caused by different sources and then analyze them individually. For identification of the transient source switching from the time to the crank-shaft angular coordinate is needed. Then most engine vibrations may be regarded as cyclo-stationary. Especially difficult is interpreting the sources during driving on the road. Changing load and additive stochastic forces from road give the background that must be subtracted. Some transients are periodic in angle domain like piston slap end valve operation (not for engines with variable valve timing), but vibration from combustion are dependent on spark ignition advance timing.

Diagnostic model of the engine should not be too complicated and it has not to include all the physical parameters of the system. It must be sensitive for failure of a component or changes in monitored process. For simplicity the stable revolution speed of engine and the stable load are assumed in models. Engine vibrations are filtered and windowed. They may be described in several ways depend on the diagnostic purpose.

2. EXPERIMENTAL SETUP

The test was performed on four-cylinder spark ignition engine 1600 with multipoint injection. The vibration signal was measured by a piezoelectric

sensor screwed on the head near fourth cylinder. During the experiment, in addition to vibration signal, two monitoring signals were also registered simultaneously, namely the digital signal of crankshaft position and the control ignition pulse from electronic control unit. With additional signals identifying the engine timing and transferring from time to crank shaft angular domain were possible [1]. Described signals are showed in Fig. 1.

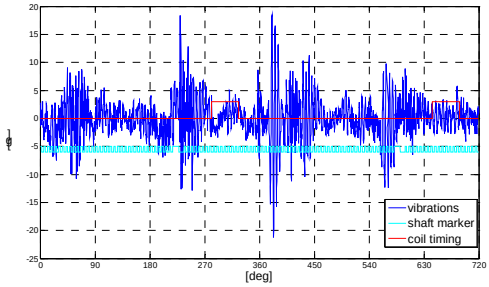

Fig. 1. Registered vibration and additional signals during one cycle of the engine operation

3. FOURIER SERIES

The vibration signal is assumed to be the sum of harmonically related elementary components that have to be periodic and complex

$$x(t) = e^{j\omega t} = \cos(\omega t) + j\sin(\omega t) \tag{1}$$

For this reason vibration signal of the engine must be preprocessed with low pass filter. It must be also transformed from time domain to shaft angle domain. After that the signal can be used for reasoning about the contribution of each cylinder to the total engine output. All the information about transient processes are lost. The signal can be expressed as [2]:

$$x(\theta) = \sum_{k=1}^{K} \left[\begin{array}{l} A_{k_{pi}} \cos\dfrac{2k}{\tau}(\theta + \varphi_i) + \\ + \left(B_{k_{pi}} + B_{k_{tr}}\right)\sin\dfrac{2k}{\tau}(\theta + \varphi_i) \end{array} \right] \tag{2}$$

where:

$A_{k_{pi}}, B_{k_{pi}}$ - the cosine and sine-terms of the k-th order harmonic components of the gas pressure torque;

$B_{k_{tr}}$ - the k-th order harmonic component of the reciprocating inertia torque;

i – the number of the cylinder;

φ_i - the firing angle of i-th cylinder;

θ - the crankshaft angle;

K – the highest number of harmonics components.

The signal $x(\theta)$ is proportional to external torques acting on the crankshaft that are inertia torque and gas-pressure torque.

Under steady-state operating conditions, the variation of the reciprocating inertia torque may be considered identical for all cylinders. The gas-pressure torque may be different from cylinder to cylinder and from cycle to cycle. Fig. 2. shows low-frequency vibrations of the engine during one operating cycle. Non-uniform operation of the one cylinder is visible. Simulated and measured vibrations during a several cycles are presented in Fig. 3. It shows regular different work of one cylinder and very small changes of cylinders operation from cycle to cycle.

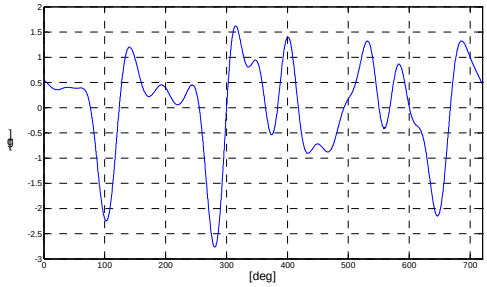

Fig. 2. Engine vibrations filtered with low pass filter during one cycle

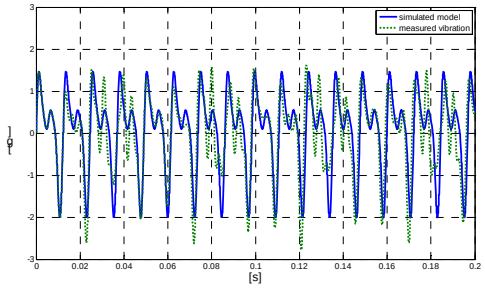

Fig. 3. Non-uniform (measured) and uniform (simulated) operation of the cylinders

4. INDEPENDENT TRANSIENTS

Assuming that transients are statistically independent some vibrations responses can be modeled as periodic transients, for instance piston slap or valve operations. Since the force applied to the engine is impulsive, the response of the system due to a unit force can be as follows:

$$x(t) = w\frac{e^{-\zeta(t)\cdot\omega_0\cdot t}}{m\cdot\omega_d(t)}\sin\left[\omega_d(t)\cdot t\right] \tag{3}$$

where:

m - mass of the element;

w - wage factor;

ω_0 - natural frequency;

$\omega_d = \omega_0\sqrt{1-\zeta^2}$ - damped frequency;

$\zeta = \dfrac{c}{2m\omega_0}$ - damping factor.

Model was identified assuming that stiffness and damping factors was changing with time, because the damped frequency was decreasing (see Fig. 4).

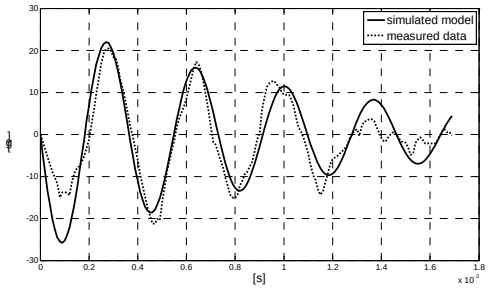

Fig. 4. Vibration response to outlet valve closing (---measured data and — simulated model)

For a single cylinder the modeled signal can be described as the transient convolved with the unit force [3]:

$$x_1(t,\theta) = w_1 \frac{e^{-\xi_1 \omega_{o1} t}}{m_1 \omega_{d1}} \sin\left(\omega_{d_1} t\right) * 1\left(\theta - \theta_{v_1} - 4k\pi\right) \qquad (4)$$

where
i – number of the cylinder;
k – number of the cycle;
θ_{v_1} - valve closing angle;
$*$ - the convolution symbol.

Simulation of this model is presented in Fig. 5.

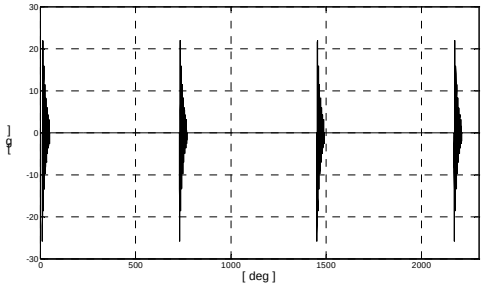

Fig. 5. Modeled signal of the outlet valve closing for a single cylinder during four cycles

This rather simple model is good only for chosen statistically independent processes. Such approach for modeling do not fit when the transients overlap each other and are buried in additive noise.

5. AUTOREGRESSIVE MODELLING

For modeling vibration signal of inlet valve operation, for example, the stationary assumption or independent transients hardly holds any more. In this case the one of statistical models should be considered, like periodically time-varying autoregressive model of the form [4]:

$$x(\theta) = \sum_{i=1}^{p(\theta)} a_i(\theta) \cdot x\left(\theta - i\right) + \varepsilon(\theta) \qquad (5)$$

where:
$\varepsilon(\theta)$ - assumed white stationary prediction error;
$a_i(\theta) = a_i\left(\theta + N\right)$ – periodically time-varying autoregressive coefficients;
$p(\theta)$ – the order of the model.

The order of the time-varying autoregressive model is related to the number of dominant sinusoidal sources of the vibration signal conditioned on each angular position. This variables are rather sensitive to non-stationarities.

At this approach the signal was preprocessed with high pass filter for removing trends and windowed with rectangular window (see Fig. 6).

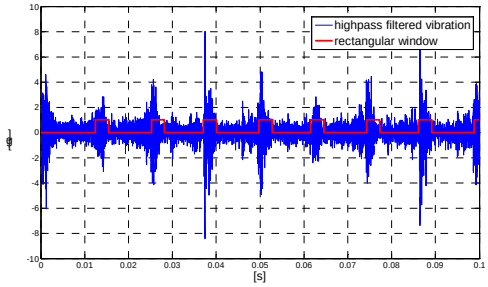

Fig. 6. Vibrations filtered with high pass filter and windowing signal for inlet valve closing

The base of the method is the assumption that measured signal can be generated using the model filter. Some works show that it can be autoregressive (AR) model with transfer function [5, 6].

$$H(z) = \frac{1}{A(z)} \qquad (6)$$

where

$$A(z) = 1 + \sum_{k=1}^{K} a_k \cdot z^{-k} \qquad (7)$$

that is submitted by a white noise with zero-mean value (see Fig.7).

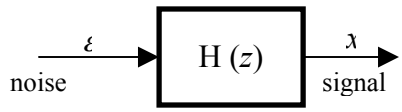

Fig. 7. Linear system driven by a zero-mean white noise

Identifying the model means finding the model coefficients a_k of the equivalent FIR filter.

Fig. 8 shows vibration response of the engine to the inlet valve opening and the simulated AR model for $K = 100$.

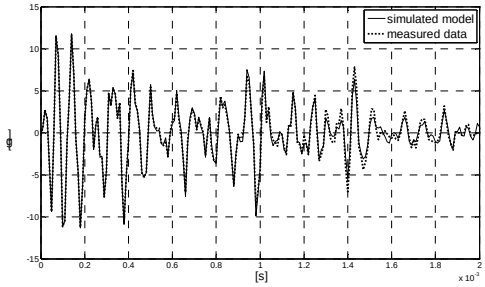

Fig. 8. Vibration response to inlet valve opening (---measured data and — simulated model)

The failure in the engine or process changes mean the change of the model-filter coefficients.

6. CONCLUSIONS

In the paper three methods of the vibration signal modeling of the reciprocating engine was presented. Each of them was dedicated to the particular process and was illustrated with the time waveform of the spark ignition engine vibration.

Non-parametric methods of power spectral density estimation like Fourier analysis are well known and often applied. But their usage is limited to stationary periodic processes. Fourier series can be applied for modeling non-uniform operation of cylinders from cycle to cycle in the reciprocating engine, for instance. In this case only low frequency components are taken. For diagnostics of other processes the different approach is more useful. Strong transients come from exhaust and inlet valve operations, fuel injection, combustion or piston slap. Assuming that transients are statistically independent some vibrations can be modeled as periodic transients. Such approach for modeling do not fit when the transients overlap each other and are buried in additive noise. Another approach is the parametric one that deals with periodically time-varying autoregressive models. It can be used for diagnostic purpose, for instance for valve mechanics or for combustion pressure rises.

BIBLIOGRAPHY

1. Komorska I: *Próba lokalizacji faz rozrządu w silniku spalinowym o zapłonie iskrowym na podstawie sygnału wibroakustycznego.* Mat. XXIII Sympozjonu Podstaw Konstrukcji Maszyn, Rzeszów – Przemyśl 2007, Tom I, pp.285-290.
2. Taraza D., Henein N. A., Bryzik W.: *Diesel Engine Diagnosis Based on Analysis of the Crankshaft's Speed Variations*, SAE paper 982540.
3. Komorska I.: *Poszukiwania modelu wibroakustycznego silnika spalinowego*, Przegląd Mechaniczny 11'07, 2007, pp.11-13.
4. McMormick, Nandi: *Condition Monitoring of Reciprocating Machinery using Cyclic Autoregressive Models*, EURASIP, Prague 1997.
5. Stranneby D.: *Cyfrowe przetwarzanie sygnałów. Metody, algorytmy, zastosowania*, Wyd. BTC, Warszawa 2004.
6. Cholewa W., Kaźmierczak J.: *Data Processing and Reasoning in Technical Diagnostics*, WNT, Warszawa 1995.

Praca naukowa finansowana ze środków na naukę w latach 2008-2010 jako projekt badawczy N N509 349834

Dr inż. **Iwona KOMORSKA** jest adiunktem w Instytucie Eksploatacji Pojazdów i Maszyn Politechniki Radomskiej. W pracy naukowej zajmuje się elektroniką samochodową, diagnostyką wibroakustyczną oraz cyfrowym przetwarzaniem sygnałów.

PREDICTION OF THE OPERATE CHARACTERISTICS OF DESIGNED PUMP BASING ON A MATHEMATICAL MODEL

Andrzej JURKIEWICZ, Piotr MICEK, Marcin APOSTOŁ, Dariusz GRZYBEK

Department of Process Control, AGH University of Science and Technology
Kraków, Poland, Tel/fax: 0048 12 617 30 80, e-mail: jurkand@agh.edu.pl

Summary

The article presents a creation process of designed pump of 7 pistons. A several FEM models are presented with a simulation results. Apart from FEM models, the mathematical model of 1/7 pump was elaborated. This model, which contains piston set with input and output valves was implemented in MATLAB Simulink program. The mathematical model was used to the definition of movement parameters: piston displacement, input and output valves displacements as well as the influence of the work pressure on the movement range. The obtained simulation results from mathematical model can replace a part of the prototype researches.

Elaborated model was verified on a laboratory stand. A verification results are shown in this article.

Keywords: FEM, mathematical model, design, pump.

PREDYKCJA WŁASNOŚCI EKSPLOATACYJNYCH PROJEKTOWANEJ POMPY W OPARCIU O MODEL MATEMATYCZNY

Streszczenie

W artykule pokazano budowę nowo projektowanej pompy 7-mio tłokowej. Przedstawiono szereg modeli MES podstawowych jej części wraz z wynikami symulacji. Oprócz modeli MES opracowano model matematyczny 1/7 pompy (stanowisko badawcze) jako zespół pojedynczego tłoka wraz z zaworami ssawnym i tłocznym, który zaimplementowano w środowisku Matlab – Simulink. Model matematyczny pozwolił na określenie parametrów ruchowych jej głównych elementów tj. przemieszczenia tłoka oraz przemieszczeń grzybków w zaworach ssawnym i tłocznym, jak i wpływu zmian ciśnienia roboczego pompy na zakres tego ruchu. Otrzymane wyniki symulacji opracowanego modelu matematycznego 1/7 pompy mogą zastąpić przeprowadzenie wielu badań i symulacji prototypu, co wiąże się ze znacznymi oszczędnościami finansowym, a także umożliwią dobór odpowiednich parametrów konstrukcyjnych głównych elementów pompy.

Słowa kluczowe: MES, model matematyczny, projektowanie, pompa.

1. INTRODUCTION

A market competition is a cause of the increase of complex degree of the design process of new product. It is possible by the wide cooperation among specialists from different field of technology and science. This cooperation basing on a use of the computer techniques, which enable concurrent design and testing of created products. A solving of the constructional problems is situated at a pre-design and design levels instead at a prototype level. The main elements of contemporary design process are – apart from CAD (computer aided design) – a selection theory, CAT (computer aided testing), FT (fast prototyping). A connection of the application mentioned above tools of new product creation and a prediction of its operate characteristics basing on mathematical models enable a getting of defined features of product without a expensive and long-lasting researches and prototype experiments.

The article presents a creation process of designed pump of 7 pistons. A several FEM models are presented with a simulation results. Apart from FEM models, the mathematical model of 1/7 pump was elaborated. This model, which contains piston set with input and output valves was implemented in MATLAB Simulink program. The mathematical model was used to the definition of movement parameters: piston displacement, input and output valves displacements as well as the influence of the work pressure on the movement range. The obtained simulation results from mathematical model can replace a part of the prototype researches.

Elaborated model was verified on a laboratory stand. A verification results are shown in this article.

2. CONSTRUCTION OF THE PUMP

The pump (Fig. 1, 2, 3) is dedicated for pumping oil and water emulsion with 3 to 5% of oil contents. The basic requirements required by the ordering party for this pump are:

- nominal pressure at the outlet: 40 MPa,
- flow capacity: 320 dm^3/min,
- motor power output: 250 kW.

The proposed solution is a new construction solution of a radial piston pump. Its main working elements are seven pistons spaced radially around the shaft axle. The pistons move in the pump body in plane and return motion forced by the properly shaped cam set on the shaft pin. Lift spaces are connected with the inlet and outlet (pumping) pipes from the outside of the immovable cylinder block. Valve timing is used as the element controlling the flow of the liquid.

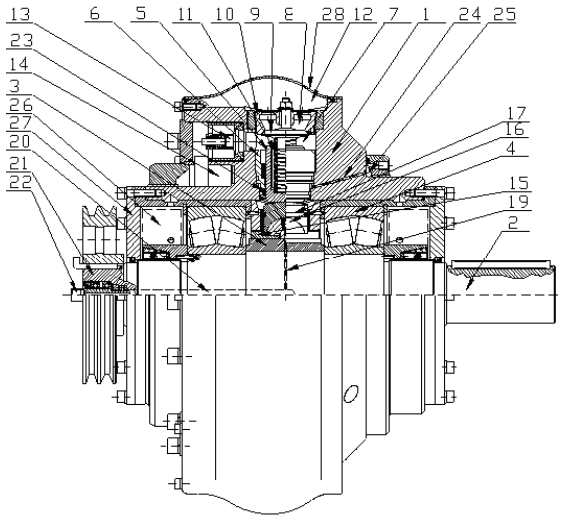

Fig. 1. Construction of the pump:
1 – pump body, *2* – shaft, 3 – eccentric pin, 4 – rolling bearings, 5 – small piston, 6 – small cylinder, 7 – lift chamber, 8 – inflow valve, 9 – inflow valve head, 10 - inflow valve seat, 11 - inflow valve spring, 12 – inflow collecting pipe, 13 – pumping valve head, 14 – pumping collecting pipe, 15 – bearing foot, 16 – ball-shaped pin, 17 - lifter, 18 – non-return valve, 19 – radial duct, 20 – axial duct, 21 – peripheral drive pin, 22 – rotating oil line, 23 - additional sealing, 24 – oil duct, 25 – oil collecting pipe, 26 - counterweights, 27 - cover, 28 - inflow collecting pipe casing

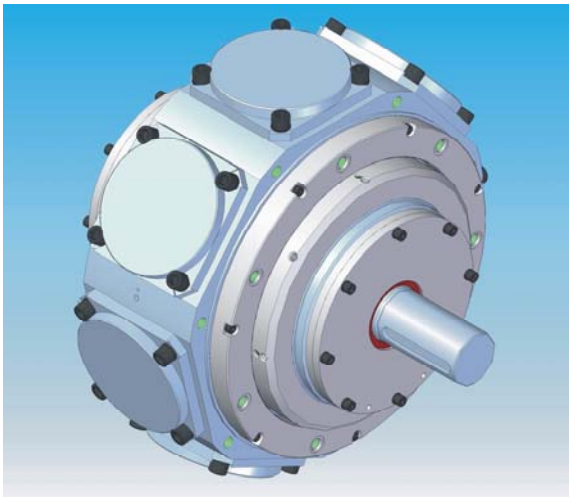

Fig. 2. View of the pump

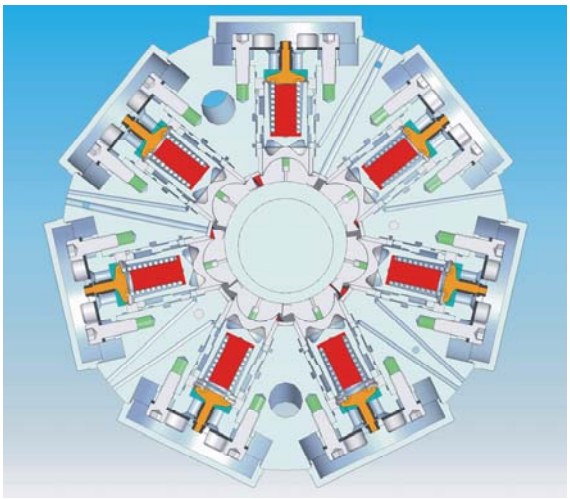

Fig. 3. Building of the pump

3. STRUCTURE OF PUMP UNIT

Main element of plunger pumps unit, which is presented in fig. 4 and 5, is radius piston pump of T7-320-40 (1).

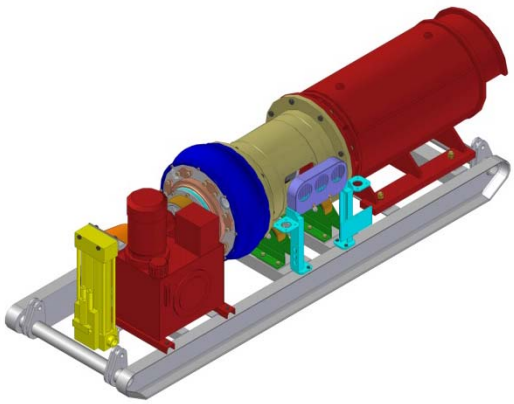

Fig. 4. View of the pump unit

The pump is preliminarily supplied by rotational pump of PJMP 65 (8). A shaft of the main pump is connected by a flexible clutch of SPR 90 (7) with motor of SGPL355 L-4 (6). The rotational pump is driven by a belt transmission (5), which are protected by shield (3). Apart from enumerated elements, the pump unit consist of following elements: water filter (4), hydraulic unit (9), manometers unit (10) and frame (2).

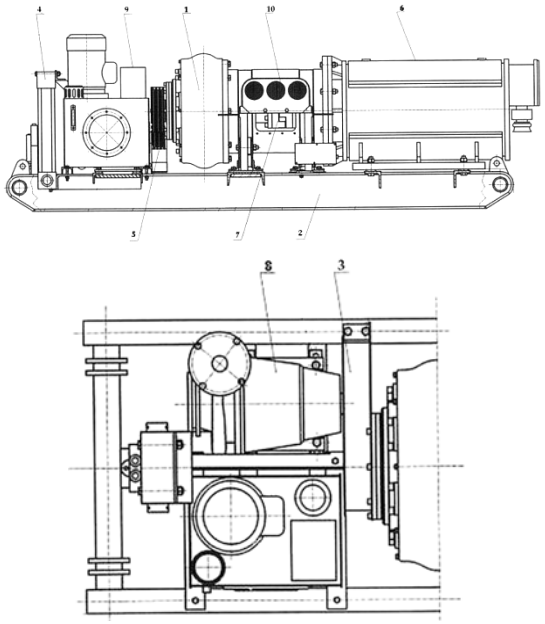

Fig. 5. Structure of the plunger pumps: 1 - radius piston pump of T7-320-40, 2 – frame, 3- shield, 4 - water filter, 5 - belt transmission, 6 – motor, 7 - flexible clutch, 8 - rotational pump, 9 - hydraulic unit, 10 - manometers unit

4. SIMULATION RESEARCHES OF CHOSEN ELEMENTS WITH THE USE OF FEM

Most important elements of new pump were verified by strength analysis in FEM. A maximal value of pressure in system was assume as a boundary condition. A strength analysis of the elements of high pressure output of pump was made by the use of flat, axial symmetric models with taking into account of interaction among components of system. A model of the plunger pump body was made as spatial solid model.

A piston of the plunger was the first tested element. The analysis enables definition of the values of maximal displacements of piston, which enables the verification values of clearance and seals clamp.

An input valve of main pump was the second tested element. Two analysis of this element were conducted for extreme work conditions. Simulation research includes also analysis of several structure of valve head in order to a limitation of its mass and an undesirable dynamic phenomena in this system.

An body shield of main pump was the third tested element. The pressure of work fluid on input side of the main pump.

A pump body was the last tested element of created pump. A solid modeling was used to the creation of body model. A shape of body was divided to four-walls elements of tetra4 type. The maximal pressure in pump system was the boundary conditions.

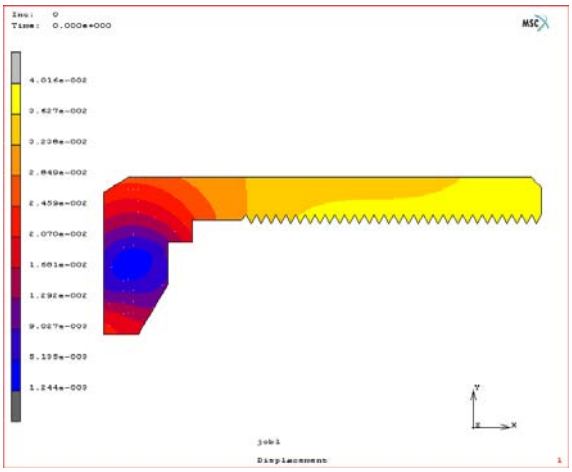

Fig. 6. Displacements distribution of the pump piston

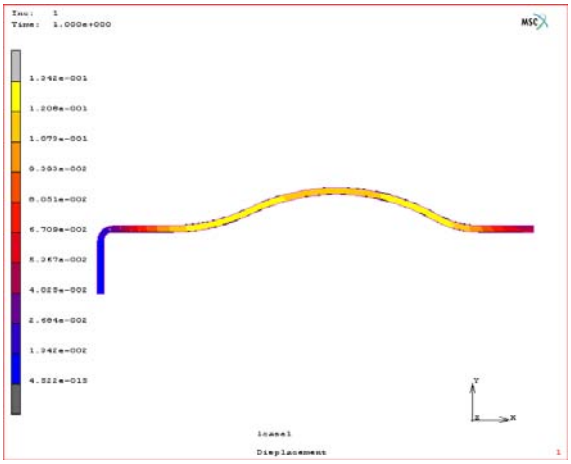

Fig. 7. Displacements distribution of the body shield

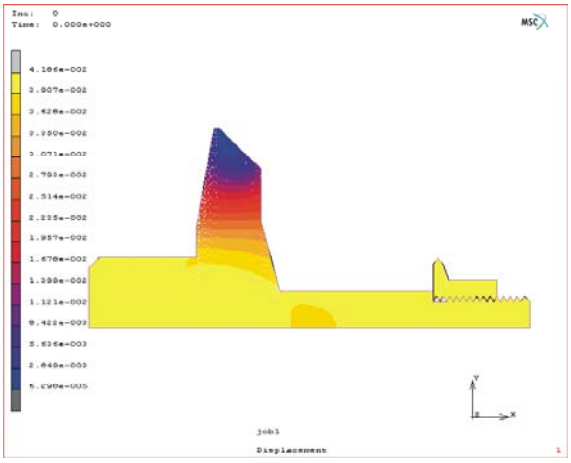

Fig. 8. Displacements distribution of the input valve

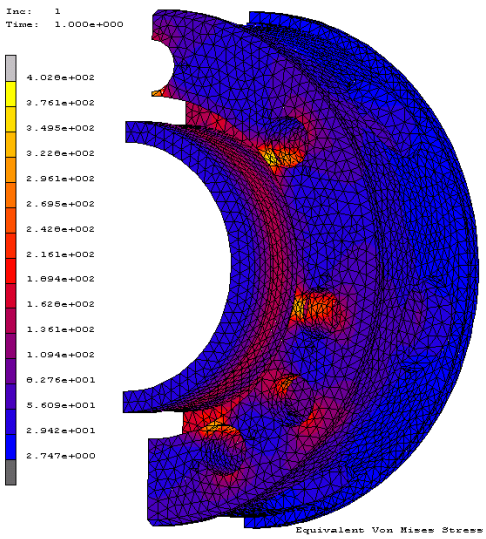

Fig. 9. Stresses distribution of the body shield

5. SIMULATION RESEARCH WITH THE USE OF MODAL ANALYSIS OF CHOSEN PUMP ELEMENTS

The object of simulation research was the body of a radius pump in the phase of concept design. The application of virtual prototyping, one of whose elements was modal analysis, was the requirement of the purchaser. The body was chosen with the connection of concentration of dynamic forces. Geometric measure and dimensions of the body were determined by assumptions determining the work of the pump as well as the measures and dimensions of other components used in the device. It allowed the execution of the technical documentation in CAD stage. On this basis, geometric model of the body was produced.

The method of finite elements and computational packet MSC Patran/Nastran were used to determine the modal model of the body. On the basic of the geometric model mentioned above a network of finite elements consisting of about 121000 quadrilateral, special elements was generated.

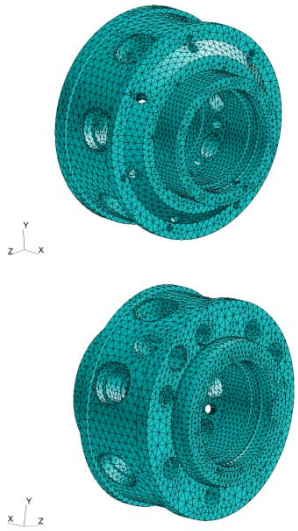

Fig. 10. The finite elements model of the body of pump

Taking into account the fact that the specific frequency and the form of specific vibrations, among others, are the functions of material properties and boundary conditions, to determine the modal model of the body we assume:

– constant material values for steel (E, ν , ρ),
– boundary conditions reflect the placement of the pump in the place of work (settled at shaft).

Taking into account the initial assumptions, parts of the body were determined, the first 10 of which are shown in table 1. The exemplary from of specific vibrations for first 2 frequencies are shown in fig.11.

Table 1. The specific frequencies of the body

L.p.	1	2	3	4
f [Hz]	1591.4	1594.7	1939.2	1975.7

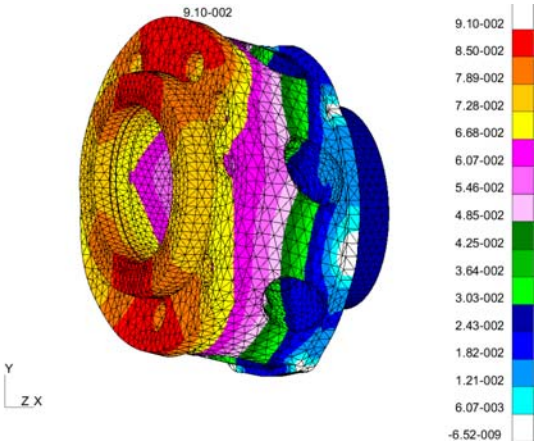

Fig. 11. The form of specific vibrations for frequencies 1591,4 Hz i 1594,7 Hz

For the designed pump following characteristic frequencies resulting from the conditions of work can be determined:

– the frequency coming from the circular velocity of shaft (for $n=1470$ *1/min*): $f_0=24,5$ *Hz;*
– the frequency coming from the periodic opening of valves on the circumference of the body: $f_z=171,5$ *Hz.*

The comparison of the acquired results with the specific frequencies of the body enables to state that force frequencies are placed in different division of value than specific frequencies. Hence we can reach constructions that at such model of force the resonance connected with these forces will not occur.

The analysis of the modal model of the body of the pump in design enables to define of following conclusions:

1. There is not threat of resonance occurrence at the characteristic frequencies resulting from the conditions of the pump's work.
2. The value of deformation of the body, which occurs at force with characteristic frequency 24,5 Hz, is leaving out.

6. MATHEMATICAL MODEL OF MAIN PUMP

6.1. Simplification assumptions

1. Constant temperature of the work fluid (constant characteristics of the work fluid).
2. Elasticity force is described by linear equation
3. Leakage doesn't appear.
4. Losses caused by local and linear resistances doesn't appear in the input conduits.
5. Force from the pressure in the gaps in input and output valves are negligible small.
6. Viscous friction force in gaps in input and output valves are negligible small.
7. Flow have a turbulent characteristic in each local elements.
8. Flow have a laminar characteristic in each linear elements.

6.2. Mathematical model

Talking into account presented above assumptions, structure of the pump and functioning of the pump, calculating schema of valves system was elaborated. This schema is presented in fig. 12. Its implementation in Matlab-Simulink is presented in fig. 13.

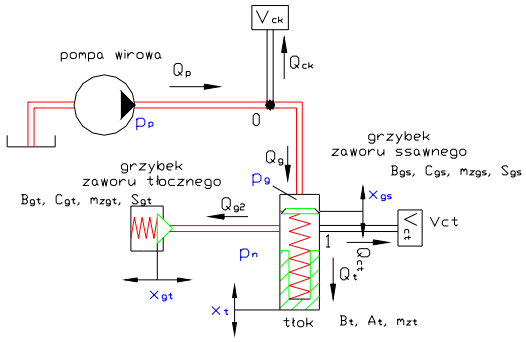

Fig. 12. Calculating schema of the plunger radius pump of T7-320-40

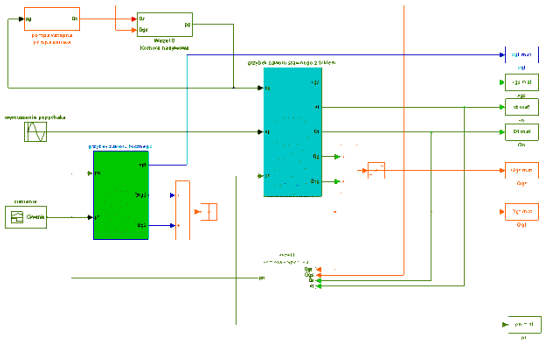

Fig. 13. Calculating diagram of the valves system of the plunger radius pump

7. SIMULATION RESEARCH RESULTS

Characteristics of the valve head displacements for input valve and output valve, piston displacement, flow intensity through valve head was got for established input parameters. Exemplary course of the valve head displacement as well as flow intensity in output valve are presented in fig. 14. Time range from 0 to 0.2 s was established from the point of view of periodicity of the motion of the pump elements.

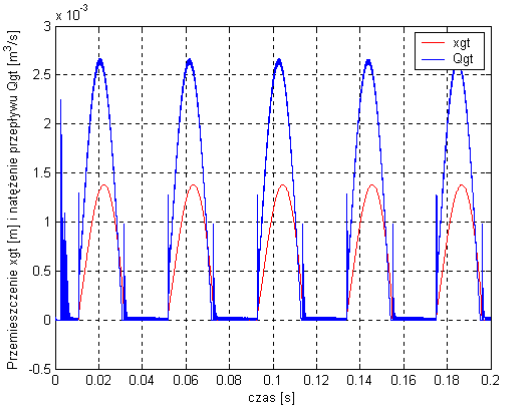

Fig. 14. Displacements of the valve head x_{gt} of the output valve and flow intensity through output valve Q_{gt}

8. CONCLUSIONS

Piston radius pump of T7-320-40, which was elaborated for water-oil emulsion, is described in this article. Measurement description of parameters and diagrams of unit is very hard because of compact construction. In case of that obtaining of pump mathematical models were needed for simulations. After implementing of model in Matlab–Simulink environment, leading series of simulations and experimental researches it was found that obtained model is enough for exact determination of real parameters diagrams. Simulation researches allow for recognition of mutual hydraulic, energetic and geometric relationships between parameters and caused in activities for unit construction optimization.

REFERENCES

[1] Dyrektywa 98/37/WE Parlamentu Europejskiego i Rady z 22 czerwca 1998 r. *W sprawie zbliżenia ustawodawstwa Państw członkowskich dotyczącego maszyn*.
[2] *Nurnikowy agregat pompowy nowej generacji o parametrach technicznych nie gorszych od określonych przez Zamawiającego*. Sprawozdanie wykonawcy z I etapu pracy naukowo-badawczej pod red. A. Jurkiewicz, Kraków 2003.
[3] Tomczyk J.: *Modele dynamiczne elementów i układów napędów hydrostatycznych.* Wydawnictwo Naukowo techniczne Warszawa 1999r.
[4] Stryczek S.: *Napęd hydrostatyczny"* Tom I i II, WNT, Warszawa 1992r.
[5] Szydlewski Z., Olechowicz J.: *Elementy napędu i sterowania hydraulicznego i pneumatycznego.* PWN Warszawa 1986r.

EVALUATION OF CERAMIC TILES DEFECTS WITH THE USE OF IMAGE ANALYSIS TECHNIQUES

Anna BZYMEK

Department of Fundamentals of Machinery Design, Silesian University of Technology at Gliwice
44-100 Gliwice ul. Konarskiego 18a, tel (032) 237 10 63, fax (032) 237 13 60, anna.bzymek@polsl.pl

Summary

In many cases ceramic tile manufacturing processes have been almost completely automated. Two stages of these process are exceptions. They are quality control and sorting at the end of the production line. These operations have been realized by the staff so identification of defects depends only on the human. Because of specific abilities of human sences, visual quality control of tiles is often not precise and reliable. Automatic visual inspection and estimation of tiles is a crucial problem in a ceramic industry. Inspection with the use of a vision stystem eliminates problems connected with the tiredness of human sences. Such systems are able to operate many hours without any breaks and are much faster and preciser. In the paper a concept of a method of the quality evaluation of the ceramic tiles, basing on digital image analysis, and the first results of the research have been presented. Three groups of defects have been distinguished, they are corner defects, edge defects and surface cracks that could be detected during the manufacturing process.

Keywords: ceramic tiles, quality evaluation, image analysis, vision system.

OCENA DEFEKTÓW PŁYTEK CERAMICZNYCH Z ZASTOSOWANIEM METOD ANALIZY OBRAZÓW

Streszczenie

Proces wytwarzania płytek ceramicznych w wielu przypadkach jest całkowicie zautomatyzowany, za wyjątkiem dwóch etapów - kontroli jakości podczas produkcji oraz sortowania płytek na końcu linii produkcyjnej. Czynności te są wciąż wykonywane przez ludzi, a kontrola jakości produktu jest zależna od zmysłów ludzkich. Z tego powodu kontrola wizualna, jest subiektywna, nie jest precyzyjna ani powtarzalna. Automatyczna kontrola jakości przeprowadzana przy użyciu systemów wizyjnych jest bardzo ważnym aspektem przemysłu ceramicznego. Automatyczna inspekcja z użyciem technik wizyjnych oraz metod przetwarzania i analizy obrazów eliminuje problemy wynikające z szybkiego męczenia się oka ludzkiego. Inspekcja taka zapewnia precyzyjną i szybką kontrolę, która dzięki temu, że system może działać bez przerw znacznie przyspiesza proces produkcji. W niniejszym referacie została przedstawiona koncepcja metody detekcji wad płytek ceramicznych bazującej na analizie obrazów cyfrowych. Wyróżniono trzy podstawowe grupy wad: wady krawędzi, naroży oraz pęknięcia płytek ceramicznych, które mogą być wykrywane już na etapie produkcyjnym.

Słowa kluczowe: detekcja wad, analiza obrazów, system wizyjny, płytki ceramiczne.

1. BACKGROUND OF THE RESEARCH

Nowadays, estimation of the ceramic tiles quality during their production has been still performed by the people usually only at the end of the production line [1, 4]. The quality of this evaluation relays only on the human sence capability, because of that such quality control is not precise and reliable. Specific features of human sences, cause fast tiredness, lack of attention, eye fatigue or even sickness of an inspector that results in low efficiency of inspection and in decrease of quality of the final product. Therefore automatic visual inspection and estimation of the quality of tiles is a crucial problem in a ceramic industry. Inspection with the use of a vision stystem eliminates problems connected with human sences. Such system can operate many hours without any breaks and is much faster and reliable.

Concerning the quality evaluation during the production process, tiles are usually inspected only when all expensive operations like glazing or pattern printing have been already performed. In such case the tile could not be easily recycled [2]. Defects of ceramic tiles could emerge on every stage of the process: during forming the biscuit on the press, during firing or pattern printing. The most important problem is to detect occuring defects as early as possible, e.g. before firing, when the demaged tile can still be recycled. In such case both material losses and production costs can be reduced. On the basis of bibliographic research [2, 5] and according to experts' opinions one can state that the most

common defects of the ceramic tiles are: edge defects, corner defects and surface cracks.

In the paper, concept of a method of the defects evaluation of the ceramic tiles, based on digital image analysis has been presented.

2. OBJECT OF INVESTIGATION

In the presented experiments objects of investigations were square ceramic tiles, of dimensions 350 x 350mm. As it was stated, three groups of defects have been distinguished as the most common. Therefore these defects have been taken into consideration in the presented research.

On the basis of experts' opinions, the area of the specimen that should be observed can be reduced to the border of the ceramic tile. The reason of such reduction is based of the specification of the considered defects. Parts of the tile that are most exposed on demages are edges and corners. In the case of surface cracks, it was stated that this kind of demage usually have its begining at the edges, from where the damage propagates. Therefore the analysed area has been also reduced only into the border region.

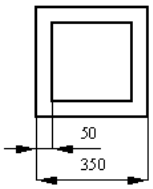

Fig. 1. Representation of the border region

In the presented experiments the border region has been limited to area of width from 20mm to 50mm. Border region has been presented in the Fig. 1.

3. VISION SYSTEM

For the research purposes, the laboratory stand consisting of a camera, illuminator and PC computer has been prepared. A schema of the laboratory stand has been presented in Fig. 3.

On that early stage of the research the specimen and the camera were stationary. However, in order to simulate the environment of the production line, the laboratory stand will be equipped with the conveyor belt and the tile will move under the stationary camera. Because of that concepts of two methods of tile observation and image acquisition have been proposed. The first method consists in observation of the whole specimen with the use of one camera. Such method allows us to acquire one image for every specimen and analysis can be performed for all border areas simultaneously. However some limitations of the minimal defect size occur. This restriction came from bigger field of view (FOV) of the camera what results in a smaller number of pixels composing the visible detail.

The second concept is based on the observation of the tile with the use of two different cameras. In this case the vision system should consist of two synchronized cameras observing parallel areas. In this case, the field of view (FOV) of the camera should be equal to half of the width of the tile and observation of border area is similar to the scanning process. Thanks to limited FOV of the camera it is possible to identify smaller defects. The schemas of two concepts have been presented in Fig. 2.

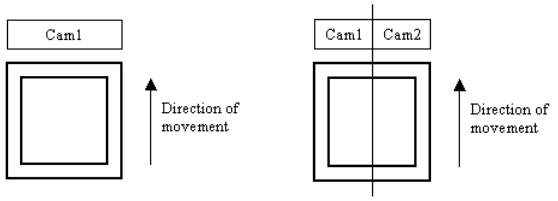

Fig. 2. The concepts of image acquisition method

Because of the possibility of limitation of the area of observation to the maximum 50 mm width of the border, the size of the acquired data can be also minimized by a region of interest (ROI), wchich is chosen before the acquisition. Concepts presented above are to be developped in the further research.

3.1. Laboratory stand configuration

In order to simplify the research at this stage of the investigation, the second presented concept of laboratory stand has been applied, but camera and the specimen were fixed. Positions of an illuminator were being changed during the experiment by changing the ditances d_1 and d_2. Such experiments have been performed in order to verify the influence of the position of the illuminator on the visibility of defects. Exemplary results have been presented in paragraph 2.1.

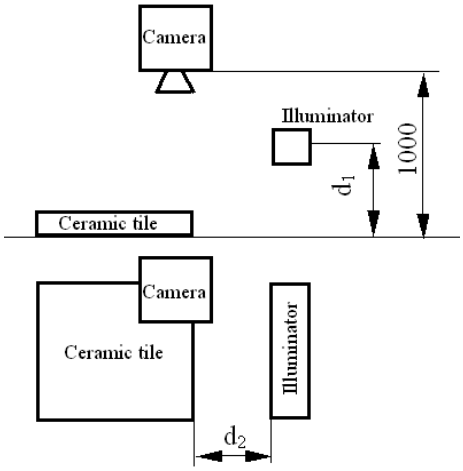

Fig. 3. Laboratory stand configuration

Parameters of the camera used in the experiment and information about the measurements precision have been presented in tab. 1.

Tab. 1. Parameters of the camera used in the investigations

Camera	Imaging Source Mono DMK 31BF03 CCD 1/3''
Resolution	1024 x 768 pixels
Pixel size	4,6 μm x 4,6 μm
Focal length	f=50mm
Specimen - camera distance	1m
Field of view	91 x 68 mm
Measurement precision	approx.0,15 mm

Exemplary images representing ROIs with the most common defects have been presented in Fig 3-7.

3.1. Methods of specimen illumination

A very important role in the image acquisition as well as analysis plays an appopriate illumination of a scene. The illumination well matched to the task enables that all information, and characteristic features of the surface are visible. It is emphasized in many references that the suitable illumination is the 70% of sucess in vision system applications [3]. In the presented reasearch, a fluorescent lamp has been used as the illuminator. Such kind of the illuminator is a source of diffused light. In order to investigate the influence of the position of the illuminator in regard to the specimen several different configurations have been tested. Changes of the illuminator possitions have been realized by changing distances between the specimen and the illuminator. Distances d_1 and d_2 pointed out in Fig. 3. were equal from 5 mm to 100 mm. Depending on the illumnator – specimen configuration one can obtain images in which defects are clearly visible, or in contrary, where defects are barely recognizable. In the paper images acquired under configuratons which reflected the biggest differences in the image quality and visibity of the defects have been presented in Fig. 4.

In the configuration where the illuminator has been remoted from the specimen (Fig. 4a) defects of the edges have been barely visible. In such case the analysis of the image was very difficult and identification of the defect were not possible. One can observe that the best results have been obtained under the configuration where the illuminator was placed on the height equal to the position of the specmen surface and very close to its edges (Fig. 4d.) In this case defects have been clearly visible and image processing and analysis were less complicated and the defects have been easily identified.

a) Distances: d_1 = 100 mm, d_2 = 100mm

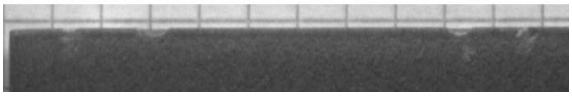

b) Distances: d_1 = 30 mm, d_2 = 40mm

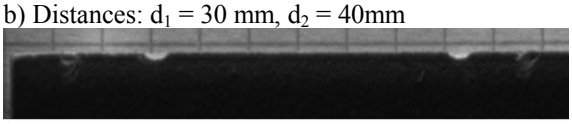

c) Distances: d_1 = 10 mm, d_2 = 20mm

d) Distances: d_1 = 5 mm, d_2 = 5mm

Fig. 4. Influence of illuminator position on the defects visibility

4. METHOD OF DEFECTS IDENTIFICATION

According to the assumption made at the beginning of the experiment, images have been acquired with the use of one camera placed 1m above the specimen. Methods based on image processing techniques have been applied in order to distinguish damages from the proper surface. The algorithm of image processing consisted in image enchancement by median filtering and normalizaton. In the next step of the algorithm, in order to limit the volume / size of processed data, regions of interest have been choosen and after that ROIs have been analysed. The operation of image analysis used in the computations were edge/line detection procedures, and morfological operations. With the use of the elaborated procedures three groups of defects were possible to be detected and sizes of edge defects were estimated.

An examplary image representing the ROI (9 x 56 mm) with proper edge has been shown in Fig. 5. It is visible that the edge is straight and can be acknowledged as ideal. An example of ROI with edge and corner defects has been presented in Fig 6.

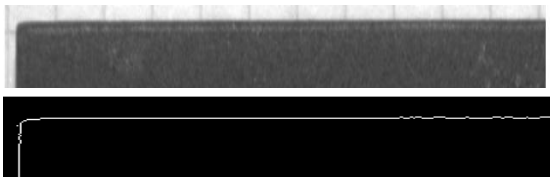

Fig. 5. Exemplary results for tile with proper edge

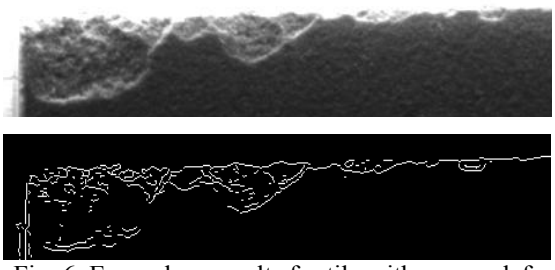

Fig. 6. Exemplary results for tile with corner defect

In this case chosen ROI is bigger than in previous case (14 x 56mm) because of sizes of damages.

The third group of defects of the tiles are scrathces and cracks. An example of the original image and image after analysis have been presented in Fig. 7.

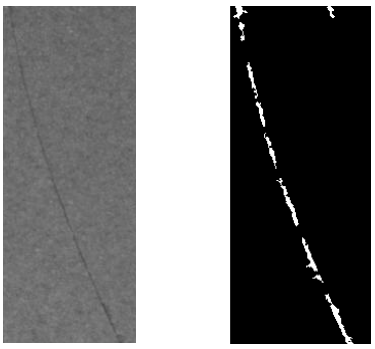

Fig. 7. Exemplary results for tile with crack

In this case morphological operations were very useful. Some kinds of filtration caused removal of the crack line from the tile surface, because of the presence of a huge number of pixels with the same gray level.

5. EVALUATION OF DEFECT SIZE

The main goal of the research, except the defect detection, was an estimation of the defect size. In Fig. 8 an example of a damaged edge has been presented. In the selected ROI four different damages are visible. For the purpose of the size evaluation, some procedures have been elaborated. Procedures were based on the searching for the stright horizontal line in a binary image, in the next step, black pixels below the line are counted. The procedure is simple but has given acceptable results.

Fig. 8. Exemplary results for tile with damaged edge.

Results of the operation of the defects size estimation procedures have been presented in Tab. 2.

Tab 2 Results of the defects size estimation

Defect number	Number of pixels of defect	Defect size [mm^2]
1	202	4,2
2	199	4,2
3	166	3,84
4	256	4,78

On this stage of the research, it is possible to estimate only the size of the defects. In further research it is planned to make possible the evaluation of the shape and mutual orientation of the defects as well.

6. CONCLUSIONS

Automatic detection of the defects of ceramic tiles is an essential task in ceramic industry. Therefore experiments of the application of image analysis methods has been undertaken, and the first obtained results have been very promising. Detection of the demaged tile and its elimination from the production process before very expensive operation such as glazing and pattern printing may keep to the minimum losses incured by the manufacturers.

LITERATURA

[1] C. Boukouvalas, J Kittler, R Marik, M. Mirmehdi, M Petrou: *Ceramic tile inspection for colour and structural defects*. Processing of AMPT95 1995, p. 390–399.

[2] C. Boukouvalas, F. De Natale, G. De Toni, J. Kittler i inni, *ASSIST: automatic system of surface inspection and sorting of tiles*, Journal of Materials Processing Technology 82 (1998), p.179-188.

[3] E. R. Davies: *Machine Vision Theory Algorithms, Practicalities* (3rd ed.). Elsevier, 2004.

[4] J. M. Valiente Gonzales, F. Acebron Linuesa, F. Lopez Garcia: *A ceramic tile inspection for detecting corner defects*. IX Spanish Symposium on Pattern Recognition and Image Analysis, isbn. 8480213515, vol. II, pp. 213-218, 2001.

[5] Z. Hocenski, T. Keser: *Failure detection and isolation in ceramic tile based on contour descriptor analysis*. Proceedings of Mediterranean Conference on Control and Automation 2007, Athens, Greece.

Anna BZYMEK is PhD student in the Department of Fundamentals of Machinery Design at Silesian University of Technology at Gliwice. The main area of her interest are vision systems in diagnostic applications. She deals with signal processing, machine vision techniques, methods of image processing, analysis and recognition.

TECHNICAL STATE ASSESSMENT OF A LIGHT RAIL TRACK WEAR BASED ON TRAMWAY DYNAMIC MODEL

Bartosz CZECHYRA, Bartosz FIRLIK, Franciszek TOMASZEWSKI

Institute of Combustion Engines and Transport, Poznan University of Technology
ul. Piotrowo 3, 60-965 Poznań (PL); tel.: 0-61 665 20 23, fax 0-64 665 22 04
bartosz.czechyra@put.poznan.pl, bartosz.firlik@put.poznan.pl, franciszek.tomaszewski@put.poznan.pl

Summary

This article presents an approach of a technical state monitoring method in aimed to the railway track wear diagnostic and its influence on the rail vehicle dynamics. The method is based on the vehicle dynamic response measurements in order to determinate principle excitations and their influence on the vehicle ride safety. Measurements are performed with accelerometers and inclinometers mounted on the measuring bogie. In this paper, authors present assumptions, methodology, the most important results and conclusions of performed numerical and experimental research.

Keywords: track wear, dynamic response, tramway.

OCENA STANU TECHNICZNEGO ZUŻYCIA TORU TRAMWAJOWEGO
W OPARCIU O MODEL DYNAMICZNY LEKKIEGO POJAZDU SZYNOWEGO

Streszczenie

W artykule przedstawiono propozycję metody monitorowania stanu technicznego toru tramwajowego w aspekcie diagnostycznym oraz wpływ jego zużycia na dynamikę pojazdu szynowego. Prezentowana metoda bazuje na pomiarze odpowiedzi dynamicznej pojazdu w celu określenia zasadniczych wymuszeń oraz ich wpływu na bezpieczeństwo jazdy pojazdu szynowego. W pomiarach wykorzystano akcelerometry i inklinometry zainstalowane na wózku pomiarowym. W referacie autorzy zaprezentowali założenia, metodykę, najważniejsze wyniki oraz podsumowanie przeprowadzonych badań numerycznych i eksperymentalnych.

Słowa kluczowe: zużycie toru, odpowiedź dynamiczna, tramwaj.

1. INTRODUCTION

The increasing use of modern light rail systems requires increasing safety standards and, consequently, accurate railway tracks. In many polish cities, light rail track wear is one of the most important factor, deciding on the light rail vehicle running safety. That's why track wear should be frequently measured in order to define proper speed limits on each track section. Nevertheless it appears that there are no widely accepted criteria of light rail vehicle running safety on a worn track profile. Consequently the light rail transit industry frequently relies on practices developed primarily for heavy rail transit and railroad freight operations that are not necessarily well suited for light rail systems [5].

For surveying tasks in the context of rail construction, many different systems exist [e.g. 1, 4, 6]. Apart from still used conventional static methods, kinematic measuring systems become more important. The most popular class of a rail track measurement devices are the one-man-track-surveying trolleys, operating with speeds of up to one to three kilometers per hour. These are commonly used by the LRV operators in many cities all over the world. Unfortunately, these systems, that are very light (3-50 kg) could not be used to study the behavior of the rails under dynamic stress for different velocities.

For these reasons, Division of Rail Vehicles (Poznan University of Technology) developed a light rail track surveying platform in co-operation with Poznan Trams Operator – MPK Poznan (PL).

2. METHODOLOGY

In polish cities, the main wheel profile for light rail vehicles is a PST profile, presented in figure 1. There are two main rail profiles used for the light rail track. The UIC-60 rail profile is commonly used in straight track sections, and the Ri59N girder groove rail is used in curves.

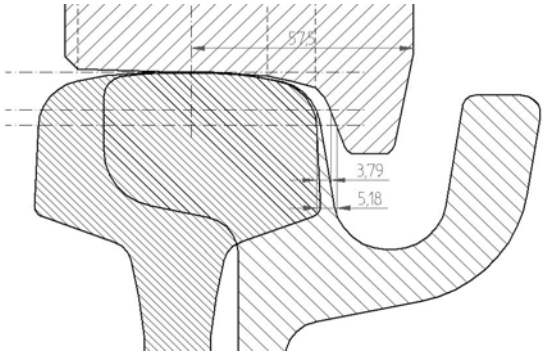

Fig. 1. Wheel/rail interface for LRV [3]

The combinations of wheel and rail profiles shown in figure 1 illustrate the various interface conditions that could be generated between the wheels and rails. The mathematical analysis has been conducted in order to understand the mechanisms involved in track and light rail by the vehicle interaction and their impact on vehicle safety. All geometric parameters in straight track and sharp curve were calculated from numerical CAD model analysis, using a Solid Edge software [3].

The basic assumptions of the presented method are:

1. The vehicle bogie is new (or after being refurbished) in order to insure constant and defined damping and stiffness parameters. Spring rate is the force per travel distance for the coil or chevron primary springs. This relationship is non-linear for long travel distances. The equivalent vertical, longitudinal, and lateral spring rates will be different.
2. The wheel profile is new, or without significant use, in order to insure stable vehicle ride on track. The wheel profile is one of the most critical vehicle parameters to consider in track design and the primary interface between the vehicle and the track structure.
3. The main modal parameters are identified. Trucks and car bodies have different natural frequencies that should also be considered. Also, car weight changes (due to different passenger load) affects the car body's natural frequency.

These assumptions guarantee, that all recorded vibrations, are due to the track wear, and not to the bogies structure faults.

3. NUMERICAL APPROACH

In order to better understand track wear influence on the vehicle dynamic response, a numerical model of the light rail vehicle was built in a simulation software Universal Mechanism (a Multibody System Dynamics package). Typical models used for rail dynamics consist of only 7 bodies. Such a model is not sufficient for a LRV, which commonly has an elastic bogie frame, that must be modeled in a different way (this elastic bogie frame ensure better ride stability on a worn track). That's why the created physical model, presented in figure 2, consists of 19 rigid bodies and 53 joint between them.

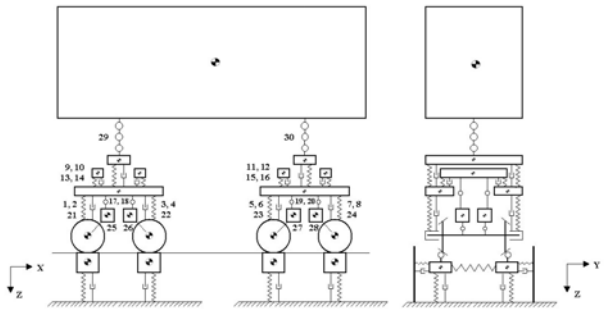

Fig. 2. Physical model of a LRV

The simulation model was created in Universal Mechanism software.

A validation of the main model parameters (natural frequency, stiffness and damping coefficients) took place on the real vehicle, by means of accelerometers and displacement sensors, performed in three stages:

1. Modal analysis of the vehicle bogie; in this research, a modal test was applied on the bogie structure, using an impact hammer, in order to determinate a Frequency Response Function (FRF) for all measuring points.
2. Wedge tests of the vehicle bogie; in this research, a quasi-static ride of a single bogie through different wedges of known geometry was performed. Measuring of wheelsets, bogie frame and motor beams acceleration permit to find a single bogie response on that kind of irregularities
3. Wedge tests of the entire vehicle; in this research, a quasi-static ride of the vehicle through different wedges of known geometry was performed.

After validating the most important model characteristic, many simulations were made, in order to find critical speeds, maximum force and maximum acceleration values under several track wear conditions – in straight track as well as in curved sections.

4. FIELD TESTS AND RESULTS

After validating all bogie parameters, ride tests of entire vehicle in normal operation tram regime were performed in the city of Poznan (PL), in order to find vehicle structure response on different kind of track irregularities. For this analysis, a measuring bogie was designed and built on the base of a standard 105N tram bogie (figure 3). Acquisition and data collection system based on a multianalyzer platform PULSE® made by Brüel & Kjær with portable data acquisition unit type B&K 3650C. That system version was fitted with a 5/1-ch. Input/Output Controller Module Type 7537 and a 12-ch in Dyn-X® technology. Input Module ensures synchronous measuring up to 17 input channels in wide frequency range from DC to

25,6 kHz [7]. Measurement system was equipped with an accelerometer set: type B&K 4504 (3 pieces), 4506, 4383 and 2 inclinometers for detection of a relative wheelsets rotation.

Fig. 3. Measuring test bogie equipped with measurement set

The first stage of this analysis, consists of testing the measuring bogie uncoupled from the carbody on different track irregularities, in order to calibrate all measuring devices, check and verify all the measuring system.

In the second stage, a measuring bogie was mounted under a standard tram and made few measurements on the tramway track in Poznan – measuring vehicle response to different track geometry, under several speed and load conditions. Representation of a tram ride via 30m curve in a vibration signal and inclinometer output is shown on figure 4.

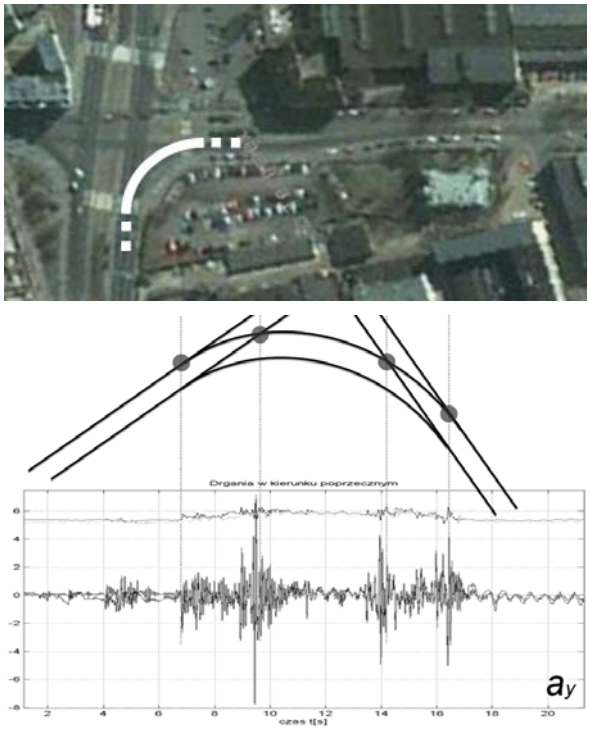

Fig. 4. Acceleration and wheelsets relative revolution signals recorded during a ride via 30m curve

Figures 5 and 6 shows the acceleration values, recorded in two axis (*y* and *z*) during a ride through the two kind of straight track section: worn and without significant use. Upper windows present time history of acceleration signal and lower windows include its spectra.

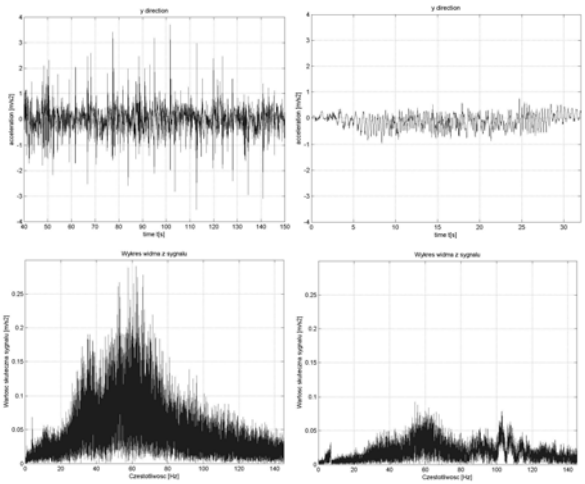

Fig. 5. Time history of acceleration signal and its spectra – *y* direct;
left – worn track
right – new track

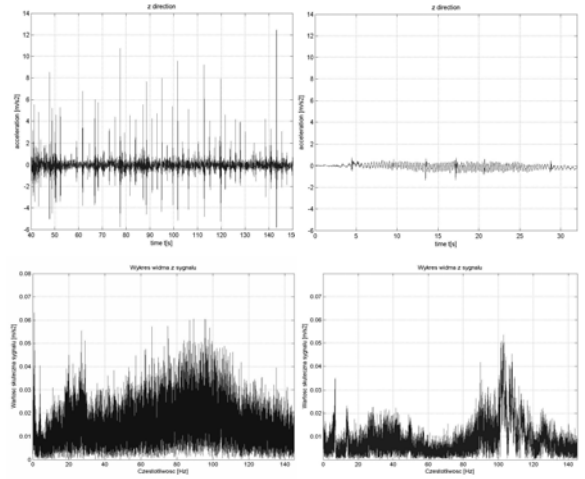

Fig. 6. Time history of acceleration signal and its spectra – *z* direct;
left – worn track
right – new track

Maximum horizontal acceleration values on a wheelset are 3.5 m/s^2 and maximum vertical acceleration values recorded in this curve are 12.5 m/s^2, but they do not cause a derailment of the measuring vehicle, in spite of the fact, that the limit value for a heavy rail vehicle is lower than this value [2]. In lower windows of the figures 5 and 6 are the analysis of a ride through the same track sections, but in frequency domain. In a 20-40 Hz frequency range an interesting signal component can be seen, that is not due to structure resonance (seen between 80-100 Hz in horizontal, and 60-80 Hz in vertical direction), but is related to track irregularities excitation.

5. CONCLUSION

The presented method is an approach of a technical state monitoring method in aimed to the railway track wear diagnostic and its influence on the rail vehicle dynamics. The analysis reveals, that there can be a relation between a track wear degree and an acceleration value of the wheelset. Frequency domain acceleration analysis could be use to determine some new, qualitative track wear global criteria for light rail track, based on RMS values in selected range. Detailed information about local irregularities can be taken from time history of acceleration and relative revolutions wheelsets signals.

The analysis shows also, that a light rail vehicle behavior on a worn track is different then for a heavy rail vehicle. It is due to different construction characteristic and destination of those vehicles, who must ride into sharp curves in city centers. Nevertheless, the derailment risk on the straight track is very low at speeds authorized for LRV (max. 70 km/h). In this situation, the most important and harder criterion in technical state assessment of a light rail track wear should be a human vibration comfort of riding.

This assumption is now verified for different track section.

REFERENCES

[1] Alippi C., Casagrande E., Scotti F., Piuri V.: *Composite Real-Time Image Processing for Railways Track Profile Measurement.* IEEE Transactions on Instrumentation and Measurement, vol. 49, no. 3, June 2000.
[2] EN 14363:2005, *Railway applications – Testing for the acceptance of running characteristics of railway vehicles – Testing of running behaviour and stationary tests.*
[3] Firlik B.: *Light Rail Vehicle Running Safety Analysis on a Worn Track Profile*, Ist International Interdisciplinary Technical Conference of Young Scientists InterTech'2008, 17-18.04.2008 Poznań.
[4] Madejski J., Grabczyk J.: *Continuous geometry measurement for diagnostics of tracks and switches.* International Conference on Switches: Switch to Delft 2002, Delft University of Technology, The Netherlands, 2002.
[5] *Transit Cooperative Research Program – Report 57, "Track Design Handbook for Light Rail Transit"* Transportation Research Board, National Research Council. National Academy Press, Washington, D.C., 2000.
[6] Wildi T., Glaus R.: *A Multisensor Platform for Kinematic Track Surveying.* 2nd Symposium on Geodesy for Geotechnical and Structural Engineering, May 21-24, 2002, Berlin.
[7] www.bksv.com

Bartosz CZECHYRA,
Dr. Eng., research scientist in Division of Railway Vehicles, Institute of Combustion Engines, Poznan University of Technology. Activities: vibro-acoustic diagnostics of the vehicles and its part, especially – an influence of a vehicle technical states on vibroacoustic climate evaluation.

Bartosz FIRLIK,
Dr. Eng., professor assistant in Division of Railway Vehicles, Institute of Combustion Engines, Poznan University of Technology. Activities: light rail vehicles dynamics, numerical methods in construction and optimization of rail vehicles

Franciszek TOMASZEWSKI,
DSc. Eng., Associate Professor, Head of Division of Railway Vehicles, Institute of Combustion Engines in Poznan University of Technology. Activities: vibroacoustic diagnostics of the vehicles and its auxiliary machines and devices, especially – technical state assessment and prediction process in diesel engines vibroacoustic diagnostics.

NEW TRENDS IN AIRPORT NOISE MONITORING SYSTEMS

Wiesław WSZOŁEK, Wojciech BATKO

Chair of Mechanics and Vibroacoustics, AGH University of Science and Technology
30-059 Kraków, Al. Mickiewicza 30, fax. (12) 636 23 14, wwszolek@agh.edu.pl, batko@agh.edu.pl

Summary

The identification process of acoustic events related to airport operations was assisted, in the existing monitoring systems, by joining noise monitoring stations with radar stations. Due to difficulties occurring in this communication system the equipment of the monitoring stations with tools allowing to recognise and classify independently the monitored noise source - will be advantageous. The concept of the application of advanced methods and techniques of artificial intelligence as analytical tools at monitoring noises originated by air traffic - is presented in the hereby paper.

Keywords: signal processing, artificial intelligence, pattern recognition.

NOWE TRENDY W SYSTEMACH MONITORINGU LOTNICZEGO

Streszczenie

W obecnych systemach monitoringu proces identyfikacji zdarzeń akustycznych związanych z funkcjonowaniem lotniska był wspomagany poprzez połączenie stacji monitoringu hałasu ze stacjami radarowymi. Z uwagi na występujące trudności w tym systemie łączności korzystnym byłoby wyposażenie stacji monitoringu w narzędzia pozwalające samodzielnie rozpoznawać i klasyfikować monitorowane źródło hałasu. W tej pracy przedstawiono koncepcję wykorzystania zaawansowanych metod i technik sztucznej inteligencji wykorzystywanych jako narzędzie analityczne przy monitorowaniu hałasu wywoływanego przez ruch lotniczy.

Słowa kluczowe: przetwarzanie sygnałów, sztuczna inteligencja, rozpoznawanie obrazów.

1. INTRODUCTION

Acoustic phenomena generated by various systems (biological, technical, related to environment, etc.) can be relatively precisely recorded and investigated by extracting acoustic parameters – both in the time and frequency domain. However, at attempts of practical applications a large number of difficulties - related to the interpretation of recorded data according to the practical needs – arise. Tasks of analysis and recognition of sound signals, which - as a residual process - are emitted by technical objects (which are to be recognised on the basis of these signals [5]), are very difficult. Finding the proper rule of the signal analysis or the proper algorithm of its recognition is really difficult [4]. This is caused by the fact, that atypical methods of signal parametrization as well as its categorization and classification are needed at the identification of technical objects by means of acoustic signals generated by them. The analysis and classification of acoustic signals generated by flying objects is discussed in the paper.

In addition, methods of signal analysis and signal recognition must be strictly adjusted to the specificity of the task being actually under testing. It seems worth mentioning, that this situation is completely different than the one occurring at a sound processing. Methods of low-pass and high-pass filtration, compression techniques or spectral transformation of sound signal algorithms neither depend on what kind of signal it is nor on the purpose of its recording and processing. Therefore the significant progress was achieved in the field of the sound signals processing and the worked out methods are of a universal character especially due to the availability of a cheap and convenient DSP methods. However, in tasks of analysis and recognition of sound signals a progress is much slower and a unification of methods meets a lot of problems. The main source of these difficulties is the fact that in nearly every task of signal analysis different features and parameters - strongly related to the specificity of the task and answering different questions - are to be exposed. In a similar fashion – in the signal recognition tasks - the criteria and aims of sound signals classification can be very different even for the same signals.

Standard methods of processing and classification of acoustic signals applied in diagnostics and classification are disappointing in all problems, in which we have to assess the noise arduousness, not the noise itself. Not standard analytical and signal interpretation methods, oriented to inferring the sound influence on human

organism and psyche and not the signal itself, are necessary. Application of an artificial intelligence can be included in those information methods, which are able to combine the possibilities of the traditional acoustic measurements technique with the requirements of modern monitoring systems of air noises. The aim of the presented paper is the investigation of effectiveness of those methods in the specific monitoring system of acoustic climate in the vicinity of one of the airports. Due to the difficulties in the existing communication system it would be advantageous to equip the monitoring station with tools allowing recognising and classifying independently the monitored noise source.

Methods originated from the artificial intelligence, which – in a natural way - are suitable for modelling vibroacoustic processes as well as for the classification of individual states and behaviour predictions can be applied for such, not standard, signal analysis. The presented hereby paper should determine the usefulness degree of picture recognition methods and neuron network technique in modelling natural reception processes and analysis of acoustic signals generated during the realization of the analysed technical process. They can also serve for the better understanding of differentiation criteria by means of the acoustic signals generated by these processes.

2. SPECIFICITY OF AN AIRPORT NOISE

Each aircraft flying above an observer emits a characteristic acoustic signal. This signal can constitute the basis for the recognition of the aircraft as well as the trajectory of its flight. As compared with environmental hazard caused by other sources the specificity of air noise is as follows [7], [6]:

- ✓ Noise influences relatively large areas.
- ✓ Aircrafts and helicopters are characterised by high levels of noise emission, but they are at a large distance from objects for which this noise is harmful.
- ✓ Propagation path of sound waves (acting from above) makes impossible the application of effective environment protections against noise, available e.g. in traffic noises.

Propagation of air noise in the environment is the most often determined by using calculation procedures (e.g. INM [1][3]). However, the basis for assessment of the noise arduousness around airports constitutes the measurement results. Such measurements are simultaneously performed in a few or a dozen or so characteristic points by means of the professional monitoring stations. Example of equipment applied in the measuring point is shown in Figure 1. The following parameters are the most often recorded in individual measuring points:

- time of event;
- sound exposure level l_{ae};
- maximal sound level l_{amax};
- equivalent sound level l_{aeq};
- duration of event t_{10};
- description of event (or eventual disturbances).

Fig.1. Typical localization of the monitoring station

Apart from recording the mentioned parameters in the monitoring system, additional information is necessary to explicitly describe the recorded acoustic event. In the case of recognizing air acoustic events (e.g. aircraft or helicopter flight) it is very difficult to find the proper principle of signal analysis or the proper algorithm of its recognition [7]. We limited ourselves in the hereby paper, to analysing acoustic events generated by aircrafts and helicopters during take offs and landings. The professional measuring equipment of the HHB, Bruel & Kjaer, Svantek Companies was applied for recording and processing of acoustic signals. The spectrum analysis in one-third-octave bands of the recorded acoustic signal in the frequency range from 20Hz to 8kHz (with time quantum Δt=0.5s) was performed for the preliminary signal processing. In this way the multispectrum W(j,k) of signals characteristic for the take off procedure was obtained (where: j – frequency coordinate, and k – time coordinate). Examples of spectra recorded in the airstrip region of the airport are shown in Figures 2 and 3. (For the sake of legibility only the dynamic spectrum fragment, corresponding to the observation time when the

[1] This method is contained in international regulations for the purpose of the Law of July 3rd 2002 – Air Law (the Journal of Law No 130, item 1112), especially in the document: Circular 2005 – AN/1/25/1988 ICAO and in the adapted for European conditions, accepted by the Directive 2002/49/WE document: ECAC CEAC Doc. 29, Report on Standard Method of Computing Noise Contours around Airports.

maximum level of sound A occurs, is presented in Figures).

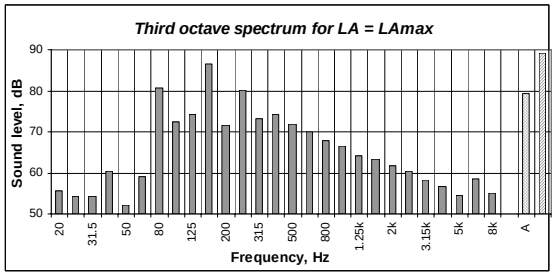

Fig. 2. Aircraft take off

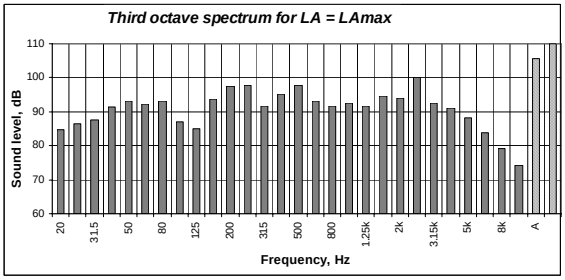

Fig. 3. Aircraft landing

Operations of taking off and landing recorded as acoustic patterns (Fig. 2 and 3), concern the same aircraft. As can be seen the patterns are quite different. Recording of helicopter noises were limited to three main phases of its flight: take off, flight and landing. Measuring microphones were placed in such a way that their axis was perpendicular towards the earth surface. Due to the specificity of helicopter noises the narrow-band analysis (Δf=const) of the recorded signal was also performed. The helicopter rotor and tail rotor are the main noise emitters. Significant participation has also engine (especially in helicopters of an older generation) and transmission systems. A singular feature of the noise spectrum emitted by a helicopter is its discrete character. The noise sources mainly decisive on its discrete characteristics are: helicopter rotor, tail rotor, transmission system and transmission gear. Within the noise spectrum of the helicopter rotor one can separate broadband noise and harmonic components (Fig. 4, Fig. 5).

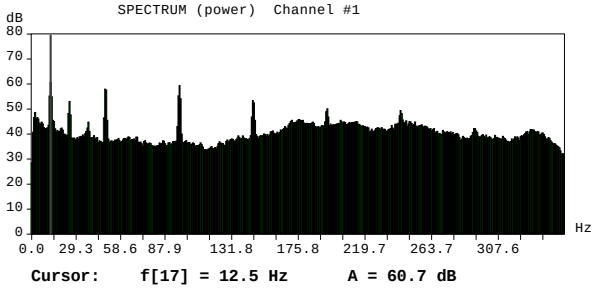

Fig. 4. Narrow-band spectrum of a 'small' helicopter during hovering

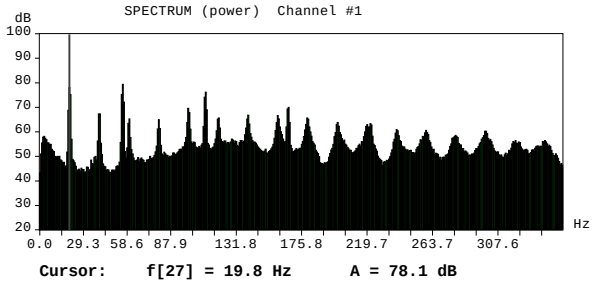

Fig. 5. Narrow-band spectrum of a 'large' helicopter during hovering

Such noise classification is a convenient instrument for the analysis of the obtained acoustic characteristics of the determined type of helicopter.

3. REQUIREMENTS TO BE MET BY THE CONTINUOUS MONITORING SYSTEMS OF AIR NOISE

The noise monitoring system can be directed towards various tasks depending on the needs. The tasks can be simple related only to the noise level estimation and environment protection or more difficult and complex corresponding to analysis and acoustic signals recognition, characterising acoustic events (e.g. noise related to flight of specific aircrafts and helicopters, flight trajectory). Finely, another essential task of the monitoring system can be the determination of the flight direction. More and more rigorous regulations concerning the permissible parameters of acoustic climate in the airports regions as well as the necessity of identification not only the facts of exceeding the permissible noise standards but also doers and circumstances of this violation are the reasons, that classic monitoring systems might not be sufficient. The listed tasks require quite different functions, measuring methods of acoustic pressure levels and completely different methods of the preliminary signal processing. „Classic" monitoring systems are based on known and standardised testing procedures and are most often directed towards continuous tracing of acoustic climate changes in the airport vicinity (Figure 6).

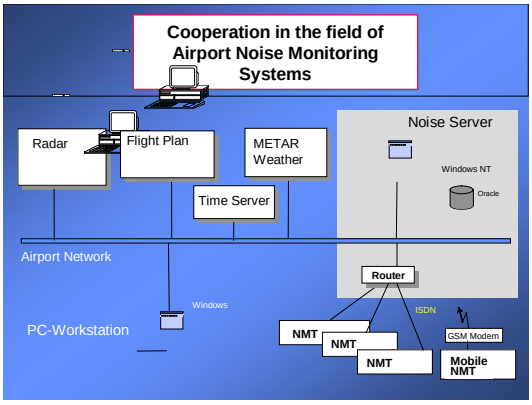

Fig. 6. Typical monitoring system of an airport noise

Those monitoring systems provide information on phenomena influencing acoustic climate in the area, on acoustic inputs related to operations of given objects, mutual superposition of signals generated by them, degree of noise arduousness and the hazardous state for inhabitants of the area. First of all they provide measurement data, which – by means of modern computer systems - can be used to obtain knowledge necessary for understanding acoustic phenomena occurring in the monitored area. Such knowledge extracted from 'raw' data is much more useful for developing the proper steps correcting the hazard caused by air transport. In diagnostics practice the environment state is monitored by applying identified diagnostic relations between the symptom under testing (space of signal feature) and its state. Formulation of such representation is extremely difficult, from the mathematic point of view, since those relations are often of a context character. Additional difficulties constitute measurement noises, which can lead to wrong diagnosis or non-explicit situations [1]. Not only acoustic parameters but also several flight and atmospheric parameters – influencing the noise propagation - should be taken into account in solving tasks related to air noise arduousness. Different, however also important, task of the monitoring system can be the determination of the flight direction needed sometimes for explicit assigning the responsibility for the disturbance to the given aircraft. This task can be realized by measuring phase differences of the measured signal (of frequency determined by the identification system of the flying object) in individual measuring microphones. The measuring system should be equipped with a special measuring probe. The photograph of the measuring probe is presented in Figure 7.

Fig. 7. Example of the measuring probe

4. RECOGNITION METHODS

The present situation in the field of a pattern recognition is briefly described below. There are many theories of a pattern recognition, which are dealing with an abstract pattern notion, understood as a set of certain features and relations. Several algorithms and instruments recognizing certain determined classes of objects were developed. However, in practical applications, it is not clear which features and relations should be assumed as the basic ones and how to single them out from the recognised patterns. It was assumed, that in order to obtain features needed at the recognition, the preliminary signal processing should occur in an identical fashion just as in visual and audio systems of humans. Out of several known recognition methods the minimum-distance methods were chosen. From this group of methods the Nearest Neighbour (NN) and the Nearest Mode (NM)[RT] methods were used. The classic neuron network of the multilayer perceptron type - taught by means of the back-propagation method – were also applied in investigations. It was assumed that networks used for the recognition and classification of collected vibroacoustic signals contain the input and output layer and at least one hidden layer. In the case of the multilayer network the input layer contains the same number of neurons as the number of coordinates of the assumed feature vector.

5. THE OBTAINED RESULTS

The objects intended for the recognition were aircrafts and helicopters the most often flying in Poland. The noise analyses were limited to the selected aircrafts (B737, ATR72, MD 80, AN24) and helicopters (small, medium and large). The analysis of the acoustic signal emitted by aircrafts was oriented to the recognition of the acoustic event doer. Many variants of the feature vector were considered in particular stages of investigations. Discussion on the correctness of the space of features selection was disregarded in this paper – since it was included in previous papers [6], [7]. Two variants of the feature vector are defined as follows:

$$<f_1, f_2, ...,f_{29}> = X_1 \quad (1)$$

where: f_i – averaged level values in the i-th frequency band,

Δf – widths of one-third-octave band,

and

$$< M_0, M_1, M_3> = X_2 \quad (2)$$

where: M_0, M_1, M_2 – spectrum moments

Table 1. Recognition results of aircrafts and helicopters

Methods of recognition	Recognition correctness, %		
	Propeller aircraft	Jet aircrafts	Helicopters
Nearest neighbour(NN)	86	85	87
Nearest Mode (NM)	87	88	88
Neural networks	96	97	97

Table 2. Recognition results of various types of aircrafts and helicopters

Object name	Recognition correctness, %	
	Method of pattern recognition (NM)	Neuron networks (BP)
B 737	79.7	95.7
MD 80	80.3	95.4
ATR 72	81.7	94.8
AN 24	80.9	96.1
Large helicopter	74.8	85.5
Medium helicopter	73.9	84.1
Small helicopter	75.1	86

6. CONCLUSIONS

The results of the aircrafts and helicopters recognition, obtained during many years of investigations with an application of the pattern recognition and neural networks techniques - are presented in the paper. It might be assumed – on the basis of these results – that recognition methods using neuron networks are more useful in the classification of flying objects. Analysis of the results achieved in successive investigation stages (modification of the signal preliminary processing method, modification of the feature space and topology of neural networks) confirms that it is possible to obtain better classification results of objects - on the basis of the generated acoustic signal. The presented research is of a practical aspect since the results were obtained by means of testing real acoustic signals. The developed algorithms and models can be directly applied in constructing new algorithms assisting the identification process of aircrafts and helicopters as well as other acoustic events. The algorithms can be implemented in already existing acoustic monitoring systems, as sub-assemblies of automatic recognition of acoustic events systems. In further stages of the research heading for obtaining higher recognition efficiency in existing systems the methods of the preliminary signal processing as well as its analysis can be modified (e.g. modification of a feature vector).

REFERENCES

[1] Wojciech BATKO, Witold CIOCH, Ernest JAMRO: *Monitoring system for grinding machine of turbine-engine blades*, Journal of Polish CIMAC; ISSN 1231-3998. – 2007 s. 37–42.

[2] Z. Engel (edit.): *Wibroakustyka maszyn I środowiska*, Wiedza i Życie, Warszawa 1995.

[3] Guding, Olmstead, Bryan, Mirsky, Fleming, Gerbi, D'Aprile: *Integrated Noise Model (INM)* Version 6.0 User's Guide, Office of Environment and Energy, September 1999, Washington DC.

[4] Tadeusiewicz R., Flasiński M.: *Rozpoznawanie obrazów*, Wydawnictwo Naukowe PWN, Warszawa 1991.

[5] Tadeusiewicz R., Wszołek W., Izworski A.: *Classification of acoustic and vibration signals by the artificial intelligence methods*. Sixth International Congress on Sound and Vibration, 5-6 July 1999, Copenhagen, Denmark, pp 3181-3188.

[6] Wszolek W., Tadeusiewicz R., Chyla A.: *Recognition of selected helicopter types based on the generated acoustic signal with application of artificial intelligence methods*, InterNoise 2001, Hague 2001, pp. 2217-2220.

[7] Wszołek W., Engel Z., Chyla A., Wszołek T.: *Założenia do opracowania systemów monitorowania hałasu śmigłowców*. Mat. XXX Zimowej Szkoły Zwalczania Zagrożeń Wibroakustycznych, Gliwice-Wisła, 2002, s.151-159.

Dr inż. **Wiesław WSZOŁEK**, absolwent Wydziału Elektrotechniki, Automatyki, Informatyki i Elektroniki Akademii Górniczo - Hutniczej w Krakowie. Pracę doktorską dotyczącą analizy i rozpoznawania sygnałów akustycznych w procesach wibroakustycznych obronił na Wydziale Inżynierii Mechanicznej i Robotyki AGH w Krakowie. Jest pracownikiem Katedry Mechaniki i Wibroakustyki AGH na stanowisku adiunkta. Prowadzi prace badawcze dotyczące zastosowania metod sztucznej inteligencji w problemach analizy i rozpoznawania sygnału mowy, ze szczególnym uwzględnieniem mowy patologicznej.

GRINDING WHEELS DEFECTS DETECTION USING NATURAL VIBRATION ANALYSIS

Włodzimierz FIKS, Andrzej ZORA

Politechnika Łódzka, Wydział Mechaniczny, Katedra Technologii Maszyn
1/15 B. Stefanowskiego str. 90-924 Łódź, Poland, tel. (042) 631-22-88, e-mail: fixwl@p.lodz.pl

Summary

In the paper defects detection method in grinding tools has been presented. The vitrified bonded grinding wheels have been put on tests due to their common usage in industry. For the examination The Dynamic Elastic Properties Analyser (DEPA) has been applied. The vibrations have been generated using Impulse Excitation Technique (IET). The tests which have been carried out proved that defects occuring in the grinding wheels cause the drop of natural vibration frequency value and distinct change of the damping curve slope angle, which allows to determine the grinding wheel defect grade. The application of this method in industrial practice can influence in the significant way work safety improvement while using these tools.

Keywords: grinding wheels, defects detection, natural vibration, frequency, damping curve.

ZASTOSOWANIE ANALIZY DRGAŃ WŁASNYCH DO WYKRYWANIA USZKODZEŃ ŚCIERNIC

Streszczenie

W artykule przedstawiono metodę wykrywania uszkodzeń w narzędziach do szlifowania. Badaniom poddano ściernice o spoiwie ceramicznym ze względu na ich powszechne stosowanie w przemyśle. Do badań wykorzystano Dynamiczny Analizator Właściwości Sprężystych (DEPA). Drgania były generowane wykorzystując technikę wzbudzenia impulsowego. Przeprowadzone badania wykazały, że występujące w ściernicy uszkodzenia powodują spadek wartości drgań własnych oraz wyraźną zmianę kąta pochylenia krzywej tłumienia, co pozwala na określenie stopnia uszkodzenia ściernicy. Zastosowanie tej metody w praktyce przemysłowej może w istotny sposób wpłynąć na poprawę bezpieczeństwa pracy tymi narzędziami.

Słowa kluczowe: ściernice, wykrywanie uszkodzeń, drgania własne, częstotliwość, krzywa tłumienia.

1. INTRODUCTION

To provide the operational reliability of applied tool during machining operations carried out in metal industry is one of the basic conditions for ensuring industrial safety. Its break-down, especially when cutting is in progress, when the tool is in contact with material and (most often) rotates with high speed, may cause workpiece or machine tool damage and – what is most important – threat safety of worker operating the stand as well as other persons working nearby.

This problem gains special importance in grinding process which characterizes significant higher cutting speed in comparison with other machining techniques. As a result there are big centrifugal forces acting on the tool during work. The problem becomes multiplied in new machining techniques (e.g. High Speed Grinding – HSG) [1] being applied more and more often, where the tool works with high tangential velocity. The full usage of HGS advantages is possible only with application of proper construction grinding machines and proper abrasive tools. The grinding wheels play here special role because they must be characterised by high strength preventing the grinding wheel disruption under the centrifugal forces within working rotation speed. The grinding wheels made of regular boron nitride (CBN) consist of body of high mechanical resistance and coat on it thin abrasive layer as well as vitrified bonded grinding wheels because of easy shaping of the grinding wheel cutting surface have found wide application in this process [2]. In addition in tests it has shown [3] that the grinding wheels of sintered corundum can be useful in HSG process with tangential velocity $v_s \cong 125$ m/s, particularly in batch production. It has an effect on number of the grinding wheels made of Al_2O_3 properties such as: significantly lower price, geometrical and topographical flexibility etc.

Insufficient grinding wheel strength, incorrect tool selection or disregard of safety rules can lead to grinding wheel damage and its emergency failure. Taking into consideration enormous kinetic energy which has the tool rotating with the high speed such accident may cause serious hazard for health or even worker's life.

Importance of the tool reliability in grinding process, in comparison with other machining techniques, results from its structure. Despite of generating new construction solutions of grinding

tools vitrified bonded grinding wheels continually play important role. In comparison with other bonds types vitrified bonded grinding wheels characterize such properties as:

- easy shaping of grinding wheel cutting surface;
- modification possibility of tool properties in dressing process and its adjustment to specific technological task;
- high abrasive wear resistance ;
- controllable in wide range porosity (in production phase).

The enumerated features cause that vitrified bonded grinding wheels in nearly every branch of industry are in common use and good cutting properties cause that most construction materials used nowadays can be machined with grinding wheels of this type. However applying for treatment vitrified bonded tools, characteristic feature of the material they are made of, conditions of their production as well as grinding process parameters must be taken into consideration.

The material that grinding wheels are made of can be considered as a composite material – i.e. agglomerated mixture of abrasive grains and bond. During grinding wheel manufacturing, after components mixing stage follows putting them into a mould, pressing and then annealing of the grinding wheel. Such a creation process of the tool body causes considerable difficulties in programming, and next in achieving expected material properties. It concerns particularly strength properties of the tool and its hardness. Because of this reason essential parameters determination of the grinding wheel is possible only by testing already accomplished tool.

Except applied materials and the tool manufacturing technology, the tool structure continuity (cracks, crush dressings, scratchs etc.) has essential influence on its strength properties. Commonly used methods of the grinding tools testing based on accelerating the grinding wheel to specified speed of rotation on special disrupting devices. Most often they are destructive tests or violating the tool structure [4], and also relatively expensive taking into consideration applied testing devices. That is why searching for another, simplier and cheaper method for strength properties determination of the grinding tools is needed.

2. RESEARCH METCHOD

The grinding wheel properties determination is possible by using adequate research techniques. Commonly known method using natural vibration frequency analysis of the tested object and subsequently on this base allowing to determine among others modulus of elasticity is one of these ways [5].

The fundamental dependence defining Young's modulus has the form:

$$Y_m = C\frac{m_s}{R^2} \tag{1}$$

where:

C – shape coefficient of tested object;
m_s – object mass;
R – value of the object natural vibration frequency.

In carried out experiments of properties testing of vitrified bonded grinding wheels The Dynamic Elastic Properties Analyser (DEPA) which is the advanced system for testing the elastic properties materials and products, using Impulse Excitation Technique (IET) has been used.

Principle of system operation is based on versatile analysis of induced in sample vibrations using Fast Fourier Transformation (FFT). Complete frequency representation of vibration signal (within a range from 0 to 11000 Hz) as FFT chart is displayed on the screen. In addition resonance frequency and signal damping curve are also displayed. On the screen except am. courses, depending on the carried out tests type, following parameters are determined and immediately displayed:

- Young's modulus;
- shear modulus;
- Poisson's ratio;
- grinding wheel hardness.

Possibility of the run analysis of vibration amplitude damping curve present in DEPA system allows to detect occurring material inhomogeneity of tested objects. If in tested sample any defects (cracks, cavities, etc.) appear they would damp vibration energy higher, what would be presented by higher value of damping coefficient than for the homogeneous material. If for two similar samples different damping coefficients occur it is the signal, that in the one of them hidden defects appeared.

Possibilities of DEPA system presented above allow to determine parameters defining grinding wheels material properties, necessary for their strength (Young's modulus, Poisson's ratio, density) and hardness calculation as well as possible damages detection.

3. TESTS RUN

The tests have been carried out on vitrified bonded grinding wheels produced in ANDRE Abrasive Articles, of different shapes and technical characteristics, using described above DEPA system.

3.1. Data logging of natural vibration run excited in grinding wheel

Vitrified bonded grinding wheels made of different abrasive materials (99A, CrA, 98C), diversified grain size (46, 60, 80) as well as different hardness (I, K, M) have been put on tests. The tests have been carried out on several grinding wheels making five repetitions for every one of

them. Hardness classes determined basing on the tests have been compatible with listed on grinding wheels characteristics (specified using model sand method). The example run of recorded grinding wheel vibration with characteristic 180x13x32 99A 60 I V-35 is shown at Fig. 1.

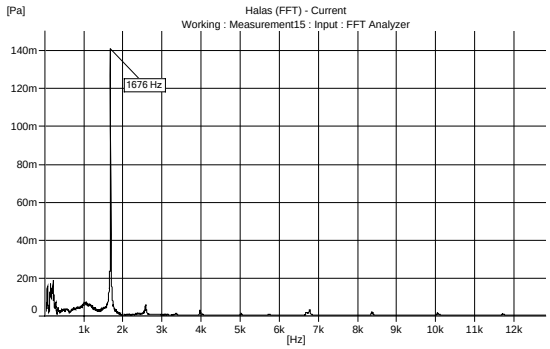

Fig. 1. FFT run of tested grinding wheel vibration

Characteristic feature of all analysed FFT runs for disc grinding wheels has been occurrence of one distinct peak of defined frequency. It testify that in this grinding wheels type homogeneous natural vibration are present, which means that there is possibility to determine properties of the grinding wheel material precisely enough.

3.2. Detection of the grinding wheel damages

The first signal informing about grinding wheel material inhomogeneity are different frequencies of natural vibrations recorded while testing depending on the excitation spot by the external impulse. In homogeneous grinding wheels the excitation spot has no influence on acquired values of natural vibration frequency.

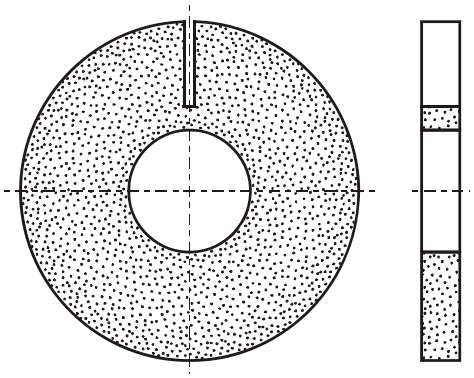

Fig. 2. Grinding wheel damage simulation by making radial kerf

In order to examine the grinding wheel damages influence on the natural vibration frequency value and the vibration damping curve run the purposely damaged grinding wheel with characteristic 180x13x32 99A 60 I V-35 has been put on tests. The grinding wheel damage consists of making kerf of different length along its radius (Fig. 2). The acquired results are presented below in table 1 and in Fig. 3 and 4.

Table 1. The grinding wheel damage influence on frequency and slope angle of damping curve

	Kerf length [%]	Frequency [Hz]	Slope angle of damping curve
1	0	1676	5,7
2	25	1653	9,5
3	50	1602	26,5
4	75	1326	68,2
5	95	867	87,1
6	100	598	87,7

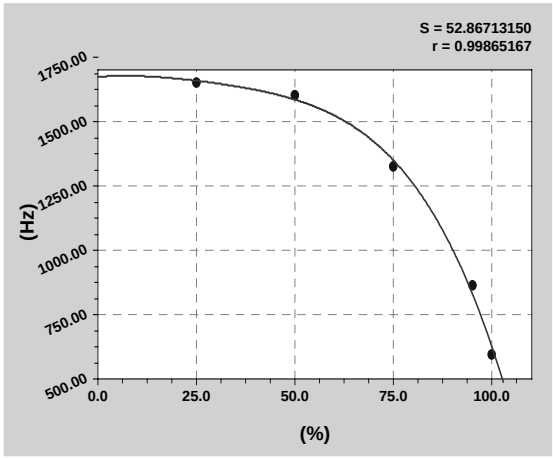

Fig. 3. The natural vibration frequency dependence on grinding wheel defect degree

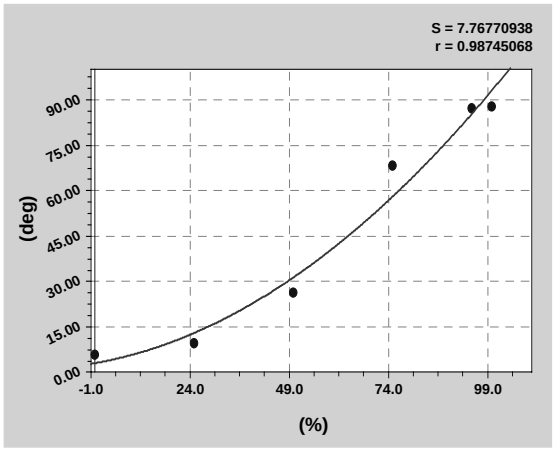

Fig. 4. The Slope angle of a damping curve dependence on grinding wheel defect degree

From presented results it can be clearly seen that simultaneously with the grinding wheel damage degree increase the natural vibration frequency of the grinding wheel decrease and significantly grows damping of these vibrations.

Cases of the grinding wheels defects which origin during their manufacturing (slight cracks) have been also detected during the grinding wheel tests carried out tests in ANDRE Abrasive Articles. The occurring cracks have caused drop of the

Young's modulus value determined for these grinding wheels. For example "proper" grinding wheel with characteristic 1-200x20x32 98C 46 K has determined Young's modulus value egual 47,2 GPa, whereas for defected grinding wheel Y_m=40,4 GPa has been achieved.

4. CONCLUSION

The results achieved during the carried out tests alow to formulate the following conclusions:

1. DEPA system which has been applied for testing is an easy-to-operate, universal tool for non-destructive evaluation of tested materials properties, also in such complex cases as composite materials of vitrified bonded grinding wheels.
2. For shapes defined in system DEPA high repeatability of basic parameters values describing grinding wheels material properties such as : natural vibration frequency, Young's modulus, density and hardness have been achieved.
3. The analysis of the damping curve run of grinding wheels natural vibration makes possible to detect defects occuring in grinding wheels, and as a result its application in industrial practice can influence in the significant way work safety improvement while using these tools.

REFERENCES

[1] Oczoś K.: *Charakterystyka trendów rozwojowych szlifowania ściernicowego.* Sekcja Podstaw Technologii Komitetu Budowy Maszyn PAN, XXIII Naukowa Szkoła Obróbki Ściernej. Rzeszów – Myczkowce, 2000, s. 13-62.

[2] Klocke F., Konig W.: *Apropriate conditioning strategies increase the performance capabilities of vitrified-bond CBN grinding wheels*. Ann. CIRP 44/1/1995, s. 305-310.

[3] Minke E., Brinksmeier E.: *The use of conventional grinding wheel in high-performance grinding processes.* Proc. 1st Int. Machining and Grinding Conference. Dearborn, USA,1995.

[4] Fiks W.: *Wytrzymałość ściernic ze spoiwem ceramicznym.* Zeszyty naukowe nr 895 Politechniki Łódzkiej, Wydawnictwo Politechniki Łódzkiej, Łódź, 2002.

[5] Konig W., Follinger H.: *Elasticity modules of grinding wheels and its impact on their in-process behaviour.* Ceramic Forum International vol. 6-7, 1987.

Włodzimierz FIKS, assistant professor, PhD, engineer, professor of The Technical University of Łódź. He obtained doctor's degree in 1981, in 2003 he was qualified as assistant profesor in the field "Machine building and Production Engineering". Employed at the professor's post at The Technical University of Łódź since 2007. He specialize in matters connected with abrasive treatment processes as well as abrasive tools resistance.

He is the author of the monograph "The resistance of vitrified bonded grinding wheels", coauthor of 3 textbooks, author or coauthor of tens articles and several elaborations for industry including 4 implemented devices construcions for dynamic resistance testing of grinding wheels. He is also the author of new method for grinding wheels resistance testing, applicating for patent in The patent Office of RP nr P-379924.

Andrzej ZORA, PhD, engineer. He obtained doctor's degree in 1998, in the field "Machine building and Production Engineering". Employed at The Technical University of Łódź since 1988. He specialize in matters connected with abrasive treatment processes monitoring as well as abrasive tools conditioning.

He is the coauthor of 2 taxtbooks, author or coauthor of several articles. He is also the coauthor of new method for evaluation of grinding wheel cutting ability.

EVALUATION OF THERMAL STATE IN REACTOR DURING PLASMA PYROLYSIS OF POLYMERS

Jarosław SZUSZKIEWICZ

Katedra Technologii Materiałów i Maszyn
ul. Oczapowskiego 11, 10-736 Olsztyn, fax. 089 523 44 65, jerry@uwm.edu.pl

Summary

Thermal conditions existing in the reactor, especially around the plasma jet, greatly influence on the course of the plasma pyrolysis including synthesis of derivative compounds. Measurements of the temperature distribution in the reactor will be helpful in carrying out the experiment of the plasma pyrolysis of polymers and also will be utilized to build the model of the plasma pyrolysis.

Keywords: plasma pyrolysis, temperature, thermal conditions, polymer.

OCENA STANU CIEPLNEGO W REAKTORZE PODCZAS PIROLIZY PLAZMOWEJ POLIMERÓW

Streszczenie

Warunki termiczne panujące w reaktorze, szczególnie w otoczeniu strumienia plazmy, mają istotny wpływ na przebieg pirolizy plazmowej, w tym na syntezę związków wtórnych. Pomiar rozkładu temperatury w reaktorze będzie pomocny w przeprowadzaniu eksperymentu pirolizy plazmowej polimerów, a także posłuży do budowy modelu pirolizy plazmowej.

Słowa kluczowe: piroliza plazmowa, temperatura, warunki termiczne, polimer.

1. INTRODUCTION

In the paper the temperature distribution during plasma pyrolysis of polymers was examined. Rubber waste was subject to plasma pyrolysis.

The thermal transformations occurring at temperatures of thousands and even tens of thousands of Kelvin are the basis of the phenomena ruling plasma pyrolysis. It seems reasonable to assume that the reactions of thermal decomposition of rubber powder will take place inside of the plasma jet (13000 K [1]), and reactions between plasma pyrolysis byproducts will take place outside the plasma jet, that is in the plasma reactor. That is why it is important to know the temperature distribution in the plasma reactor to anticipate what processes might occur inside the reactor. The knowledge of the temperature distribution will enable controlling plasma pyrolysis in more precise way.

2. EXPERIMENT SET-UP

For the measurement of the temperature in the plasma reactor [2] a thermometer EMT – 07 was used. The principle of its operation is based on thermocouples [3]. The temperature measured by that thermometer ranges from 190 K do 1500 K.

The temperature was measured in the four cross-sections of the plasma reactor, I-IV (fig. 1).

The cross-section I was established right over the nozzle of the plasmatron, prior to the outlet of the plasma jet, in the place out of the direct influence of the plasma jet. The cross-sections II and III were established to measure the space, where samples of gas products are taken to the analysis. The measurement in the cross-section IV was established to evaluate the temperature of gas outgoing from the reactor. Regarding to relatively small diameter of the outlet opening (60 mm) of the reactor, the thermocouple was inserted to the cross-section IV at angle (15 - 30°).

The thermocouples were inserted into the plasma reactor through openings, which were secured to limit the presence of ambient air inside of the reactor.

The gas temperature in the cross-section I was measured in the selected points in the distance of 4 cm to 14 cm to the longitudinal axis. In the cross-sections II and III the temperature was measured in the axis and points distant to the axis from 1cm to 14 cm. In the cross-section IV the gas temperature was measured only in two points – in the longitudinal axis of the plasma reactor and in the distance of 3 cm of the axis.

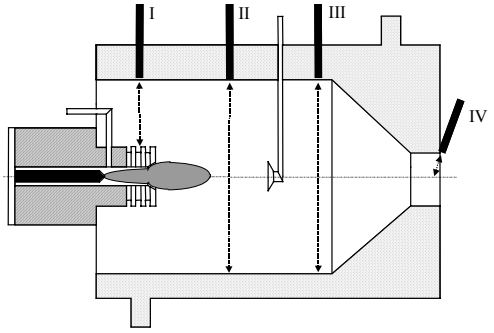

Fig. 1. Scheme presenting the cross-sections in the reactor where the temperature was measured

3. RESULTS

The temperature distribution in the cross-section I of the plasma reactor is presented in the fig. 2. The measurement was carried out for Ar plasma (gas flow rate Q=5808 l/h, current I=500 A, no rubber - g=0 kg/h). According to the fot. 2 it follows that the temperature in the plasma reactor decreases while the distance to the longitudinal axis increases. The maximum temperature in that cross-section equals to 621 K.

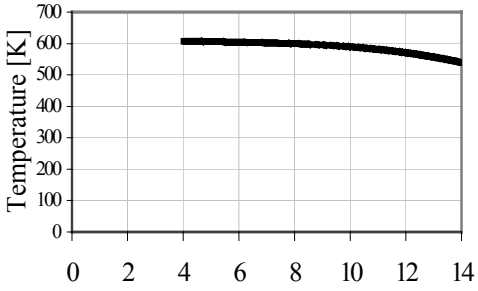

Fig. 2. Temperature distribution in the cross-section I of the reactor: Ar plasma, Q=5808 l/h, I=500 A, g=0 kg/h

In the cross-section II four series of measurements were carried out: for "clean" Ar plasma (Q=5808 l/h, I=500 A, no rubber), for "clean" Ar + 5.9 % H_2 plasma (Q=5538 l/h, I=500 A, no rubber) and during the plasma pyrolysis of the rubber powder in Ar plasma (Q=5808 l/h, I=500 A, g=4.39 kg/h) and in Ar + 5.9 % H_2 plasma (Q=5538 l/h, I=500 A, g=4.39 kg/h). The temperature distribution in the cross-section II is presented in the fig. 3. It results from the figure, that the temperature inside of the plasma reactor increases while approaching to the axis of the reactor. However, in the axis of the plasma reactor the temperature is lower than it is nearby (from 18 K to 85 K in the examined range of work parameters of the plasmatron). It seems that the reason of the decrease of the temperature in the axis of the reactor is relatively small distance of the cross-section II from the outlet of the plasma jet from the nozzle-anode of the plasmatron. That decrease of the temperature might be caused by the huge axial velocity of the plasma operating gas, gas transporting the rubber powder and outgoing gas flow rate. The maximum temperature in the cross-section II occurred for "clean" Ar + 5.9 % H_2 plasma. It is equal to 1096 K.

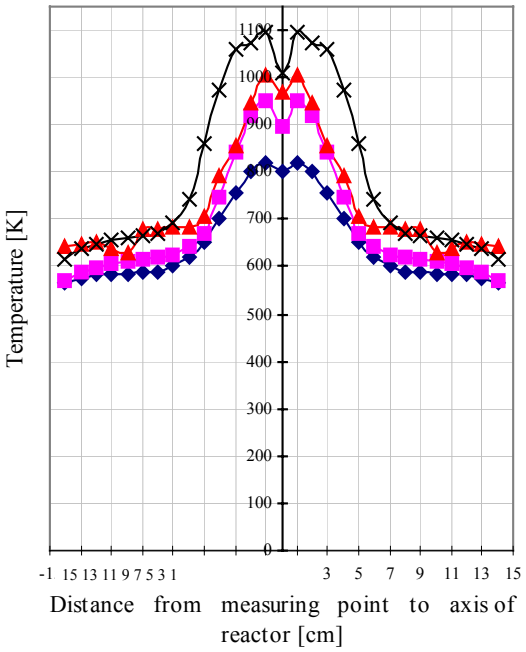

Fig. 3. Temperature distribution in the cross-section II of the reactor:

- Ar plasma (Q=5808 l/h, I=500 A)
- Ar plasma (Q=5808 l/h, I=500 A, g=4.39 kg/h)
- Ar + 5.9 % H_2 plasma (Q=5538 l/h, I=500 A)
- Ar + 5.9 % H_2 plasma (Q=5538 l/h, I=500 A, g=4.39 kg/h)

In the cross-section III also four series of measurements were carried out, i.e. for "clean" Ar plasma (Q=5808 l/h, I=500 A, no rubber), "clean" Ar + 5.9 % H_2 plasma (Q=5538 l/h, I=500 A, no rubber) and for the plasma pyrolysis of the rubber powder in Ar plasma (Q=5805 l/h, I=500 A, g=4.39 kg/h), Ar + 5. % H_2 plasma (Q=5538 l/h, I=500 A, g=4.39 kg/h). The results of the measurements in the cross-section III of the plasma reactor were shown in the fig. 4. The temperature distribution in the cross-section III does not have a minimum in the axis of the reactor. In the cross-section III the temperature in the axis is maximal and it equals 848 K. The reason of that state is fact that the cross-section III is situated almost in twice longer distance away from the outlet of the plasma jet from the nozzle-anode than the cross-section II. The lowest temperature (573 K) was registered along the walls of the reactor for the pyrolysis of the rubber powder in Ar plasma (Q=5808 l/h, I=500 A, g=4.39 kg/h), and highest for "clean" Ar + 5.9 % H_2 plasma (Q=5538 l/h, I=500 A, g=0 kg/h).

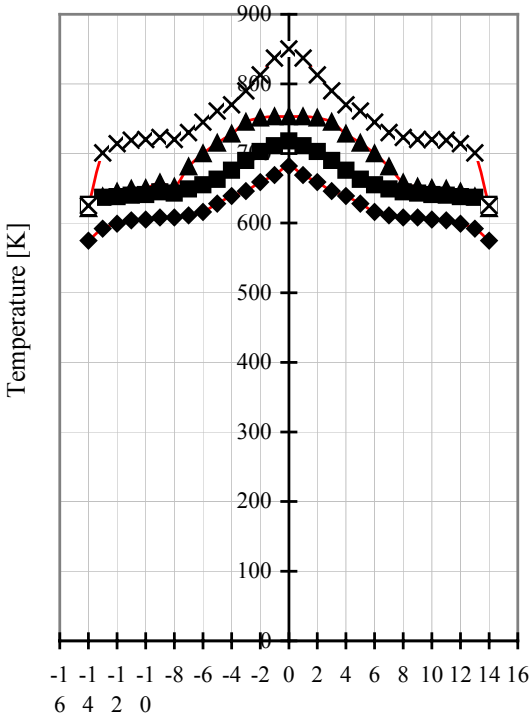

Fig. 4. Temperature distribution in the cross-section III of the reactor:
- Ar plasma (Q=5808 l/h, I=500 A)
- Ar plasma, (Q=5808 l/h, I=500 A, g=4,39 kg/h)
- Ar + 5,9 % H_2 plasma (Q=5538 l/h, I=500 A)
- Ar + 5,9 % H_2 plasma (Q=5538 l/h, I=500 A g=4,39 kg/h)

In the cross-sections II and III similar influence of work parameters of the plasmatron on change of temperature was observed: injection of the rubber powder into the plasma jet was causing the decrease of the temperature in the reactor and adding of H_2 to the plasma operating gas was increasing the temperature.

In the cross-section IV of the reactor, i.e. nearby the outlet of the reactor, the temperature was measured only in two points, because of its small diameter. The first measuring point was established in the axis of the reactor, and the second in the distance of 3 cm away from it. The temperature was measured for "clean" Ar plasma (Q_1=5325 l/h, I_1=500 A and Q_2=6970 l/h, I_2=500 A; in both cases with no rubber powder in the plasma jet), for "clean" Ar + 5.9 % H_2 plasma (Q=5538 l/h, I=500 A, no rubber), for the pyrolysis of the rubber powder in Ar plasma (Q_1=5325 l/h, I_1=500 A and Q_2=6970 l/h, I_2=500 A; g=4.39 kg/h in both cases) and Ar + 5.9 % H_2 plasma (Q=5538 l/h, I=500 A, g=4.39 kg/h). The results of the measurements were presented in the fig. 5.

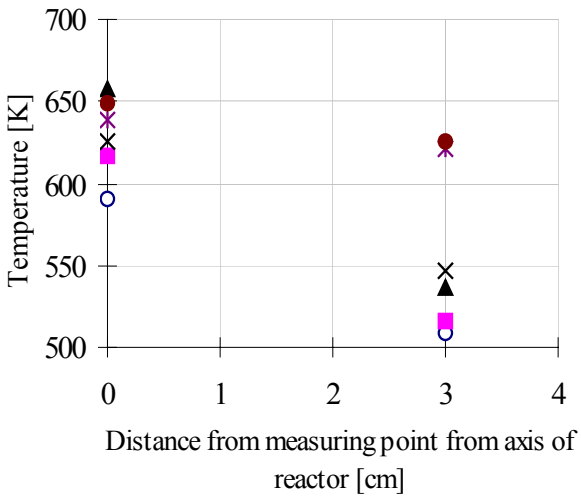

Fig. 5. Temperature distribution at the outlet of the reactor (cross-section IV):
- ▲ - Ar plasma (Q_1=5325 l/h, I_1=500 A)
- ■ - Ar plasma (Q_2=6970, I_2=500 A)
- × - Ar plasma (Q_1=5325 l/h, I_1=500 A, g_1=4.39 kg/h)
- ○ - Ar plasma (Q_2=6970 l/h, I_2=500 A, g_2=4.39 kg/h)
- ✳ - Ar plasma + 5.9 % H_2 (Q=5538 l/h, I=500 A)
- ● - Ar + 5.9 % H_2 plasma (Q=5538 l/h, I=500 A, g=4.39 kg/h)

The lowest temperature (509 K) appeared in the distance of 3 cm from the axis of the plasma reactor for the case of the pyrolysis of the rubber powder in Ar plasma. At the same time it is the lowest registered temperature in the reactor. The highest temperature (657 K) was registered at the axis of the reactor for "clean" Ar plasma (no rubber). The influence of the work parameters of the plasmatron on the temperature in cross-section IV was different than in the cross-sections II and III: the temperature measured during the pyrolysis of the rubber powder in Ar and Ar + 5.9 % H_2 plasmas is higher than the temperature registered for "clean" Ar and Ar + 5.9 % H_2 plasmas. The difference could have been caused by the direct contact of the outgoing gas from the reactor with the surrounding atmosphere. It is important to pay attention to slight differences between the measured temperatures nearby the outlet of the reactor.

The longer the distance from the plasma jet in the longitudinal axial direction of the reactor was, the lower the temperature occurred. That dependence is illustrated in the fig. 6.

In order to examine the influence of the plasmatron power on the temperature in the reactor, two series of measurements were carried out for: "clean" Ar plasma (Q=5808 l/h, no rubber) and plasma pyrolysis of the rubber powder in Ar plasma (Q=5808 l/h, g=4.39 kg/h).

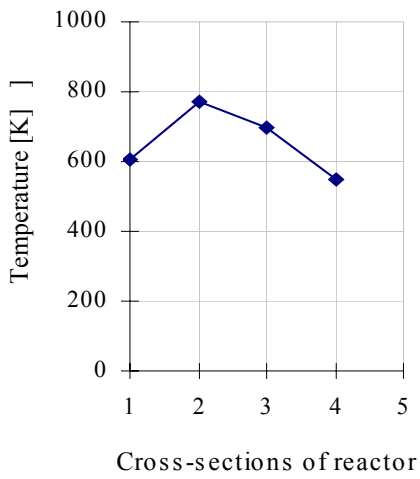

Fig. 6. Temperature distribution in the reactor along its longitudinal axis for Ar plasma (Q=5808 l/h, I=500 A, g=0 kg/h). The temperature measured in the distance of 3 cm away from the axis of the reactor

The measurements were done in the cross-section II of the reactor, in the axis. The received dependencies of the temperature in the function of the plasmatron power are presented in the fig. 7. According to the fig. 7 the temperature in the axis of the reactor is increasing while the plasmatron power is increasing. The higher temperatures occur for "clean" Ar plasma than during the plasma pyrolysis of the rubber powder.

4. CONCLUSIONS

Adding up, on the basis of the carried out measurements it results that at the constant work parameters of the plasmatron the temperature in the reactor decreases while the distance to the longitudinal axis and the distance to the plasma jet in axial direction increases. It is reasonable. Adding H_2 to Ar results in the increase of the temperature in the reactor in the case of "clear" plasma as well as in the case of the plasma pyrolysis of the rubber powder. However generally, spraying the rubber powder into the plasma jet causes the decrease of the temperature in the reactor. The reason of such a state might be more intensive cooling of the plasmatron, caused by the increased total flow rate of the gas by the flow of Ar transporting the rubber powder. The other reason of that decrease of the temperature can be consumption a part of the energy of the plasma jet for decomposition of the rubber powder during plasma pyrolysis.

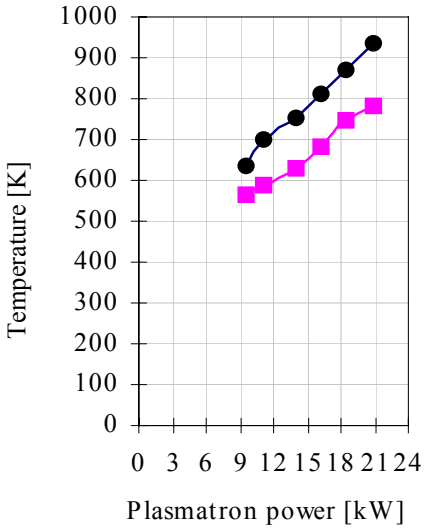

Fig. 7. Temperature in the cross-section II in the axis of the plasma reactor as the function of the plasmatron power:

LITERATURE

[1] Chen F.: *Introduction to Plasma Physics and Controlled Fusion*, 2nd. Edition, Springer 1984.
[2] *Dokumentacja techniczno - ruchowa plazmotronu Plancer PN120*, IBJ Świerk, 1978.
[3] Kerlin T.: *Practical Thermocouple Thermometry*, Instrumentation Systems, May 1999.

Jarosław SZUSZKIEWICZ, Ph. D., is an employee of the Chair of Materials and Machines Technology of the Faculty of Technical Sciences, University of Warmia nad Mazury in Olsztyn, Poland. His main fields of specialty are: environmental protection, plasma pyrolysis of polymers and Computer Aided Manufacturing.

THE ENERGETIC DIAGNOSTICS OF NAVAL PROPULSION SYSTEM WITH NAVAL GAS TURBINE

Bogdan POJAWA

Polish Naval Academy, The Institute of Ships Construction and Vessels Operation
ul. Śmidowicza 69, 81-103 Gdynia, pojawabogdan@o2.pl

Summary

The method of determining the energetic balance of naval power unit with the naval gas turbine is presented in the essay. The laboratory station with the gas turbine was used in introductory researches.

Elaborating the energetic balance of the engine allows to conduct an analyze of energetic processes which occur inside. Results of the analyses may be used due to improving the economy of the engine work what is equal with the increase of its effective efficiency. What is more, in respect of qualitative and quantitative changes of particular components of energetic balance it can be used as an indicator of change of the engine running-in or a change of its technical state.

Keywords: diagnosing, a energetic balance, a naval gas turbine.

DIAGNOSTYKA ENERGETYCZNA OKRĘTOWEGO UKŁADU NAPĘDOWEGO Z OKRĘTOWYM TURBINOWYM SILNIKIEM SPALINOWYM

Streszczenie

W referacie przedstawiono metodę wyznaczania bilansu energetycznego okrętowego układu napędowego z turbinowym silnikiem spalinowym. Do badań wstępnych wykorzystano stanowisko laboratoryjne z turbinowym silnikiem spalinowym.

Opracowanie bilansu energetycznego silnika (układu napędowego) pozwala na analizę zachodzących w nim procesów energetycznych. Wyniki tych analiz mogą służyć do poprawienia ekonomiczności pracy silnika, a więc podwyższenia jego sprawności efektywnej tzw. karnotyzacja. Ponadto ze względu na ilościowe i jakościowe zmiany poszczególnych składników bilansu energetycznego, może on być przyjęty jako wskaźnik zmiany przebiegu docierania silnika lub zmiany jego stanu technicznego.

Słowa kluczowe: diagnozowanie, bilans energetyczny, okrętowy turbinowy silnik spalinowy.

1. INTRODUCTION

The need of constant control and diagnosing of naval gas turbines is significant in the process of exploiting. It caused the necessity of creating a range of methods of diagnosing. Thanks to them it is possible to estimate the technical condition and determine the range and frequency of essential service maintenance which is the result of the exploiting strategy. The strategy is focused on reliable long-term functioning at the lowest cost.

The wear of parts of engine as well as of the whole engine may occur while exploiting gas turbine engines. Most common processes which affect such consumption and simultaneously the possibility of loss of usefulness for the further exploiting are following: fatigue, low-cycle fatigue of material, creeping, vibro-creeping, changes in the material structure, erosion, corrosion, brittle cracking and rubbing rotating parts of an engine with immovable ones. In processes of the energy exchange, in the result of use of operational properties of machine elements, as well as of the machine as such, the dissipation of energy may appear. The amount of the energy which is possible to dissipate is restricted by the boundary value E_G. This is the value for which the machine is unfit for use. The current amount of dissipated energy $E_Z(\Theta)$ in a particular period of exploiting may be regarded as dimension of the advancement of use processes [2].

The quantitative assessment of the dissipated energy allows to conduct the energetic balance in the process of the naval power unit exploiting. The energetic balance composes the quantitative comparison of the energy which supplies the engine while working. There is a possibility to determine the effective efficiency of the engine on the basis of the energetic balance. The effective efficiency expresses the quantitative percentage of the provided energy which is changed into output mechanical energy.

The method of determining the energetic balance of naval power unit with the gas turbine engine is presented in the essay. The laboratory station with the gas turbine GTD-350 was used in introductory researches.

2. THE RESEARCH OBJECT IDENTIFYING

The laboratory station contains miniaturized naval power unit with the gas turbine [3]. A propulsion unit consist of: a main engine, a clutch, a gear, an engine shafting as well as a screw propeller. In the station a Froude's water brake of HWZ-3 type is the mechanical energy receiver. In respect of operation principles the brake puts under load the engine in similar way as the screw propeller with changing spiral lead. A general view of the laboratory station with gas turbine GTD-350 power unit is shown in the figure 1.

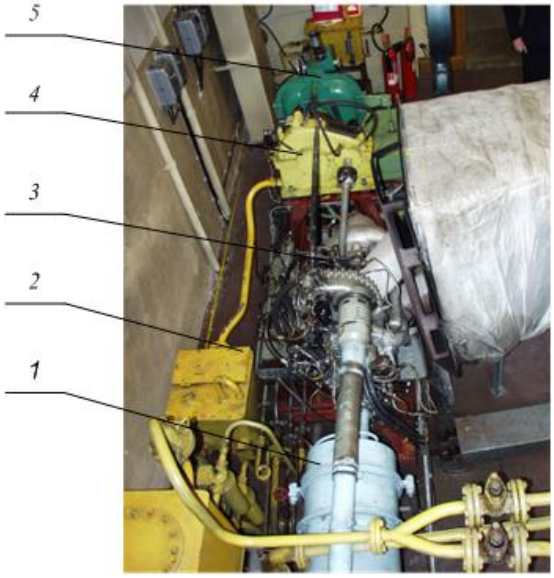

Fig. 1. The laboratory station with the gas turbine GTD-350: 1 - air admission installation; 2 - container of the oil installation of the reduction gear; 3 - the gas turbine GTD-350; 4 - the reduction gear; 5 - the water brake HWZ-3

The station is used in a didactic process of exploiting naval gas turbines as well as in initial researches about exploiting and diagnosing [3, 4].

3. THEORETICAL BASIS OF ENERGY BALANCE ELABORATING

The energy balance is a quantitative configuration of all types of energy which take part in energetic processes in particular machines or devices. The energy balance is determined on the basis of energy and mass conservation laws [1, 5, 6].

If a particular object is in a steady working state (in a thermodynamic equilibrium state) the changes of energy of the system does not appear $\Delta E_u = 0$. Therefore, the input energy (input energy flux) will be equal with the output energy (output energy flux). It may be shown by the following equation [1, 5, 6]:

$$\dot{E}_d = \dot{E}_w \tag{1}$$

The above assumption is also related to the equation of substance balance which can be presented as:

$$m_d = m_w \tag{2}$$

At the beginning of the energy balancing of a particular object it has been separated by a conventional control balance shield. It can be crossed not only by energy in a heat and work form, but also by the substance which brings the kinetic and potential energy. Such a thermodynamic system is treated as an open system which is motionless in respect of reference level. It is assumed that the flow is unidirectional, homogenous in every section which is orthogonal to the axis of flow direction determined by the control shield. It allows to assign equal, in every point of the section, medium value of parameters of the state and the function of the state to particular control sections. The input working substance (working medium) is air and fuel and output substance is exhaust gas. Moreover, it is assumed that in a propulsion engine processes of compression and expansion are adiabatic and irreversible and the process of combustion is treated as total and complete. It is also assumed that the particular thermodynamic system is in a state which is steady in time (in a thermodynamic equilibrium state) [1, 5, 6].

For the thermodynamic system which is defined in such way, taking into account equations (1) and (2), the equation of the energy balance may be presented in following way:

$$\dot{I}_{pal} + \dot{Q}_d + \dot{I}_{pow} = \dot{I}_{spal} + P_e + \dot{Q}_{ot} \tag{3}$$

$\dot{I}_{pal}$ – a stream of fuel enthalpy;

$\dot{I}_{pow}$ – a stream of air enthalpy;

$\dot{I}_{spal}$ – a stream of emission enthalpy;

P_e – effective mechanical energy which is formulated by the effective power transferred to the energy receiver;

$\dot{Q}_d$ – a stream of fuel chemical energy;

$\dot{Q}_{ot}$ – a stream of output energy losses.

In the respect of II principle of thermodynamics, according to which during changing the heat into the work the energy is dissipated, it is possible to introduce to the equation (3) a dimensionless quantity which is called propulsive efficiency [5,7]:

$$\eta_n = \frac{\dot{E}_{mech\_uż}}{\dot{E}_d} = \frac{P_e}{\dot{I}_{pal} + \dot{Q}_d + \dot{I}_{pow}} \tag{4}$$

The propulsive efficiency express the efficiency of all devices which enter into the composition of the considered object which are: the propulsion engine, gear with the clutch as well as the energy receiver [7]. Then, the equation (4) will be presented as follows:

$$\eta_n = \eta_e \cdot \eta_{PR} \cdot \eta_h \tag{5}$$

η_e – effective efficiency of the engine;

η_{PR} – efficiency of the gear with the clutch, it ranges from 0,97 to 0,99;

η_h – brake efficiency, for water brakes it ranges from 0,97 to 0,99.

Those efficiencies express mostly the mechanical losses connected with friction, doing a work to the propulsion of all underslung devices which are indispensable in providing with proper work and transfering turning moment to the energy receiver.

4. INITIAL RESEARCHES

Preliminary researches were aimed at measuring physical quantities of the considered object during working under the particular load. Those quantities were indispensable in determining the energy balance in entire range of load changing. A measuring-recording computer system AMW-34AIN was used in measuring and recording physical quantities.

On the basis of results reduced to normal weather conditions summands of the balance equation (3) were determined. The results of calculations are presented in the figure 2.

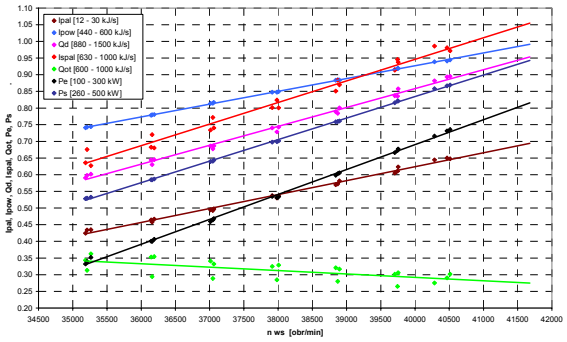

Fig. 2. The dependence of components of energy balance equation of the considered object on the engine load

On the basis of results it was also possible to determine the efficiency of the considered propulsion η_n as well as the effective efficiency of the engine η_e. Relationship between propulsion efficiency η_n, effective engine efficiency η_e and load is shown in the figure 3.

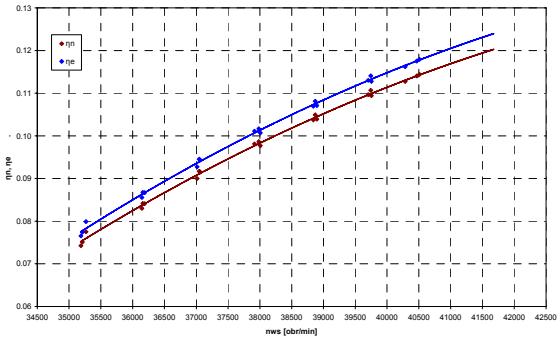

Fig. 3. The dependence of the propulsion η_n and the effective efficiency η_e on the engine load

On the basis of the elaborated energy balance it can be stated that values of particular components of the balance are related and proportional to the load of an engine. Those relationships show a linear dependence. On the grounds of dependence courses of particular components of the balance on the engine load, which are presented in figure 2, it can be stated that:

– changes of energy which is pulled out together with emission $\left(\dot{I}_{spal}\right)$, the mechanical effective energy $\left(P_e\right)$ as well as the power delivered to the compressor stay in the permanent proportions in the entire range of load changing. It is stated that participation of the energy pulled out with the emission $\left(\dot{I}_{spal}\right)$ in the whole range of load changes is about 50% of input energy. Similarly, the participation of the power delivered to the compressor is about 20% of the input energy;
– in the energy balance the participation of the energy losses $\left(\dot{Q}_{ot}\right)$ decreases with the load engine increase. It causes an increase of the effective engine efficiency showed in the figure 3 and a decrease of specific fuel consumption;
– the participation of energy losses $\left(\dot{Q}_{ot}\right)$ in the considered range of engine load changes decreases from 25% to 14% of input energy, while the participation of mechanical effective energy $\left(P_e\right)$ increases from 7% to 12%.

On the Sankey diagram the graphical illustration of the percentage participation of particular components of energy balance related to the input energy can be presented. Using the dependence of particular components of energy balance equation it is possible to create the Sankey diagram for any engine load. In the figure 4 there is presented the exemplary Sankey diagram created for nominal engine load.

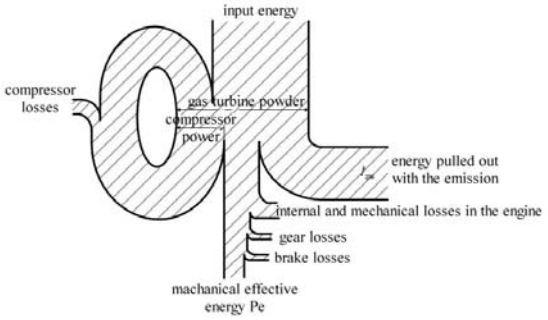

Fig. 4. Sankey diagram created for nominal engine load

According to the above figure low effective efficiency η_e is characterized for the engine. In the considered range of engine load changes this efficiency ranges from 7% to 13%. In such cases it is possible to make the engine more similar to the Carnot cycle what can be achieved by, for instance, regeneration of the heat which is pulled out with the emission.

5. SUMMARY

The elaborated method of determining the energy balance of naval propulsion unit with a gas turbine allows to conduct a quantitative analysis of internal energetic processes. It allows also to define in a quantitative way components of the balance equation and their dependence on the engine load. Results of these analysis may be used in improving the economy of their work what is equal with increase of effective efficiency. Crucial matter for diagnosing is a possibility of quantitative evaluation of dissipated energy in the exploiting which can be measure of the degradation of the technical state of the considered object. What is more, in the respect of quantitative changes of particular components of the energy balance, it can be regarded as an indicator of change of engine running-in course or its technical condition.

6. BIBLIOGRAPHY

[1] Çengel Y. A., Boles M. A.: *Termodynamics an engineering approach*. Fifth edition, The McGraw-Hill Companies 2006.
[2] Orłowski Z.: *Diagnostyka w życiu turbin parowych*. WNT, Warszawa 2001.
[3] Pojawa B.: *Stanowisko laboratoryjne dwuwirnikowego silnika turbinowego*. XXVI Sympozjum Siłowni Okrętowych SYMSO, Gdynia 2005.
[4] Pojawa B.: *Rozwiązanie problemu niedostatecznej możliwości obciążania silnika GTD-350 na stanowisku laboratoryjnym*, Zeszyty Naukowe AMW nr 4(167)/2006, Gdynia 2006, str. 71–86.
[5] Pudlik W.: *Termodynamika*. Wydawnictwo Politechniki Gdańskiej, Gdańsk 1998;
[6] Szargut J.: *Termodynamik*a. PWN, Warszawa 1998.
[7] Wojnowski W.: *Okrętowe siłownie spalinowe część I*. Wydawnictwo AMW, Gdynia 1998.

Bogdan POJAWA D. Eng. – assistant professor in Institute of Ships Construction and Vessels Operation, Polish Naval Academy in Gdynia. His main research interests include exploiting and diagnosing naval propulsion units. He is a member of Polish Society of Technical Diagnosis as well as Polish Scientific Society of Combustion Engines.

LABORATORY WEAR ASSESSMENT OF CAMSHAFTS' CAMS

Zbigniew STANIK, Kazimierz WITASZEK

Politechnika Śląska, Wydział Transportu, Katedra Eksploatacji Pojazdów Samochodowych
40-019 Katowice, ul. Krasińskiego 8

Summary

In this work results of laboratory wear tests of specimens made of spheroidal graphite cast iron grade EN-GJS-900-2 have been presented. This cast iron is used for camshafts of FIAT cars manufacturing. The iron has been heat–treated to obtain a hardness, ranging from 37 up to 53 HRC. Dry sliding and lubricated wear tests have been carried out. Their results have been utilized to work out mathematical wear models of the investigated cast iron. These models enabled the assessment of the influence of: lubricant presence, pressure, cam and pusher hardness on the wear rate of the tested material.

Keywords: camshafts, cams, wear rate, spheroidal graphite cast iron, sliding friction.

LABORATORYJNA OCENA ZUŻYCIA KRZYWEK WAŁKÓW ROZRZĄDU

Streszczenie

W pracy przedstawiono wyniki laboratoryjnych badań zużycia próbek wykonanych z żeliwa sferoidalnego gatunku EN-GJS-900-2 stosowanego na wałki rozrządu samochodów osobowych marki FIAT. Żeliwo to poddano obróbce cieplnej w celu uzyskania twardości od 37 do 53 HRC. Badania przeprowadzono przy tarciu na sucho i w obecności oleju silnikowego. Ich wyniki wykorzystano do opracowania matematycznych modeli zużycia badanego żeliwa sferoidalnego. Modele te pozwoliły na ocenę wpływu takich czynników jak obecność środka smarnego, nacisk, twardość krzywki i popychacza na intensywność zużycia badanego materiału.

Słowa kluczowe: wałki rozrządu, krzywki, intensywność zużywania, żeliwo sferoidalne, tarcie ślizgowe.

1. INTRODUCTION

The mating cam of a camshaft – pusher plays an important role in internal combustion engines, because it is responsible for controlling the movement of valves. Elements of this mating are subjected to a tribological wear, that changes their shapes. This phenomenon has an undesirable influence on an engine properties in service. Cams and pushers are made of wear resistant materials and work in lubricating friction conditions, thus their wear has usually a very low rate. So their shape remains almost unchanged during the whole service period of an engine. Fig. 1 presents an appearance of a normally worn cam, made of spheroidal graphite cast iron, and an optical micrograph of its working surface. In the latter one vertical dark and light strips, that are remains of grinding marks (made during its manufacturing), are still visible. Oblique wear grooves (Fig. 1 b) are very shallow and narrow.

Sometimes in service occur cases of severe wear of cams, that results in significantly reduced life of camshafts. An example of severely worn cam is presented in Fig. 2. Deep wear grooves, pits and plastically deformed material is present on its working surface (Fig. 2 b). Plastic deformation of cast iron matrix facilitates formation of adhesive joints, that subsequently break, causing tearing out of some portion of specimen metal and thus pits and grooves formation [1]. So the appearance of the severely worn cam surface indicates that an adhesive wear mechanism has been dominant in this case.

Severe wear of cams can be influenced by different factors. During the service of an engine they interact. From that reason it is difficult to isolate them to determine their effect on the cams' wear behaviour. Laboratory wear tests enable to control each factor, so its influence on the investigated phenomenon is easy to determine. Thus in the present work laboratory test results have been used to study wear behaviour of the cams.

a)

b)

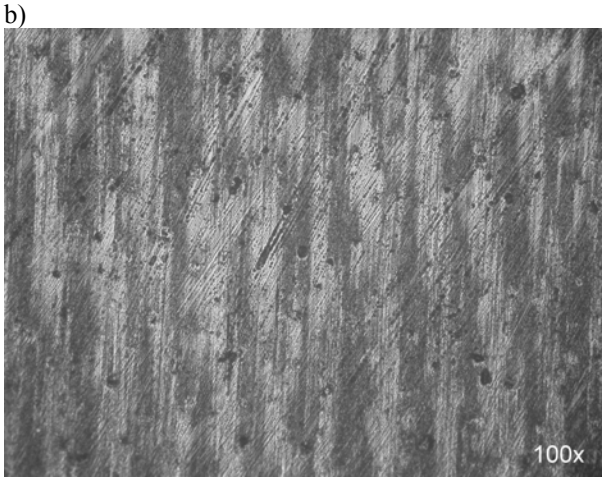

Fig. 1. The appearance (a) and the optical micrograph of working surface (b) of a normally worn cam, made of spheroidal graphite cast iron

a)

b)

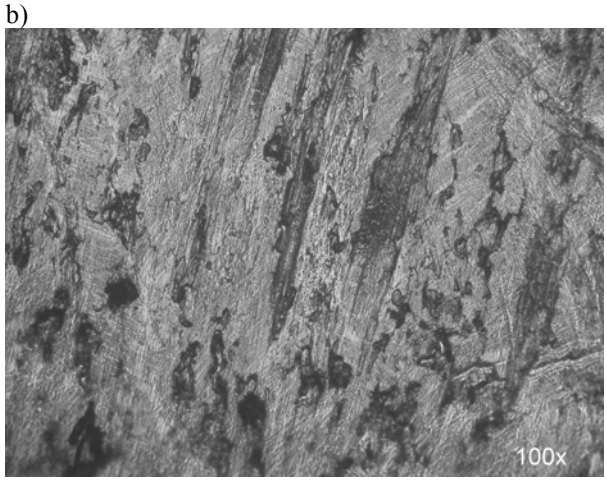

Fig. 2. The appearance (a) and the optical micrograph of working surface (b) of a severely worn cam, made of spheroidal graphite cast iron

2. WEAR TESTS

A pin-on-disc apparatus has been utilized to carry out the wear tests in the present work. Pins were machined from a spheroidal graphite cast iron grade EN-GJS-900-2 (according to the PN-EN 1563:2000 Standard), used for camshafts of FIAT cars manufacturing. To obtain a non-conformal contact, like the one of the cam and pusher, the shape of the pin tips was a half-sphere. Its radius was of 1.5 mm. Pins were water-quenched and tempered to obtain three ranges of hardness: 37 - 38 HRC, 43 - 44 HRC and 53 - 55 HRC. Discs with a diameter of 46 mm and thickness of 4 mm were made of a grey cast iron grade GJ-250, used for pushers. Tis cast iron has been hardened to a Rockwell C Harness Number of 46 – 48. The chemical compositions of the tested materials are presented in Table 1.

Test parameters are given in Table 2. Wear behaviour of pins in dry and oil lubricated friction conditions has been studied. For the latter ones the Aquila SG/CD 15W/40 engine oil have been used. In the all tests a constant load of 49.05 N and sliding speed of $1\ m \cdot s^{-1}$ have been applied. Sliding distance of a single test run ranged from 20 m for dry sliding to 1000 m for oil lubricated conditions. During each test a wear scar on the specimen surface has formed. Its area has been wear dependent. So the pin wear has been determined on the basis of wear scar diameter.

Table 1. Chemical composition of the cast irons for pins and disks

Element	C	Si	Mn	P	S	Cr	Ni	Mo	Mg	Cu
Pin	3.38	2.65	0.50	0.02	0.01	0.05	-	-	0.025	0.11
Disc	3.35	2.40	0.78	0.10	0.04	1.05	0.42	0.46	-	0.10

Table 2. Test parameters

Parameter	Values
Friction	dry, oil lubricated
Load, N	49.05
Sliding speed, m $\cdot$ s^{-1}	1
Sliding distance, m	20 – 1000
Pin hardness, HRC	37, 38, 43, 44, 53, 55
Disc hardness, HRC	46 – 48

3. TEST RESULTS

An example of test results is presented in Fig. 3. As can be seen in that figure the longer the sliding distance the greater the wear volume (volume loss) and the lower the pressure. The pressure decrease is caused by the increase of the apparent contact area, that often takes place during the sliding wear tests with a non-conformal contact [2].

a)

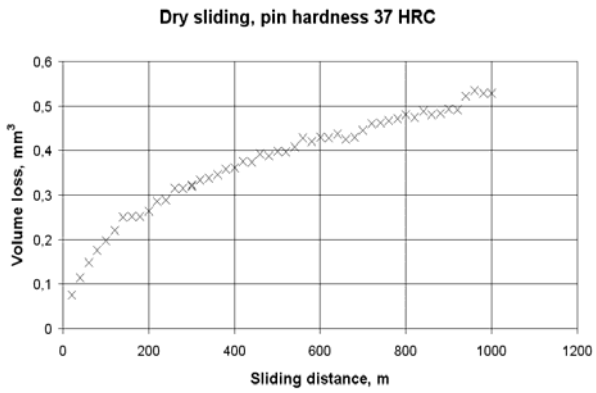

b)

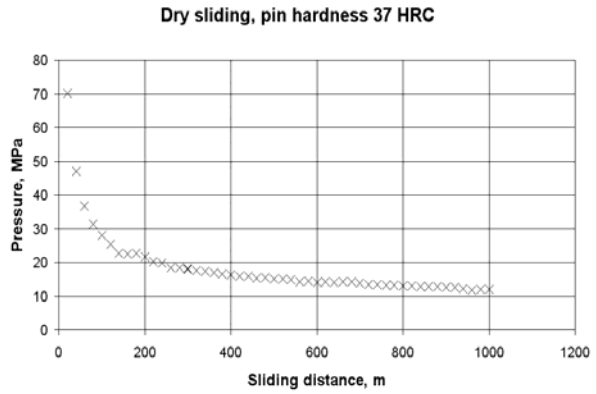

Fig. 3. Wear volume (a) and pressure (b) vs. sliding distance

4. DISCUSSION

To study the influence of the tested factors on the wear rate of the tested cast iron the dimensional analysis has been utilized [3]. With its aid the following function has been worked out:

$$\frac{Z}{l} = f\left(\frac{p}{\mathrm{H}_1}, \frac{\mathrm{H}_2}{\mathrm{H}_1}\right), \tag{1}$$

where:

Z – linear wear ($Z=V/A$), mm,
V – volume loss, mm^3,
A – apparent contact area, mm^2,
p – pressure in the pin-disc contact ($p=P/A$), MPa,
P – load, N
H_1, H_2 – hardness of pin and disc respectively, HB,
l – sliding distance, km.

A ratio Z/l is often called a linear wear rate [4]. According to Ref. [5] the following mathematical form of the function (1) has been chosen:

- for dry sliding:

$$\frac{Z}{l} = -0.020 \cdot \left(\frac{p}{\mathrm{H}_1}\right) - 0.022 \cdot \left(\frac{\mathrm{H}_2}{\mathrm{H}_1}\right) - 0.005 \cdot \left(\frac{p}{\mathrm{H}_1}\right)^2 + 0.007 \cdot \left(\frac{\mathrm{H}_2}{\mathrm{H}_1}\right)^2 - 0.003 \cdot \sqrt{\frac{p}{\mathrm{H}_1}} + 0.015 \cdot \sqrt{\frac{\mathrm{H}_2}{\mathrm{H}_1}} + 0.034 \cdot \frac{p}{\mathrm{H}_1} \cdot \frac{\mathrm{H}_2}{\mathrm{H}_1}, \tag{2}$$

- for oil lubricated sliding:

$$\frac{Z}{l} = 0.078 \cdot \left(\frac{p}{\mathrm{H}_1}\right)^2 + 0.003 \cdot \left(\frac{\mathrm{H}_2}{\mathrm{H}_1}\right)^2 - 0.043 \cdot \sqrt{\frac{p}{\mathrm{H}_1}} + 0.043 \cdot \frac{p}{\mathrm{H}_1} \cdot \frac{\mathrm{H}_2}{\mathrm{H}_1}, \tag{3}$$

Equations (2) and (3) contain some numerical coefficients. Values of these coefficients have been determined with the aid of a regression, whose accuracy has been determined with coefficients of correlation. Their values were 0.89 and 0.96 for the equations (2) and (3) respectively. They are high enough to accept the determined dependences for the further analysis. The influence of pressure, pin and disc hardness on wear rate of the tested cast iron is presented in Figs 4 and 5.

In Figs. 4 and 5 can be seen, that the pin wear rate Z/l for oil lubricated sliding is significantly lower than the one for dry conditions. The latter one caused very intense pressure decrease in the beginning of the test. So it was unable to obtain test results for high pressures in the dry friction conditions. It is the reason that the pressure range in Fig. 4 is much wider than in Fig. 5. The pressure increase increases the wear rate, especially for low pin hardness, both in dry and lubricated conditions. High pressure facilitates plastic deformation and microcutting, thus intensifying abrasion and adhesion [6, 7]. These effects can be responsible for wear rate increase. Higher pin hardness causes greater wear resistance of the tested cast iron, visible especially in dry friction – high pressure conditions. Harder subsurface material is much more difficult to deform under high pressures and

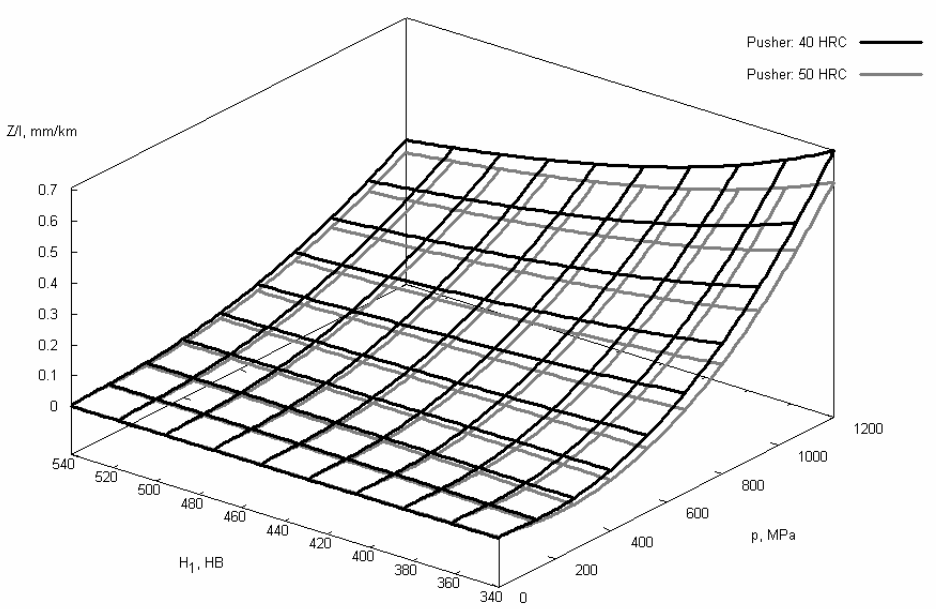

Fig. 4. The influence of pressure, pin (cam) and disc (pusher) hardness on wear rate of the tested cast iron in oil lubricated conditions

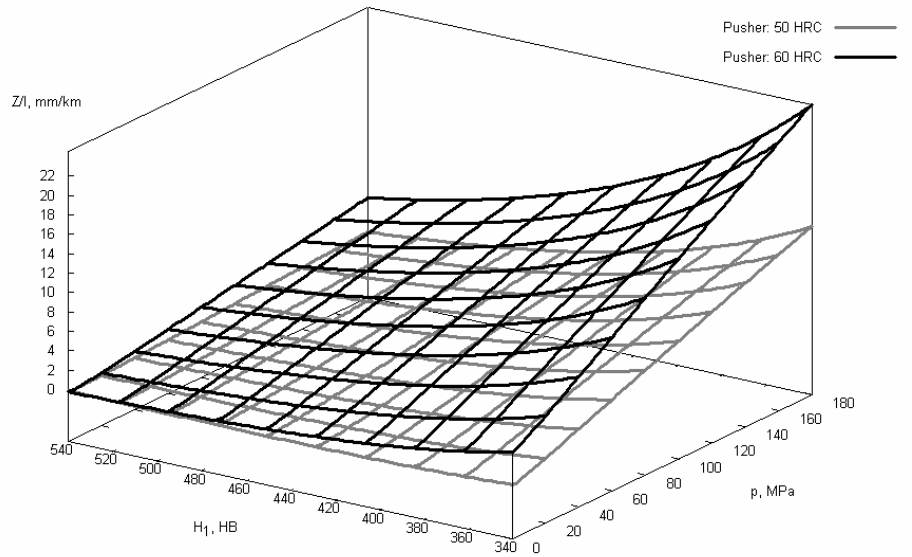

Fig. 5. The influence of pressure and pin hardness on wear rate of the tested cast iron in dry sliding conditions

can support thick films of oxides, that prevent metal – to metal contact and adhesion [6, 7], thus reducing the wear rate. Since presence of the engine oil prevents adhesive joints forming, wear rate decrease with the hardness increase in lubricated conditions (Fig. 4) is less severe than the one visible in Fig. 5.

The formulas (2) and (3) enable an assessment of the effect of the disc (pusher) hardness H_2 on the pin (cam) wear rate. As can be seen in Fig. 4 this effect in oil-lubricated conditions is negligible. It ranges within the scatter of the test results. On the other hand the hardness H_2 significantly influences the pin wear rate in dry sliding conditions. Its increase increases this rate. It can be attributed to the abrasive wear intensification, because harder asperities of disc can more easily plough and microcut pin material, especially when it exhibit low hardness.

6. CONCLUSIONS

The results of the tests and calculations carried out in the present work have drawn to the following conclusions:

- the presence of the lubricant influences the most significantly wear rate of the tested cast iron. the lubricant absence dramatically increases the wear rate. it can be explained by adhesive wear intensification.
- adhesive and abrasive wear can be intensified as pressure grows and pin (cam) hardness

drops off, especially in dry sliding conditions. So pin wear rate increases when its hardness decreases or the pressure increases. That effect is much less severe than the one of the lubricant absence (Fig. 4 and 5).

- disc (pusher) hardness significantly influences the wear rate of pins (cams) only in dry sliding conditions. its increase intensifies abrasive wear, thus increasing the wear rate.
- to understand the possible causes of severe wear of cams a further study of the effect of other factors, such as oil type, temperature and sliding speed, on the wear rate of cams is necessary. Its results can be helpful to find the best ways to prevent this wear.

REFERENCES

[1] Witaszek M.: *The influence of load and sliding speed on dry sliding wear of a bainitic steel*. 16th International Colloquium Tribology 2008. Esslingen 15 - 17.01.2008 r. s. 99+ 5 str. CD.

[2] Kozyrev Yu. P, Ginzburg B. M., Priemskii N. D., Tochilnikov D. G., Bulatov V. P.: *Express investigations of wear process by means of cylindrical counterbodies. Part I: Calculations and technique*. Wear, 171 (1994), 71-75.

[3] Müller L.: *Zastosowanie analizy wymiarowej w badaniach modeli*. Warszawa, PWN, 1983.

[4] *Wybrane zagadnienia zużywania się materiałów w ślizgowych węzłach tarcia*. Praca zbiorowa pod redakcją W. Zwierzyckiego. PWN, Warszawa - Poznań, 1990.

[5] Polański Z.: *Planowanie doświadczeń w technice*. PWN, Warszawa 1984.

[6] Haseeb A. S. M .A., Islam A. M., Bepari M. M. A.: *Tribological behaviour of quenched and tempered, and austempered ductile iron at the same hardness level*. Wear, 244 (2000), s. 15-19.

[7] Islam M. A., Haseeb A. S. M. A., Kurny A. S. W.: *Study of wear of as-cast and heat-treated spheroidal graphite cast iron under dry sliding conditions*. Wear, 188 (1995), s. 61-65.

BEARING CONDITION DIAGNOSTICS USING ENTROPY OF SIGNAL IN FREQUENCY DOMAIN

Bogdan WYSOGLĄD

Department of Fundamentals of Machine Design, Silesian University of Technology, Poland
Konarskiego 18a, 44-100 Gliwice, bwysoglad@posl.pl

Summary

This paper focuses on the application of entropy of the vibration signal in frequency domain for rolling element bearing defect detection and diagnosis. Impacts, which are results of bearing faults, cause instantaneous changes of vibration signal in frequency domain. Presented method of diagnosing is based on an assumption that mentioned above changes of signal can be estimated with use of entropy of signal in frequency domain. During the research the Shannon entropy and the relative entropy (Kullback – Leibler entropy) were applied. Distribution of signal in frequency domain was estimated with use Fourier Transform (normalized Power Spectrum Density) or Discrete Wavelet Transform. In the paper the influence of: rotational speed of shaft, radial load of bearing and additional noise of signal on efficiency of proposed method was presented.

Keywords: diagnostics, vibrations, signal processing, entropy, rolling element bearings.

DIAGNOZOWANIE ŁOŻYSK Z ZASTOSOWANIEM ENTROPII SYGNAŁU W DZIEDZINIE CZĘSTOTLIWOŚCI

Streszczenie

Artykuł przedstawia przykłady zastosowania entropii widma sygnału do wibroakustycznej diagnostyki łożysk tocznych. Impulsy drgań, które są wynikiem uszkodzeniem łożyska wywołują chwilowe zmiany sygnału w dziedzinie częstotliwości. Prezentowana metoda diagnozowania bazuje na założeniu, że te zmiany sygnału mogą być oceniane z wykorzystaniem entropii widma sygnału. W badaniach zastosowano entropię Shanona i entropię względną (Kullback – Leibler entropy). Rozkłady sygnałów w dziedzinie częstotliwości wyznaczano z zastosowaniem transformacji Fouriera (znormalizowane widmo mocy sygnału) albo dyskretnej transformacji falkowej. W artykule przedstawiono wyniki opisujące wpływ: prędkości obrotowej wału, obciążenia promieniowego łożyska i zakłóceń sygnału na wyniki zaproponowanej metody.

Słowa kluczowe: diagnostyka, drgania, analiza sygnałów, entropia, łożyska toczne.

1. ROLLING ELEMENTS BEARING VIBRATION

Most modes of failure for rolling-elements bearing involve the growth of discontinuities (fatigue cracks) on the bearing raceway or on a rotating element. Rollers or balls rolling over a local fault in the bearing produce a series of force impacts (a sequence of shocks). The majority of methods concerning the rolling bearing diagnostics are based on observation and analysis of vibrations caused by these shocks [7].

The impact caused by crossing of rolling elements over a fatigue crack (as a unit delta function) produces a broad spectrum of energy in the frequency domain. Natural frequencies of the bearing elements and housing are excited up to a few dozens kilohertz.

General assumption of the research is that impulses, which are results of bearing faults cause instantaneous changes of signal in frequency domain. These changes of signal can be estimated with use of entropy of signal in frequency domain.

During the research the Shannon entropy and the relative entropy (Kullback – Leibler entropy) were applied. Spectral entropy of signal is a measure of the degree of order/disorder of the signal, so that it can provide useful information about the underlying dynamical process associated with the signal.

2. THE METHODS OF BEARING DIAGNOSIS

2.1. The method using Shannon entropy

In the following, the signal is assumed to be given by the sampled values $x = \{x_n, n = 1, 2 \ldots, N\}$, corresponding to an uniform time grid with sampling time Δt.

In order to study temporal evaluation, the analyzed signal is divided in i overlapping temporal windows of length K and for interval L (were K and L are natural numbers). On the basis of laboratory test of bearing with diffrent faults, the best results

were obtained when time period of signal windows (short segment) was equal 1 ÷ 4 [ms].

Temporal window number i of signal x one can write $x^i = \{x^i_k\} = \{x_n, n = i \cdot L, i \cdot L+1, \ldots, i \cdot L+K\}$. The number of temporal windows is equal to $I = (N-K)/L$. The time period between two windows is equal to $\Delta t_L = L \cdot \Delta t$.

For each short signal windows $\{x^i_k\}$ distribution of power in frequency domain $\{p^i_j\}$ is estimated. Distributions in frequency domain were estimated with use of Fourier Transform or Wavelet Transform.

In the case of Fourier Transform a normalized Power Spectrum Density represented spectral distribution of signal. In the case of Wavelet Transform in order to obtained an orthogonal results of decomposition a Discrete Wavelet Transform was applied [1, 4].

The number of distribution levels was equal to the number of wavelet decomposition levels. Decomposition was taken up to the level j = 24 or 32. During the research as mother wavelet function was applied the Daubechies 7.

Relative wavelet energy for the resolution level j of spectral distribution p_j is define as

$$p_j = \frac{E_j}{E_{tot}} \tag{1}$$

where E_j - energy for the resolution level j, E_{tot} – total energy of signal window.

Then the Shannon entropy values H^i of each spectral distribution $\{p^i_j\}$ is estimated. Entropy is a measure of the uncertainty or disorder in a given distribution. We define the entropy of signal in the frequency domain as [2]

$$H\ (p) = -\sum_{j=1}^{J} p_j \cdot \log_2[p_j] \tag{2}$$

$$\sum_{j=1}^{J} p_j = 1$$

where:

p_j *(j = 1, 2, ... n)* – distribution *{p_j}* of signal segment in frequency domain, J – the number of the levels of distribution.

The obtained value of the entropy is assigned to the central point of the time window. A vector of entropy values (signal of entropy) is created. The vector included I values with sampling time Δt_L .

Bearings condition is not determined on the basis of maximum value of entropy as effects of bearing faults. Fundamental to its state identification is the frequency of instantaneous changes of entropy value. At the end power spectrum density of the vector of entropy values is estimated.

Confirmation of the bearing fault is a distinct magnitude of this spectral line, whose frequency is equals to the frequency of crossing of a roller over the cracks (bearing characteristic frequency) [6].

Fig. 1 presents obtained results in case of fault of outer ring, while distributions in frequency domain were estimated with use of Fourier Transform. The distinct magnitude of the spectral line whose frequency is very close to the bearing characteristic frequency (BPFO = 192 Hz) confirmed existence of the fault of the outer ring.

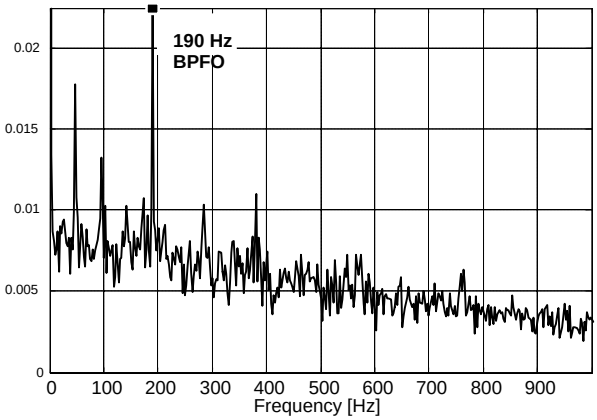

Fig. 1. Spectrum of vector of entropy values while the outer ring had medium fault while distribution of signal was estimated with use Fourier Transform

2.2. The method using relative entropy

The purpose of analysis is to recognize instantaneous changes of signal in frequency domain. Relative entropy (Kullback – Leibler entropy) gives a measure of the degree of similarity between two distributions [3, 5].

We define the relative entropy between two (basic and reference) distributions in frequency domain of short segments of signal as

$$H_R(p/q) = \sum_{j=1}^{J} p_j \cdot \log_2\left[\frac{p_j}{q_j}\right] \tag{3}$$

$$\sum_{j=1}^{J} p_j = 1 \qquad \sum_{j=1}^{J} q_j = 1$$

where:

p_j *(j = 1, 2, ... n)* – distribution in frequency domain *{p_j}* of basic signal window,

q_j *(j = 1, 2, ... n)* – distribution in frequency domain *{q_j }* of reference signal window,

J – the number of the levels of distribution (spectral lines).

The successive transformations of signals during the analysis with use of relative entropy were:

- division of vibration signal into basic and reference short windows. In order to study temporal evaluation, the analyzed signal was divided in i overlapping basic windows of length K and for interval L (were K and L were natural numbers). For each basic window nonoverlapping reference window of length K and for interval L=K was determined.
- estimation of distribution in frequency domain of each window.

- estimation of relative entropy value for each corresponding basic and reference signal window.
- creation vector of relative entropy values (signal of relative entropy).
- spectral analysis of the vector of relative entropy values.

3. RESULTS OF BEARINGS DIAGNOSTICS

3.1. Analysed signals

Analysed signals were recorded on a laboratory stand. Bearings faults were artificially produced by an electric pen. A radial acceleration signal was picked up from the top of the tested bearing casing by a piezoelectric accelerometer. During measurements of vibration of one bearing 20 records of samples were recorded. Each record included 8192 acceleration values sampled at a frequency equal to 51.2 kHz. MatLab programs were implemented to execute signal analyses.

3.2. Efficiency of the proposed method of bearings diagnosis

In the chapter the influence of: rotational speed of shaft, radial load of bearing and additional noise of signal on efficiency of proposed method was presented.

As mentioned above confirmation of the bearing fault is a distinct magnitude of this spectral line, whose frequency is equals to the bearing characteristic frequency. The distinction between the spectral line with the characteristic frequency and adjoining lines was described with application of HAR. A harmonic amplitude ratio (HAR) is defined as the amplitude value of the spectral line $a(f_k)$, whose frequency is equal to the bearing characteristic frequency, over the average value of amplitude of the spectrum a_{av}

$$HAR = \frac{a(f_k)}{a_{av}} \quad . \tag{4}$$

The influence of rotational speed of shaft on efficiency of proposed method was presented in Fig. 2. In more cases of application of both entropy and relative entropy the faults of bearings were identified. The best results were obtained while the rotational frequency was high. The reason of that was the difference between the powers of impulses produced by a fault in different speed conditions.

Fig. 3 presents obtained results in case of fault of different bearing elements while bearing load in radial direction was changed. The results of the analysis of signals recorded for different loads were similar.

The signals were recorded on a laboratory stand that allows simulating vibration interferences. While the vibrations of bearing were measured vibration interferences (noise) was caused by additional bearing (mounts on the shaft) with large corrosion of the raceways. Shaft rotation velocity was 2900 rpm.

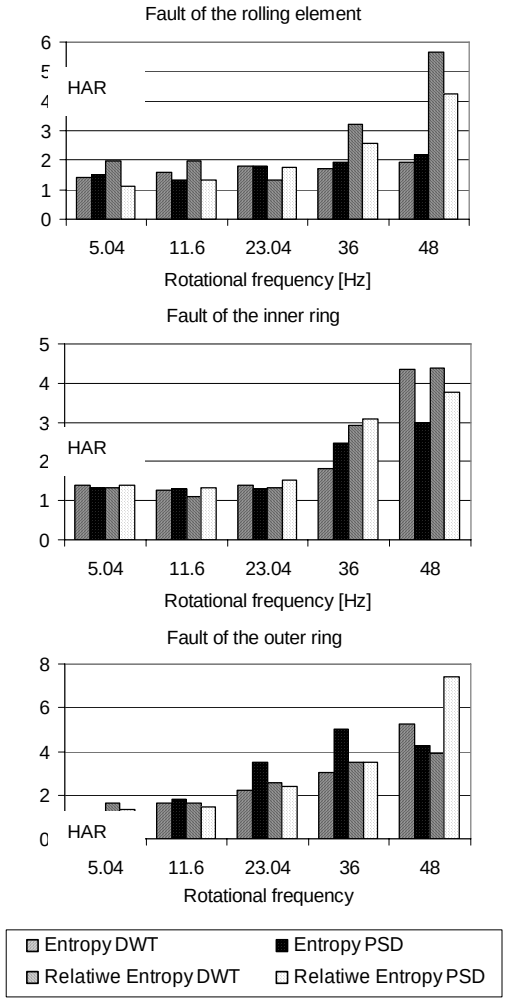

Fig. 2. The influence of rotational speed of shaft on the harmonic amplitude ratio HAR

Fig. 4 presents obtained results while vibration interferences were changed. The influence of additional noise on efficiency of proposed method was small. We can suppose that practical application of proposed method will be detecting failures while additional sources of vibrations (noise) are present.

4. CONCLUSIONS

Results of the research presented in the paper proved that the application of the presented method enables us to obtain distinct symptoms of bearing faults.

In more cases of analysis the best results were obtained while the relative entropy (Kullback – Leibler entropy) was applied and distribution of signal in frequency domain was estimated with use Fourier Transform (normalized Power Spectrum Density).

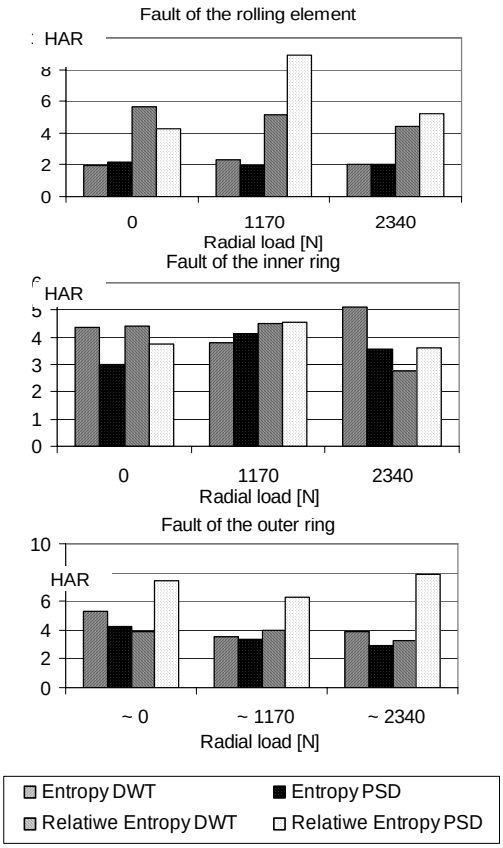

Fig. 3. The influence of bearing load in radial direction on the harmonic amplitude ratio HAR

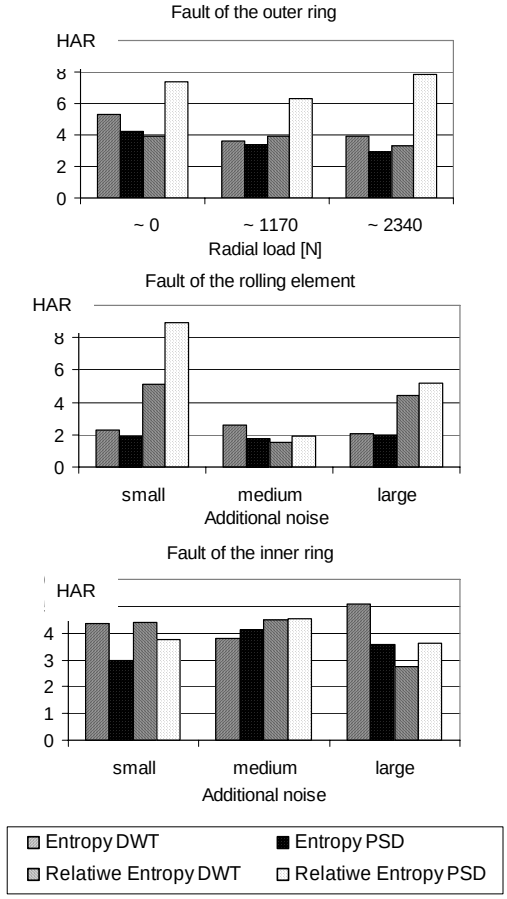

Fig. 4. The influence additional noise on the harmonic amplitude ratio HAR

REFERENCES

[1] Białasiewicz J. T.: *Wavelet and approximations*. (in Polish) WNT, Warszawa 2000.
[2] Majera J., McCowan I., Bourland H.: *Speech/music segmentation using entropy and dynamism features in a HMM classification framework.* Speech Communication 40 (2003) pp. 351-363.
[3] Mączak J.: *On a certain method of using local measures of fatigue-related damage of teeth in a toothed gear.* COMADEM, Cambridge 2003.
[4] Mori K., Kasashima N., Yoshioka T., Ueno Y.: *Prediction of spalling on ball bearing by applying the discrete wavelet transform to vibration signals.* Wear 195(1996), pp.162-165.
[5] Radkowski S.: *Wibroakustyczna diagnostyka uszkodzeń niskoenergetycznych.* Instytut Technologii Eksploatacji, Warszawa-Radom 2002.
[6] Scheithe W.: *A method for early detection of rolling element bearing failures.* Proceedings of Carl Schenck AG, Darmstadt.
[7] Tandon N., Choudhury A.: *A review of vibration and acoustic measurement methods for the detection of defects in rolling element bearings.* Tribology Int. 32(1999), 469-480.

Bogdan WYSOGLĄD is an assistant professor in the Department of Fundamentals of Machinery Design at Silesian University of Technology. He conducts research in the field of machine building and maintenance. His researches are focused on: technical diagnostics of machinery, signal analysis and application of methods of Artificial Intelligence.

WIRELESS TRANSMISSION SYSTEM FOR A RAILWAY BRIDGE SUBJECT TO STRUCTURAL HEALTH MONITORING

Damian SALA[1], Jerzy MOTYLEWSKI[1,2], Przemysław KOŁAKOWSKI[1,2]

[1]Smart-Tech Centre, Institute of Fundamental Technological Research,
Polish Academy of Sciences, Warsaw, Poland, http://smart.ippt.gov.pl
[2]Adaptronica sp. z o.o., R&D Company, Łomianki, Poland, http://www.adaptronica.pl

Summary

One of the fast-developing research topics in electronics is the wireless data transmission, which is a highly desirable component in health monitoring of engineering structures. The paper describes a newly-designed system of wireless data transmission for structural health monitoring of a railway bridge.

Keywords: wireless transmission of data, structural health monitoring.

SYSTEM BEZPRZEWODOWEJ TRANSMISJI DANYCH DO MONITOROWANIA STANU TECHNICZNEGO MOSTU KOLEJOWEGO

Streszczenie

Jednym z prężnie rozwijających się tematów badawczych w elektronice jest bezprzewodowa transmisja danych, na którą jest duże zapotrzebowanie w monitorowaniu stanu konstrukcji inżynierskich. W artykule opisano nowo projektowany system bezprzewodowej transmisji danych do monitorowania stanu technicznego mostu kolejowego.

Słowa kluczowe: bezprzewodowa transmisja danych, monitorowanie stanu konstrukcji.

1. INTRODUCTION

This paper describes a wireless transmission system to be operating on a real bridge structure. The investigated bridge (Fig. 1) is a single-span, 40-meter-long, steel truss structure providing support for a single railway track. The program of monitoring of the bridge includes two major issues. First, monitoring of structural health and its potential degradation due to e.g. corrosion is planned. Second, monitoring of railway car mass and speed is of interest to the owner of the railway infrastructure. The monitoring will be performed using piezoelectric strain sensors.

Consequently, the proposed integrated monitoring system [1] will consist of two hardware parts. The first part installed nearby an investigated bridge is supposed to weigh trains in motion (Fig. 2). This way the parameters of dynamic load acting on the bridge will be known in contrast to frequently used unknown ambient excitation like wind. Information from part 1 will be transferred to a remote analysis centre using a module of wireless transmission of data. The part 2 installed directly on the bridge should record time responses of the structure induced by train passage. The time responses will be then transferred to the analysis centre (independently from part 1) using another module of wireless transmission.

Having the information both about the dynamic load and the structural response to this load, monitoring of the bridge health can be performed by solving an inverse problem in the framework of the Virtual Distortion Method [2]. Deterioration of the bridge can be interpreted as stiffness degradation and/or mass loss for every element of the truss bridge.

The undertaken in-situ monitoring campaign, started mid 2007, fits in the fast-developing research area called Structural Health Monitoring (SHM) [3]. The principal idea behind is that a structure should be subject to a permanent monitoring (performed not necessarily round the clock, but repeatedly). The main advantage of such monitoring is the ability to track changes in responses during the lifetime of a structure, raise alerts in case of significant deviations from normal behaviour and estimate the usable lifetime until demolition or general repair. The *in-situ* monitoring system consists of two major components, depicted in Fig. 3, i.e. some sensors collecting responses in time and the central data processing unit (DP), providing basic signal processing and data transfer to a remote computational centre.

The sensors may communicate with the DP unit either via cables or wirelessly. The latter way is the subject of consideration in this paper.

Fig. 1. Railway truss bridge monitored in Nieporet

Fig. 2. Excitation by train – weigh in motion (WIM)

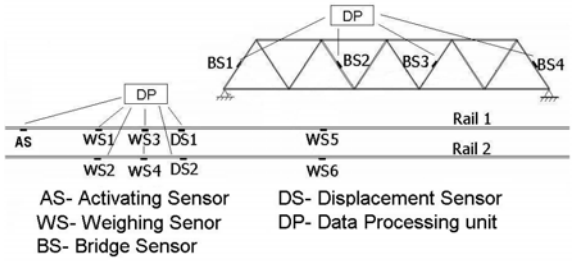

Fig. 3. A scheme of the bridge equipped with sensors and data acquisition unit

The wireless method of data transmission has been the subject of intensive research in the SHM community. The reasons of this fact are the following:

- cables may be used only for local transmission of data, far-range transmission to a remote location seem to be realizable only by wireless methods,
- installation time of standard cable connections between sensors and DP unit is very long and the process may be troublesome,
- cost of cabling for large structures is high,
- cables used for data transmission are prone to devastation.

2. THE GENERAL CONCEPT

Several types of topologies for wireless communication networks, shown in Fig. 5, are currently in use [4]. The authors plan to configure their wireless system as a set of independent sensors controlled by a central data processing unit, which corresponds to the star topology. Both hardware parts of the system will have their own autonomous DP units.

The WIM sensors is connected to the WIM DP unit with standard cables because the distances between the sensors and the unit are small. The bridge sensors communicate with the bridge DP unit via nearby-range wireless transmission, because they may be mounted far away from one another, depending on bridge size.

The far-range wireless transmission of data takes place independently for the WIM DP unit and bridge DP unit. This is due to the fact that monitoring of rail traffic should be performed on-line and monitoring of bridge health can be done off-line. Therefore the amount of data and frequency of transmission for the WIM and bridge DP units will be different. Another explanation is that the WIM point may be located too far from the bridge, so one unit for the whole monitoring system might be impractical.

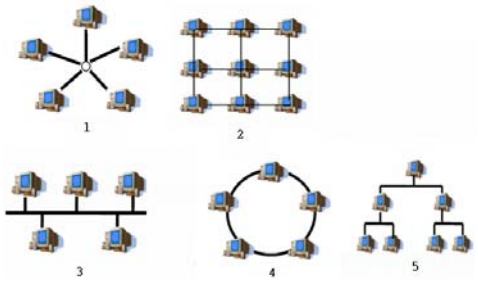

Fig. 4. Types of wireless networks: 1) star, 2) net, 3) rail, 4) circle, 5) tree

The major challenges to be faced from the electronic viewpoint are:

- equipping the system with a maintenance-free source of power,
- designing durable small-size and energy-saving components of the wireless transmission system,
- pre-processing of time signals in situ and optimizing them for far-range wireless transfer.

Fig. 5. Piezoelectric sensor for collecting strains

Piezoelectric sensors were chosen to collect strain responses in time. An example of a piezo-ceramic sensor is shown in Fig. 5.

3. TIME SIGNALS TO BE TRANSFERRED

As the integrated system consists of two blocks, there are two types of time signals recorded by piezo-sensors. These time signals need to be pre-processed in situ before starting their wireless transfer to a remote centre.

The first type of signal corresponds to the load identification block and the associated weigh in motion procedure for running trains. An example of the time signal detected by the weighing sensors (WS), is depicted in Fig. 6.

The second type of signal corresponds to the bridge health monitoring block and the associated damage identification procedure. An example of the time signal captured by bridge sensors (BS) is shown in Fig. 7.

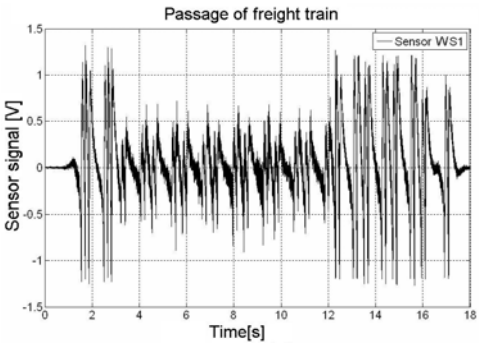

Fig. 6. Signal captured by a weighing sensor

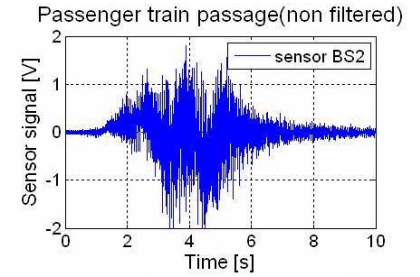

Fig. 7. Signal captured by a bridge sensor

4. WIRELESS TRANSMISSION SYSTEM

In the authors' opinion, the wireless system for SHM should be characterized by a relative simplicity, high reliability and low energy consumption.

The complete system proposed in this paper can be divided into two subsystems – for weighing trains in motion and for health monitoring of the bridge. Detailed proposition of the wireless solutions will be focused on the latter subsystem only. The reason is that both the nearby-range and far-range transmission has to be considered for the bridge.

The proposed bridge system, schematically shown in Fig. 8, consists of three major components – a number of the measuring units integrating piezoelectric sensors with associated electronics described as BS, the DP unit and two activating sensors (AS). The role of the activating sensors is to wake the system up for the time of train ride only and put it in a passive mode afterwards.

Each measuring unit collects analogue signals from the piezoelectric sensors mounted on the bridge and transfers them to the DP unit via an embedded transceiver using a local mode of wireless transmission. A scheme of the integrated bridge sensor is shown in Fig. 9.

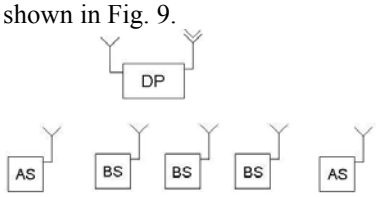

Fig. 8. Scheme of the local wireless transmission system

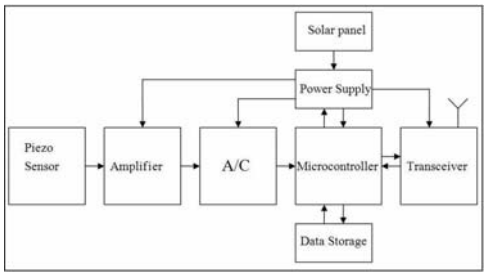

Fig. 9. Scheme of the integrated bridge sensor

The proposed electronics associated with each measuring unit is not sophisticated in order to keep the power supply at the 50 mW level. At first stage of testing, a lithium-ion battery will be used. Subsequently, a solar cell should be provided to recharge an in-built battery for long-term, maintenance-free operation. A crucial feature of the system resulting in significant energy savings will be its intermittent operation. The system will be activated by one AS from each direction. It will remain active only during the passage of a train over the bridge. Otherwise it will switch to a passive, energy-saving mode. The only sensor operating in the stand-by mode will be the two activating sensors. The difference in energy consumption is 3 order of magnitude as the microcontroller of the DP unit needs 0.4 mA when active and just 0.6 μA when passive.

The integrated bridge sensor will perform analogue to digital conversion of a signal before sending it to the DP unit. To this end, a 12-bit analogue-digital converter providing proper sampling will be used. The available nearby transmission distance is estimated to reach approx. 100 m. All measuring units are supposed to start data acquisition simultaneously thus have to be properly time-synchronized by triggering signals from the DP unit.

The tasks of the DP unit are: sequential collection of digital signals from the bridge sensors, signal compression and transfer to a remote computing centre for analysis. Thus the DP unit

should consist of a transceiver to collect the signals from various measuring units, microcontroller for signal processing, sufficient memory buffer enabling storage of data and additional RS-232 port for possible *in-situ* acquisition. A scheme of the DP unit is depicted in Fig. 10. Advantage of the GSM system is taken to transfer the digital data to a remote computational centre.

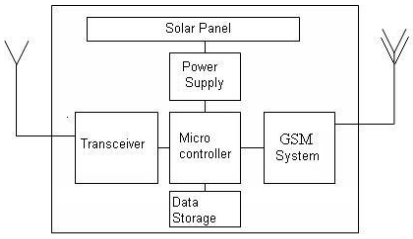

Fig. 10. Scheme of the DP unit

Several tests of the proposed system are planned, starting from a check of the performance of a single measuring unit, through the design of the DP unit, finally leading to the installation of the system *in situ* and its subsequent verification.

Currently the work is focused on development of specific modules (see Fig. 11) of the system for both the local and far-range wireless transmission. The next step is to assemble all the modules in the planned items i.e. the BS and DP units. It is planned to install and test the whole system of wireless transmission in situ in 2009. The local transmission will be checked first.

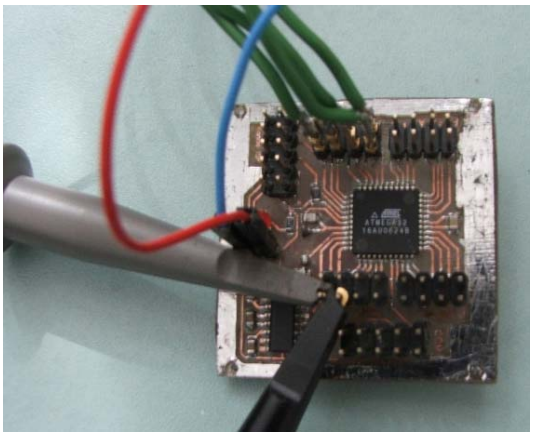

Fig. 11. Module of the wireless system ready for lab testing

4. CONCLUSIONS

High demand from the Structural Health Monitoring community is the reason for fast development of wireless transmission systems applicable to real structures. A prototype of the proposed system will be implemented and tested on a railway bridge. Further development of the system, taking into account fidelity of transmission, durability and cost-effectiveness of hardware will be the subject of future work.

General conclusions are the following:

- wireless transmission of data is very important for permanent SHM,
- it is relatively easy to adapt the wireless system to various applications e.g. structures, water networks,
- fidelity of data processing and durability of hardware should be major features of the wireless system.

ACKNOWLEDGEMENTS

The authors gratefully acknowledge the financial support from the projects R03 015 02, 2007-2010 and N N506 3072 33, 2007-2009, granted by the State Committee for Scientific Research in Poland.

REFERENCES

[1] Adaptronica sp. z o.o. & Contec sp. j.: *Sposób i układ do monitorowania konstrukcji kratownicowej mostu*. Zastrzeżenie patentowe nr P 387115, Urząd Patentowy RP, 2009.
[2] J. Holnicki-Szulc (ed.): *Smart Technologies for Safety Engineering*, Wiley, 2008.
[3] P. Kolakowski, K. Sekula, A. Swiercz: *A Concept of Long-Term Monitoring of a Railway Truss Bridge Excited by Trains*, Proc. of 4th European Workshop on SHM, Kraków, 2-4 July, 2008.
[4] I. Stojmenovic (ed.): *Handbook of Sensor Networks*, Wiley, 2005.

Mr. **Damian SALA** is a mechanical engineer with electronic background. He is a PhD student in the Smart-Tech Centre at IPPT PAN in Warsaw. His research is concentrated on wireless transmission systems applicable to SHM.

Dr. **Jerzy MOTYLEWSKI** is an electronic engineer. He has almost 50 years' experience in vibroacoustic measurements with a special interest in noise mitigation. His comprehensive expertise ranges from the power industry to aeronautics.

Dr. **Przemysław KOŁAKOWSKI** is a civil engineer. He did his PhD on optimization of trusses. Then he worked as a consultant in Atkins plc for four years. His current research is focused on smart technologies, in particular on vibration-based SHM.

INTERNAL COMBUSTION ENGINE VIBRATION BASED FAULT DETECTION USING WAVELET PACKET TRANSFORM

Henryk MADEJ

Faculty of Transport, Silesian University of Technology
40-019 Katowice, ul. Krasińskiego 8, fax (+48) 32 6034108, email: henryk.madej@polsl.pl

Summary

In this paper, the wavelet transforms of vibration acceleration signals which were acquired from the cylinder head and engine block for various faulty and healthy conditions of IC engine was used to fault detection. The engine which has been tested is 4-cylinder 4-stroke with eight valves fed with petrol and LPG. Many mechanical fault detection techniques based on vibration analysis have been developed over the last few decades. The analyssis of vibration signals associated with internal combustion engines is complicated due to the complexity of the engines and diffrent sources of vibration. The engine vibration signal is inherently a transient one even in engine steady operation. The time-frequency localization features of the wavelet transforms make them suitable for IC engine fault diagnosis and monitoring. In the present investigation, a fault diagnosis technique based on wavelet packet transform (WPT) i used to engine fault detection. The experimental results show that proposed method is useful for detection the faults in various engine working conditions.

Keywords: wavelet transform, IC engine, diagnostics.

PRZETWARZANIE SYGNAŁÓW ZA POMOCĄ TRANSFORMACJI FALKOWEJ W DIAGNOSTYCE WIBROAKUSTYCZNEJ SILNIKÓW SPALINOWYCH

Streszczenie

W artykule przedstawiono przykłady zastosowania analizy falkowej sygnałów przyspieszeń drgań zarejestrowanych na kadłubie i głowicy silnika ZI w celu wykrycia symulowanych uszkodzeń. Obiektem badań był 4-ro cylindrowy silnik spalinowy zasilany alternatywnie benzyną i LPG. W ostatnich latach opracowano i rozwinięto wiele metod diagnozowania opartych na pomiarach drgań. Analiza sygnałów drgań związanych z pracą silnika spalinowego jest utrudniona ze względu na złożony sygnał wywołany jednoczesnym działaniem wielu źródeł. Sygnał przyspieszeń drgań rejestrowany na kadłubie i głowicy silnika jest niestacjonarny i zawiera składowe impulsowe. Dlatego w diagnostyce drganiowej silników korzystne jest stosowanie metod czasowo-częstotliwościowych takich jak analiza falkowa, które umożliwiają tworzenie użytecznych cech diagnostycznych. W artykule przedstawiono przykłady zastosowania pakietu analizy falkowej (WPT) do wykrywania symulowanych uszkodzeń silnika. Z badań wynika, że zastosowana metoda może być użyteczna do diagnozowania różnych uszkodzeń silnika spalinowego.

Słowa kluczowe: analiza falkowa, silniki spalinowe, diagnostyka drganiowa.

1. INTRODUCTION

The diagnosing systems used in modern combustion engines aim at locating the element or system which, due to natural wear or damage, cannot further perform its function as specified by the manufacturer.

Increasing requirements concerning the durability and reliability of combustion engines and the minimisation of costs and disadvantageous influence upon the environment necessitate the acquiring of information on their condition during operation. Introduction of the obligation of manufacturing motor vehicles compliant with the OBDII standard resulted in the possibility of accessing data stored in the programmers of individual systems. Owing to this solution, new possibilities of diagnosing the technical condition of those systems arise [12].

The greatest efficiency of the on-board diagnostics system was assured in the area of monitoring the emission of toxic compounds. However, some types of damage, such as: growing wear of valve-seats and valve faces, a shift of the valve train phase, or wear of the cylinder bearing surface to a degree exceeding the dimensions allowable for a particular engine, in many cases in practice, do not result in a response of the diagnosing system. The most frequent reason for this are the used adaptive controlling algorithms for combustion engines. It is about controlling the processes with changeable dynamic properties and

of changeable stochastic disturbance properties, during which estimation is carried out of the process model parameters and disturbance, so as to update the controlling algorithm [3, 7]. Adaptive control of an engine can lead to a situation where the appearing errors will be hidden or adapted. Mechanical defects and operational wear, in particular in the early phases of development, are compensated by adaptive adjustment systems as a result of permissible ranges of adjustment. Only after occurrence of a major failure, the course of the regulation process is so much disturbed, that finding the defect will be relatively easy, because the system will switch to an emergency mode.

In the modern engines, the detection algorithms of combustion knocking are a component of the engine controller system IC. A change of the ignition advance angle has a significant influence on the nature of the measured vibration signal. This poses a danger of masking the mechanical defects by control systems and can be the cause of more serious failure.

Therefore, changes of the technical condition of an engine, induced by early phases of its wear, are difficult to detect. An important issue in vibroacoustic examination of engines is a correct interpretation of complex measured signals by applying more and more proficient methods of their processing [1, 5, 9, 14, 16]. The main tasks in diagnostics include: separation of a useful vibroacoustic signal and selection of characteristic, damage-sensitive features of the processed signal.

2. DIAGNOSING OF COMBUSTION ENGINES WITH USE OF VIBROACOUSTIC METHODS

One of the methods of acquiring diagnostic information is to measure the vibration generated by the engine. A combustion engine is subject to the action of inner and outer forces. They encompass mainly:

- combustion pressure,
- movement of the crank-piston system,
- forces induced by the timing gear system,
- forces from the work of engine accessories, such as the alternator, compressor, and the like,
- forces transferred from the vehicle body and the power transmission system.

One of the significant forces appearing during the crank-piston system work are piston strokes while changing its movement direction. The value of the force depends significantly on the clearance between the piston and the cylinder wall [4, 5, 6], caused by wear and tear of the engine. The value of force is a function of combustion pressure and rotational speed of the engine.

The vibration signal recorded in any place on the engine block is a weighted sum of the engine block response to all elementary events (Fig. 1); convolutions with pulse functions of transfer from the place of generation to the reception place of the diagnostic signal are the weights here [2].

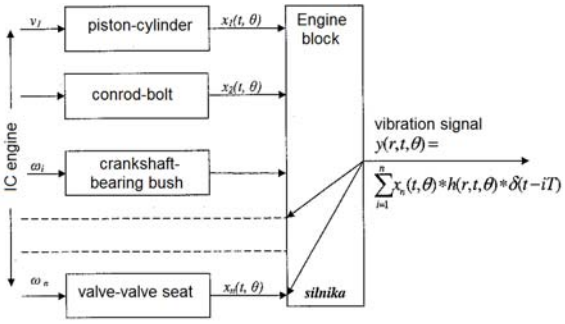

Fig. 1. Diagram of generating engine vibration signals

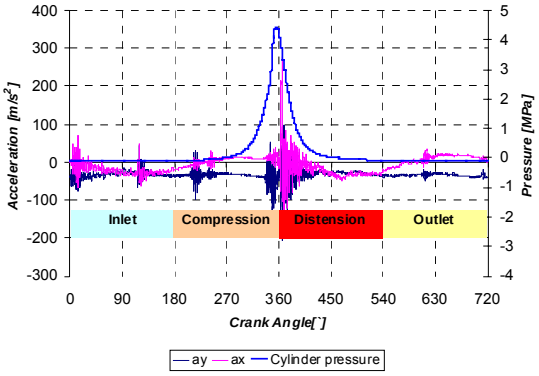

Fig. 2. An exemplary course of a working cycle of a single-cylinder combustion engine

All systems of the combustion engine work in a specific order (Fig. 2). The elementary events taking place in kinematic pairs are ordered, as well. In that case, the kinematic pair of an engine, which produced a percussive impulse, can be determined by the location of the impulse vis-à-vis the reference signal.

The vibroacoustic signal generated by the combustion engine can be presented in a simplified form:

$$x(t) = \sum A_i \cos(\omega_i t + \varphi_i) + \sum\sum B_{ij}(t) u(t - t_j) \cos(\omega_{ij} t + \varphi_{ij}) \quad (1)$$

where:
A_i and $B_{ij}(t)$ - amplitudes of signal components,
ω_i and ω_{ij} - frequencies of vibration components,
$u(t)$ - pulse function,
t_j - time determining the occurrence of pulsing phenomenon,
φ_i and φ_{ij} - signal component phases.

The first component of the equation reflects the main harmonic components, which are normally characterized by high amplitude values. After removing the low-frequency components, a residual signal containing high-frequency impulse components is obtained.

The above signal transformation facilitates isolating the summary signal of the investigated kinematic pair by means of time or angle selection. Vibroacoustic signals generated by individual kinematic pairs and combustion engine tooling are most frequently nonstationary due to the occurrence of nonlinear phenomena provoked, inter alia, by clearance, nonlinearity of elastic components' characteristics. Frequency characteristics of signals essentially depend on transmittance of the propagation route of component signals from their source to the measuring point. Vibration measured on a block is of a complex nature due to the overlapping signals which originate from various sources. For these reasons, diagnosing of combustion engine faults is a difficult process.

3. SIGNAL ANALYSIS IN THE TIME-SCALE DOMAIN

A simultaneous analysis of the time and frequency related properties of signals by means of a wavelet transform is more and more frequently used in diagnosing combustion engines [5, 10, 11, 14, 15, 16, 17].

The continuous wavelet transform of a finite energy function, $x(t) \in L^2(R)$, is defined as follows:

$$W_x(a,b) = \langle x(t), \psi_{a,b}(t) \rangle = |a|^{-\frac{1}{2}} \int_{-\infty}^{+\infty} x(t) \psi \frac{(t-b)}{a} dt \quad (2)$$

$$a, b \in R, a \neq 0$$

An inverse transform of the transformation $W_x(a,b)$ takes the following form:

$$x(t) = \frac{1}{C_\psi} \int_{-\infty}^{+\infty} W_x(a,b) \psi_{a,b}(t) \frac{da db}{a^2} \quad (3)$$

Based on the definition, the function $\psi(t) \in L^2(R)$ is an acceptable elementary wavelet, if:

$$C_\psi = \int_0^\infty \frac{|\Psi(\omega)|^2}{\omega} d\omega < \infty \quad (4)$$

where $\Psi(\omega)$ is the Fourier transform of the function $\psi(t)$.

Wavelet coefficients $W_x(a,b)$ are the function of scale a and shift b. A change of the scale is tantamount to wavelet compression or stretch $\psi_{a,b}$. The coefficients $W_x(a,b)$ are the measure of signal's $x(t)$ correlation with the wavelet $\psi_{a,b}(t)$: for narrow wavelets, they represent the content of high-frequency components, and for wide wavelets, low-frequency components. The Continuous wavelet transform (CWT) is very excessive; after sampling its parameters, time t and coefficient of scale a, the coefficients of a dyadic wavelet series are obtained. A discrete wavelet analysis of signal $x(t) \in L^2$ becomes reduced to determining its discrete wavelet transforms, which are the scalar products of signal x and a sequence of function $\psi_{j,k}$. These products are called wavelet coefficients. The wavelet coefficients represent common characteristics of signal x and wavelet $\psi_{j,k}$. Parameter k localises the moment in which the analysis is being made, while parameter j enables choosing the scale level (range of frequency), at which the signal spectrum is investigated.

The discrete wavelet transform finds broader and broader application the diagnosing of machines. Its expansion is reflected in the so-called wavelet packages, which enable multiple decomposition of signals. Wavelet packages consist of a linear combination of the wavelet function expansion:

$$\psi^i_{j,k}(t) = 2^{j/2} \psi^j\left(2^j t - k\right) \quad (5)$$

$i = 1,2,3...,$
j – scale parameter,
k – shift parameter.

Function ψ^i is defined by the following relations:

$$\psi^{2j}(t) = \sqrt{2} \sum_{k=-\infty}^{\infty} h(k) \psi^i(2t-k) \quad (6)$$

$$\psi^{2j+1}(t) = \sqrt{2} \sum_{k=-\infty}^{\infty} g(k) \psi^i(2t-k) \quad (7)$$

Discrete filters $h(k)$ and $g(k)$ are mirror filters connected with the scaling functions and wavelet functions [1, 13]. The algorithm of multiple signal decomposition by means of wavelet packages (WPT) is presented in the block diagram (Fig. 3).

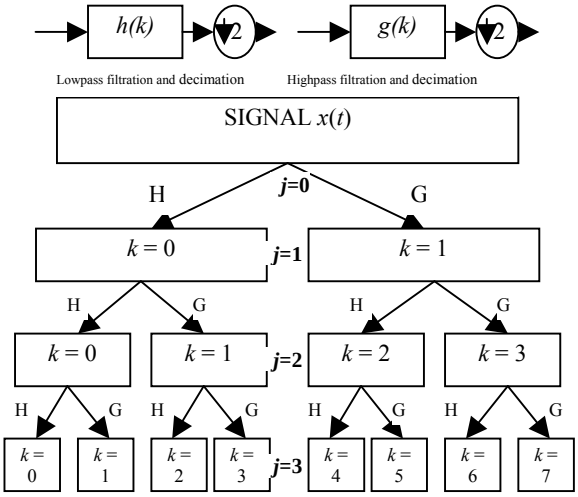

Fig. 3. Algorithm of decomposition by means of wavelet packages

The algorithm makes a frequency analysis of the signal through iteration of the double-channel set of filters consisting of low- and high-pass filters. Signal obtained as a result of filtration in the previous step undergoes further filtration. As a result of each iteration, a high-frequency component, called a detail, and a low-frequency component, called approximation, are obtained. The signal decomposition process is a multilevel iteration process, where further details and approximations are subject to further decomposition. The calculation algorithm (fig. 3) has the from of a set of filters with a binary tree structure, where the low- and high-pass branches are developed by means of a pair of the same filters. This type of analysis has been widely applied recently, because it enables creating standard sets of diagnostic characteristic used as input data of neuron classifiers[14, 16].

The above-mentioned properties of wavelet analysis make it more and more popular in diagnosing combustion engines, where non-stationary signals with impulse components are processed.

4. RESEARCH OBJECT AND TESTING PROCEDURE

Tests of vehicles equipped with 1.2 and 1.3 dm^3 spark ignition engines were conducted on a BOSCH chassis test bench, FLA203. During the tests, accelerations of the engine block and head vibration, rotational speed and location of the crankshaftwere recorded as a function of time. The signals were recorded with use of an eight-channel NI PCI-6143 data acquisition card, controlled with a programme developed in the Lab View 7.1 environment. A diagram of the measuring system is shown in Fig. 4.

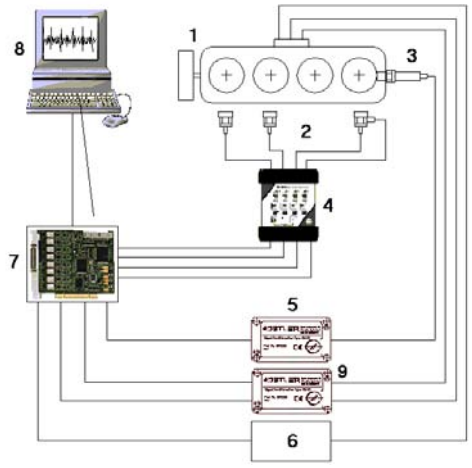

Fig. 4. Diagram of the measuring system l-combustion engine, 2-piezoelectric acceleration sensors, 3-piezoelectric pressure sensor, 4-charge amplifier, 5-signal amplifier, 6- signal converter of the subatmospheric pressure inlet system, 7-data acquisition card, 8-computer with LabView software, 9-amplifier of the rotational speed sensor signal and crankshaft position

The main purpose of the study was to determine the influence of the lack of the LPG fuel inflow into individual cylinders on the vibration signal characteristics. As part of the tests, 7 various states of engine operation were simulated (operational engine; cylinders 1, 2, 3 and 4 disengaged one by one; cylinders disengaged in pairs: 1-4 and 2-3).

In addition, the effect was examined of the simulated local fatigue crack of exhaust valve of the first cylinder in the 1.3 engine on the changes of the wavelet decomposition coefficients.

5. RESEARCH RESULTS

The time courses of vibration accelerations and their decomposition into low- and high-frequency constituents, performed with use of wavelet filtration for one working cycle of an engine during idle run, in the case of switching off the fuel inlet to cylinders 1 and 4, is shown in Fig. 5. In the signal filtered out by means of wavelet decomposition, it is possible to notice low-frequency interference induced by the simulated condition of the engine. Fig. 6 presents the results of approximation A5 and Fig. 7 shows details D4 for five simulated states of the engine operation. On the basis of the presented results of the wavelet analysis, the energy measures can be easily determined from the distributions at different levels of decomposition. The energy of wavelet decomposition coefficients for the selected decomposition level, j and the band range, k, is determined as follows:

$$E_{j,k} = \sum_{k} \left| c_{j,k} \right|^2 \tag{8}$$

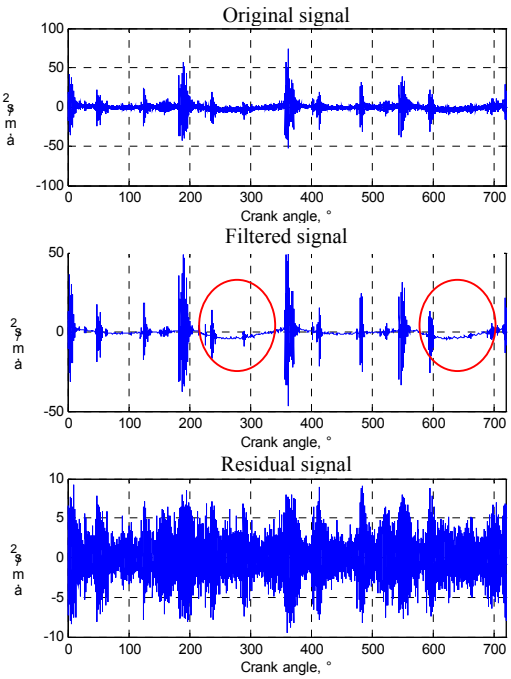

Fig. 5. Decomposition of vibration acceleration signal for an engine with cylinders 1 and 4 off, within one working cycle of the engine

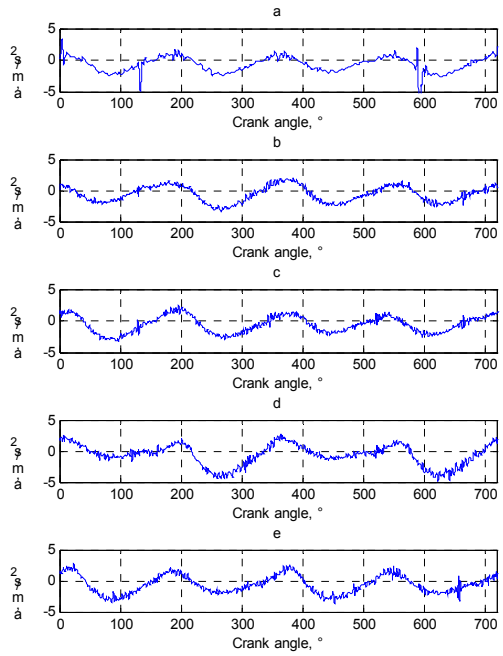

Fig. 6. Approximations at the A5 level, a-operational engine, b)1st cylinder off, c-2nd cylinder off, d- 1st and 4th cylinders off, e- 2nd and 3rd cylinders off

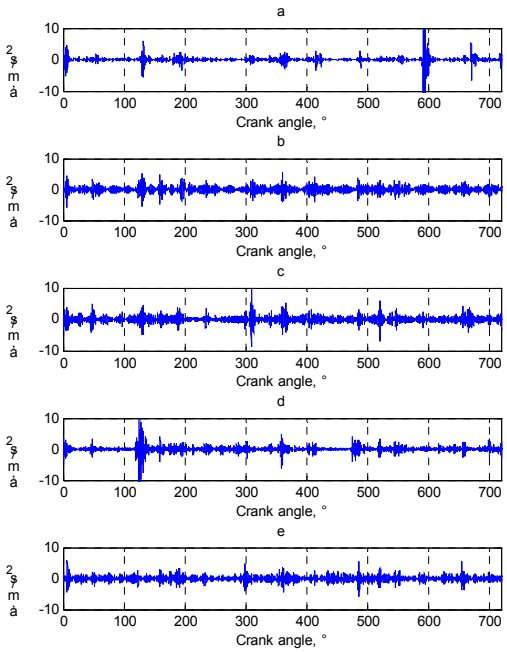

Fig. 7. Details at the D4 level, a-operational engine, b)1st cylinder off, c-2nd cylinder off, d- 1st and 4th cylinders off, e- 2nd and 3rd cylinders off

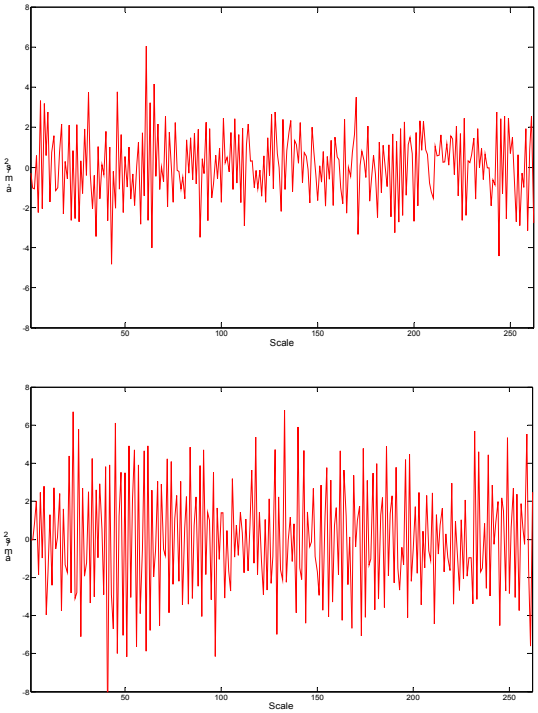

Fig. 8. Results of WPT decomposition for j=4 and k=1 for an operational engine (upper graph) and an engine with a simulated crack of the exhaust valve (lower graph)

Figure 8 shows the selected results of the decomposition by means of WPT for the engine with a simulated crack of the exhaust valve head in the first cylinder. The damage provoked a significant increase of $E_{j,k}$ wavelet coefficients' energy in the selected point of the decomposition tree. When compared to the fully operational engine, the

simulated damage provoked a significant increase of energy of wavelet coefficients $E_{j,k\ uszk}$ / $E_{j,k\ spr}$= 2.97.

6. CONCLUSIONS

On the basis of the examinations carried out and the papers published recently, it can be concluded that the multiple wavelet decomposition is a proper tool for the construction of a set of diagnostic characteristics. This type of analysis has been widely applied recently, because it enables creating standard sets of diagnostic features used as input data of neuron classifiers.

REFERENCES

[1] Batko W., Ziółko M.: *Zastosowanie teorii falek w diagnostyce technicznej*. Problemy Inżynierii Mechanicznej i Robotyki, nr 7, Kraków 2002.
[2] Cempel Cz.: *Diagnostyka wibroakustyczna maszyn*, Państwowe Wydawnictwo Naukowe, Warszawa 1989.
[3] Dąbrowski Z., Madej H.: *Masking mechanical damages in the modern control systems of combustion engines*. Journal of Kones, Vol. 13, No 3/2006.
[4] Dąbrowski Z., Madej H.: *O użyteczności symptomów wibroakustycznych w nowoczesnej diagnostyce silników spalinowych*. Przegląd Mechaniczny nr 1 / 2007, s. 32-35
[5] Fabis P., Flekiewicz M., Flekiewicz B., Madej H., Wojnar G.: *Influence of piston slap on engine block vibration*. SAE Paper No. 2007-01-2163.
[6] Geveci M.: *An investigation of crankshaft oscillations for cylinder health diagnostics*. Mechanical Systems and Signal Processing 19 (2005) 1107–1134.
[7] Isermann R.: *Diagnosis methods for electronic controlled vehicles*, Vehicle System Dynamics, Vol. 36, No. 2-3.
[8] Janecki J., Gołąbek S.: *Zużycie części i zespołów pojazdów samochodowych*. Warszawa, WKiŁ 1984.
[9] Liu B.: *Selection of wavelet packet basis for rotating machinery fault diagnosis*. Journal of Sound and Vibration 284(2005) 567-582.
[10] Madej H., Flekiewicz M., Wojnar G.: *Spatial-phase selection of diesel engine vibroacustic signal for piston slap diagnostic*. Journal of Kones. Powertrain and Transport vol. 14 no. 2 / 2007, s. 133-144.
[11] Madej H., Flekiewicz M., Wojnar G.: *Zastosowanie ciągłej transformaty falkowej (cwt) do analizy drgań siników spalinowych*. Teka Komisji Motoryzacji PAN, zeszyt nr 33-34, Kraków, str. 259-267.
[12] Merkisz J., Mazurek S.: *Pokładowe systemy diagnostyczne pojazdów samochodowych*. WKiŁ, Warszawa 2004.
[13] Peng Z. K., Chu F. L.: *Application of the wavelet transform in machine condition monitoring and fault diagnostics: a review with bibliography*. Mechanical Systems and Signal Processing 18(2004) 199–221.
[14] Wu J. D., Liu C. H.: *Investigation of engine fault diagnosis using discrete wavelet transform and neural network*. Expert Systems with Applications, 35 (2008) 1200-1213.
[15] Wu J. D., Chen J. C.: *Continuous wavelet transform technique for fault signal diagnosis of internal combustion engines*. NDT&E International,39(2006),304-311.
[16] Yan R., Gao R. X.: *An efficient approach to machine health diagnosis based on harmonic wavelet packet transform*. Robotics and Computer–Integrated Manufacturing, 21(2005) 291-301.
[17] Zhang Z., Tomita E.: *Knocking detection using wavelet instantaneous correlation metod*. JSAE Review 23(2002) 443-440.

Henryk MADEJ, Ph.D., D.Sc. Eng. work as a professor in the Department of Automotive Vehicle Construction Silesian University of Technology in Katowice. He deals with IC engines and powertrains diagnostics with the application of vibroacustical signal analysis, also with minimization of machine vibroactivity. Member of Polish Society of Technical Diagnostics.

The results presented in the paper were obtained with the support of the Polish Scientific Committee.

ANALYSIS OF AE-SIGNAL GENERATED DURING FRICTION TEST OF DLC-LAYERS

Anna PIĄTKOWSKA[1], Tadeusz PIĄTKOWSKI[2]

[1]Institute of Electronic Material Technology, Wólczyńska 133, 01-191 Warsaw
e-mail: Anna.Piatkowska@itme.edu.pl
[2]Institute of Optoelectronics, Military University of Technology, Kaliskiego 2, 00-908 Warsaw

Summary

In the present work the results of tribological and simultaneous AE measurements of the DLC layers deposited on Si substrate are presented. The layers studied were 18nm, 200nm and 650nm thick. The best properties were obtained for the films with thickness of 18nm and 650nm. The value of average friction coefficient was stable and equal to 0,1 and no wear was observed. The 200nm layer had a very low adhesion to the substrate. Intense acoustic emission signals accompanied the friction.

Keywords: DLC-film, Acoustic Emission, sliding friction, adhesion, damage.

ANALIZA EMISJI AKUSTYCZNEJ GENEROWANEJ PODCZAS PRÓBY TARCIA WARSTW DLC

Streszczenie

W pracy przedstawione zostały wyniki badań tribologicznych i równoczesnych pomiarów emisji akustycznej na warstwach DLC na podłożu Si. Badano warstwy o grubościach: 18nm, 200nm i 650nm. Najlepszymi właściwościami charakteryzowały się warstwy 18nm oraz 650nm. Współczynnik tarcia był stabilny i wynosił 0,1 a warstwy nie uległy uszkodzeniom. Bardzo słabą adhezją do podłoża odznaczała się warstwa o grubości 200nm. Tarciu towarzyszyła intensywna emisja sygnałów akustycznych

Słowa kluczowe: warstwa DLC, emisja akustyczna, tarcie ślizgowe, adhezja, uszkodzenia.

1. INTRODUCTION

Excellent mechanical, tribological, optical and electronic properties of diamond like carbon (DLC) coatings are exploited in different domains of industry. The major application of DLC is a chemical hard coating for mechanical or chemical protection [1]. Among numerous practical examples the DLC-fine film is used for resistant-coverage and anti-wear coating of optical-infrared elements, where good resistance of abrasion is very important.

In this paper the adherence and tribological properties of DLC-coating are described.

Simultaneous acoustic emission (AE) measurements are used to obtain additional information on the process and the phenomena occurred during the sliding friction in DLC layers.

2. EXPERIMENTAL DETAILS

2.1. Specimens

The DLC-fine films were deposited on Si-substrate by RF reactive sputtering, using a graphite target under various pressures of Ar and H_2. Finally, three thicknesses of DLC films were chosen for analysis: 18nm, 200nm and 650nm.

As the substrate three separate Si-wafers of 2" in diameter with thickness of 0.5mm were used. The surface of substrate was polished (average roughness Ra=5nm on the measurement section 400μm).

2.2. Experimental equipment

Tribological properties and adhesion of the studied films were determined using a "ball-on-disc" tribometer. During dry friction sliding the momentary friction forces were recorded. Then they were converted to the momentary friction coefficient. Three sensors of acoustic emission (AE) measure simultaneously the acoustic signals generated during friction. Schematic diagram of the set-up is presented in Fig. 1.

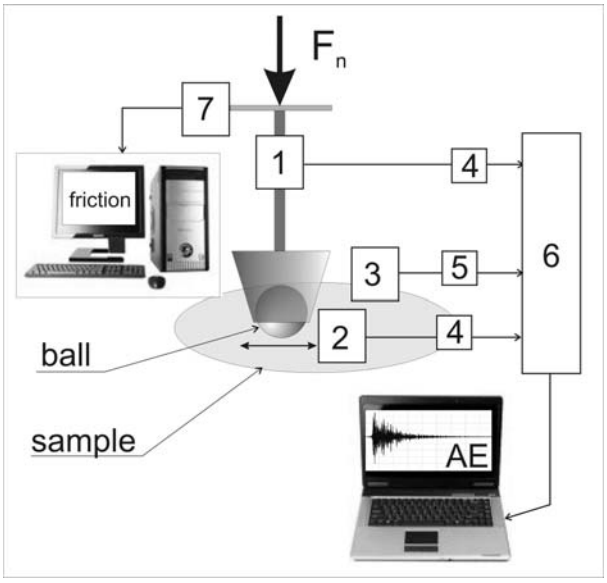

Fig. 1. Schematic diagram of the set-up for the measurement of friction and acoustic signals.
1 – AE sensor freq. Range: 400-750 kHz
2 – AE sensor freq. Range: 60-1950 kHz
3 – Accelerometer freq. Range: 5-60 kHz
4 – AE Preamplifier
5 – Signal Conditioner
6 – Data Acquisition Card
7- Friction force Sensor

The proposed set-up for the measurements of vibroacoustic and acoustic emission is composed with three sensors: two high-frequency sensors (1) and (2), and accelerometer (3) shown in Fig. 1. Sensors (2) and (3) were fixed on the surface of samples with DLC-film in a distance of about 15mm to the wear track. The sensor (1) is placed in the holder of ball with intention to measure acoustic emission signals generated from damages of the ball. Registration of the vibroacoustic and acoustic emission signals was in the 60 s periods in the same way for all tests.

Tribological conditions are described in [2]. The performed tests were a kind of multi-pass with sliding velocity 0.21 mm/s and wear trace length.

2.3. Methodology

The aim of this work is an analysis of the relation between the tribological properties and the generated and recorded AE signals. The values and changes of the momentary friction coefficient and of the AE signals amplitudes recorded as a function of test-time in several time periods (A, B, C…) are compared. We verify if the fluctuations of momentary friction coefficient are accompanied by simultaneous impulses of AE signals. AE signal is analyzed in relation to impulses number, their duration and reproducibility determined from AE-time plots. The frequency spectra were calculated. Due to the non stationary character of AE signals the Short-Time Fourier Transform (STFT) was applied. The STFT transform divides up the signal into small time segments and performs Fourier transforms on each segment of time to derive the spectra. The Kaiser-Bessel window was used due to its higher selectivity than other types of gaps [3-4].

During the friction test several AE signal measurements were performed in dependence of the appearance of fluctuation of the momentary friction coefficient. We named the tests as stage A, stage B.

3. RESULTS AND DISCUSSION

Generally, DLC-films are characterized by very low friction coefficient approx. 0,1 [1, 5] and their key feature is an excellent adhesion to the substrate [5, 6].

In this work we present the results of tribological tests of DLC-films on Si-substrate characterized by different adhesion to the support.

The DLC layers of 18nm thick were characterized by high wear resistance and excellent adhesion to the Si substrate. Multi-pass friction tests performed on the 18nm DLC layer did not show substantial surface damages. The abrasion of the counterbody was observed only together with a transfer of wear products. The corresponding AE signals described the equipment noise and the ball abrasion. Some AE impulses appeared in data registered by sensor1 located in the support of the counterbody. The results obtained due to friction on the 650nm layer are presented in Fig. 2. The undamaged DLC-film resulted in non- AE activity [4, 5].

During the friction test the value of average friction coefficient decreases from 0,15 to 0,08, however in the 60s periods: A, B, C its variations are related to the changes of the movement direction of sliding. The arrows mark one pass of the ball shift. Few AE impulses were recorded and their amplitudes were very low. They were registered only by sensor1. From this fact and from the analysis of the friction trace one can conclude that the AE signals originated from small damages of the ball. Spectra obtained for the subsequent friction stages showed the higher amplitude of the registered AE signals in the frequency range of several to 100kHz.

Average value of friction coefficient for the 18nm DLC layer was about 0,10 during the entire test. AE impulses were not generated and the background level did not change in the next stages of friction. The increase of the load also did not cause any damage on the layer.

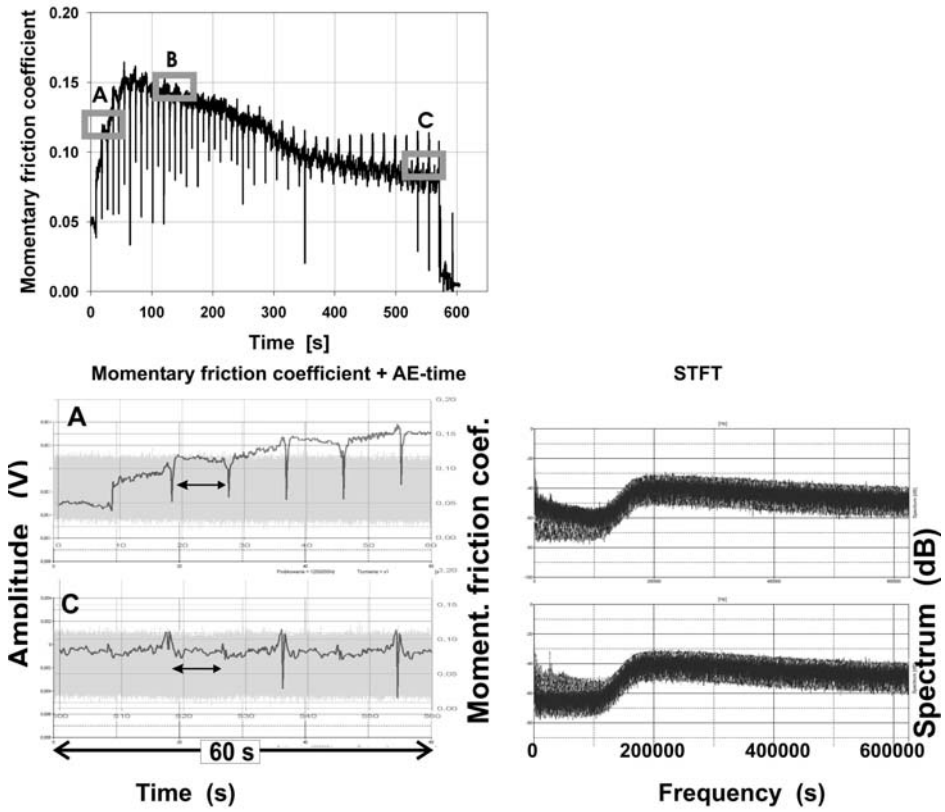

Fig. 2. Results of tribological and AE signal measurement on 650nm thick DLC layer, registered by sensor1

Completely different properties revealed the 200nm thick DLC layer. During the friction test three phases of the average friction coefficient values were observed (Fig. 3).

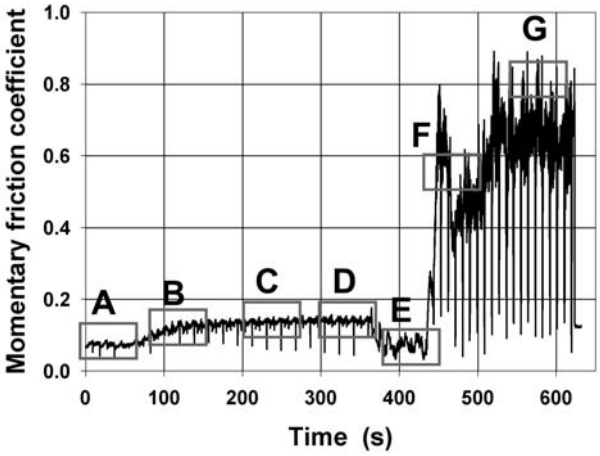

Fig. 3. Plot of changes of the friction coefficient values during test on 200nm thick DLC layer

In the first phase (stages A to D), the value of average friction coefficient was constant (μ=0,08). It lasted up to 200-300s and corresponded to 20-30 passes. In the next phase a decrease of average friction coefficient was registered, however, significant fluctuations were observed. This phase lasted about 100s (10 passes of ball). After that the average friction coefficient value increased catastrophically up to 0,7 with momentary fluctuations in the range of 0,55 to 0,9. The boxes in Fig. 3 mark the registered AE signals. Our intention was the starting of the recording of AE signals when the first changes of the momentary friction coefficient values occur.

First phase of friction indicated by low momentary friction coefficient values shows similar aspects of the generated AE signals as those obtained in the case of 18nm thick layer. The diagrams of AE amplitudes variation and the plots of momentary friction coefficient superimposed with the same time axis are presented on the left in Fig. 4. On the right in Fig. 8 the STFT spectra for A and D stages are shown.

The amplitude of AE signal is comparable for all measurements of this non-wear phase. The STFT spectra for the whole range of frequencies from several to 600kHz do not manifest any rise of amplitude. The single peaks for frequencies: 156kHz, 280kHz and 320kHz are the result of counterbody movements and the activity of tribometer.

The amplitudes amplification is stable for the whole range frequencies and does not exceed -50dB.

The comparison of these results and the amplification level of noise –90dB provide information about increase of amplitudes of AE continuous signals. The next two phases of friction presented in Fig. 5 have numerous AE impulses recorded.

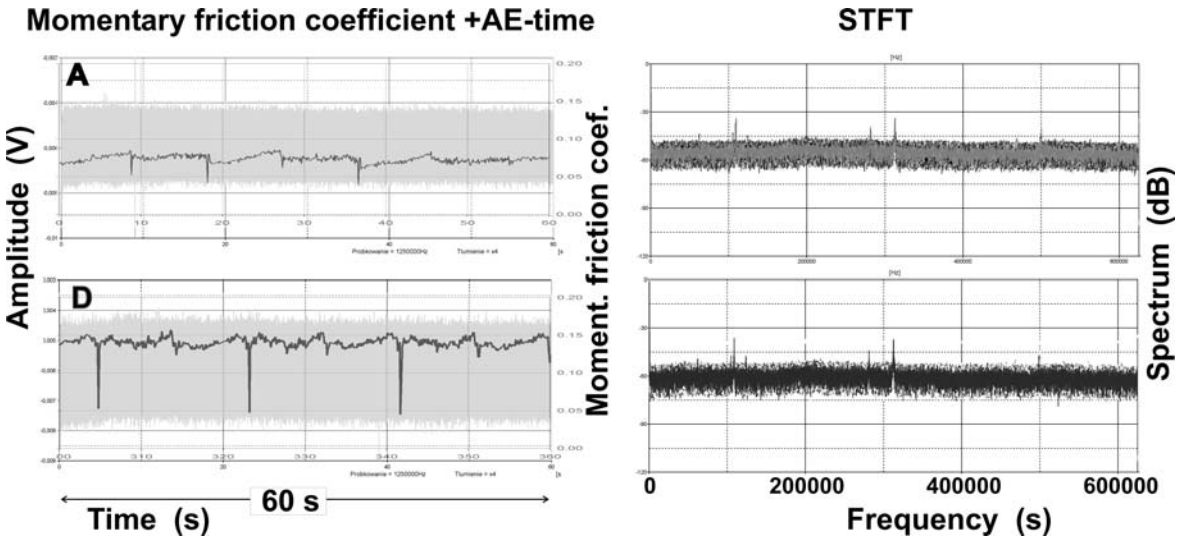

Fig. 4. Diagrams of momentary friction coefficient (dark line) and AE-time (gray lines) registered on 200nm DLC layer and STFT spectra for A and D stages of friction

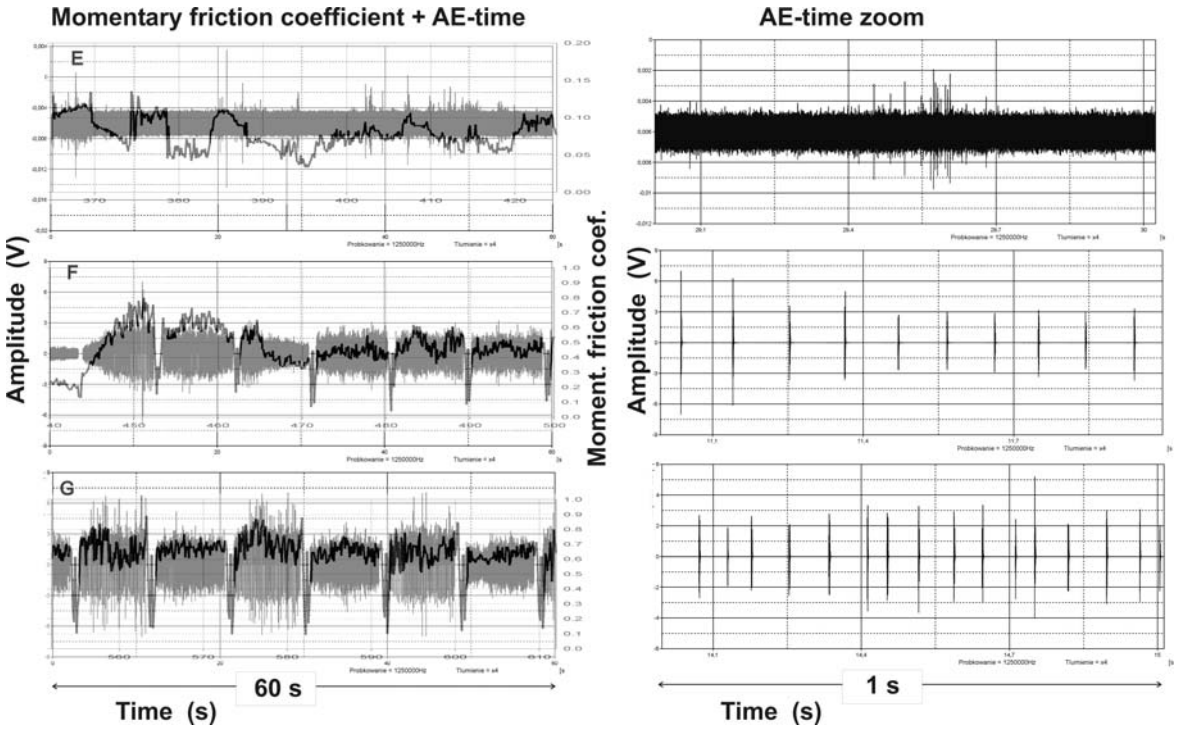

Fig. 5. Diagrams of momentary friction coefficient (dark line) and AE-time (gray lines) registered on DLC layer of 200nm thick

During E stage of friction non-stationary, incoherent groups of trancient impulses were generated. Analysis of the AE signal and the momentary friction coefficient shows weak correlation between these parameters. Spectra STFT for this stage show the amplitude rise for frequencies range from 480kHz to 560kHz. During friction at the E stage trancients amplitudes increase 200 times. Perturbations of momentary friction coefficient correspond to AE-time. The rise of momentary friction coefficient is accompanied by augmentation of AE amplitude. Regular pauses decline of AE signal and low value of friction coefficient coincide with change of movement direction of counterbody. It permits they exact superimpose and comparison of diagrams. At G stage the momentary friction coefficient value increases as well as number of trancients. At both F and G stages simple impulses generated are repetitive. Phenomenon of reappearance is presented by zoom of one second diagram AE time (Fig. 5 on the right). Intervals between successive trancients indicate the tendency to diminution of break during friction-time. Thus for F stage intervals among impulses is 100ms in average, however for G stage is 65ms. At both cases

a certain signal modulation occurred. Higher frequency is obtained for G stage than for F stage. Another difference between tribological behavior at F and G stages was shown by AE signals. Only during G stage the distinction of AE signals takes place. Values of amplitudes depend on the sliding direction. They have much higher values in a return direction. Parallelly momentary friction coefficient is varied. STFT spectra calculated for AE signal of G stage are presented in Fig.6. STFT spectra calculated from whole 60s AE show amplitudes magnification for all range of frequencies. Diagrams in Fig.6 b and c expose 8s section of AE registered respectively by sensor1 and sensor2 (see Fig. 1). This selected AE time part includes strong signals generated during one pass of friction.

In contrary to the results for the whole range of AE at G stage, STFT spectra of part AE time show some preferences of frequencies. For the signal registered by sensor2 fixed to the surface of the sample a higher amplification of amplitudes exists at a frequency about 262kHz. Different appearance is observed for the spectrum STFT calculated from AE-time registered by sensor1 attached to holder of counterbody. Fig.6c presents the rank of frequencies: 110kHz, 140-170kHz, 183kHz 198kHz, 240kHz, 267kHz, 345kHz, 445kHz, 476kHz characterizing trancients with maximal amplitudes.

Between impulses recorded by sensor1 and 2 we do not observe phase difference. Impulses have similar profiles and they happen at identical time.

Duration of these two multiple impulses is comparable. But it seems that sensor 2 is more sensible and it recorded the biggest number of tribological events.

Vibroacoustic sensor 3 recorded small number of impulses and only for terminal friction stage. STFT spectra exhibit impulses at level –40dB and in the range of frequencies from several to 15kHz.

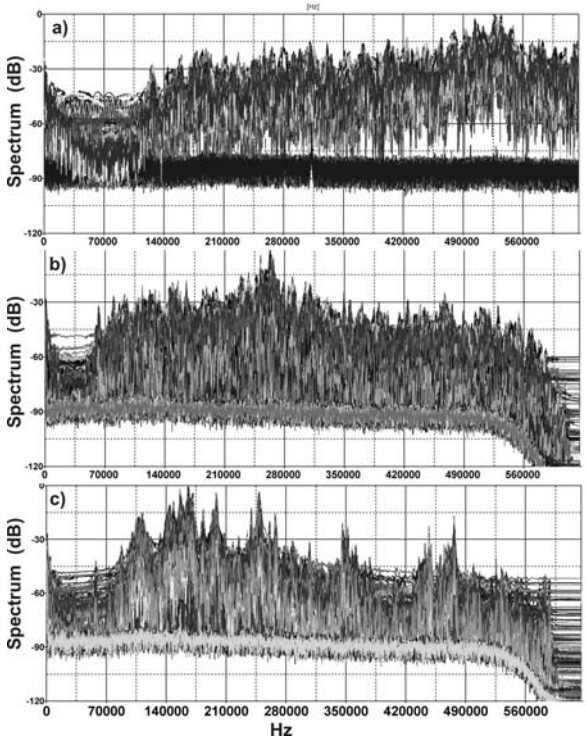

Fig. 6. STFT spectra calculated for G stage a) from 60s AE recorded by sensor2, b) from 8s part of AE recorded by sensor2, c) from 8s part AE, recorded by sensor1

The presented results of tribological and AE measurements were correlated with the topography of wear traces. DLC layer 18nm thick and 650nm thick were not damaged. The only effects of friction are the abrasion and product of couterbody transferred on the surface of sample. This kind of wear generates AE response with higher amplitude of continuous signal. Similar results obtained for plastically deformation were described at [7].

The friction of the sample with 200nm thick layer significantly damaged its surface, but damages appeared after relatively long time of friction. When tribological test was stopped during first phase of friction where average friction coefficient was low and AE impulses were not recorded, we did not observe any wear (by optical microscope with Nomarski contrast). In E stage first microcracks and spalling of DLC layer became visible. Next cycles of friction catastrophically demolished surface. Fig. 8 presents SEM images after 630s of friction, it is after 70 passes of ball.

The topography of wear trace was observed by scanning electron microscope – Fig. 7. For analysis of all wear tracks succeeding scans were realized with 200 time magnification.

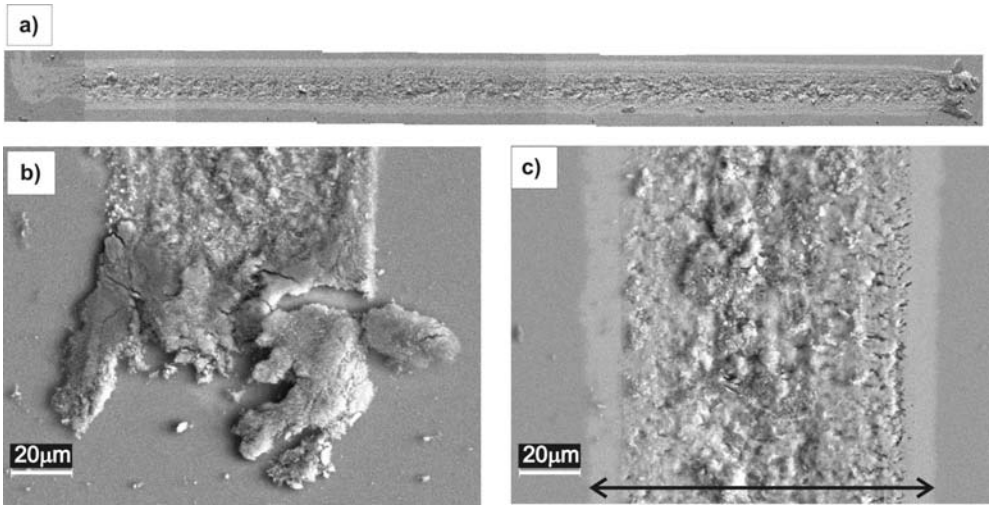

Fig. 7. SEM images of wear trace after friction on DLC layer 200nm thick
a) topography whole track b) zoom of track extremity

In whole trace area shown in Fig. 7a appear almost uniformly spread damages: spallings, microcracks, agglomerations of wear particles. On one extremity of trace presented in Fig. 7b occurred large accumulation of wear particles. It is crushed, pressed conglomerate of wear particles. Fig. 7c shows magnification of central trace fragment. Width of trace marked by arrow, is about 100µm. Clear gray strip zone along wear track is showed on the Si-substrate. Sideways wear trace were occurred delaminating of DLC layer. Probably the break took place during E stage of friction. Products of wear: DLC, Si (counterbody), Si-substrate particles were mixed agglomerates of various dimensions. On the right of trace (Fig. 8c) numerous microcracks of Si-substrate are manifested. The surface of trace is very rough and wear particles are strongly agglomerated. During F stage number of Fine cracks are slightly increased, but they are covered by wear particles.

3. CONCLUSION

Tribological properties of DLC layers depend on their thickness, on the method and parameters of processes. The DLC layers 18nm and 650nm thick produced by RF sputtering were coated by one sputtering process and they characterized very good abrasion resistance and excellent adhesion to Si-substrate. The average friction coefficient is stable and have low value of 0,1.

In this case the identification of wear using a registration of AE signal wasn't useful and non provided new information for discussion of results. The amplification of amplitudes signal level is sign of slight200nm abrasion of couterbody. The DLC layer has a limited abrasion and delamination resistance. In the beginning of friction damages do not appear. This non-wear phase is at 200-300s, according to associated events. The first changes are small spallings, short, single cracks and plastic deformation of DLC-coating. These damages generated measurable activity of AE signal. During this stage when adhesion is lost the average friction coefficient is diminished. In this moment non-regular and non-stationary AE signals appear. Their frequencies is the range: 480-560kHz. Terminal phase of friction consists of the damages formation and the transfer of wear products. The average friction coefficient rises catastrophically until value 0,9. In this stage the friction is accompanied by numerous AE trancients. Size of destruction intensivity can be described by quantity of AE impulses generated per second. This number rises from 10 to 15 impulses/second in terminal 70^{th} pass of friction. It means 50% rise of the origin number of AE impulses or number of damages (tribological events). Considering continuous regularity of impulses it is probably appearance of cracks in substrate.

The measurement AE signal adopted at tribological tests made possible the damage detection and identification of the beginning of cracking of DLC layer, microcutting of Si-counterbody and breakage of Si-substrate.

Friction monitoring by registering AE signals provided observation of wear intensification, that was not visible by measuring the changes of momentary friction coefficient.

Acknowledgements

The study was performed under Grant No.1661/T07/2005/29 from the Polish Ministry of Science and Higher Education.

REFERENCES

[1] Hauert R.: *An overview on the tribological behaviorof diamond-like carbon in technical and medical applications*. Tribology International 37 (2004) 991-1003
[2] Piatkowska A., Piatkowski T.: *Measurement and anaysis of acoustic emission in the tribological system ball-on-disc*. Diagnostyka 4 (44)/2007 43-48.
[3] Aric K. Menon, Zine-Eddine Boutaghou: *Time-frequency analysis of tribological systems-partI: implementation and interpretation*. Tribology International Vol. 31 No.9 (1998) 501-510
[4] Chen G. X., Zhou Z. R.: *Time-frequency analysis of friction-induced vibration under reciprocating sliding conditions*. Wear 262 (2007) 1-10.
[5] Wei Zhang, Akiro Tanaka: *Tribological properties of DLC films deposited under various conditions using a plasma-enhanced CVD*. Tribology International 37 (2004) 975-983.
[6] Zaidi H., Djamai A., Chin K. J., Mathia T.: *Characterisation of DLC coating adherence by scratch testing*. Tribology International 39 (2006) 124-128.
[7] Löhr M.., Spaltmann D., Binkowski S., Santner E., Woydt M.: *In situ Acoustic Emission for wear life detection of DLC coatings during slip-rolling friction*. Wear 260 (2006) 469-478.

Anna PIĄTKOWSKA is a specialist in the micro- and nano-tribological research. She obtained a doctoral degree (Ph.D) from the Institute of Electronic Materials Technology, where she is an assistant professor. Her principal research subjects are: ion implantation, micro-, nano-mechanical and structural properties of implanted materials and SEM imaginig. Dr Piątkowska is a member of Polish Society of Tribology.

Tadeusz PIĄTKOWSKI graduated from the Faculty of Precision Engineering (1981) and Faculty of Electronics of Warsaw University of Technology (1984). He received his PhD from Military University of Technology in 2003. He is now an assistant professor at the Institute of Optoelectronics of Military University of Technology. His research area is mainly in fusion sensors systems, remote temperature measurements. He took part in 19 research projects and he is an author and co-author of 30 publications.

THE DIAGNOSIS OF ON BOARD GENERATORS

Andrzej GĘBURA, Tomasz RADOŃ
Instytut Techniczny Wojsk Lotniczych, ul. Księcia Bolesława 6, 01-494 Warszawa, skr. Poczt,. 96,
tel. 0-22-685 22 42, e-mail. andrzej.gebura@itwl.pl

Summary

In the paper select problems related to diagnosis of onboard generators and alternators with control systems are discussed. Problems refer to commutator generators and synchronous single and three phase alternators.

Special attention is paid to commutation effects. Results of incorrectness and possibility to detect them are discussed. There are also discussed effects concomitant with changes in a character of a pulsation during short-circuits or isolating clearance in a wiring of a rotor or a stator. Possibility of diagnosis of generator's or alternator's parts by means of analysis of pulsation component parameters is indicated.

In a case of alternators, there are discussed a number of diagnostic methods based on an observation of shape changes of voltage or frequency modulation. It provides to detect numerous mechanical or electrical faults of generators, alternators or their control systems.

Keywords: technical diagnostic, frequency modulation, turbine engine, rolling bearing.

DIAGNOZOWANIE POKŁADOWYCH PRĄDNIC LOTNICZYCH

Streszczenie

Starzejąca się technika lotnicza wymaga poważnego podejścia do problemu oceny trwałości statku powietrznego w tym, do niedawna nie zawsze doceniane, trwałości instalacji elektroenergetycznej. Szeroko pojęty system elektryczny statku powietrznego wpływa swą, często obniżoną, na skutek procesów starzeniowych, kondycją, na obniżenie trwałości wszystkich innych systemów.

W pracy omówiono wybrane problemy związane z diagnozowaniem pokładowych prądnic lotniczych wraz z układem regulacji. Problematyka poruszana w tym artykule dotyczy komutatorowych prądnic prądu stałego oraz przemiennego (synchronicznych prądnic jednofazowych i trójfazowych).

Podczas omawiania problemów diagnozowania prądnic prądu stałego szczególną uwagę zwrócono na zjawiska komutacji – omówiono objawy nieprawidłowości i możliwości ich wykrywania. Omówiono również pewne zjawiska towarzyszące zmianom w charakterze pulsacji podczas zwarć lub przerw w uzwojeniach w wirniku lub stojanie – wskazano na możliwość diagnozowania tych elementów prądnic za pomocą analizy parametrów składowych pulsacji. Zaproponowano zastosowanie metody obserwacji szczególnych korelacji pulsacji do wykrywania zwarć wirnika lub stojana. Analizując kształt i amplitudę składowej pulsacji prądnicy komutatorowej prądu stałego, można wykrywać zwarcia i przerwy w obwodzie wirnika. W przypadku przerw w obwodzie wirnika zmniejszeniu ulega amplituda składowej pulsacji a w przypadku zwarcia obraz charakterystyczny składowej pulsacji. Zwarte uzwojenie podczas przemieszczania się wirnika pod kolejnym biegunem stojana wywołuje wielokrotnie zwiększoną pulsację komutatorową. Dzięki pogłębieniu wiedzy doświadczalnej na ten temat możliwe było diagnozowanie szeregu uszkodzeń zarówno prądnic prądu stałego jak i całych węzłów elektroenergetycznych.

W przypadku prądnic prądu przemiennego omówiono szereg metod diagnostycznych opartych na obserwacji zmian kształtu przebiegu modulacji napięcia lub częstotliwości, umożliwiających wykrywanie wielu wad mechanicznych i elektrycznych prądnic oraz ich układów regulacji. Referat omawia aspekty diagnostyczne związane z obserwacją parametrów dynamicznych lotniczych pokładowych pierwotnych i wtórnych źródeł prądu przemiennego. Omówione zostały właściwości diagnostyczne takich parametrów jak: a) impulsy przepięciowe i zanikowe dla stanów przejściowych obciążenia sieci pokładowej, b) amplituda obwiedni, c) zniekształcenia kształtu przebiegu (całkowita zawartość harmonicznych, wartość poszczególnych harmonicznych, współczynnik amplitudy, odchylenie od kształtu sinusoidy), d) dewiacja częstotliwości, e) precesja częstotliwości, f) wartość harmonicznych cząstkowej transformaty Fouriera częstotliwości;
g) przebieg zmian wartości chwilowej częstotliwości.

Słowa kluczowe: diagnostyka techniczna, modulacja częstotliwości, silnik turbinowy, łożysko toczne, pulsacje żłobkowe, pulsacje komutatorowe, impulsy zanikowe, impulsy przepięciowe.

1. PULSATION CHARACTERISTIC OF A GENERAT

In a standard, school formulation, a commutate generator can be presented as it shown on Figure 1. Figure 2 shows an electromotive force. The commutate generator consists of:

- a motionless stator, which can be presented as a pair of permanent magnets (fig. 1), where: "N"- north pole, "S"- south pole generating permanent magnetic field with an intensity of B and a sense from "N" to "S";
- a rotor turned with a velocity of ω_2 by an outside mechanical force. On the rotor there is a rolled winding in which the electromotive force e is induced. The induced electromotive force (EMF) can be described by a formula:

$$e = \left| k \cdot B \cdot \sin(\omega_2 t) \right| \qquad (1)$$

where: k – design coefficient of the generator, B – magnetic induction, ω_2 – angular velocity of the generator's rotor;

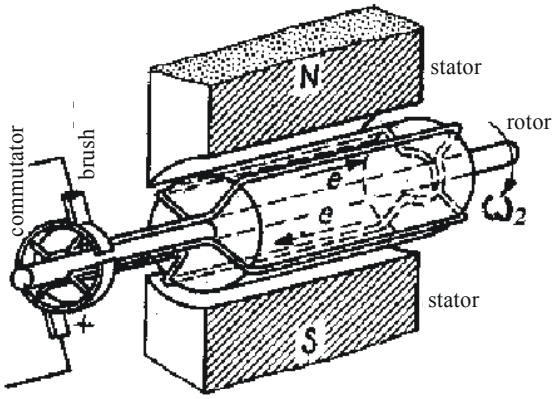

Fig. 1. The rotor with two coil elements and four-segment commutator

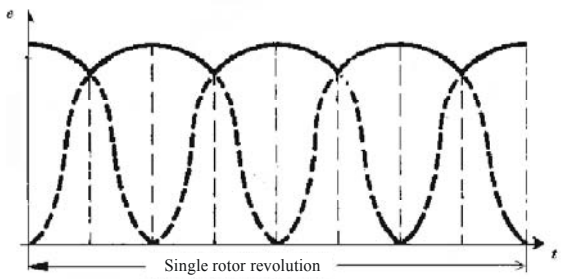

Fig. 2. The course of electromotive force between the brushes in the d.c. generator

- a commutator as a ring made of conducted material. This ring is cut and its segments are insulated. Segments create so-called sectors (staves) of the commutator. End of the winding is connected to each sector – the commutator is a mechanical current rectifier;
- electric brushes "+" and "-", which slide along commutator's sectors. Conductors conducting electric current to loads are conducted to brushes.

In order to increase induction B, rotor's windings are placed on a core made of silicon sheet pack. The value of electromotive force (EMF) is amplified about 10 000 times. For good mechanical connection windings on the rotor with the core, they are placed in special grooves called skewed slots. In a cross-section of the rotor's core these skewed slots have shape of teeth, therefore a term of "rotor's teeth" is used. A comparison of a function described by formula (1) – (Fig. 2) with the generator's pulsation component (Fig. 3) does not show their similarity.

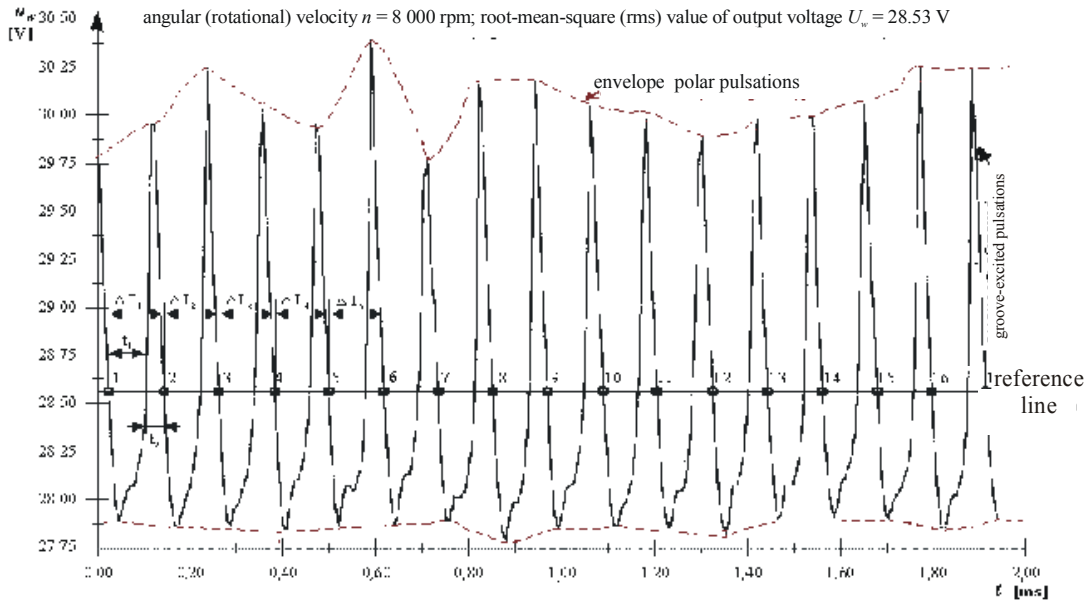

Fig. 3. Fluctuations in pulsation component for an aircraft d.c. generator under minimum load

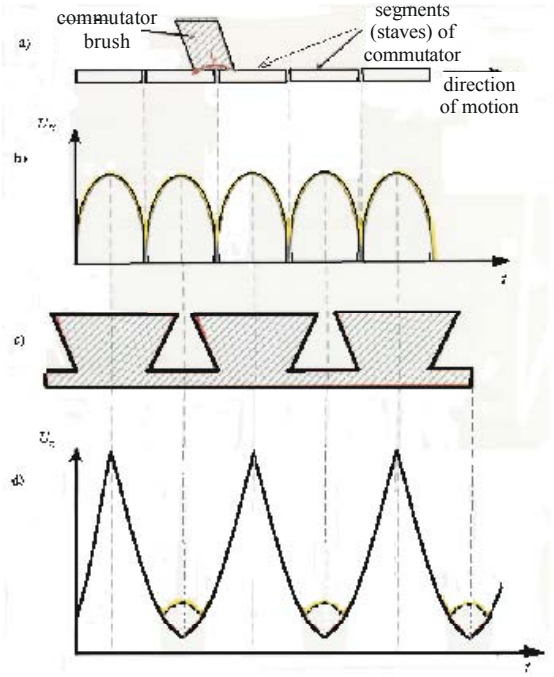

Fig. 4. The shape of pulsation curve plotted for the d.c. generator: a) developed view of mechanical components of the commutator node, b) commutator-excited pulsations – $U_K = f(t)$, c) developed view of rotor grooves, groove-excited pulsations (solid line) – $U_ż = f(t)$, with commutator-excited pulsations indicated (broken line)

Groove pulsation of generator output arises as a result of changes of reluctance, caused by rotation of a tooth rotor. The frequency of groove pulsation f_g according to [1 – 4] can be expressed by the formula:

$$f_g = Z\ n/60$$

where: Z – number of rotor's grooves, n – rotational speed.

In the references [1 – 3] pole pulsation of voltage is related to so-called rotational pulsation considering their similarity. A phenomena of pole and rotational pulsation is visible as amplitude modulation of commutate generator's output voltage. The envelope presented on Figure 3 testifies to it. The modulation frequency is directly proportional to product of number of stator's poles and rotor's angular velocity but amplitude's depth is proportional to changes of magnetic reluctance between the rotor and the stator. The frequency of pole pulsation f_p can be presented by formula:

$$f_p = 2pn/60$$

where: p – number of pairs of stator's magnetic poles.

The signal of pole modulation brings information about anisotropy of plates of generator's magnetic circuit. In special references pole modulation is usually related to rotational modulation, which is characterized by frequency of that type modulation equal to frequency of first or second harmonic (in some cases first sub harmonic) of generator rotor's rotational velocity.

This signal brings diagnostic information about errors:

- accomplishment of the generator, particularly about inaccuracy of geometric dimensions, appearing as asymmetry of an air-gap between the stator and the rotor;
- assembly of the generator, such as parallelism error, i.e. shift of the generator's rotor shaft axis in relation to the drive shaft, named sometimes as eccentricity error, as well as angular error of shift of the rotor' s shaft in relation to the drive shaft.

The voltage commutate pulsation is related to co-operation brushes and the commutator. During rotation of armature, brushes short-circuit different number of winding coils, what changes a number of coils in parallel branches and creates periodic pulsation of voltage on brushes. The frequency of that pulsation f_k depends on the number of commutator's sectors and can be expressed by the formula [1-2]:

$$F_k = K\ n/60$$

where: K – number of commutator's sectors.

2. GROOVE PULSATION

The phenomena of different groove pulsation is described in references related to induction alternators [1, 2]. Alternators do not have the winding rotors and useful signal is received from the winding winded on the stator. The rotor made of ferromagnetic (most often of silicon-steel sheet pack) has milled grooves (teeth) and the magnetic field strength of permanent magnets is modulated. In these alternators groove pulsation is the basic phenomena of the useful signal to be arisen. Because there is not the winding on the rotor, as in typical commutate alternator, only alternating component of pulsation occurs (commutate pulsation does not appear considering the lack of the commutator and the rotor's winding). On the base of information from reference [1-2], it is known that in order to obtain the output voltage signal in the highest degree approximate sine curve, skew teeth (fig. 4b) are most often used in induction alternators.

Rotors with grooves of "swallow's tail", presented on Figure 4c, are rarely used in induction alternators because they have asymmetrical shape of output voltage [1]. This shape of grooves is generally used in typical commutate generators. It ensures windings are good fastened on the rotor. Time between groove pulsation crossings the reference level for the alternator rotor's angular velocity ω_2 = const depends only on angle error of cuts of teeth. Because these errors appear periodically after each full rotation of the rotor, they can be easy filtered. Incontestable is the fact of rigid mutual angle position of grooves in relation to themselves. In this connection for ω_2 = var, time between succeeding crossings "zero" level (after filtering cut errors of rotor's grooves) is the measure of changes of rotor's angular velocity. Described

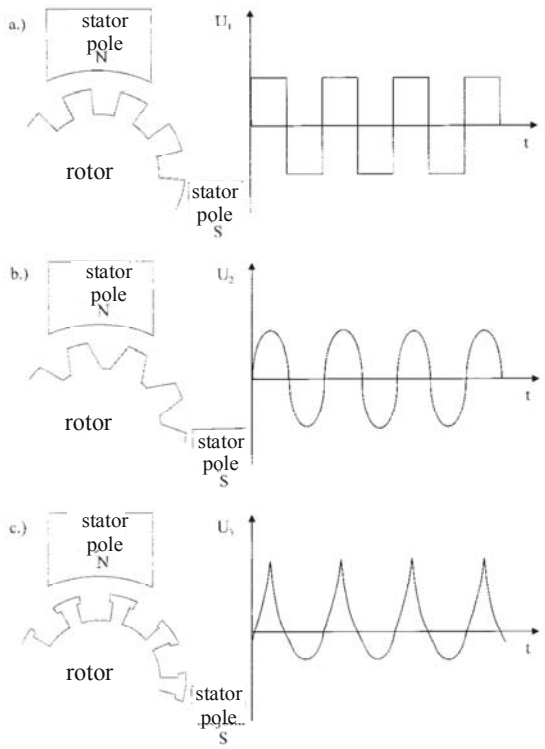

Fig. 5. Typical courses of output voltage of induction generators with a) trapezoid, b) rectangular, and c) 'swallow-tail' shaped rotor grooves

properties of groove pulsation have been used as a source of diagnostic information about technical condition of the alternator's power unit. It was the base to elaborate FDM-A diagnostic method, which is discussed in the another scientific description [5].

The measurement of amplitude of groove pulsation provides to locate brakes in rotor's winding. From data obtained during investigations [7] appears that after a failure of winding relative value (related to rms value of alternator's output voltage U_o) of groove pulsation $\delta_ż$ decreases. This value can be expressed by formula:

$$\delta_ż = \Sigma\,(U_{maxm} - U_{minm}) \cdot 100\% / Ż \cdot U_o$$

where: m – natural number as a number of succeeding period of groove pulsation, U_{maxm} – maximal value of voltage of pulsation component in given period m, U_{minm} – minimal value of voltage of pulsation component in given period m, Ż – number of rotor's grooves.

Simultaneously after the failure of generator's winding, changes of rms value of output voltage ΔU_o occur practically imperceptible, especially for lower values ω_2). They are presented in Table 1 – on the base of data from [7]. Relative value of these changes for the failure of one winding of the rotor δU_o does not exceed 0,01%. In practice to notice the failure of alternator, i.e. the break in winding, by aircrew during operation is impossible. As it results from practice of staff managed by authors to notice the failure is possible by using special measure apparatus.

The failure of alternator's winding, e.g. its break, causes decreasing of value of groove pulsation given in Table 1 as coefficient $\Delta\delta_ż$ from 0,8% to 1,6%, what can be measured using measure apparatus of class 0,1%.

3. POLE PULSATION

The phenomena of pole pulsation can be observed on the curve of output voltage [5] of the generator as the amplitude modulation shown on Figure 3. The frequency of modulation is directly proportional to the product of the number of stator's poles and rotor's angular velocity, but the amplitude's depth is proportional to changes of magnetic reluctance between the rotor and the stator. This signal brings information about anisotropy of plates of the generator's magnetic circuit. The modulation can cause small errors of ΔT_i measurement. It is easy to filter, considering recurrence of it, characteristic for the given generator.

Relative pole pulsation δ_p can be expressed by the formula:

$$\delta_p = \{(U_{max0} - U_{min0})\ 100 / (U_{max0} + U_{min0})\}_{MAX} \quad (6)$$

where: 0 – natural number meaning number of succeeding period of pole pulsation; U_{max0} – maximum value of pulsation component voltage in period 0; U_{min0} – minimal value of pulsation voltage component in given period 0.

Pole pulsation brings some diagnostic information:

a) phase parameter informs about errors of geometrical distribution of stator's pole pieces,
b) pulsation amplitude (envelope shown on Figure 3) generally testifies to irregularity of magnetic field's distribution under stator's magnetic poles but in a few cases also to short-circuit or break of winding of rotor or stator:

– if amplitude of pole pulsation reaches, uniformly extended, in a whole period, values approximated amplitude of rotor's groove pulsation it means surcharge of one coil in consequence extended leakance of its insulation or partial short – circuit with ground or between rotor's coils in the given groove;
– if amplitude of pole pulsation reaches unequal values in the whole period, e.g. for one rotor's rotation peak value of that envelope decreases, it means surcharge of one coil in consequence extended leakance of its insulation or partial short – circuit with ground or between coils of one stator's pole;
– if amplitude of pole pulsation decreases uniformly in the whole period of rotor's rotation, as it is shown in table 2, it can indicate break of rotor's winding.

Considering diagnostic complexity of signal and its small amplitude in relation to carrier component (groove pulsation) to localize damaged

Table 1. Parameters of groove-excited pulsations prior to and after a failure to the generator

ω_2 →	rpm	4000	4500	5000	5500	6000	6500	7000	7500	8000	8500	9000	9500	Condition of winding
U_{ws}	V	28,6	28,5	28,5	28,5	28,6	28,7	28,7	28,6	28,6	28,6	28,6	28,9	Fit for use
$\delta_{\dot{z}}$	%	6,3	5,8	5,6	5,8	5,5	5,6	5,7	5,8	5,4	5,4	5,9	5,5	
U_{wz}	V	28,6	28,5	28,5	28,9	28,6	28,6	28,5	28,9	28,6	28,6	28,5	28,5	Damaged
$\delta_{\dot{z}}$	%	5,0	3,6	4,7	4,0	4,4	4,6	4,1	4,2	4,5	4,3	4,8	4,7	
ΔU_w	V	0	0	0	-0,4	0	0,1	0,2	-0,3	0	0	0,1	0,4	Indices effected by comparison between parameters
δU_w	%	0,00	0,00	0,00	-0,01	0,00	0,00	0,01	-0,01	0,00	0,00	0,00	0,01	
$\Delta\delta_{\dot{z}}$	%	1,3	2,2	0,9	1,8	1,1	1	1,6	1,6	0,9	1,1	1,1	0,8	

Table 2. Parameters of pole pulsations prior to and after a failure to the generator

ω_2 →	rpm	4000	4500	5000	5500	6000	6500	7000	7500	8000	8500	9000	9500	Condition of winding
U_{w1}	V	28,6	28,5	28,5	28,5	28,6	28,7	28,7	28,6	28,6	28,6	28,6	28,9	Fit for use
δ_{b1}	%	4,2	4,2	3,9	4,4	4,1	4,1	4,0	4,4	4,1	4,1	4,3	4,3	
U_{w2}	V	28,6	28,5	28,5	28,9	28,6	28,6	28,5	28,9	28,6	28,6	28,5	28,5	Broken
δ_{b2}	%	3,6	3,2	3,6	3,3	3,4	3,6	3,4	3,5	3,4	3,3	3,7	3,5	
$\Delta\delta_b$	%	0,6	1	0,3	1,1	0,7	0,5	0,6	0,9	0,7	0,8	0,6		Comparison

windings by means of the measurement of pole pulsation is not enough precise. Signal of pole pulsation grows significantly in the case of failure, e.g. short – circuit of any winding – its amplitude grows several times in comparison with amplitude of groove pulsation. Because during short – circuit of coil commutate pulsation amplitude considerably grows, phenomena of short – circuit is discussed below.

4. COMMUTATE PULSATION

The phenomena of commutate pulsation is not used in method FDM-A [5 i 6], because it has been admitted to be interference signal. Previous investigations carried out by authors [5, 8] have showed that value of amplitude of that pulsation is directly proportional to level of current load. Figure 4 presents interdependence between commutate and groove pulsation as well as localization of rotor's grooves and commutate staves. From experiments with using onboard generator it results that for generator's load current below 10% rated value - amplitude of commutate pulsation (fig. 4b) is almost imperceptible against a background of groove pulsation (fig. 4d). For load 10% pulsation is scarcely visible on output voltage. Angle displacements of each half – sinusoid of commutate pulsation (fig. 4d) change in relation to groove pulsation and are individually displaced during mechanical vibration of brushes in a brush – holder as well as generator's current load. In this connection commutate pulsation can not be used for diagnosis of failure value of power unit's kinematics pairs.

For rated load peak value of commutate pulsation reaches level about 50% of groove pulsation. It means that it can be used as a source of diagnostic information of failures e.g. generator's commutate – brush kinematics pair.

Interesting data were given by controlled short – circuit in the rotor. When midpoint of one winding was shorted, it appeared that pole pulsation, visible as slow changing component, was predominant (fig. 5) but commutate pulsation was fast changing (fig. 6).

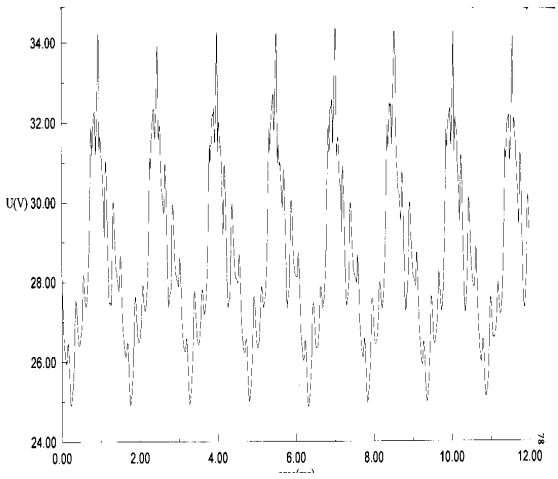

Fig. 6. Output voltage of the d.c. generator at the rotor winding fault (inter-turn short-circuit fault).

As far as component of pole pulsation was stable, in respect of frequency and amplitude, the component of commutate pulsation reached maximal value at the moment of passing under succeeding pole of the generator's stator. A univocal change of relation between amplitude of pulsation components provide to detect short – circuits in rotors of commutate generators.

5. SUMMARY

In the paper different kinds of pulsation of generator's output voltage have been discussed. However in practice they appear simultaneously, amplitude – phase relation between them are very different. Special references describe individually each of them. Authors, based on own developing, try to present practical relations between them. Pulsation component brings much diagnostic information about both technical condition of power unit as well as information source, i.e. generator. It is not mentioned in references. Diagnostic symptoms, contained in pulsation and precisely recognized, are used in professional practice of authors. Others having more than one meaning and not identified will be able to use after many arduous investigations that will provide to find precise relations between succeeding parameters of kinematics failures and parameters of output voltage component.

LITERATURE

1. Wróbel T.: *Studium teoretyczne i eksperymentalne zagadnienia pulsacji napięcia prądnic tachometrycznych prądu stałego.* Dodatek do Biuletynu WAT nr 3(259), Warszawa 1974.
2. Wróbel T.: *Studium zagadnienia pulsacji napięcia prądnic tachometrycznych o wyjściu stałoprądowym*. Dodatek do Biuletynu WAT nr 6(298), Warszawa 1977 (in Polish).
3. Liwschitz-Garik M.: *Direct-current machines* D. Van Nostand Company, New York 1962.
4. Plamitzer M.: *Maszyny elektryczne.* Wydawnictwo Naukowo-Techniczne, Warszawa 1962.
5. Biarda D., Falkowski P., Gębura A., Kowalczyk A.: Opis patentowy PL 175674B1: *Sposób diagnozowania technicznego elementów sprzęgających silnik, a zwłaszcza lotniczy silnik spalinowy, z prądnicą prądu stałego.* Zgłoszenie 08.07.1996, udzielenie patentu 29.01.1999.
6. Biarda D., Falkowski P., Gębura A., Kowalczyk A.: Opis patentowy PL 175645B1: *Sposób diagnozowania technicznego elementów sprzęgających silnik, a zwłaszcza lotniczy silnik spalinowy, z prądnicą prądu stałego.* Zgłoszenie 08.07.1996, udzielenie patentu 29.01.1999.
7. Gębura A., Prażmowski W., Kowalczyk A., Falkowski P., Głowacki T., Budzyński P., Pisarska K.: *Sprawozdanie z pracy – określenie związków pomiedzy parametrami jakości energii prądnic pokładowych a stanem zużycia skrzyń napędowych.* Warszawa, czerwiec 1997r, niepublikowane, nr BT ITWL 11818/I.
8. Gębura A., Prażmowski W., Kowalczyk A., Falkowski P., Głowacki T., Budzyński P., Gajewski T., Pisarska K.: *Sprawozdanie z pracy – określenie związków pomiędzy parametrami jakości energii prądnic pokładowych a stanem zużycia skrzyń napędowych. Część I.* Warszawa czerwiec 1997, niepublikowane, nr BT ITWL 12023/I.

AVERAGED WAVELET POWER SPECTRUM AS A METHOD OF PISTON – SKIRT CLEARANCE DETECTION

Grzegorz WOJNAR, Henryk MADEJ

Silesian University of Technology, Faculty of Transport, ul. Krasińskiego 8, 40-019 Katowice
tel: (032) 603 41 93, e-mail: Grzegorz.Wojnar@polsl.pl

Summary

Vibration of engine block and head is caused by many input functions and their structure changes together with the occurrence of mechanical damage, wear and tear, and anomalies occurring in the combustion process. Due to the above reasons, the vibration signal measured on an engine block or head is of complex nature, it is non-stationary and contains transient components. In such case, the traditional methods, such as Fourier analysis are of little use; it is necessary to apply processing methods as far as time and frequency are concerned.

This paper presents an attempt to define the clearance in the piston – cylinder system based on the vibration acceleration signal. A single-cylinder Diesel engine and a four-cylinder engine with spark ignition (SI) were tested. In order to obtain damage sensitive symptoms, the vibration acceleration signals were analyzed with use of a continuous wavelet transform (CWT). Based on the wavelet analysis, the averaged wavelet power spectra (ASWPS) were defined, which reflect the energy distribution on a scale being the frequency function. Based on the results obtained, it has been shown that the averaged wavelet distribution of signal energy can be useful in diagnosing clearance in the piston – cylinder system.

Keywords: combustion engines, diagnostics, wavelet transform, clearance in the piston – cylinder system.

UŚREDNIONE FALKOWE WIDMO MOCY JAKO METODA DIAGNOZOWANIA LUZU W UKŁADZIE TŁOK-CYLINDER

Streszczenie

Drgania bloku i głowicy silnika są spowodowane wieloma wymuszeniami, a ich struktura zmienia się wraz z pojawianiem się uszkodzeń mechanicznych, zużycia eksploatacyjnego oraz występowania anomalii w procesie spalania. Z powyższych powodów sygnał drganiowy mierzony na bloku lub głowicy silnika ma złożony charakter, jest niestacjonarny i zawiera składowe impulsowe. W takim przypadku tradycyjne metody takie jak analiza Fouriera są mało przydatne, konieczne staje się stosowanie metod przetwarzania w dziedzinie czasu i częstotliwości.

W artykule przedstawiono próbę określania luzu w układzie tłok – cylinder na podstawie sygnału przyspieszeń drgań. Badaniom podano jednocylindrowy silnik z zapłonem samoczynnym (ZS) i czterocylindrowy silnik z zapłonem iskrowym (ZI). W celu uzyskania symptomów wrażliwych na uszkodzenie sygnały przyspieszeń drgań analizowano za pomocą ciągłej transformaty falkowej (CWT). Na podstawie analizy falkowej określono uśrednione falkowe widma mocy (ASWPS), które odzwierciedlają rozkład energii w dziedzinie skali będącej funkcją częstotliwości. Na podstawie uzyskanych wyników można stwierdzić, że uśredniony falkowy rozkład energii sygnału może być przydatny w diagnozowaniu luzu w układzie tłok – cylinder.

Słowa kluczowe: silniki spalinowe, diagnostyka, transformata falkowa, luz w układzie tłok cylinder.

1. INTRODUCTION

For the detection of mechanical defects in motor vehicles, operating processes are used as information carriers, in which the processing of one energy type into another or its transfer takes place. The carrier of information on the technical condition of combustion engines, which is used more and more frequently, is a vibroacoustic signal [2, 3, 4, 5, 7, 8, 10]. The diagnostic systems used in the modern combustion engines [9] aim at locating the element or system which, due to natural wear or damage, cannot further perform its function as specified by the manufacturer.

From the point of view of their effects, mechanical damages can be divided into:

– damages causing the increase of toxic compounds emission or the increase of fuel consumption,
– damages having direct influence upon the safety of driving.

– non-emmission damages of the power transmission system, imparing the vehicle's dynamics.

Increasing requirements concerning the durability and reliability of combustion engines and the minimisation of costs and disadvantageous influence upon the environment necessitate the acquiring of information on their condition during operation. Introduction of the obligation of manufacturing motor vehicles compliant with the OBDII standard resulted in the possibility of accessing data stored in the programmers of individual systems. Owing to this solution, new possibilities of diagnosing the technical condition of those systems arise [9]. The main sources of vibrations and noise generated by the piston combustion engine, are thermodynamic processes taking place in it, including the combustion process, percussion phenomena in the piston – cylinder system and operation of the timing gear system. Combustion of the material filling the cylinder is a quickly-changing process and it occurs in a small range of the crankshaft rotation angle corresponding to the piston location close to its top dead point (GMP). The impulse nature of inductions initiates the vibrations of the resonant engine structure. Vibration acceleration signal are registered on the head and engine block may be used in tests aiming at limiting vibroactivity of combustion engines and they are a good source of diagnostic information on the condition of various engine kinematic pairs.

2. AVERAGED WAVELET POWER SPECTRUM (ASWPS)

The vibration signal measured on engine block or head is complex, non-stationary and contains transient components, and therefore, traditional methods, such as Fourier analysis, are of little use here. In recent years, diagnostic methods are developed which use signal analysis in time and frequency respect (Wigner—Ville distribution – WV) or in respect of time and scale, being a frequency function – continuous wavelet transform (CWT) [1] defined by the following equation:

$$CWT_x(a,b) = C_{ab} = \frac{1}{\sqrt{a}} \int_{-\infty}^{\infty} \psi^* \left(\frac{t-b}{a} \right) \cdot x(t)dt \,, \quad (1)$$

where:

a – means scale parameter,
b – value of the analysing function shift,
$\psi(t)$ - analysing wavelet,
$x(t)$ – signal analysed.

Characteristics obtained by means of wavelet transformation are called scalograms or time and scale characteristics and they are usually presented as SD or 3D charts. The time axis of the characteristics corresponds to the time shift the base wavelet is subject to, whereas another axis contains the values of scale which are the frequency function. Similarly to spectogram which is the square of *STFT* Fourier transformation module, the scalogram is the square of wavelet transformation module, that is, time-scale representation:

$$S_x^{SCAL}(a,b) = \left|CWT_x(a,b)\right|^2 = \left|C_x(a,b)\right|^2 . \quad (2)$$

Based on this transformation, it is possible to determine the so-called scale wavelet power spectrum used for the evaluation of energy change of the signal analysed in selected scopes of scale and crankshaft rotation angle:

$$E(a) = \int_{b_1}^{b_2} \left|C_x(a,b)\right|^2 db = \int_{b_1}^{b_2} S_x^{SCAL}(a,b)db \,. \quad (3)$$

where:

b_1, b_2 – limits of integration, corresponding to the analysed scope of time or crankshaft rotation angle.

Based on the spectrum so determined, it is possible to define the signal energy in a selected range of scale $a_1 \div a_2$ and the crankshaft rotation angle $b_1 \div b_2$:

$$E = \int_{a_1}^{a_2} E(a)da = \int_{a_1}^{a_2}\int_{b_1}^{b_2} S_x^{SCAL}(a,b)dadbb \,. \quad (4)$$

3. ANALYSIS OF SI ENGINE SIGNALS

During the tests of a vehicle equipped with a spark ignition engine of 1.2 dm^3 capacity acceleration of vibration was recorded in the function of time and the crankshaft rotation angle. In the measurements, a DPA crank angle encoder produced by Kistler and ICP vibration acceleration converters produced by PCB were used together with an SV006 signal amplifier. Three converters were used, two of them were located close to the fourth cylinder. One of them allowed recording vibration in a direction perpendicular to the cylinder axis and the other one – paralelly. The third sensor was placed on the head near the first cylinder and it allowed recording the vibrations parallel to the cylinder axis. The signals were recorded with use of an eight-channel NI PCI-6143 data acquisition card, controlled with a programme developed in the Lab View 7.1 environment.

Fig. 1 shows the courses of vibration accelerations, recorded in the direction perpendicular to the cylinder axis and simultaneously, perpendicular to the piston pin axis in case of an engine operating with a rotational speed of 2500 RPM. The measurements were performed before and after the repair of the engine, consisting of replacement of the pistons worn out.

Based on the tests results analysis it was stated that the repair performed did not influence the peak values of vibration accelerations (Fig. 1). It did not influence the root-mean-square value of vibration accelerations, calculated based on the root-mean-square values of 23 cycles of engine's operation (Fig. 2).

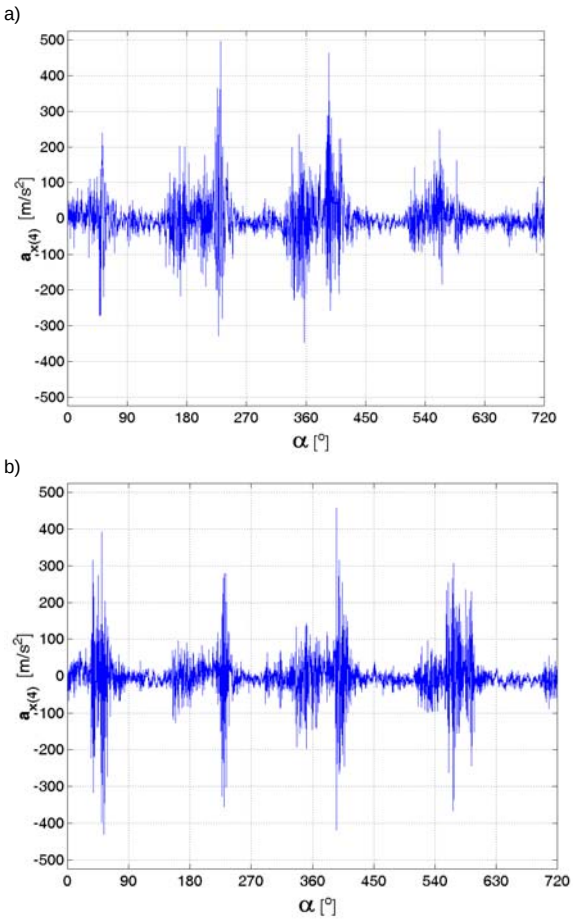

Fig. 1. Course of the vibration accelerations recorded on the fourth cylinder in the direction perpendicular to the cylinder axis and simultaneously perpendicular to the piston pin axis: a) before engine repair, b) after engine repair

Similarly, the results of the spectrum analysis of vibration signal in the scope of low frequencies from 0 to 500 Hz do not show significant differences in the bands connected with the induction frequency equaling 83.34 Hz (Fig. 3). It is possible to note a small amplitude change in the spectrum of vibration acceleration recorded after the engine repair in the band connected with the ignition. Spectrum analysis was conducted for the time course comprising fifteen full working cycles of the engine tested.

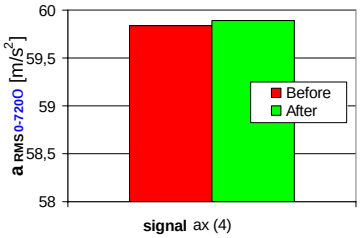

Fig. 2. Comparison of root-mean-square value calculated based on the vibration accelerations registered on the fourth cylinder in the direction perpendicular to the cylinder axis before and after the engine repair

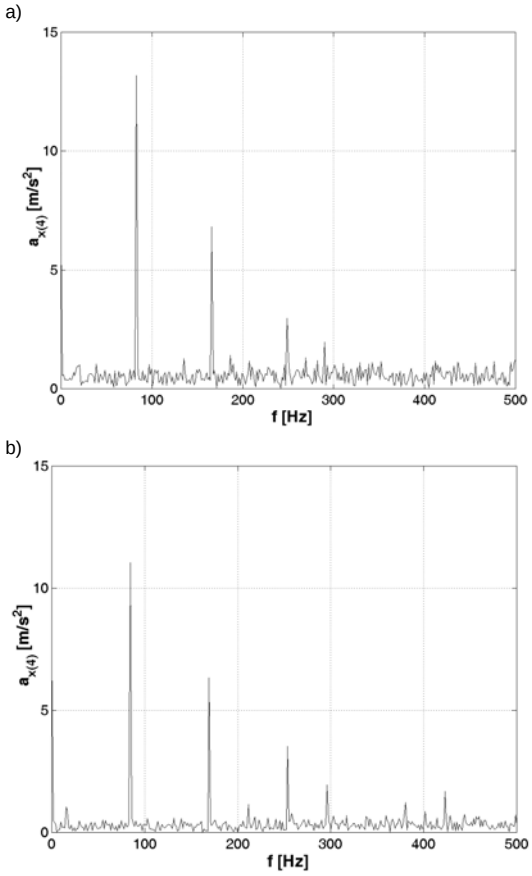

Fig. 3. Spectra of vibration accelerations recorded on the fourth cylinder in the direction perpendicular to the cylinder axis before (a) and after (b) repair of the engine

In the studies described in papers [7, 8], a nonaveraged wavelet power spectrum was applied for clearance detection in the piston – cylinder system of Diesel engine. Due to the existence of a stochastic constituent of the vibration signal and, for example, the possibility of misfiring, this method may lead to untrue conclusions. For this reason, in this article, a method of diagnosing clearance in the piston – cylinder system has been suggested, which method is based on the averaged scale - wavelet power spectrum (ASWPS), determined according to the diagram presented in Fig. 4. Using the Morlet wavelet, a wavelet transform was calculated based on 23 full engine's working cycles. Next, the scope

of analysis was narrowed to the crankshaft rotation angle of 350-420°, since in this scope the piston hits the cylinder wall. Fig. 5 shows the scale wavelet power spectra (SPWT) of 23 engine's working cycles before and after its repair: In order to enable easier comparison of spectra obtained for the conditions before and after the engine repair, they were averaged. It is possible to see in Fig. 6 that after the repair, the values of constituent amplitudes of obtained spectra decreased. The energy of CWT coefficients, calculated from the dependence 4 on the basis of SWPS (Fig. 7) was proposed to be the diagnostic measure. The measure proposed is sensitive to the clearance change in the piston – cylinder system (Fig. 8).

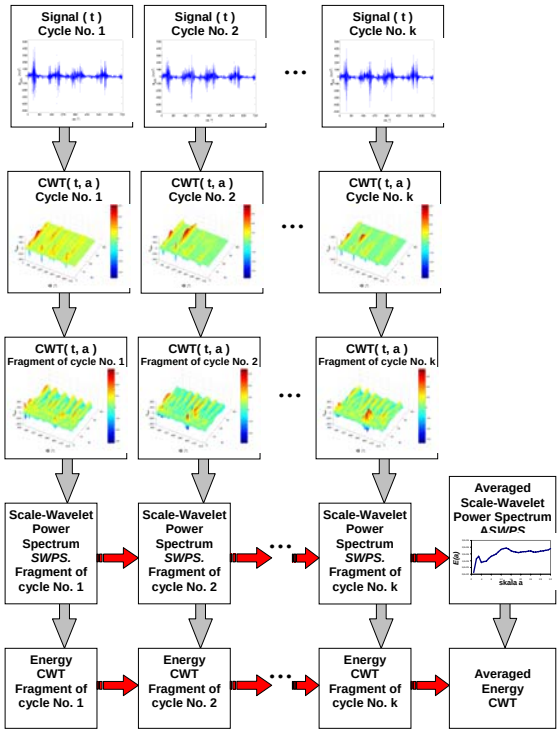

Fig. 4. Diagram of calculating the Averaged Scale Wavelet Power Spectrum (ASPWT)

4. ANALYSIS OF DIESEL ENGINE SIGNALS

In order to check the usefulness of the method suggested, another object of analysis were vibration signals of a single-cylinder Diesel engine with direct injection, produced by Ruggerini of 477 cm^3 capacity and of 91mm cylinder diameter. In the tests, the following items were recorded:

- pressure inside the cylinder,
- vibration accelerations of engine wall blocks in the direction parallel to the cylinder axis and perpendicular to the cylinder axis and simultaneously in the direction perpendicular to the piston pin axis,
- crankshaft rotation angle and GMP (top dead point) of piston,
- engine's torque,
- subatmospheric pressure in the suction manifold.

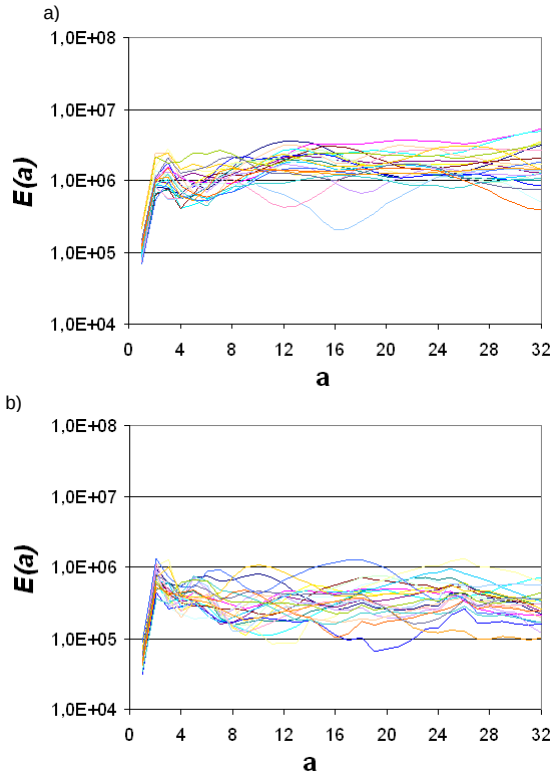

Fig. 5. Scale wavelet power spectra (SPWT) – measurement on the fourth cylinder in the direction perpendicular to the cylinder axis: a) before, b) after repair of the engine

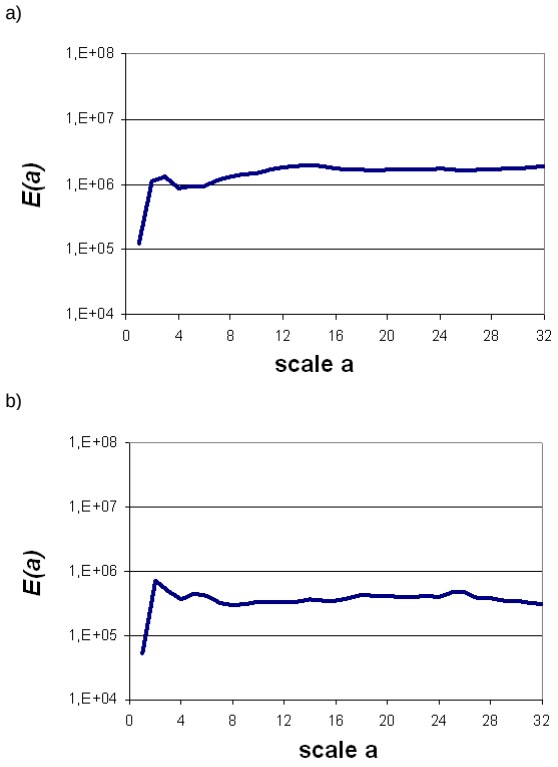

Fig. 6. Averaged scale wavelet power spectra (ASPWT) – of 23 engine's operating cycles in the direction perpendicular to the cylinder axis: a) before, b) after repair of the engine

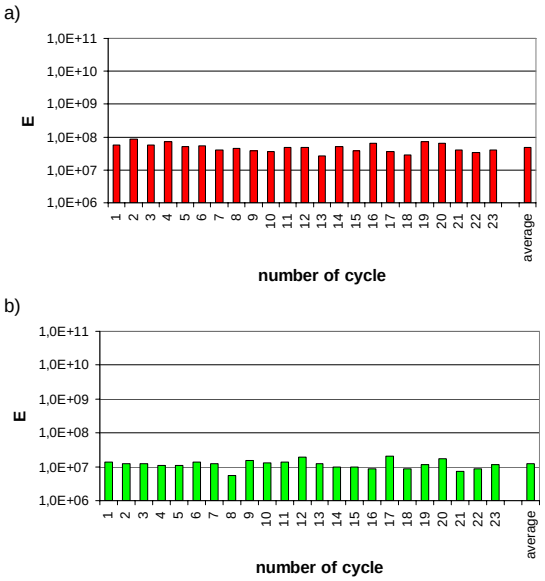

Fig. 7. Energy of CWT coefficients of 23 cycles of engine operation - measurement on the fourth cylinder in the direction perpendicular to the cylinder axis: a) before, b) after repair of the engine

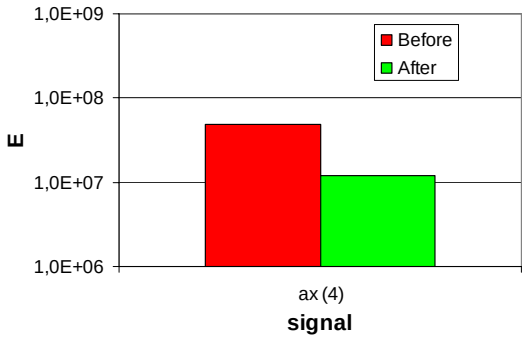

Fig. 8. Average energy of CWT coefficients of 23 engine's operating cycles - measurement on the fourth cylinder in the direction perpendicular to the cylinder axis

During the tests, the engine operated with a rotational speed of about 1250 [r.p.m.] and was loaded with torque of 2.8 [Nm].

The measurements were conducted for three clearance values: nominal clearance, double nominal clearance and four times nominal clearance. For the selected experimental clearance values, the compression pressure on the same level was kept.

Observing the presented in Fig. 9 averaged wavelet power spectra (ASPWT) of the signals registered in two mutually perpendicular directions, it can be noted that the amplitudes of those spectra in the whole scope of scale increase together with the increase of clearance in the piston – cylinder system. Similarly, the energy of CWT coefficients changes (Fig. 10).

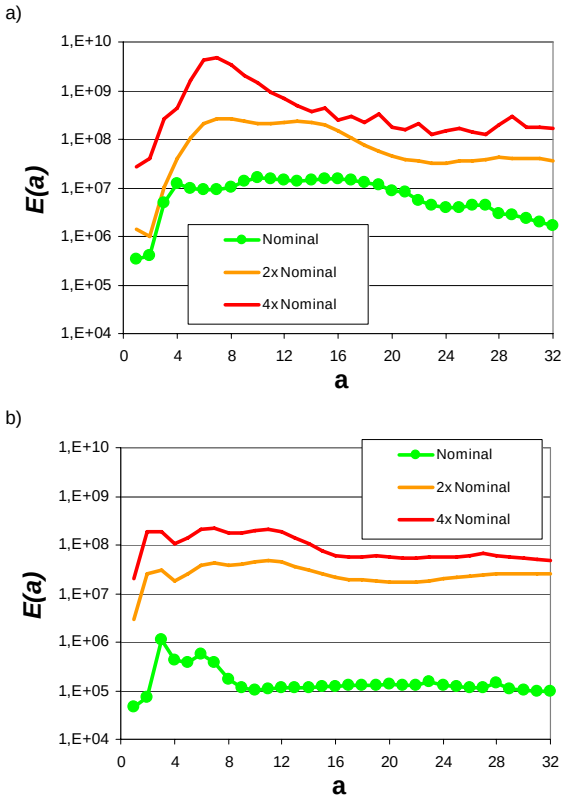

Fig. 9. Averaged scale wavelet power spectrum (ASPWT) – 30 cycles of engine operation: a) of vibration acceleration signal of engine block, b) of head

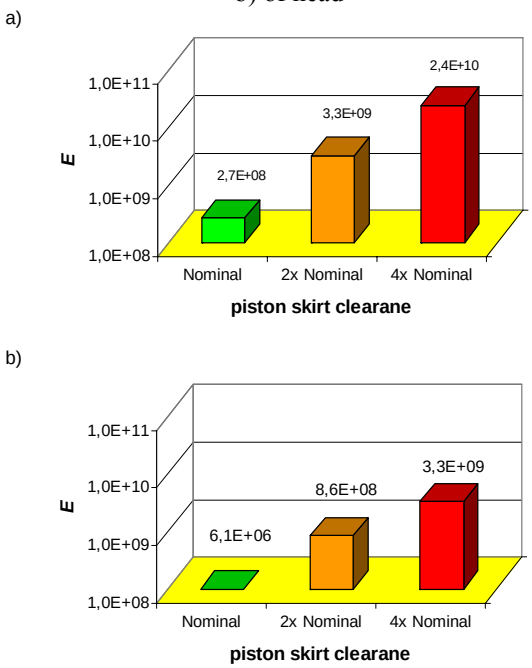

Fig. 10. Average coefficient CWT energy of vibration accelerations signal a) of engine block, b) of head

5. CONCLUSIONS

Based on the research and analyses performed, the following conclusions have been formulated:

- Based on an appropriate phase and spectrum analysis, it is possible to determine appropriate measures of vibration signal, sensitive to operational wear of the piston – cylinder system.
- In case of both engines, the suggested measure, based on the averaged wavelet power spectrum (ASWPS) was sensitive to the clearance change in the piston – cylinder system.
- Using the vibration signals in diagnosing mechanical combustion engines is more effective when applying signal decomposition by means of time-frequency (scale) representations.
- Differences in the obtained spectra for the tested engines may be caused by:
  - a different number of cylinders – SI engine has 4 cylinders, whereas Diesel engine has 1 cylinder,
  - maximal pressures in combustion chamber - SI and Diesel engines,
  - construction of the engine – SI engine is cooled with liquid and Diesel engine is cooled with air.
- It seems reasonable to develop appropriate algorithms supplementing OBD systems, allowing the detection of mechanical defects in engines, which can be masked by electronic control devices of the contemporary automotive vehicles.

REFERENCES

[1] Batko W., Dąbrowski Z., Engel Z., Kiciński J., Weyna S.: *Nowoczesne metody badania procesów wibroakustycznych*. ITE, Radom 2005.
[2] Cempel C.: *Diagnostyka wibroakustyczna maszyn*. PWN, Warszawa 1989.
[3] Dąbrowski Z., Madej H.: *O użyteczności symptomów wibroakustycznych w nowoczesnej diagnostyce silników spalinowych*. Przegląd Mechaniczny nr 1 / 2007, s. 32-35.
[4] Fabis P., Flekiewicz M., Flekiewicz B., Madej H., Wojnar G.: *Influence of piston slap on engine block vibration*. SAE Paper No. 2007-01-2163.
[5] Flekiewicz M., Madej H.: *Wstępna identyfikacja źródeł drgań silnika spalinowego ZI*. Konferencja IX Szkoła Analizy Modalnej, Kraków 2004.
[6] Geng Z., Chen J.: *Investigation into piston-slap-induced vibration for engine condition simulation and monitoring*. Journal of Sound and Vibration, 282, pp. 731-751, 2004.
[7] Madej H., Flekiewicz M., Wojnar G.: *Zastosowanie ciągłej transformaty falkowej (CWT) do analizy drgań siników spalinowych*. Teka Komisji Engineyzacji PAN oddz. Kraków zeszyt 33-34.
[8] Madej H., Flekiewicz M., Wojnar G.: *Różne aspekty diagnostyki WA silników spalinowych z wykorzystaniem analiz w dziedzinie czasu i skali*. XIII Konferencja Naukowa Wibroakustyki i Wibrotechniki i VIII Ogólnopolskie Seminarium Wibroakustyka w Systemach Technicznych WibroTech 2007 Warszawa - Jachranka 2007 r. s. 177-186.
[9] Merkisz J., Mazurek S.: *Pokładowe systemy diagnostyczne pojazdów samochodowych*. WKiŁ, Warszawa 2004.
[10] Peng Z. K., Chu F. L.: *Application of the wavelet transform in machine condition monitoring and fault diagnostics: a review with bibliography*. MSSP 18 (2004) 199-221.

Grzegorz WOJNAR PhD. Eng. adjunct of Silesian University of Technology. Scientific interest: modelling dynamic processes, diagnostics of tooth gear, machine design and signal processing methods.

Henryk MADEJ, Ph. D., D. Sc. Eng. work as a professor in the Department of Automotive Vehicle Construction Silesian University of Technology in Katowice. He deals with IC engines and powertrains diagnostics with the application of vibroacustical signal analysis, also with minimization of machine vibroactivity. Member of Polish Society of Technical Diagnostics.

DIAGNOZOWANIE WYCIEKÓW Z RUROCIĄGÓW PRZESYŁOWYCH Z WYKORZYSTANIEM NOWEJ INFORMACJI DIAGNOSTYCZNEJ – SYGNAŁÓW SŁABYCH INTERAKCJI MIĘDZYOBIEKTOWYCH

Paweł OSTAPKOWICZ

Politechnika Białostocka, Wydział Mechaniczny, Katedra Automatyki i Robotyki
15-351 Białystok, ul. Wiejska 45C, fax.: (085)7469248, email: ostad@pb.bialystok.pl

Streszczenie

Rurociągi są obiektami, które wykazują ograniczenia lub nawet brak podatności diagnostycznej, ściśle związanej z możliwością pomiaru ilościowo i jakościowo dostępnej informacji diagnostycznej. Ma to zasadniczy wpływ na mało zadowalającą skuteczność obecnie stosowanych metod diagnozowania wycieków opartych na informacji diagnostycznej w postaci pomiarów natężenia przepływu i ciśnienia w rurociągu. Wśród takich metod można wyróżnić techniki oparte na detekcji fal ciśnienia. Ich skuteczność może ulec polepszeniu poprzez zastosowanie opracowanej metody polepszania podatności diagnostycznej rurociągów. Metodę tą umownie nazwano metodą słabych interakcji międzyobiektowych. Ideę metody stanowi pozyskiwanie nowej informacji diagnostycznej, tj. sygnałów diagnostycznych. W niniejszym artykule poza teoretycznym opisem proponowanej metody przedstawiono wyniki badań przeprowadzonych z jej zastosowaniem na 380-cio metrowej długości laboratoryjnym rurociągu.

Słowa kluczowe: diagnostyka procesów przemysłowych, rurociągi, diagnozowanie wycieków.

DIAGNOSING OF LEAKAGES FROM TRANSMISSION PIPELINES BASED ON NEW DIAGNOSTIC INFORMATION – SIGNALS OF WEAK INTERACTIONS BETWEEN OBJECTS

Summary

Transmission pipelines are the objects showing limitations or even a partial absence of the diagnostic susceptibility, which is closely connected with a possibility of the measurement of quantitatively-available and qualitatively-available diagnostic information. It has an essential influence on a hardly satisfactory efficacy of currently used leak detection methods based on diagnostic information in the form of flow and pressure measurements in pipeline. Among such methods are techniques based on pressure wave detection. The efficacy of such techniques can be improved by the use of an elaborated method of improving the diagnostic susceptibility of pipelines. This new method has been conventionally named the method of weak interactions between objects. Its essence consists in acquiring new diagnostic information i.e. diagnostics signals. Except a theoretical description of the proposed method this paper presents the results of research conducted on a 380-metre-long laboratory pipeline.

Keywords: diagnostics of industrial processes, pipeline, leakages diagnosing.

1. WSTĘP

Diagnozowanie nieszczelności i wycieków z rurociągów przesyłowych obejmuje następujący zakres zadań:

- wykrycie wycieku (z wygenerowaniem alarmu),
- zlokalizowanie wycieku,
- oszacowanie natężenia wycieku (a dodatkowo ilości medium, które wypłynęło z rurociągu).

Realizacja powyższych zadań odbywa się przy użyciu odpowiednich metod diagnozowania, na podstawie których opracowuje się system diagnostyczny typu LDS (leak detection system).

Metody diagnozowania wycieków ogólnie można podzielić na dwie kategorie rozwiązań:

- metody bezpośrednie (zewnętrzne) – gdzie detekcja i lokalizacja wycieku wiąże się z ujawnieniem tłoczonego produktu na zewnątrz rurociągu, poprzez zastosowanie badań organoleptycznych lub użycie specjalnych urządzeń,
- metody pośrednie (analityczne, wewnętrzne) – gdzie diagnozowanie wycieku wynika z pomiarów i analizy parametrów przepływu (ciśnienia, natężenia/prędkości przepływu).

Ograniczając obszar zainteresowania niniejszej pracy do rurociągów przesyłowych cieczy, w przypadku tego typu obiektów powszechne zastosowanie znalazły głównie metody wewnętrzne.

Wśród wielu metod wewnętrznych stosowanych do diagnozowania wycieków z rurociągów

przesyłowych cieczy można wyróżnić *metody oparte na detekcji fal ciśnienia*. Metody takie dają możliwość bardzo szybkiego wykrycia i zlokalizowania zaistniałych wycieków. Są one szczególnie przydatne do identyfikacji nagłych wycieków[1]. Ich skuteczność jest jednak mało zadowalająca. Pozwalają one wykrywać jedynie duże wycieki (tj. o wartości powyżej 1 % nominalnego natężenia przepływu – według informacji odnajdywanych w literaturze, a nawet o wartości 3÷5 % – według informacji podawanych przez operatorów rurociągów) i lokalizować je ze zgrubną dokładnością (rzędu od kilkuset metrów, nawet do kilkunastu kilometrów).

Przyczyn takich problemów należy upatrywać w podatności diagnostycznej rurociągu, która jest ściśle związana z możliwością pomiaru ilościowo i jakościowo dostępnej informacji diagnostycznej. Do sytuacji, gdy systemy diagnostyczne LDS dysponują tylko częścią użytecznych danych pomiarowych może dochodzić dość często [8].

Skutecznym sposobem polepszania podatności diagnostycznej rurociągów przesyłowych jest nowo opracowana metoda, umownie nazwana *metodą słabych interakcji międzyobiektowych*.

2. METODY OPARTE NA DETEKCJI FAL CIŚNIENIA

Metody te wykorzystują towarzyszące wyciekom zjawisko powstawania i rozchodzenia się fal ciśnienia. Fale te powstają wskutek nagłego spadku ciśnienia w miejscu, w którym wystąpił wyciek i rozchodzą się od tego miejsca w obu kierunkach rurociągu z prędkością dźwięku c. W przypadku nagłych wycieków fale mają wyraźnie widoczne czoła (rys. 1), a dla wycieków narastających powoli, z uwagi na bardziej łagodny przebieg zmian ciśnienia, mają wygładzony kształt. Za czołem fali ciśnienie w rurociągu maleje o tym mniejszą wartość, im większa jest odległość danego punktu od miejsca wycieku.

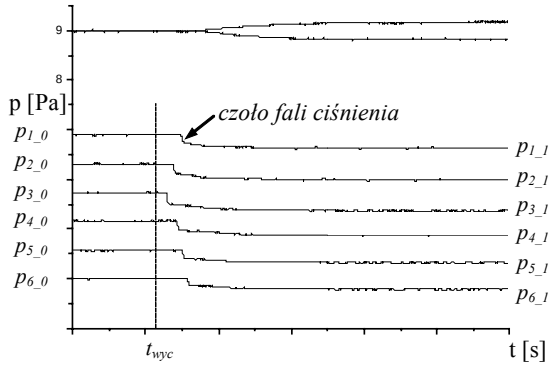

Rys. 1. Przebiegi sygnałów ciśnienia w punktach pomiarowych 1-6 rozmieszczonych wzdłuż rurociągu

[1] Nagły wyciek – jego natężenie osiąga wartość nominalną w krótkim czasie od momentu pojawienia się nieszczelności.

w stanach z wyciekiem, który miał miejsce pomiędzy punktami 2 i 3; t_{wyc} – początek wycieku

Przykładem takich rozwiązań jest *metoda śledzenia czół fal ciśnienia* [7]. Pozwala ona wykryć i zlokalizować wyciek w oparciu o zaobserwowane zmiany wartości ciśnienia w rurociągu wywołane propagacją fal ciśnienia powstałych wskutek wystąpienia wycieku. Takie zmiany w postaci spadków ciśnienia pojawiają się najpierw w punktach pomiaru najbliżej położonych miejsca wycieku, a następnie z pewnym opóźnieniem w kolejno odległych punktach.

Lokalizacji wycieku dokonuje się na podstawie ustalonych chwil $t\_(z_n)$ detekcji przejść czół fal ciśnienia przez poszczególne punkty pomiarowe z_n. Znając kolejność przejść fal ciśnienia przez poszczególne punkty pomiarowe i odległość pomiędzy punktami, miejsce wycieku można wyznaczyć na podstawie wykresu (rys. 2), jako punkt przecięcia prostych *A-C* i *C-B*, według zależności (1). Punkt *A* na wykresie określa czas przejścia czoła fali ciśnienia od miejsca wycieku do początku rurociągu, a punkt *B* czas przejścia czoła fali ciśnienia do końca rurociągu.

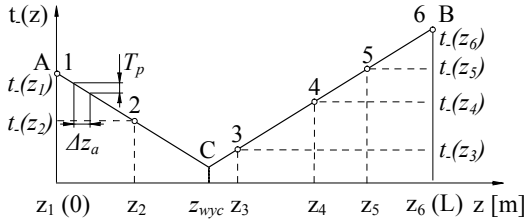

Rys. 2. Rozkład czasu przejścia czół fal ciśnienia wzdłuż rurociągu po wycieku w punkcie $z = z_{wyc}$

$$z_{wyc} = \frac{a_k}{a_p + a_k} \cdot l + \frac{t_l(0) - t_l(L)}{a_p + a_k} \tag{1}$$

gdzie: $a_p = 1/c_p$, $a_k = 1/c_k$ – współczynniki nachylenia prostych *A-C* i *C-B*; c_p, c_k – średnie prędkości dźwięku na odcinkach: $0 < z < z_{wyc}$, $z_{wyc} < z < L$; L – długość rurociągu; $t_l(0)$, $t_l(L)$ – ustalone chwile dotarcia czół fal ciśnienia do punktów: $z = 0$, $z = L$.

Metoda ta jest stosunkowo szybka, przy rozmieszczonych co kilka – kilkanaście kilometrów, bezinercyjnych przetwornikach ciśnienia (bez wygórowanych wymagań co do ich dokładności). Wymaga jednak precyzyjnej synchronizacji pomiaru czasu w trakcie dokonywania pomiarów ciśnienia w poszczególnych punktach rurociągu. Szczególną uwagę należy też zwrócić na okres próbkowania sygnałów T_p, który decyduje o błędzie $\Delta z_a = (1 \div 3)\, c \cdot T_p$, z jakim śledzone jest położenie czoła fali ciśnienia. Okres ten powinien wynosić setne, a nawet tysięczne części sekundy. Należy też pamiętać, że jeżeli wyciek nie zostanie od razu zauważony (np. wskutek chwilowego zawieszenia

lub wyłączenia systemu LDS), nigdy już nie zostanie wykryty tą metodą.

3. METODA SŁABYCH INTERAKCJI MIĘDZYOBIEKTOWYCH

W dotychczasowym podejściu, rozpatrując funkcjonowanie rurociągu zgodnie z zasadami automatyki jako obiektu regulacji – taki opis jest dokonywany z wykorzystaniem transmitancji obiektu i może tu być użyta następującą zależność:

$$Y = G\,Z \tag{2}$$

gdzie: G – transmitancja obiektu; Z – transformata zakłócenia (wynikającego z oddziaływania otoczenia na obiekt, takim zakłóceniem jest wyciek); Y – transformata sygnału wyjściowego obiektu (takim sygnałem jest mierzony sygnał ciśnienia).

Analizując wzór (2) nietrudno dojść do wniosku, że praktycznie rzecz biorąc zmiany dostępnego sygnału Y mogą wynikać ze zmian stanu technicznego obiektu opisanego parametrami transmitancji G i/ lub ze zmian oddziaływania otoczenia na obiekt, reprezentowanego tu przez sygnał Z. Taka właśnie sytuacja jest charakterystyczna dla niepodatnych diagnostycznie obiektów technicznych (w tym rurociągów) – diagnosta dysponuje jednym równaniem z dwiema niewiadomymi, zatem problem diagnozowania takiego obiektu staje się niemożliwy do jednoznacznego rozwiązania.

3.1. Idea metody

Proponowane podejście polega na polepszaniu podatności diagnostycznej rurociągów poprzez zastosowanie układów korekcyjnych (opisanych i stosowanych w automatyce) do pozyskiwania nowej informacji diagnostycznej (sygnałów diagnostycznych) [3, 4, 5, 6].

Informacją tą, w odróżnieniu od dotychczas stosowanych sygnałów ciśnienia, są mierzalne sygnały oddziaływań, wynikające z pracy specjalnych obiektów badawczych (korektorów) dołączonych do diagnozowanego rurociągu.

Sprowadzając rurociąg do UAR i wprowadzając element korekcyjny – korektor (o transmitancji G_K), otrzymuje się układ zgodny z rys. 3.

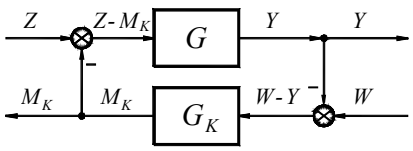

Rys. 3. Układ z badanym obiektem (rurociągiem) o transmitancji G i dołączonym korektorem o transmitancji G_K: M_K – transformata sygnału wyjściowego z korektora

Dla układu można otrzymać następujące relacje pomiędzy sygnałami:

$$\begin{aligned} Y &= (Z - M_K)G \\ M_K &= (W - Y)G_K \end{aligned}, \tag{3}$$

a po przekształceniach zależność:

$$Z = \frac{WM_K}{W - Y}, \tag{4}$$

opisującą zakłócenie Z działające na obiekt (którym jest wyciek) w funkcji dostępnych sygnałów: Y, W, M_K. Zgodnie z powyższą zależnością i po uwzględnieniu, że sygnałem zadanym do korektora W jest wartość sygnału wyjściowego Y w chwili poprzedniej, zakłócenie (wyciek) może być identyfikowane bez znajomości transmitancji obiektu G, która wskutek powstałego uszkodzenia uległa zmianie i może być nieznana.

3.2. Praktyczna realizacji metody

Praktyczna realizacja proponowanej metody polega na dołączeniu do diagnozowanego rurociągu minimum dwóch korektorów o odpowiednio dobranych transmitancjach G_{K1} i G_{K2}: na początku i końcu rurociągu.

Schemat konstrukcji korektorów przedstawiono na rysunku 4. Zasadniczym elementem korektorów jest zasobnik ciśnieniowy (akumulator hydrauliczny), składający się z dwóch komór, rozdzielonych przeponą.

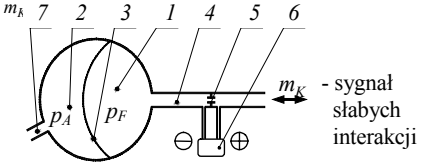

Rys. 4. Schemat konstrukcji korektora: *1* – komora z cieczą; *2* – komora z powietrzem; *3* – przepona; *4* – kanał pomiarowy; *5* – kryza pomiarowa; *6* – czujnik różnicy ciśnień; *7* – zawór

Zastosowane na obiekcie rurociągowym korektory – jako urządzenia pomiarowe – mają służyć do obserwacji zmian ciśnienia w rurociągu, w szczególności fal ciśnienia, wywołanych przez pojawienie się wycieku. Dotyczy to fal o wyraźnie widocznych czołach, generowanych przez nagłe wycieki. Przy wystąpieniu takich zmian ciśnienia, dochodzi do „zadziałania" korektora (zmiany położenia przepony) i w jego kanale pomiarowym pojawia się fluktuacja przepływu m_K – określana jako *sygnał słabych interakcji międzyobiektowych*. Wielkość tej fluktuacji jest miarą wzajemnych oddziaływań pomiędzy rurociągiem a korektorem, a jej pomiaru dokonuje się na kryzie z użyciem czujnika różnicy ciśnień.

Korektory mają również stanowić zabezpieczenie przewodu rurociągu przed skutkami nagłego wzrostu ciśnienia, wywołanego przez zatrzymanie pomp, zamknięcie zaworów.

W celu poprawy skuteczności metody w zakresie poziomu wykrywalności wycieków, skrócenia czasu ich wykrycia i poprawy błędów lokalizacji, zakłada się rozmieszczenie kilku dodatkowych korektorów wzdłuż rurociągu, np. w obrębie stacji zasuw.

4. WERYFIKACJA METODY SŁABYCH INTERAKCJI Z WYKORZYSTANIEM MODELU FIZYCZNEGO RUROCIĄGU

4.1. Stanowisko badawcze

Proponowana metoda została poddana weryfikacji eksperymentalnej na stanowisku badawczym z modelem fizycznym rurociągu o długości $l = 380$ m, wykonanym z rur z polietylenu PE80 DN40 o średnicy wewnętrznej $d = 34$ mm (rys. 5). Rurociągiem tłoczono wodę.

Rurociąg modelowy wyposażono w odpowiednie standardowe przyrządy i przetworniki pomiarowe, umożliwiające pomiar ciśnienia, natężenia przepływu i temperatury.

Korektory badawcze M_{K1} i M_{K2} do wywoływania sygnałów słabych interakcji zamontowano na początku i końcu rurociągu, w pobliżu punktów pomiaru ciśnienia P_1 i P_6 (rys. 5).

Informacje na temat zastosowanych przetworników ciśnienia i przetworników różnicy ciśnień zamontowanych w korektorach oraz lokalizacji tych urządzeń zestawiono w tabeli 1.

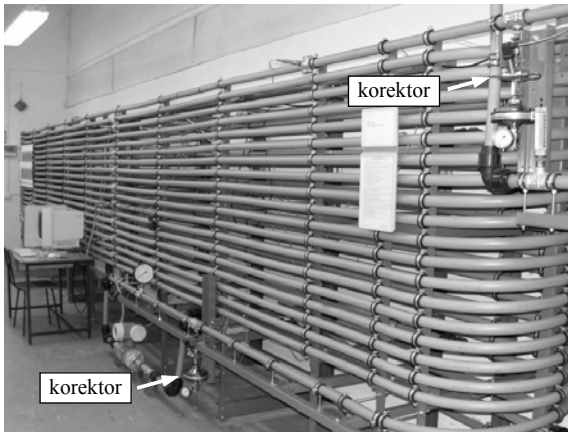

Rys. 5. Widok rurociągu modelowego i zamontowanych korektorów

Tab. 1. Lokalizacja i charakterystyki urządzeń

Urządzenie	Przetworniki ciśnienia	Korektory przetworniki różnicy ciśnień
lokalizacja [m] z_n	P_1=1; P_2=75; P_3=141; P_4=281; P_5=355; P_6=378	M_{K1}=-3; M_{K2}=379,2
charakterystyki pomiarowe	*zakres:* 0÷10 [bar] *dokładność:* 0,1% zakresu	*zakres:* -0,5÷0,5 [Δbar] *dokładność:* 0,2% zakresu
błąd*	± 0,026 [bar]	± 0,0036 [Δbar]
błąd* = przetwornik + 12-bit A/C karta pomiarowa		

Do symulowania wycieków użyto ręcznie sterowanych zaworów kulowych wyposażonych w specjalne gniazda z wymiennymi kryzami o różnych średnicach otworów. Zawory zainstalowano w kilkunastu wybranych punktach rurociągu.

Prowadzone na stanowisku eksperymenty obejmowały różne nastawy punktu pracy rurociągu oraz miejsca, wielkości i tempo symulowanych wycieków.

4.2. Charakterystyka nowo pozyskanych sygnałów. Ocena wpływu korektorów na działanie rurociągu

W trakcie badań ustalono, że w reakcji na wyciek sygnały słabych interakcji (jako różniczkowane postacie sygnałów ciśnienia) przyjmują kształt charakterystycznych impulsów (rys. 6c). Parametry takich impulsów są zależne od wielkości, położenia i tempa narastania wycieku. Osiągają one najbardziej pożądane wielkości (tj. najwyższe amplitudy i najkrótsze szerokości) dla nagłych wycieków z wyraźnie widocznymi czołami fal ciśnienia. Dla wycieków narastających wolniej parametry impulsów pogarszają się.

Na podstawie analizy przebiegów sygnałów i relacji do ich pól błędów stwierdzono, że w przypadku sygnałów słabych interakcji wykraczają one poza pola błędów (rys. 6d), czego nie można powiedzieć o sygnałach ciśnienia (rys. 6b). Pomiar sygnałów słabych interakcji jest zatem bardziej dokładny (wiarygodny) od pomiaru sygnałów ciśnienia.

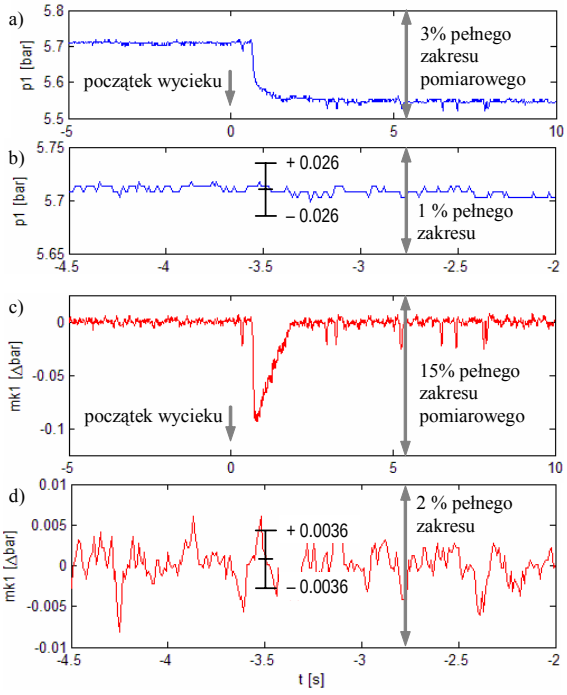

Rys. 6. Porównanie przebiegu sygnału słabych interakcji m_{K1} (z pierwszego korektora) z przebiegiem sygnału ciśnienia p_1, z zaznaczonymi polami błędów pomiaru; dla przypadku 6 % nagłego wycieku symulowanego na 195 m rurociągu

Ustalono również, że dołączenie do rurociągu korektorów nie wpływa na jakość jego funkcjonowania i jest łatwe do zrealizowania. Korektory w obszarach ich zamontowania obniżają poziom pulsacji ciśnienia w rurociągu o około 10%.

5. ZASTOSOWANIE NOWEJ INFORMACJI DIAGNOSTYCZNEJ – SYGNAŁÓW SŁABYCH INTERAKCJI DO DIAGNOZOWANIA WYCIEKÓW

Nowo pozyskane sygnały diagnostyczne – sygnały słabych interakcji poddano ocenie w zakresie możliwości ich zastosowania do diagnozowania wycieków metodą śledzenia czół fal ciśnienia, mając na uwadze polepszenie skuteczności tej metody.

5.1. Opracowane procedury diagnostyczne

Zasadniczym elementem takiej oceny było opracowanie algorytmów przetwarzania sygnałów słabych interakcji i sygnałów ciśnienia, które pozwalałby wykryć zaistniały wyciek, uzyskać informacje o propagacji fal ciśnienia, a następnie zlokalizować wyciek.

Badania przeprowadzono w oparciu o następujące założenia:

- pozyskiwanie sygnałów z okresem próbkowania $T_P = 0{,}01\,\mathrm{s}$,
- użycie pakietu sześciu sygnałów ciśnienia: $p_1 - p_2 - p_3 - p_4 - p_5 - p_6$ z przetworników rozmieszczonych wzdłuż rurociągu (pakiet A), a następnie dla porównania zastąpienie skrajnych sygnałów ciśnienia sygnałami słabych interakcji z korektorów, uzyskując w ten sposób kolejny pakiet sygnałów: $m_{K1} - p_2 - p_3 - p_4 - p_5 - m_{K2}$ (pakiet B),
- porównanie wyników uzyskanych przy użyciu pierwszego pakietu sygnałów z wynikami uzyskanymi przy użyciu drugiego pakietu sygnałów,
- uwzględnienie występowania zakłóceń – zaszumienie porównywanych sygnałów szumem gaussowskim o zerowej wartości średniej i odchyleniu standardowym równym 0,2 % i 0,5 % wielkości ich zakresów pomiarowych i wynikająca stąd konieczność zmiany przyjętych progów alarmowych,
- ustalenie wartości progów alarmowych dla sygnałów słabych interakcji i sygnałów ciśnienia, niezaszumianych i zaszumianych, w sposób zapewniający niewystępowanie alarmu dla stanów bez wycieku (w całej rozpatrywanej serii eksperymentów).

Do wykrywania i lokalizowania wycieków przy użyciu sygnałów słabych interakcji i sygnałów ciśnienia zastosowano identyczne procedury. Ich podstawę stanowi algorytm (rys. 7), opracowany w oparciu o rozwiązania opisane w pracach [1, 2, 7]. Służy on do wykrywania fal ciśnienia z jednoczesnym określeniem momentów przejścia ich czół przez poszczególne punkty pomiaru sygnałów słabych interakcji i sygnałów ciśnienia.

Działanie algorytmu oparte jest o:

- filtrowanie rekursywne poszczególnych sygnałów x_n: p_1, p_2, p_3, p_4, p_5, p_6, m_{K1}, m_{K2}; gdzie przyjęto identyczne nastawy współczynników korekcyjnych dla filtrów $\alpha = 0{,}995$,
- obliczanie odchyleń (residuów) Δx_n,
- filtrowanie rekursywne obliczonych residuów z funkcjami wynikowymi $f\Delta x_n$, które po przekroczeniu wartości odpowiadającego im progu alarmowego P_x_n informują o pojawieniu się czoła fali ciśnienia, z jednoczesnym zapisem chwili czasowej t_x_n dla takiego przekroczenia; gdzie przyjęto identyczne nastawy współczynników korekcyjnych dla filtrów $\beta = 0{,}900$.

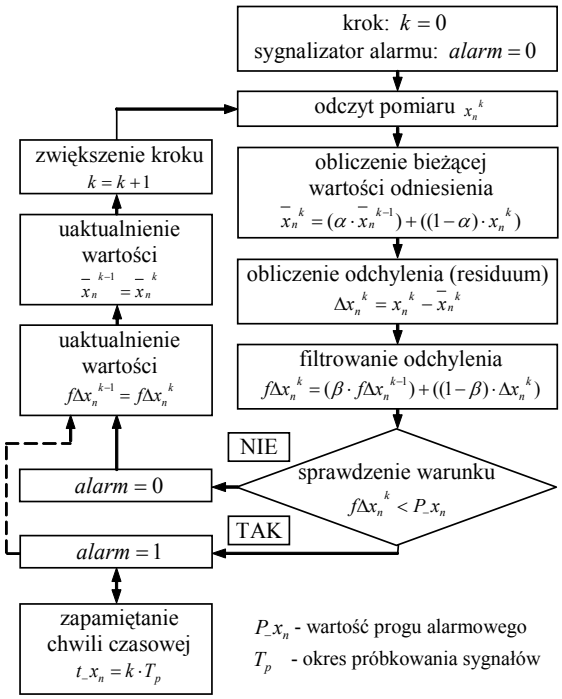

Rys. 7. Algorytm wykrywania czół fal ciśnienia

Na rysunkach 8a i 8b przedstawiono przykładowe przebiegi funkcji $f\Delta x_n$ ($f\Delta p_1$ – dla sygnału ciśnienia p_1 i $f\Delta m_{K1}$ – dla sygnału słabych interakcji m_{K1}), z zaznaczonymi wartościami progów alarmowych P_x_n (P_p_1 i P_m_{K1}), a dodatkowo również funkcji Δx_n (Δp_1 i Δm_{K1}). Analizując przebiegi funkcji $f\Delta x_n$ i Δx_n można zauważyć, że zastosowane filtrowanie rekursywne residuów Δx_n pozwala wyeliminować zakłócenia, dzięki czemu można zawęzić margines pola alarmowego. Wprowadza to jednak opóźnienie w wykryciu czoła fali ciśnienia, która zostaje

wykryta w chwilach $t\_x_n^{(I)}$ ($t\_p_1^{(I)}$ i $t\_m_{K1}^{(I)}$), co może następnie skutkować błędami w lokalizacji wycieku.

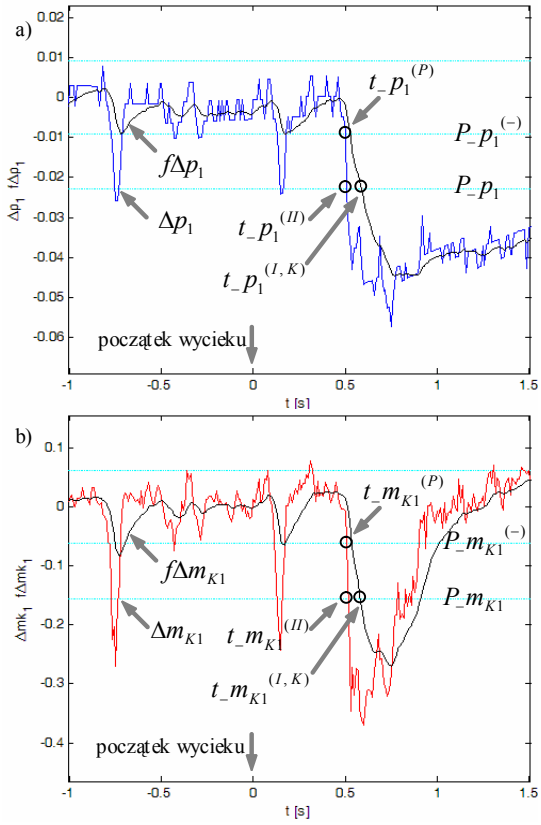

Rys. 8. Przebiegi funkcji $f\Delta x_n$ i Δx_n oraz sposób określania chwil $t\_x_n^{(I)}$ i $t\_x_n^{(II)}$: a) dla sygnału ciśnienia p_1, b) dla sygnału słabych interakcji m_{K1}; 2 % nagły wyciek symulowany na 115 m rurociągu

Zaproponowano zatem modyfikację powyższych procedur. Polega ona na zastąpieniu ujawnionych chwil czasowych $t\_x_n^{(I)}$ przez nowe chwile $t\_x_n^{(II)}$.

Chwile $t\_x_n^{(II)}$ dla poszczególnych sygnałów wyznaczane są w oparciu o specjalnie wydzielany przedział czasowy $T\_x_n =< t\_x_n^{(P)}, t\_x_n^{(K)} >$, jako pierwsze zaobserwowane w przedziale przekroczenie przez funkcję residuum Δx_n progu alarmowego P_x_n (rys. 8). Początek przedziału ustalany jest jako najbliższy wstecz względem wyznaczonej chwili $t\_x_n^{(I)}$ moment $t\_x_n^{(P)}$ jednoczesnego przekroczenia przez obie funkcje $f\Delta x_n$ i Δx_n poza wprowadzony dodatkowy próg $P\_x_n^{(-)}$ – definiowany według zależności (5). Końcem przedziału jest chwila $t\_x_n^{(K)} = t\_x_n^{(I)}$.

$$P\_x_n^{(-)} = b \cdot P\_x_n , \tag{5}$$

gdzie: b – jest współczynnikiem.

Po wykryciu wycieku, na podstawie ustalonych chwil czasowych $t\_x_n^{(I)}$ lub $t\_x_n^{(II)}$ przejścia czół fal ciśnienia przez poszczególne punkty pomiarowe, następuje jego lokalizacja w oparciu o zależność (1).

5.2. Zastosowanie opracowanych procedur do diagnozowania symulowanych wycieków

Opisane procedury zostały zastosowane do diagnozowania symulowanych wycieków. Wyniki ich użycia prezentowane poniżej dotyczą serii badań przeprowadzonych przy następujących warunkach:

– funkcjonowaniu rurociągu modelowego w warunkach stanu ustalonego przed wyciekiem z: ciśnieniem na wlocie $p_1 \approx 5{,}7$ bara, ciśnieniem na wylocie $p_6 \approx 2{,}2$ bara, nominalnym natężeniem przepływu $q_0 \approx 95$ l/min, średnią temperaturą tłoczonego medium $T_{wody} \approx 20$ °C,

– symulowaniu nagłych wycieków (poprzez bardzo szybkie pełne otwarcie zaworów kranków upustowych) o wielkościach 1÷8 % nominalnego natężenia przepływu q_0 w punktach o współrzędnych: 155 , 195 , 235 m.

Istotnym elementem poprawnego działania opracowanych algorytmów wyznaczania chwil czasowych $t\_x_n^{(I)}$ i $t\_x_n^{(II)}$ był odpowiedni dobór wartości progów alarmowych P_x_n.

Dla rozpatrywanych poszczególnych sygnałów ciśnienia i sygnałów słabych interakcji, niezaszumianych i zaszumianych, doboru wartości progów alarmowych dokonano pod kątem jak najmniejszych opóźnień w wykrywaniu czół fal ciśnienia, w oparciu o uzyskane minimalne wartości funkcji $f\Delta x_n$ w stanach bez wycieku. W przypadku sygnałów zaszumianych, w celu wyeliminowania fałszywych alarmów, dodatkowo uwzględniono ich kilkukrotne zaszumianie. Informacje na temat przyjętych wartości progów alarmowych przedstawiono w tabeli 2.

Tab. 2. Wartości przyjętych progów alarmowych

Sygnały		Zaszumianie		
		bez (A)	0,2% ($A_{0,2}$)	0,5% ($A_{0,5}$)
ciśnienia	p_1	-0,0230	-0,0280	-0,0570
	p_2	-0,0185	-0,0255	-0,0555
	p_3	-0,0170	-0,0250	-0,0540
	p_4	-0,0180	-0,0260	-0,0550
	p_5	-0,0160	-0,0240	-0,0530
	p_6	-0,0165	-0,0245	-0,0535
słabych interakcji	m_{K1}	-0,155	-0,160	-0,170
	m_{K2}	-0,125	-0,130	-0,140

W tabeli 3 przedstawiono wyniki lokalizacji symulowanych wycieków oraz ich błędy. Wyniki dotyczą użycia standardowego pakietu sygnałów ciśnienia (pakiet A) i pakietu obejmującego sygnały słabych interakcji (pakiet B), niezaszumianych (A) i zaszumianych ($A_{0,2}$, $A_{0,5}$), z uwzględnieniem lokalizacji wycieku w oparciu o ustalone chwile czasowe $t\_x_n^{(I)}$ (metoda I) oraz chwile czasowe $t\_x_n^{(II)}$ (metoda II).

Tab. 3. Porównanie wyników lokalizacji symulowanych wycieków, gdzie obliczone miejsca wycieków są wartościami średnimi z trzech eksperymentów; „–" oznacza nie wykrycie i nie zlokalizowanie danej wielkości wycieku

Wycieki		Szum	Zastosowane pakiety sygnałów							
			Pakiet A: $\mathbf{p_1 - p_2 - p_3 - p_4 - p_5 - p_6}$				Pakiet B: $\mathbf{m_{K1} - p_2 - p_3 - p_4 - p_5 - m_{K2}}$			
			Metoda I		Metoda II		Metoda I		Metoda II	
[m]	[% q_0]		miejsce [m]	błąd [m]	miejsce [m]	błąd [m]	miejsce [m]	błąd [m]	miejsce [m]	błąd [m]
155	1,0 %	A	–	–	–	–	–	–	–	–
		$A_{0,2}$	–	–	–	–	–	–	–	–
		$A_{0,5}$	–	–	–	–	–	–	–	–
	1,5 %	A	164,2	+9,2	172,9	+17,9	–	–	–	–
		$A_{0,2}$	172,2	+17,2	132,6	-22,4	–	–	–	–
		$A_{0,5}$	–	–	–	–	–	–	–	–
	2,0 %	A	158,6	+3,6	155,4	+0,4	161	+6	156,7	+1,7
		$A_{0,2}$	160,1	+5,1	164,3	+9,3	152,2	-2,8	163,2	+8,2
		$A_{0,5}$	–	–	–	–	147,3	-7,7	135,9	-19,1
	2,5 %	A	159	+4	158	+3	158,2	+3,2	159,3	+4,3
		$A_{0,2}$	158,9	+3,9	157,5	+2,5	150,8	-4,2	159,8	+4,8
		$A_{0,5}$	–	–	–	–	117,3	-37,7	132,9	-22,1
	3,0 %	A	153,7	-1,3	153,7	-1,3	151,2	-3,8	153	-2
		$A_{0,2}$	150	-5	157	+2	141,4	-13,6	154,2	-0,8
		$A_{0,5}$	199,8	+44,8	179,7	+24,7	151,6	-3,4	137,4	-17,6
	4,0 %	A	152,3	-2,8	151,4	-3,6	152,6	-2,4	152,9	-2,1
		$A_{0,2}$	157,3	+2,3	156,3	+1,3	153,2	-1,8	153,8	-1,2
		$A_{0,5}$	165	+10	133,5	-21,5	134,9	-20,1	136,8	-18,2
195	1,0 %	A	–	–	–	–	–	–	–	–
		$A_{0,2}$	–	–	–	–	–	–	–	–
		$A_{0,5}$	–	–	–	–	–	–	–	–
	1,5 %	A	187,9	-7,1	195,2	+0,2	–	–	–	–
		$A_{0,2}$	180,6	-14,4	198,5	+3,5	–	–	–	–
		$A_{0,5}$	–	–	–	–	–	–	–	–
	2,0 %	A	185,6	-9,4	190,5	-4,5	186,9	-8,1	192,6	-2,4
		$A_{0,2}$	186,6	-8,4	190,2	-4,8	175,9	-19,1	186,3	-8,8
		$A_{0,5}$	–	–	–	–	178	-17	192,8	-2,2
	2,5 %	A	185,7	-9,3	190,5	-4,5	184,7	-10,3	190,4	-4,6
		$A_{0,2}$	185,7	-9,3	190,1	-4,9	178,5	-16,5	190	-5
		$A_{0,5}$	208,4	+13,4	210,8	+15,8	204,2	+9,2	187,7	-7,3
	3,0 %	A	192	-3	191,1	-3,9	191,4	-3,6	191,9	-3,1
		$A_{0,2}$	194,7	-0,3	189,4	-5,6	191,4	-3,6	189,4	-5,6
		$A_{0,5}$	187,7	-7,3	181,4	-13,6	173,1	-21,9	184,6	-10,4
	4,0 %	A	193,2	-1,8	195,5	+0,5	192,6	-2,4	196,1	+1,1
		$A_{0,2}$	190,6	-4,4	196,7	+1,7	188,6	-6,4	194,4	-0,6
		$A_{0,5}$	187,9	-7,1	182,9	-12,1	189,5	-5,5	189,9	-5,1
235	1,0 %	A	–	–	–	–	–	–	–	–
		$A_{0,2}$	–	–	–	–	–	–	–	–
		$A_{0,5}$	–	–	–	–	–	–	–	–
	1,5 %	A	213,3	-21,7	225,5	-9,5	–	–	–	–
		$A_{0,2}$	217,6	-17,4	224,5	-10,5	–	–	–	–
		$A_{0,5}$	–	–	–	–	–	–	–	–
	2,0 %	A	222,1	-12,9	228,2	-6,8	222,2	-12,8	228,8	-6,2
		$A_{0,2}$	219,4	-15,6	224	-11	215,8	-19,2	228,1	-6,9
		$A_{0,5}$	–	–	–	–	–	–	–	–
	2,5 %	A	228,2	-6,8	230,7	-4,3	228,2	-6,8	232,7	-2,3
		$A_{0,2}$	227,3	-7,7	235,4	+0,4	227,2	-7,8	235,3	+0,3
		$A_{0,5}$	221	-14	224,1	-10,9	240,3	+5,3	223,6	-11,4
	3,0 %	A	226,9	-8,1	228,3	-6,7	228	-7	227,7	-7,3
		$A_{0,2}$	229,5	-5,5	227,7	-7,3	231,4	-3,6	227,9	-7,1
		$A_{0,5}$	248,8	+13,8	230,6	-4,4	259,3	+24,3	226	-9
	4,0 %	A	227,8	-7,2	226,5	-8,5	227,3	-7,7	225,4	-9,6
		$A_{0,2}$	232,4	-2,6	231	-4	230,5	-4,5	229,5	-5,5
		$A_{0,5}$	220,3	-14,7	231,9	-3,1	231,8	-3,2	237,1	+2,1

Dokonując lokalizacji wycieków, występujące we wzorze (1) współczynniki a_p i a_k nachylenia prostych wyznaczano w oparciu o dwa podzbiory danych $\{z_n, t\_x_n\}$: początkowy – dla pierwszej trójki czujników z danego pakietu i końcowy – dla drugiej trójki czujników z danego pakietu, wykorzystując metodę aproksymacji średniokwadratowej, zwanej także metodą najmniejszych kwadratów.

Do określenia wartości progów $P\_x_n^{(-)}$ przyjęto identyczne wartości współczynników $b = 0{,}4$.

Na podstawie analizy uzyskanych wyników można stwierdzić, że przy użyciu pakietu standardowych niezaszumianych sygnałów ciśnienia możliwe było wykrycie i zlokalizowanie nagłych wycieków o wielkościach 1,5 %, gdzie dla porównania przy użyciu pakietu obejmującego niezaszumiane sygnały słabych interakcji poziom wykrywalności wycieków wynosił 2 %, a błędy ich lokalizacji nie odbiegały znacząco od wyników uzyskanych dla sygnałów ciśnienia.

Wraz ze wzrostem poziomu zaszumienia sygnałów, w przypadku użycia sygnałów ciśnienia znacznemu pogorszeniu uległy poziom wykrywalności i błąd lokalizacji wycieków, gdzie dla porównania w przypadku użycia sygnałów słabych interakcji zmiany nie były aż tak znaczne.

Wzrost zaszumienia spowodował również konieczność zmiany przyjętych progów alarmowych P_x_n dla poszczególnych sygnałów, gdzie w przypadku sygnałów słabych interakcji poziom zmian był niewielki, a w przypadku sygnałów ciśnienia po identycznym ich zaszumieniu wartości progów należało zmienić na kilkukrotnie wyższe.

Zaobserwowano również wzrost dokładności lokalizacji wycieków, poprzez zastosowanie modyfikacji opracowanych procedur w zakresie zastąpienia ujawnionych chwil czasowych $t\_x_n^{(I)}$ przez nowe chwile czasowe $t\_x_n^{(II)}$.

Prezentowane wyniki potwierdziły istnienie problemów związanych z wykrywaniem i lokalizowaniem wycieków w odniesieniu do użycia standardowych sygnałów ciśnienia. Dla porównania, pomimo użycia sygnałów słabych interakcji tylko z dwóch korektorów, uzyskano większą odporność na możliwość wystąpienia zakłóceń (zaszumianie) oraz lepszy poziom wykrywalności i błędów lokalizacji wycieków.

PODSUMOWANIE

Dołączenie do rurociągów korektorów stwarza możliwość pozyskiwania cennej informacji diagnostycznej, którą są sygnały słabych interakcji międzyobiektowych. Sygnały te mają dobre własności metrologiczne: są czułe na wycieki i odporne na zakłócenie. Dzięki tym sygnałom możliwe jest polepszenie podatności diagnostycznej rurociągów, a stąd skuteczności diagnozowania wycieków, realizowanego w oparciu o metodę śledzenia czół fal ciśnienia. Sygnały słabych interakcji mogą stanowić cenne uzupełnienie dotychczas stosowanych sygnałów ciśnienia.

LITERATURA

[1] Billman L., Isermann R.: *Leak detection methods for pipelines*. Automatica, vol. 23, no. 3, 1987, pp. 381-385.

[2] Kowalczuk Z., Gunawickrama K.: *Detekcja i lokalizacja wycieków w rurociągach przesyłowych*. Rozdział 21 pracy zbiorowej pod red. J. Korbicza, J. Kościelnego, Z. Kowalczuka i W. Cholewy: Diagnostyka procesów. Modele, metody sztucznej inteligencji, zastosowania. Warszawa, WNT, 2002.

[3] Lindstedt P.: *Weak interactions between objects in the signal-based and parametric diagnostics of transport-dedicated complex engineering systems*. Aircraft Engineering and Aerospace Technology: An International Journal, vol.77 no.3/2005, pp. 222-227.

[4] Lindstedt P., Ostapkowicz P.: *Zastosowanie elementów korekcyjnych automatyki w diagnostyce obiektów technicznych*. XV Krajowa Konferencja Automatyki, Warszawa 27-30. czerw. 2005, Wydaw. PAN, str. 181-186.

[5] Ostapkowicz P.: *Signals of weak interobject interactions in diagnosing of lekages from pipelines*. Eksploatacja i niezawodność, nr 33, 1/2007, str. 31-45.

[6] Ostapkowicz P.: *Sygnały słabych interakcji międzyobiektowych w diagnostyce wycieków z rurociągów*. Rozdział w pracy zbiorowej pod red. J. Korbicza, K. Patana, M. Kowala: Diagnostyka procesów i systemów. Warszawa, Wydaw. EXIT, 2007, str. 323-330.

[7] Sobczak R.: *Lokalizacja nieszczelności w rurociągach metodą śledzenia czół fal ciśnienia*. Przemysł Chemiczny, nr 83, 6/2004, str. 296-299.

[8] Zhang J.: *Statistical pipeline leak detection for all operating conditions*. Pipeline & Gas Journal, February 2001, pp. 42-45.

Praca finansowana przez Politechnikę Białostocką – praca statutowa S/WM/3/06.

Dr inż. **Paweł OSTAPKOWICZ** – absolwent i pracownik Wydziału Mechanicznego Politechniki Białostockiej, gdzie w 1998 roku ukończył studia, a w 2007 roku uzyskał stopień doktora.
Tematyka badawcza: budowa i eksploatacja maszyn, automatyka, miernictwo dynamiczne, diagnostyka maszyn. Prace dotyczyły głównie: diagnozowania wycieków z rurociągów, polepszania podatności diagnozowanych obiektów technicznych, wibroakustyki.

MODELE SYGNAŁÓW GENEROWANYCH PRZEZ OKRĘTOWY KOCIOŁ PAROWY

Andrzej ADAMKIEWICZ*, Artur BEJGER**, Krzysztof KOŁWZAN***

*Akademia Morska, Wydział Mechaniczny, Instytut Technicznej Eksploatacji Siłowni Okrętowych
Wały Chrobrego 1-2, 70-500 Szczecin, andrzej.adamkiewicz@am.szczecin.pl
**Akademia Morska, Wydział Mechaniczny, Katedra Diagnostyki i Remontów Maszyn
ul. Podgórna 51/53, 70-205 Szczecin, artur.bejger@am.szczecin.pl
***Polski Rejestr Statków S.A, Al. Gen. J. Hallera 126, 80-416 Gdańsk, krzysztof.kolwzan@prs.pl

Streszczenie

Ograniczona dostępność pomiarowa sygnałów generowanych podczas pracy zautomatyzowanych kotłów pomocniczych zmusza do wykorzystywania w procesie tak modelowania jak i rzeczywistego dozorowania stanów kotłów na podstawie wybranych sygnałów odwzorowujących stan techniczny kotłów. Przeprowadzono dekompozycję strukturalną i funkcjonalną okrętowego pomocniczego kotła parowego. Sygnały podzielono na: cieplno-przepływowe, emisji toksycznych zanieczyszczeń w strumieniu spalin wylotowych, jak również wibroakustyczne. Przedstawiono estymację parametrów sygnałów na podstawie wyników pomiarów wielkości wyjściowych ogólnego modelu kotła. W pracy zdefiniowano sygnały tworzące relacje diagnostyczne, jakich można oczekiwać w procesie oceny stanów kotłów okrętowych. Ich identyfikacja może być uzasadnieniem do wdrożenia strategii eksploatacji kotłów okrętowych z tzw. obsługiwaniem quasidynamicznym.

Słowa kluczowe: kocioł parowy, sygnał, diagnoza, parametr, okrętowy układ energetyczny, obsługiwanie.

MODELS OF SIGNALS GENERATED BY A SHIP BOILER

Summary

The especially limited measurement availability of signals generated at operation of automated auxiliary boilers enforces the application of modeling as well as actual monitoring of their condition on the basis of a significant number of reliable measurement signals. A structural and functional decomposition of an auxiliary ship boiler has been carried out. Signals have been divided into: thermal-flow, exhaust toxic pollutant emissions in gas flows of marine boilers, as well vibroacoustic and acoustic. Estimation of signals parameters, basing on the results of measurements of output values for a general boiler model, has been suggested. Diagnostic relations which can be expected to be valid for ship boilers have been defined. Establishing their validity may be a justification for implementing a ship boiler quasidynamic maintenance.

Keywords: ship boiler, signal, diagnostic, parameter, marine power plants, maintenance.

1. ISTOTA ROZPATRYWANEGO PROBLEMU BADAWCZEGO

Okrętowe kotły parowe są eksploatowane z zastosowaniem strategii eksploatacji opartej na metodzie planowo – zapobiegawczej. Strategia ta nie obejmuje nieplanowanych czynności obsługowych, jako konsekwencji zaistniałych losowo w historii użytkowania kotłów zdarzeń – niezdatności [1, 2]. Stan taki, zachęca do stosowania zróżnicowanych metod postępowania eksploatacyjnego w celu wypracowania tak diagnozy użytkowej jak i obsługowej.

Szersze zastosowanie diagnostyki w eksploatacji kotłów, pozwoli na dynamiczne podejmowanie decyzji eksploatacyjnych, utrzymanie w stanie zdatności, wzrost dyspozycyjności kotłów, uprzedzając ewentualne zaistnienie niezdatności.

Powstawanie osadów, od strony spalin i kamienia kotłowego od strony wodnej, jest niesprawnością charakterystyczną dla kotłów, rozwijającą się w procesie eksploatacji ewolucyjnie, a jej skutki powodują znaczną liczbę niezdatności i awarii kotłów [1]. Z tego powodu wynika znaczenie faktu odpowiednio wczesnego rozpoznawania wszelkich niezdatności. Możliwość rozróżniania uszkodzenia lub stanu technicznego zależy od własności diagnozowanego obiektu – typu kotła. Wymagana rozróżnialność wiąże się z jego wyposażeniem w odpowiedni zbiór urządzeń pomiarowych.

Przedstawione zagadnienie rozpatrzono kompleksowo, w oparciu o model diagnozowanego rzeczywistego obiektu technicznego – okrętowego kotła parowego i wyniki pomiarów.

Identyfikacja parametrów modelu może nastąpić metodą bezpośredniego pomiaru lub pośrednimi

metodami obliczeniowymi. Ograniczenia i stosowalność każdej z tych metod wynikają z przeznaczenia modelu i specyfiki struktury konstrukcyjnej kotła. Do ekstrakcji cech kotłów stosowane są przede wszystkim metody analizy sygnałów, obejmujące opis sygnałów i modele sygnałów. Od ich relacji z cechami stanu zależne są metody rozróżnialności niesprawności kotłów.

2. SYGNAŁY W RELACJACH DIAGNOSTYCZNTCH KOTŁÓW

Dysponowanie wiarygodnymi metodami diagnozowania kotłów bez ich wyłączania z ruchu związane jest z identyfikacją cech sygnałów generowanych przez kocioł podczas pracy. Jednocześnie ich znajomość jest niezbędna do oceny warunków pracy kotła dla potrzeb sterowania procesem w kierunku realizacji racjonalnego sposobu eksploatacji zdefiniowanego przez uogólnione kryterium wybranej strategii. W pierwszym przypadku będą wykorzystywane modele diagnostyczne relacji typu [7, 9]:
parametry sygnałów – parametry stanu

$$\mathbf{Y_i = F_1 (X)} \tag{1}$$

oraz
parametry sygnałów – stany

$$\mathbf{Y_i = K (W)} \tag{2}$$

w drugim:
parametry sygnałów – miara eksploatacji

$$\mathbf{Y_i = G_1 (L)} \tag{3}$$

oraz
miara eksploatacji – parametry sygnałów

$$\mathbf{L = G_2 (Y_i)} \tag{4}$$

gdzie:

- $\mathbf{Y_i}$ – zbiory parametrów sygnałów „i",
- $\mathbf{X}$ – zbiory parametrów stanu,
- $\mathbf{W}$ – zbiory stanów,
- $\mathbf{L}$ – zbiory miar eksploatacji,
- i – identyfikator rodzaju sygnału.

Każda z relacji (1) – (4) jest modelem obiektu technicznego/kotła, jak i modelem procesów przetwarzania energii i procesów towarzyszących – resztkowych, również innych urządzeń współpracujących z kotłem [6, 8].

W pracującym kotle, funkcjonującym w środowisku okrętowym zachodzą procesy fizyko-chemiczne, między innymi takie jak: przepływ strumieni energii z równoczesną konwersją, strumieni masy wody, pary, powietrza, paliwa i spalin, drgania, emisję akustyczną, promieniowanie ciepła itp., które są źródłem generowanych sygnałów. Opisują je przebiegi w czasie wielkości fizycznych transmitujących informację w sposób zależny od rodzaju sygnału (jego właściwości). Składowe sygnału, niosące informację są parametrami sygnału [9]. Przy nieznajomości pełnego modelu, a taka sytuacja jest rozpatrywana, do detekcji uszkodzeń kotła wykorzystywane są metody kontroli ograniczeń oraz związków między zmiennymi procesowymi [7, 9]. Postępowanie takie zastosowano w odniesieniu do kotła w eksploatacji, gdy podstawą oceny jego stanu mają być wyniki badań procesów: głównego roboczego, cieplno-przepływowego i procesów resztkowych: emisji produktów spalania oraz wibroakustycznych.

3. OBIEKT, PRZEDMIOT, WARUNKI I PROGRAM BADAŃ

Identyfikację parametryczną sygnałów przeprowadzono w oparciu o instalację kotłową układu energetycznego m/f „Polonia". Układ wyposażony jest w 3 pomocnicze kotły parowe produkcji Anders Halvorsen A/S Flekkefjord – Norwegia [10]. Jeden typu PARAT Mod. B – 3, jest poziomym kotłem płomieniówkowym, z palnikiem ciśnieniowym typu Weishaupt 132/150-2 opalanym paliwem ciężkim HFO, o wydajności pary 6000 kg/h, ciśnieniu projektowym pary 9 bar, ciśnieniu roboczym dla stanu eksploatacyjnego 7 bar. Kocioł jest użytkowany przede wszystkim podczas postoju statku w porcie. Dwa kotły utylizacyjne typu PARAT o wydajności pary każdy 1250 kg/h, zasilane spalinami z silników głównych, pracują wyłącznie podczas podróży morskiej. Ogólną budowę obiektu badań, kotła opalanego, przedstawiono na rysunku 1.

Przedmiotem przeprowadzonych badań były parametry sygnałów generowanych przez pomocniczy kocioł opalany. Procesy zachodzące w czasie pracy kotła generowały sygnały wielowymiarowe, opisywane przez zbiory wielu parametrów.

Badania przeprowadzono w trybie eksperymentu biernego, w warunkach eksploatacyjnych statku. Instalacja kotła opalanego znajdowała się w stanie pełnej zdatności technicznej, po wykonanym stoczniowym przeglądzie klasyfikacyjnym. Woda zasilająca kocioł o temperaturze 85 – 95 ºC, w zakresie zalecanym przez producenta, była odgazowana i uzdatniona chemicznie. Kocioł opalany był paliwem ciekłym o temperaturze 160^{o} C i zawartości siarki 1,49%. Kocioł pracował w trybie automatycznym, cyklicznie włączając palnik przy ciśnieniu pary świeżej 5,1 bar i wyłączając przy ciśnieniu 6,3 bar, w zależności od zapotrzebowania na parę przez okrętowe instalacje pary grzewczej. Dopuszczalny zakres zmian ciśnienia pary w kotle podczas automatycznej pracy kotła wynosił 4,4 – 7,0 bar. Wykonano dwie serie pomiarów, po kilkadziesiąt obserwacji w każdej. Na rys. 2 pokazano przykładowy fragment przebiegu zmian parametrów eksploatacyjnych układu energetycznego, w tym ciśnienia pary w kotle, na monitorze centrali kontrolno – manewrowej siłowni statku, w funkcji czasu pracy.

Wybór punktów pomiarowych sygnałów podyktowany był konstrukcją kotła i jego

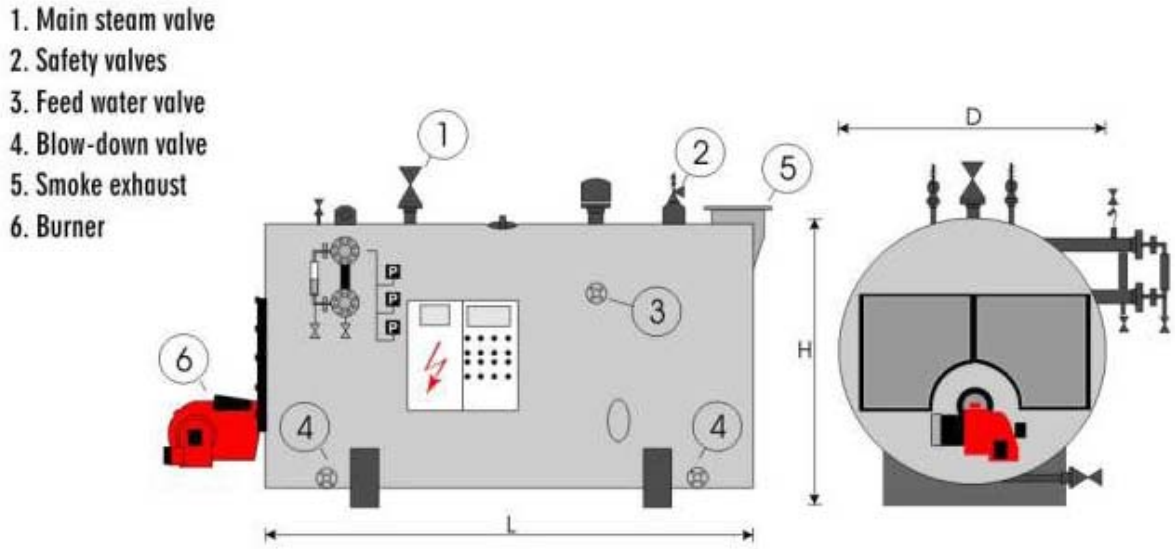

Rys. 1. Schemat ogólnej budowy pomocniczego kotła opalanego typu Parat Mod. B – 3 [11]: 1 -główny zawór parowy, 2 - zawory bezpieczeństwa, 3 - zawór zasilania wodnego, 4 - Zawór szumowania dolnego, 5 - wylot spalin, 6 – palnik

podzespołów, układem monitorowania parametry pracy siłowni oraz rodzajem badanego sygnału. Ocena stanu dynamicznego kotła za pomocą generowanych procesów fizycznych wymaga jednoznacznego skojarzenia jego parametrów funkcjonalnych ze zbiorem miar procesów wyjściowych oraz kryteriów ich oceny. Identyfikacja charakteru sygnałów i mechanizmu ich generacji musi w diagnozowaniu kotłów poprzedzać zastosowanie informacji zawartych w emitowanych procesach wyjściowych.

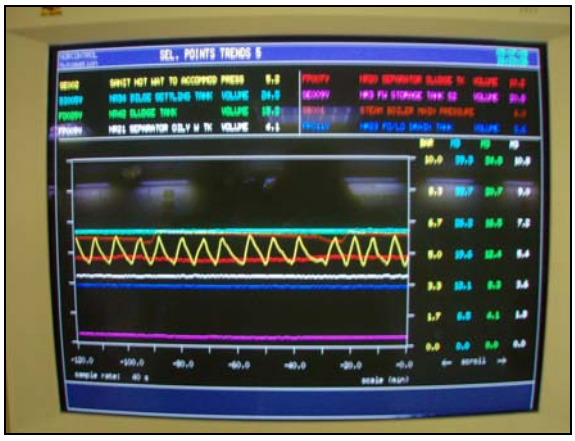

Rys. 2. Przykładowy fragment przebiegu zmian ciśnienia pary w kotle na monitorze centrali kontrolno – manewrowej siłowni statku w funkcji czasu pracy (linia żółta)

4. IDENTYFIKACJA PARAMETRÓW SYGNAŁÓW GENEROWANYCH PRZEZ PROCESY ZACHODZĄCE W KOTLE

Źródłem sygnałów generowanych przez kocioł okrętowy jest główny proces roboczy wymiany ciepła pomiędzy produktami spalania strumienia paliwa w atmosferze strumienia powietrza, wodą i parą wodną z udziałem materiałów elementów kotła Nadzorowanie pracy kotła odbywa się przede wszystkim w oparciu o wartości parametrów sygnału cieplno – przepływowego oraz metodami wizualizacyjnymi. Stosując jednak jedynie te metody nie można sterować procesem eksploatacji kotła.

4.1. Sygnał cieplno - przepływowy

Parametry sygnału cieplno-przepływowego, stanowią integralny składnik systemu regulacji i sterowania pracą kotła. Międzynarodowe standardy opierają się aktualnie na stacjonarnych modelach entalpowych [6]. Miarą jakości przemian w takich modelach są sprawności i jednostkowe zużycia ciepła. Dla pomocniczego kotła parowego będzie to sprawność η_{Kh} definiowana zależnością w postaci

$$\eta_{Kh} = \frac{\dot{m}_{pary1}\left(i_{pary1} - i_{wz}\right)}{\dot{m}_{pal} W_d + \dot{m}_{pow0} i_{pow0}} \tag{5}$$

gdzie:

- $\dot{m}_{pary1}, i_{pary1}$ – strumień masy i entalpia pary wodnej opuszczającej kocioł,
- i_{wz} – entalpia wody zasilającej kocioł,
- $\dot{m}_{pal}$ – strumień masy paliwa zasilającego kocioł,
- $\dot{m}_{pow0}, i_{pow0}$ – strumień masy i entalpia powietrza atmosferycznego zasilającego kocioł,
- W_d – wartość opałowa dolna paliwa.

Zmienne modelu (5) są zmiennymi zależnymi od wielkości wejścia i wyjścia podzespołów kotła. Dla potrzeb analizy sygnałów kocioł zdekomponowano rozróżniając w nim: walczak, komorę spalania i palnik. Modelami entalpowymi F_h sygnału będą

wówczas związki między cieplno-przepływowymi wielkościami zależnymi, a parametrami cieplno-przepływowymi niezależnymi i geometrią walczaka, komory spalania oraz palnika. W takim ujęciu model jest określony przez układ równań bilansowych masy i energii dla walczaka W, komory spalania KS wraz z palnikiem P, zapisany symbolicznie w postaci

$$\eta_{Kh} = F_h\left\{D_{pary}\left(p_{p1}, t_{p1}\right) f_{KS}\left[KS, f_W\left(W\right)\right]\right\} \quad (6)$$

gdzie:

$D_{pary}\left(p_{p1}, t_{p1}\right)$ – wydajność pary przy ciśnieniu p_{p1} i temperaturze t_{p1},

$$KS = \{p_{pal}, t_{pal}, W_d, p_{pow0}, t_{pow0}; m_{pal}, m_{pow0}, i_{pow0}; współcz.korekc.\} \quad (7)$$

– zbiory zmiennych (rozdzielone średnikami), niezależnych, zależnych i współczynników korekcyjnych komory spalania,

$$W = \left(t_{wz}, p_{p1}, t_{p1}; \dot{m}_{pary1}, i_{wz}, i_{pary1}; L, D, H, ...\right) \quad (8)$$

– zbiory zmiennych (rozdzielone średnikami) niezależnych, zależnych i wymiarów geometrycznych podzespołów, które decydują o własnościach cieplno-przepływowych walczaka kotła/elementów przepływowych.

Przez zmienne niezależne determinujące stan cieplny kotła w zapisach (6) – (8) rozumiane są zbiory parametrów z danymi początku (indeks 0) i końca (indeks 1) procesu odparowania wody w kotle. Parametry niezależne mogą być zadawane jako zbiór zmiennych wejścia/zewnętrznych (outside parameters) lub stanowić zbiór wielkości mierzonych/kontrolowanych. Niektóre z nich mogą być/są dla kotła parametrami alarmowymi.

Modele sygnałów cieplno-przepływowych budowane są jako zero wymiarowe (o parametrach skupionych). Przy zidentyfikowanych parametrach sygnału miarą degradacji kotła będą różnice między wartościami aktualnymi i wartościami referencyjnymi wybranych parametrów sygnału cieplno-przepływowego.

4.2. Sygnał emisji produktów spalania

Współczesne kotły okrętowe opalane są paliwami płynnymi, produktami destylacji ropy naftowej lub gazowymi. W składzie paliw dla kotłów występują: węgiel < (85 – 90)%, wodór (10 – 12)%, siarka < (0,6 – 2)%, tlen i azot 0,5% oraz inne domieszki.

W procesie zupełnego spalania paliwa następuje utlenianie cząstek palnych, a w rezultacie reakcji egzotermicznej emitowane są w postaci gazowej: z węgla – CO_2 (dwutlenek węgla), wodoru – H_2O (woda), siarki – SO_2 (dwutlenek siarki) lub w postaci dymu. Reszty w postaci osadów, które są lub nie są korodujące oraz mogą, ale nie muszą, hamować przenikania ciepła mogą częściowo pozostawać w kotle. Azot i tlen w spalinach pochodzi z powietrza podawanego do paleniska, a także w niewielkiej ilości z paliwa [1, 4, 5, 8, 11].

Podczas spalania paliwa przy niedostatecznej ilości podawanego powietrza pozostają oprócz cząstek CO_2 również i CO oraz nie spalone węglowodory, które mogłyby podlegać dalszemu utlenianiu. Jednakże spalanie to poza komorą jest wysoce utrudnione ze względu na zbyt niskie temperatury, zbyt małą ilość tlenu lub/oraz niedostateczną w mieszanie składników palnych.

Miarą oceny jakości funkcjonowania kotła na podstawie parametrów sygnału emisji produktów spalania jest sprawność kotła η_{KA} definiowana zależnością z uwzględnieniem straty wylotowej q_{Af} i straty niezupełnego spalania q_{Ag} w postaci [4, 5, 8]

$$\begin{aligned}\eta_{KA}[\%] &= 100[\%] - q_{Af}[\%] - q_{Ag}[\%] \\ &= \eta_{Af}[\%] - q_{Ag}[\%]\end{aligned} \quad (9)$$

gdzie:

$$\eta_{Af}[\%] = 100[\%] - q_{Af}[\%] \quad (10)$$

jest sprawnością procesu spalania w kotle określaną z wykorzystaniem straty wylotowej q_{Af}

$$q_{Af}[\%] = \left(t_{spal}\left[^oC\right] - t_{pow0}\left[^oC\right]\right)\left(\frac{A_1}{CO_2[\%]} + B\right) \quad (11)$$

gdzie:

A_1,B – współczynniki Siegerta [4, 5, 8] charakterystyczne dla danego paliwa,

q_{Ag} – strata niezupełnego spalania, obliczana w oparciu o zmierzoną zawartość CO_{zmierz} w spalinach wg wzoru.

$$q_{Ag} = \frac{\alpha\ CO_{zmierz}[\%]}{CO_{zmierz}[\%] + CO_2[\%]} \quad (12)$$

gdzie:

α – współczynnik charakterystyczny dla danego rodzaju paliwa, tutaj dla oleju opałowego α =48,

CO_2 – zawartość objętościowa dwutlenku węgla CO_2 w spalinach, obliczona z zależności.

$$CO_2 = CO_{2\max}\left(1 - \frac{O_{2zmierz}[\%]}{20{,}95[\%]}\right) \quad (13)$$

gdzie:

CO_{2max} – współczynniki Siegerta [4, 5, 8] charakterystyczne dla danego paliwa,

20,95% – zawartość tlenu O_2 [%] w czystym powietrzu,

$O_{2zmierz}$ – zmierzona zawartość tlenu O_2 [%].

Strata niezupełnego spalania określa procentową stratę ciepła spowodowaną obecnością gazów palnych CO w spalinach. Wśród szkodliwych składników emitowanych w spalinach oprócz tlenku

węgla *CO* i tlenku azotu *NO* spaliny zawierają również wyższe tlenki, głownie NO_2. Stężenie tlenku azotu, wyrażone w (ppm) można z dużą dokładnością wyrazić jako sumę stężeń *NO* i NO_2. Jeżeli analizator nie posiada czujnika dwutlenku azotu NO_2, a jedynie czujnik tlenku azotu *NO*, wówczas zawartość NO_2 jest szacowana na podstawie zmierzonej koncentracji *NO*. Najczęściej przyjmuje się, że tlenek azotu *NO* występujący w spalinach stanowi około 95% ogólnej ilości tlenków azotu NO_X wówczas

$$NO_x[ppm] = \frac{NO_{zmierz}[ppm]}{0{,}95} \tag{14}$$

Wpływ na zawartość tlenków siarki SO_X w spalinach ma ilość siarki w paliwie.

W praktyce niemożliwym jest takie rozdrobnienie paliwa, aby wszystkie molekuły otrzymały jednocześnie niezbędną do spalenia ilość powietrza. Współczynnik nadmiaru powietrza λ z zastosowaniem parametrów emisji produktów spalania obliczany jest na podstawie znanej dla danego paliwa wartości CO_{2max} oraz zmierzonej wartości $CO_{2zmierz}$ w spalinach według związku

$$\lambda = \frac{CO_{2\max}}{CO_{2zmierz}} \tag{15}$$

lub poprzez pomiar w spalinach zawartości tlenu O_2

$$\lambda = \frac{20{,}95\%}{20{,}95\% - O_{2zmierz}[\%]} \tag{16}$$

Jest on zmienną zależną wyjścia palnika.

Niezbędne do wyznaczenia sprawności kotła związki (9) – (16) można, analogicznie do zależności (6) – (8), zapisać w postaci ogólnego modelu sygnału emisji produktów spalania pomocniczego kotła okrętowego w postaci:

$$\eta_{KA} = F_A\left\{O_2, skl.pal, \lambda, f_{Af}\left[AF, f_{Ag}(AG)\right]\right\} \tag{17}$$

gdzie:

skl.pal – skład paliwa,

Af – zbiory zmiennych (rozdzielone średnikami), niezależnych, zależnych i współczynników korekcyjnych związanych ze stratą wylotową,

$$Af = \{t_{pow0}, O_2; t_{gaz}, q_{Af}; Cwpal, A_1, B, 20{,}95\} \tag{18}$$

t_{gaz} – temperatura spalin wylotowych,

Cwpal – zawartość węgla w paliwie,

Ag – zbiory zmiennych (rozdzielone średnikami) niezależnych, zależnych i wymiarów geometrycznych palnika związanych z niezupełnym spalaniem,

$$Ag = \{O_2, CO, \alpha, skl.pal; q_{Ag}; wym.geom.pal\} \tag{19}$$

Do pomiarów parametrów sygnału emisji produktów spalania posłużono się analizatorem spalin typu IMR 3000 P [4, 5], którego widok ogólny przedstawiono na rysunku 3. Pomiary parametrów sygnału prowadzono w stanach załączenia, stanach pośrednich i wyłączania palnika kotła, rejestrując podczas jednej obserwacji kilkadziesiąt sekwencji czasowych wzrostu i zmniejszania ciśnienia w kotle. Na rysunku 4 przedstawiono przykładowy wydruk protokółu pomiaru parametrów sygnału emisji produktów spalania uzyskany przy pomocy analizatora spalin.

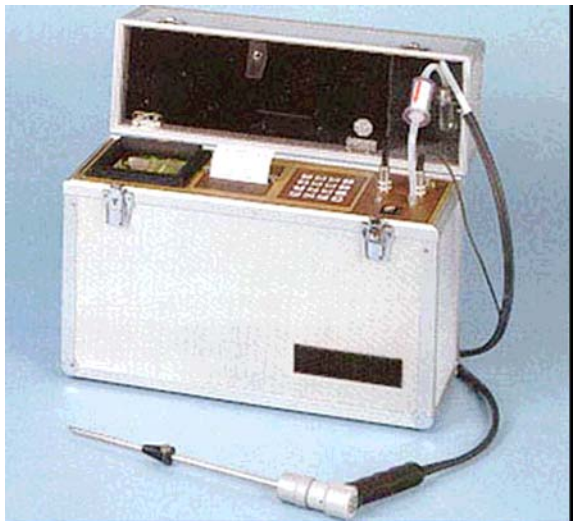

Rys. 3. Widok ogólny zastosowanego do pomiarów analizatora spalin IMR 3000 P [4]

Dokumentuje on wartości parametrów sygnału emisji produktów spalania oleju opałowego, w prezentowanym protokóle przy najwyższym osiągalnym w kotle ciśnieniu pary 6,3 bar.

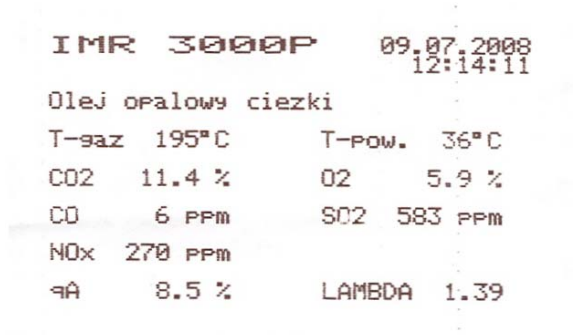

Rys. 4. Wybrany protokół pomiaru parametrów sygnału emisji produktów spalania w chwili wyłączenia palnika

Szkodliwe produkty spalania z okrętowych kotłów parowych CO, CO_2, SO_X i NO_X wpływając destrukcyjnie na stan techniczny kotłów okrętowych stanowią realne zagrożenie dla środowiska morskiego, szczególnie podczas postojów w portach, stoczniach i żegludze w pobliżu lądu. Dopuszczalne wartości udziałów związków toksycznych w strumieniu emitowanych produktów spalania ropopochodnych paliw okrętowych zostały objęte przepisami Konwencji MARPOL. Stosując reguły wnioskowania diagnostycznego ich przekroczenie klasyfikuje formalnie kocioł do stanu niezdatności, natomiast wartości parametrów sygnału emisji produktów spalania jako skutek jakości organizacji

tego procesu są nośnikami informacji diagnostycznej.

4.3. Sygnał wibroakustyczny

W kotle obserwuje się dwa rodzaje wymuszeń generujących sygnały wibroakustyczne związane ze zjawiskami przepływowymi, z których pierwsze jest spowodowane przez procesy zachodzące w komorze paleniskowej, pozostałe natomiast przez zjawiska występujące podczas omywania pęczków w ciągu konwekcyjnym. Pewien wpływ mogą mieć również wymuszenia ze strony pompy paliwowej i wentylatora powietrza.

W komorze spalania, przy ciśnieniu spalin wynoszącym 10 kPa, mogą pojawić się charakterystyczne drgania widoczne w częstotliwości rzędu 30 - 200 Hz. Zmiany te przenoszą się na ściany komory i związane z nimi elementy, a. zjawisku towarzyszy hałas. Oprócz drgań akustycznych mogą też występować infradźwięki o częstotliwościach 3 - 10 Hz, które są trudne do zaobserwowania. Widmo drgań może zmieniać się na skutek zmian: obciążenia kotła (poboru pary), stanu eksploatacyjnego pracy palnika (parametrów powietrza, rodzaju dysz, stosunku nadmiaru powietrza) oraz rodzaju i parametrów paliwa[8, 11].

Częstotliwości drgań własnych można określić w zależności od przyjętego modelu źródła drgań, w którym odpowiednie wymuszenie generuje fale stojące o częstotliwości podstawowej określonej prawami akustyki. Dla komory spalania może to być model typu zamkniętej rury, otwartej lub rezonatora Helmholtza. Przy długościach fali wyraźnie większych od wymiarów komory, modele rezonatora Helmholtza i rury jednostronnie otwartej stają się identyczne [11]. Na skutek doprowadzania energii płomienia do gazów wypełniających komorę paleniskową występują pulsacje ciśnienia wywołujące takie zjawiska jak:

– rezonans układu zasilania paliwem i komorą spalania,
– pulsacje spowodowane niestabilnością procesu spalania,
– szum spalania.

Ciśnienie akustyczne strumienia spalin emitowane przez płomień może oddziaływać na komorę spalania, generując jej drgania. Mogą być one przyczyną drgań akustycznych, w zależności od rozmiarów kotła. Płomień wytwarza szum o szerokim zakresie częstotliwości. Składa się on z szumu przepływu turbulentnego i szumu spalania od fal ciśnienia wywołanych chwilowymi wzrostami objętości podczas spalania. Szum turbulentny i szum spalania zależą od typu palnika i obciążenia kotła. Spalanie znacznie podwyższa poziom hałasu w stosunku do przepływu burzliwego.

Uproszczone modele sygnałów drgań własnych i emisji akustycznej można znaleźć w stosownej literaturze, między innymi np. [3, 8]. Z modeli tych wynika, że każdy kocioł może generować drgania o właściwych tylko dla siebie częstotliwościach własnych.

Największy problem przy korzystaniu z tych modeli stanowi określenie wielkości wynikających z cech konstrukcyjnych kotła, np. stałych charakteryzujących sposób mocowania rury, logarytmicznego dekrementu tłumienia itp. Wielkości te można wyznaczyć jedynie doświadczalnie poprzez pomiary połączone z rejestracją amplitudy i czasu zanikania drgań własnych po wzbudzeniu.

Dla pomiarów parametrów drganiowych i emisji akustycznej wyróżniono stany: z pracującym palnikiem i z wyłączonym płomieniem a pracującą tylko dmuchawą palnika. Badania ukierunkowano na określenie pasma częstotliwości sygnału drganiowego i emisji akustycznej kotła związanego bezpośrednio z pracą:

– pompy paliwowej zasilającej pracujący palnik (pomiar na kadłubie pompy),
– na kołnierzu mocującym pracujący palnik do kotła – pomiar w kierunku poziomym,
– przepływem strumienia powietrza dostarczanego przez dmuchawę bez pracującego palnika.

Akwizycja i archiwizacja danych sygnału drganiowego oparta była na platformie multianalizatora PULSE® firmy Brüel & Kjær z przenośną kasetą pomiarową typu B&K 3650C. System ten był wyposażony w pięciokanałowy moduł kontrolera wejścia/wyjścia typu 7537 oraz 12 kanałowy moduł wejściowy z technologią Dyn-X®. Moduł wejściowy umożliwia synchroniczny pomiar do 17 sygnałów w szerokim paśmie częstotliwości od 0 do 25,6 kHz. System pomiarowy współpracował z przetwornikami przyspieszeń drgań typu B&K 4514B oraz B&K 4504A również firmy Brüel & Kjær. Na rysunku 4 przedstawiono wybrane widmo przyśpieszeń drgań zarejestrowane na kadłubie pompy paliwowej zasilającej pracujący palnik kotła.

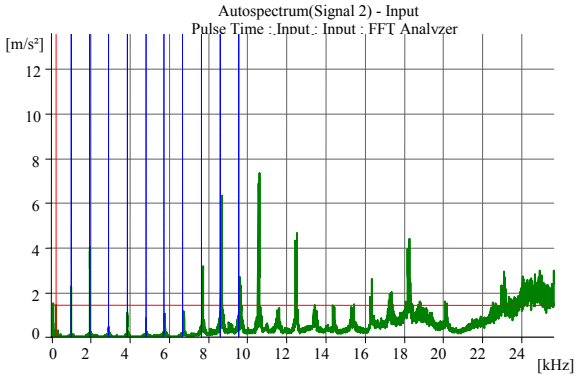

Rys. 4. Przykładowe widmo przyśpieszeń drgań zarejestrowane na kadłubie pompy paliwowej pracującego palnika

Analizując otrzymane wyniki pomiarów sygnału drganiowego zidentyfikowano charakterystyczne składowe harmoniczne związane z procesem spalania, widoczne dla częstotliwości 10,5 kHz oraz składowe harmoniczne napędu pompy paliwowej palnika w niskim paśmie częstotliwości rzędu 60 i 180 Hz, obliczone z prędkości obrotowej napędu pompy. Są one widoczne na widmie przyśpieszeń drgań zarejestrowanych na kołnierzu mocującym palnik do walczaka kotła.

W przypadku rejestracji sygnałów emisji akustycznej istotne znaczenie ma wybór doświadczalnie wyselekcjonowanego punktu pomiaru. W celu zapewnienia skutecznej separacji sygnałów związanych z pracą kotła parowego zastosowano układ wzmacniający sygnał czujnika emisji akustycznej charakteryzujący się niskimi szumami własnymi i ściśle określonym pasmem przenoszonych częstotliwości.

Do pomiarów zastosowano aparaturę opracowaną w Pracowni Analizy Sygnału Emisji Akustycznej Instytutu Podstawowych Problemów Techniki PAN, pod kierunkiem prof. dr hab. inż. Zbigniewa Ranachowskiego. Ponieważ sygnał z typowego czujnika emisji akustycznej posiada niski poziom napięć (rzędu miliwoltów) i pasmo od około 0,1 kHz do 1,5 MHz, konieczne było uprzednie odpowiednie przekształcenie sygnału. Sygnał emisji akustycznej był najpierw wzmacniany w przedwzmacniaczu, a następnie odfiltrowany. Do rejestracji sygnałów szumowych emisji akustycznej generowanych przez przepływ paliwa oraz powietrza zasilającego, potrzebny był wzmacniacz niskoszumny o impedancji wejściowej > 0.5 Ohma i paśmie przenoszenia 0.5 – 40 kHz. Zastosowano tu zapis sygnału z następującymi parametrami: wejście liniowe, częstotliwość próbkowania 88,2 kHz, rozdzielczość 16 bitów, waga najmłodszego bitu z zastosowaniem wzmocnienia X 100–2 mikrowolty.

Na rysunku 6 przedstawiono wybrany przebieg czasowy sygnału źródłowego emisji akustycznej z pracującej pompy paliwowej zasilającej kocioł i na rysunku 6 jego wizualizację amplitudowo częstotliwościową.

.

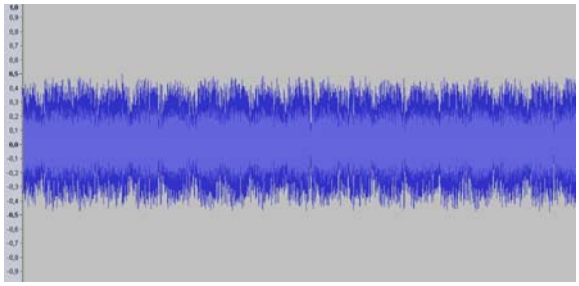

Rys. 5. Przebieg czasowy sygnału źródłowego emisji akustycznej z pracującej pompy paliwowej zasilającej kocioł

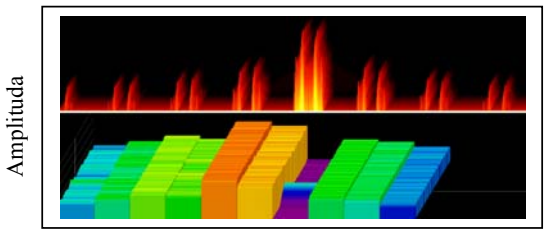

Rys. 6. Wizualizacja procesu emisji akustycznej z pompy paliwowej zasilającej pracujący palnik kotła

Wizualizację sygnału emisji akustycznej dla przepływu powietrza podawanego przez dmuchawę, bez pracy palnika przedstawiono na rysunku 7.

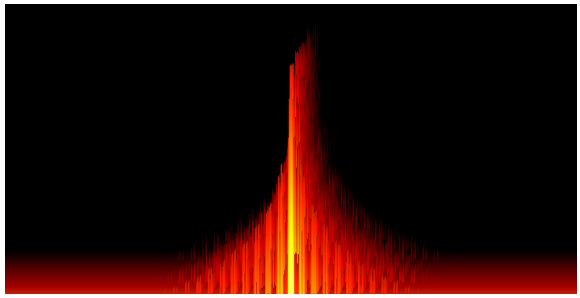

Rys. 7. Wizualizacja sygnału emisji akustycznej dla przepływu powietrza podawanego przez dmuchawę (bez pracy palnika)

Klasyczne metody Fouriera nie mogą być stosowane do analizy procesów niestacjonarnych. Nie dają one informacji na temat lokalnych rozkładów częstotliwościowych. Zamiast klasycznej transformacji Fouriera zastosowano transformację falkową, gdzie częstotliwość reprezentowała współczynnik skalujący. Na rysunku 8 przedstawiono dekompozycję falkową sygnału emisji akustycznej kotła z zapalonym palnikiem.

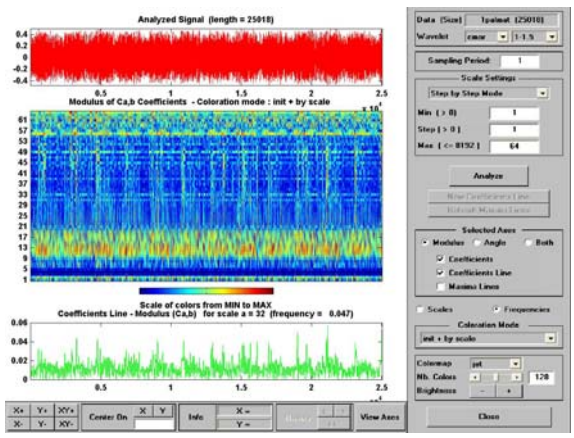

Rys. 8. Dekompozycja falkowa sygnału emisji akustycznej kotła z pracującym palnikiem

Stosując metodę dekompozycji falkowej analizowano sygnał z gorszą rozdzielczością w dziedzinie częstotliwości w porównaniu z przekształceniem Fouriera, natomiast można było pozyskać informację o ewentualnych zmianach charakterystyki widmowej sygnału w kolejnych, względnie krótkich, przedziałach czasu pracy kotła.

Skutki degradacji i niesprawności odwzorowuje wzrost drgań i zmiana charakteru widma czasowo-widmowego generowanego sygnału wibroakustycznego kotła. Do jego opisu mogą/są powszechnie stosowane modele diagnostyki wibroakustycznej [3, 9, 10].

5. WNIOSKI KOŃCOWE I PODSUMOWANIE

Nadzór eksploatacyjny kotła odbywa się dotychczas przede wszystkim w oparciu o wartości parametrów sygnału cieplno – przepływowego oraz metodami wizualizacyjnymi. Osady i zanieczyszczenia kotła wpływają znacząco na jakość procesu przejmowania ciepła, a regulacja palnika na proces spalania paliwa. Dlatego spośród sygnałów generowanych przez parowy kocioł okrętowy za podstawowy w nadzorowaniu poprawności funkcjonowania kotła należy uznać sygnał cieplno – przepływowy. Jego modele doczekały się w literaturze dostatecznie wszechstronnych opracowań [6, 8, 11, 12].

Ze względu na łatwość pozyskiwania wartości parametrów sygnału emisji produktów spalania modele (9) – (19) mogą mieć one zastosowanie w uwiarygodnianiu parametrów modeli cieplno – przepływowych (5) – (8). Wynik tej konfrontacji będzie dobrym uzupełnieniem uzasadnienia podejmowanych obsługowych decyzji eksploatacyjnych. Zależność (9) dzięki swej prostocie dobrze oddaje tendencje zmian wartości sprawności kotła, natomiast sprawność spalania η_{Af} obliczona ze związku (10) jest wygodna jako parametr kontrolny podczas regulacji palnika. Modele te mogą być również pomocne w ocenie skuteczności przeprowadzanych obsług – odtwarzania stanu technicznego powierzchni wymiany ciepła kotła (czyszczenia) i regulacji palnika.

Kotły parowe podczas pracy generują drgania, hałas i pulsacje czynników roboczych. Są one przyczynami i/lub efektami degradacji stanu technicznego kotłów. Bezpośrednim powodem emisji akustycznej może być zmiana naprężeń, temperatury, promieniowanie, erozja a nawet korozja materiału kotła. Zaistnienie emisji akustycznej nabytej w trakcie eksploatacji należy uznać za sygnał degradacji/zmiany własności struktury warstwy wierzchniej i wnętrza materiału elementu konstrukcji. Sygnał ten ze względu na doraźny charakter pozyskiwania jego parametrów należy uznać za źródło informacji diagnostycznej, po wnikliwej ich identyfikacji w ramach systemu diagnostycznego.

Zebrane doświadczenia i pozyskane wyniki podczas eksperymentalnej identyfikacji parametrów sygnału wibroakustycznego nasuwają w badaniach celowość pomiarów:

a/ w komorze spalania:
- ciśnienia akustycznego – czujnikami ciśnienia,
- częstotliwości w komorze spalania,
- ciśnienia akustycznego do określenia zmiany fazy,

b/ dla elementów kotła:
- drgań czujnikami prędkości i przyśpieszenia,
- natężenia dźwięku wyemitowanego przez elementy kotła.

Przedstawione modele sygnałów generowanych przez kotły i otrzymane wyniki ich identyfikacji parametrycznej wnoszą zachęcające przesłanki do wdrożenia quasidynamicznego obsługiwania kotłów okrętowych.

LITERATURA

[1] Adamkiewicz A., Kołwzan K.: *Influence Of Combustion Products On Faults In Ship Auxiliary Boilers.* Materiały XXVIII Sympozjum Siłowni Okrętowych. Akademia Morska w Gdyni, 15 – 16 listopada 2007, Gdynia 2007.

[2] Adamkiewicz A., Tomaszewski F.: *Analysis Of Possibilities Of Applying Ship Boiler Maintenance Strategies With Quasidynamic Diagnostics.* 27-th International scientific conference DIAGO® 2008. Technical diagnostics of machines and Manufacturing equipment. Vysoká škola báňská – Technická univerzita Ostrava. Asociace technických diagnostiků ČR o.s., Rožnov pod Radhoštěm, 5. - 6. February 2008.

[3] Cempel Cz., Tomaszewski F.: *Diagnostyka maszyn. Zasady Ogólne. Przykłady zastosowań.* Międzynarodowe Centrum Naukowe Eksploatacji Majątku Trwałego, Radom 1992.

[4] Combustion Gas Analyzer IMR 3000. IMR Environmental Equipment, Inc., St. Petersburg, www.imrusa.com

[5] *Flue Gas Analyzer GA-20 plus.* Operating manual 01/2003. MADUR Electronics, 01/2003.

[6] Głuch J., Krzyżanowski J.: *Diagnostyka cieplno-przepływowa obiektów energetycznych*. Wydawnictwo IMP PAN, Gdańsk 2004.

[7] Korbicz J., Kościelny J. M., Kowalczuk Z., Cholewa W.: *Diagnostyka procesów. Modele. Metody sztucznej inteligencji. Zastosowania.* WNT, Warszawa 2002.

[8] Kruczek S.: *Kotły. Konstrukcje i obliczenia.* Oficyna wydawnicza Politechniki Wrocławskiej. Wrocław 2001.

[9] Niziński S., Michalski R.: *Diagnostyka obiektów technicznych.* Wydawnictwo Instytutu Technologii Eksploatacji, Radom 2002.

[10] PARAT Andes Halvorsen A/S.: *Operator's Manual For Parat Steam Boiler Plant*. Flekkefjord, Norway, Steam and Heat Industry, Boiler Factory, 1995.
[11] Pronobis M.: *Modernizacja kotłów energetycznych.* Warszawa, Wydawnictwa Naukowo-Techniczne, 2002.
[12] Zajczyk R.: *Modele matematyczne systemu elektroenergetycznego do badania elektromechanicznych stanów nieustalonych i procesów regulacyjnych*. Gdańsk, PAN Komitet Elektrotechniki, 2003.
[13] http://www.parat.no/index2.htm
[14] www.imrusa.com

Andrzej ADAMKIEWICZ dr hab. inż. prof. nadzw. na Wydziale Mechanicznym Akademii Morskiej w Szczecinie. Doktoryzował się w Instytucie Maszyn Przepływowych PAN w Gdańsku. Stopień doktora habilitowanego uzyskał na Wydziale Maszyn Roboczych i Transportu Politechniki Poznańskiej. Reprezentowane dyscypliny i specjalności: budowa i eksploatacja maszyn: cieplne maszyny wirnikowe, siłownie okrętowe i diagnostyka maszyn. Pracę naukową i dydaktyczną realizuje w zakresie okrętowych układów energetycznych: maszyn przepływowych, turbin okrętowych, napędów parowych, a w tym kotłów parowych opalanych, utylizacyjnych i fluidalnych oraz szeroko rozumianych zagadnień ochrony środowiska morskiego. Członek Sekcji Podstaw Eksploatacji KBM PAN, Zachodniopomorskiego Zespołu Środowiskowego Sekcji Podstaw Eksploatacji KBM PAN, członek Rady Technicznej Polskiego Rejestru Statków, Polskiego Towarzystwa Naukowego Silników Spalinowych oraz Zespołu Techniki Morskiej Sekcji Technicznych Środków Transportu Komitetu Transportu PAN.

Artur BEJGER dr inż. jest adiunktem w Katedrze Diagnostyki Maszyn Okrętowych Akademii Morskiej w Szczecinie. Prodziekan ds. studiów dziennych Wydziału Mechanicznego AM. Pracę dydaktyczną realizuje na przedmiotach związanych z diagnozowaniem oraz technologią remontów maszyn okrętowych. Działalność naukową koncentruje wokół problematyki diagnozowania maszyn (ze szczególnym uwzględnieniem układów wtryskowych silników wysokoprężnych) z wykorzystaniem sygnału emisji akustycznej. Jest współautorem nowej metodyki badawczej (z opracowaniem przenośnego urządzenia pomiarowego) układów wtryskowych silników wysokoprężnych. Członek Zachodniopomorskiego Zespołu Środowiskowego Sekcji Podstaw Eksploatacji KBM PAN oraz Polskiego Towarzystwa Naukowego Silników Spalinowych.

Krzysztof KOŁWZAN, mgr inż., pracownik Inspektoratu Konwencyjnego Polskiego Rejestru Statków S.A. Absolwent Wyższej Szkoły Morskiej w Gdyni. Pracę magisterską obronił w 1985 r. (promotor prof. mgr inż. Andrzej Perepeczko).
Zainteresowania naukowe autora obejmują zagadnienia: eksploatacji statków i siłowni okrętowych ze szczególnym uwzględnieniem wymagań stawianych im przez międzynarodowe konwencje o ochronie środowiska morskiego oraz diagnostykę okrętowych maszyn i urządzeń. Jest ekspertem Ministerstwa Infrastruktury w czasie sesji Międzynarodowej Organizacji Morskiej (IMO) oraz przewodniczy polskiej sekcji Komitetu Ochrony Środowiska Morskiego (IMO MEPC).

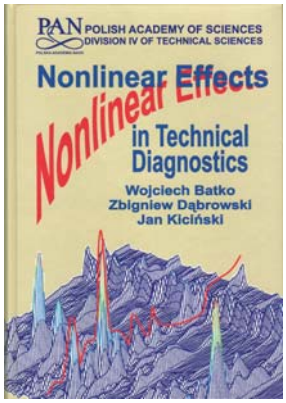

Wojciech BATKO
Zbigniew DĄBROWSKI
Jan KICIŃSKI

Nonlinear Effects in Technical Diagnostics

ITE, Radom, 2008

The presented in the book considerations lead to the conclusion that a classic diagnostic task very often requires application of a nonlinear description. The following postulate can be formulated on the basis of numerous papers (including papers of the authors).

A new ('after an initial usage') machine can be described with an adequate accuracy by a linear model. During exploitation certain nonlinear disturbances related to wear and tear – occur. Thus, an observation of nonlinear effects allows solving a diagnostic task.

This postulate is also true for technical devices, which operations require a nonlinear description from the "very beginning" (e.g. piston-and-crank mechanism). In such situation we will observe an increase of nonlinear disturbances.

Resonant increases of the amplitude in bands, in which the vibration level in a new machine was low, local losses of motion stability, generation of self-exited vibrations, as well as strong dependence of parasitic vibration processes on the load – are typical symptoms frequently utilised in vibroacoustic diagnostics.

Thus, purposefulness of application nonlinear descriptions seems to be doubtless similarly as looking for vibration measures (more precisely: methods and techniques of signal analysis) sensitive to the nonlinear disturbances evolution.

The Authors considerations are illustrated by many technical examples from the field of rotating machinery and new nonlinear materials.

Diagnostyka

Obszar zainteresowania czasopisma to:
- ogólna teoria diagnostyki technicznej
- eksperymentalne badania diagnostyczne procesów i obiektów technicznych;
- modele analityczne, symptomowe, symulacyjne obiektów technicznych;
- algorytmy, metody i urządzenia diagnozowania, prognozowania i genezowania stanów obiektów technicznych;
- metody detekcji, lokalizacji i identyfikacji uszkodzeń obiektów technicznych;
- sztuczna inteligencja w diagnostyce: sieci neuronowe, systemy rozmyte, algorytmy genetyczne, systemy ekspertowe;
- diagnostyka energetyczna systemów technicznych;
- diagnostyka systemów mechatronicznych i antropotechnicznych;
- diagnostyka procesów przemysłowych;
- diagnostyczne systemy utrzymania ruchu maszyn;
- ekonomiczne aspekty zastosowania diagnostyki technicznej;
- analiza i przetwarzanie sygnałów.

Topics discussed in the journal:
- General theory of the technical diagnostics,
- Experimental diagnostic research of processes, objects and systems,
- Analytical, symptom and simulation models of technical objects,
- Algorithms, methods and devices for diagnosing, prognosis and genesis of condition of technical objects,
- Methods for detection, localization and identification of damages of technical objects,
- Artificial intelligence in diagnostics, neural nets, fuzzy systems, genetic algorithms, expert systems,
- Power energy diagnostics of technical systems,
- Diagnostics of mechatronic and antropotechnic systems,
- Diagnostics of industrial processes,
- Diagnostic systems of machine maintenance,
- Economic aspects of technical diagnostics,
- Analysis and signal processing.

Wszystkie opublikowane artykuły uzyskały pozytywne recenzje wykonane przez niezależnych recenzentów.

All the published papers were reviewed positively by the independent reviewers.

Druk:
Centrum Graficzne „GRYF”, ul. Pieniężnego 13/2, 10-003 Olsztyn, tel. / fax: 089–527–24–30

Oprawa:
Zakład Poligraficzny, UWM Olsztyn, ul. Heweliusza 3, 10-724 Olsztyn
tel. 089-523-45-06, fax: 089-523-47-37

Wszystkie opublikowane w czasopiśmie artykuły uzyskały pozytywne recenzje, wykonane przez niezależnych recenzentów.
Redakcja zastrzega sobie prawo korekty nadesłanych artykułów.
Kolejność umieszczenia prac w czasopiśmie zależy od terminu ich nadesłania i otrzymania ostatecznej, pozytywnej recenzji.
Wytyczne do publikowania w DIAGNOSTYCE można znaleźć na stronie internetowej:
http://www.uwm.edu.pl/wnt/diagnostyka

Redakcja informuje, że istnieje możliwość zamieszczania w DIAGNOSTYCE ogłoszeń i reklam.
Jednocześnie prosimy czytelników o nadsyłanie uwag i propozycji dotyczących formy i treści naszego czasopisma.
Zachęcamy również wszystkich do czynnego udziału w jego kształtowaniu poprzez nadsyłanie własnych opracowań związanych z problematyką diagnostyki technicznej. Zwracamy się z prośbą o nadsyłanie informacji o wydanych własnych pracach nt. diagnostyki technicznej oraz innych pracach wartych przeczytania, dostępnych zarówno w kraju jak i zagranicą.